

GPO PRICE \$ \_\_\_\_\_

CFSTI PRICE(S) \$ \_\_\_\_\_

Hard copy (HC) 3.25

Microfiche (MF) 1.00

# 653 July 85

# INVESTIGATIONS OF SPACE STORABLE PROPELLANTS

(OF  $2/B_2H_6$ )

N66 39930

FACILITY FORM 502  
(ACCESSION NUMBER) 184  
(PAGES) CR 54741  
(NASA CR OR TMX OR AD NUMBER)

(THRU)

(CODE)

(CATEGORY) 27

Prepared for

NATIONAL AERONAUTICS AND SPACE ADMINISTRATION

CONTRACT NAS 3-2553

**Thiokol** CHEMICAL CORPORATION  
REACTION MOTORS DIVISION  
DENVER, NEW JERSEY

### NOTICE

This report was prepared as an account of Government sponsored work. Neither the United States, nor the National Aeronautics and Space Administration (NASA), nor any person acting on behalf of NASA:

- A.) Makes any warranty or representation, expressed or implied, with respect to the accuracy, completeness, or usefulness of the information contained in this report, or that the use of any information, apparatus, method, or process disclosed in this report may not infringe privately owned rights; or
- B.) Assumes any liabilities with respect to the use of, or for damages resulting from the use of any information, apparatus, method or process disclosed in this report.

As used above, "person acting on behalf of NASA" includes any employee or contractor of NASA, or employee of such contractor, to the extent that such employee or contractor of NASA, or employee of such contractor prepares, disseminates, or provides access to, any information pursuant to his employment or contract with NASA, or his employment with such contractor.

Requests for copies of this report should be referred to

National Aeronautics and Space Administration  
Office of Scientific and Technical Information  
Attention: AFSS-A  
Washington, D.C. 20546

NASA CR-54741  
Report RMD 6039-F

FINAL REPORT

INVESTIGATION OF SPACE  
STORABLE PROPELLANTS -  $\text{OF}_2/\text{B}_2\text{H}_6$

prepared for

NATIONAL AERONAUTICS AND SPACE ADMINISTRATION

10 June 1966

CONTRACT NAS 3-2553

Technical Management  
NASA Lewis Research Center  
Cleveland, Ohio  
Liquid Rocket Technology Branch  
Daniel Bachkin  
Paul N. Herr

THIOKOL CHEMICAL CORPORATION  
Reaction Motors Division  
Denville, New Jersey





## ACKNOWLEDGMENT

This program was sponsored by the Office of Advanced Research and Technology, NASA Headquarters, under the direction of Mr. Henry Burlage. Technical cognizance was under the Lewis Research Center with Messrs. Daniel Bachkin and Paul N. Herr and Technical Managers.

Contributions to the technical content of this report were made by a number of individuals at Thiokol-RMD. Overall technical direction was handled by the Thiokol-RMD Advanced Technology Section, M. Sussman, Section Supervisor. Project Engineer was M. Luperi. The detailed activities were supported by the following:

Ablative Materials	H. Feigel, S. Tick, F. Forte
2000 lb Thrust Injector Studies	R. Fash, R. Billings, E. Tepper
Specific Heat of OF <sub>2</sub>	A. Lum, M. McCallister
Advanced Thrust Chamber Design Studies	S. Kurzeja, S. Tick
Test Setup Design	A. Mock, D. Totten
Test Instrumentation	H. Mey, Jr.
Test Operations	R. Axt, J. Rossi, D. Doney, T. Wilk, J. Kipp, J. Stewart
AEDC Liaison	R. Axt
AEDC Data Analysis	A. Merrill, R. Billings



## ABSTRACT

Sea level testing was accomplished at the 2000-pound space thrust level with  $\text{OF}_2 / \text{B}_2\text{H}_6$  propellants to checkout hardware for subsequent altitude performance tests. Tests conducted with propellant-cooled and heat sink type vortex injectors demonstrated that  $\text{OF}_2 / \text{B}_2\text{H}_6$  can deliver high specific impulse. Allowing for nozzle divergence losses and combustion efficiency, 98% of theoretical vacuum shifting equilibrium specific impulse was obtained. Injector and combustion chamber heat transfer data were acquired to provide design data for  $\text{OF}_2 / \text{B}_2\text{H}_6$  combustion containment.

Altitude performance tests, conducted at AEDC with the sea level injector-combustion chamber in conjunction with a 40:1 area ratio conical nozzle extension demonstrated that  $\text{OF}_2 / \text{B}_2\text{H}_6$  delivers high specific impulse at altitude conditions ( $\geq 125,000$  ft). A maximum specific impulse of 384 lbf-sec/lbm was obtained. Comparisons of the experimental performance data were made with the theoretical shifting and frozen equilibrium performance and also the predicted kinetic performance.

The specific heat of liquid  $\text{OF}_2$  was experimentally determined over a range of temperatures and pressures typical of those for space operation.

Design studies were conducted to investigate the feasibility of reliable thrust chamber concepts capable of extended firing durations over many cycles of operation with  $\text{OF}_2 / \text{B}_2\text{H}_6$ . Detailed analysis of the most promising advanced thrust chamber concepts have been completed.

PRECEDING PAGE BLANK NOT FILMED.



## CONTENTS

	Page
I. INTRODUCTION	1
II. SUMMARY	4
III. PROGRAM CONCLUSIONS AND RECOMMENDATIONS	8
IV. DISCUSSION	10
A. Sea Level Injector Investigations	10
1. Objective	10
2. Test Program	10
3. Test Hardware Design and Fabrication	11
4. Test Facility	24
5. Propellant-Cooled and Heat Sink Injector Performance and Heat Transfer Tests	26
B. Altitude Performance Evaluation of $\text{OF}_2/\text{B}_2\text{H}_6$	63
1. Objectives	63
2. Test Program	63
3. Test Hardware	63
4. Test Facility	65
5. Data Reduction	68
6. Test Results	71
C. 2000-Pound Thrust Ablative Combustion Chamber	83
1. Objectives	83
2. Design and Fabrication	83
D. Specific Heat Determination of Liquid $\text{OF}_2$	88
1. Objective	88
2. Test Program	88
3. Test Apparatus	88
4. Apparatus Calibrations and Test Procedures	91
5. Test Results	91

CONTENTS (cont)

	Page
E. $\text{OF}_2/\text{B}_2\text{H}_6$ Combustion Containment Design Studies	96
1. Objective	96
2. Design Studies	96
3. Cooling Concept Evaluation	111
4. Radiamic Thrust Chamber Design Analysis	116
REFERENCES	137
APPENDIXES	
A Heat Transfer Calculations	
B Thermochemical and Kinetic Performance Analysis	
C Test Procedure for the Determination of the Specific Heat of Liquid $\text{OF}_2$	

## ILLUSTRATIONS

Figure		Page
1	Mid-Diameter Vortex Injector	12
2	Mid-Diameter Vortex Oxidizer Injector	12
3	Full Diameter Vortex Injector Assembly	12
4	OF <sub>2</sub> Injector Heat Transfer Data	15
5	Typical Instrumented Heat Sink Oxidizer Injector Assembly	16
6	Two-on-One Heat Sink Type Injector	18
7	Two-on-One Heat Sink Type Injector Design Ablative Cap	18
8	One-on-One Heat Sink Injector - 20 Orifices	19
9	One-on-One Heat Sink Injector - 30 Orifices	19
10	Oxidizer Injector Braze Photographs	21
11	Uncooled Heat Sink Thrust Chamber Assembly	23
12	OF <sub>2</sub> /B <sub>2</sub> H <sub>6</sub> Test Facility	25
13	Uncooled Thrust Chamber Installed in Test Facility	27
14	Propellant-Cooled Mid-Diameter Vortex Injector Sea Level Performance (Used at AEDC)	36
15	Propellant-Cooled Mid-Diameter Vortex Injector Sea Level Performance	37
16	Heat Sink Vortex Injector Sea Level Performance	38
17	Heat Sink Injector Sea Level Performance	40
18	Post-Test Photographs, Two-on-One Heat Sink Injectors	41
19	X316540 S/N 4-5 Heat Sink Injector After Five Tests	47

# ILLUSTRATIONS (cont)

Figure		Page
20	Gas Side Wall Temperature Data - S/N 4-3 Heat Sink Oxidizer Injector, Test Run 6CX1492	48
21	Oxidizer Injector Heat Flux S/N 4-3, Two-on-One Heat Sink Test Run 6CX1492	49
22	Gas Side Wall Temperature Data - S/N 1-1 Heat Sink Oxidizer Injector Test Run 6CX1492	51
23	Average Oxidizer Injector Heat Flux S/N 1-1, One-on-One Injector	52
24	Heat Sink Oxidizer Injector Heat Flux vs Vortex Annulus Gas Film Parameter	53
25	Heat Sink Full-Diameter Vortex Injector Design	54
26	Gas Film Heat Transfer Coefficient vs Axial Location RMD Sea Level Test Data	56
27	Gas Film Heat Transfer Coefficient vs Thermocouple Station - AEDC Data	57
28	Oxidizer Injector Water Flow Model	59
29	Typical Oxidizer Injector Spray Pattern, S/N 0-6 Injector	59
30	Altitude Evaluation Thrust Chamber and Nozzle Extension Assembly	64
31	Thrust Chamber Assembly Installation in Propulsion Engine Test Cell J-2 at Arnold Center	66
32	Location of Engine Instrumentation Parameters - AEDC Tests	67
33	Experimental Altitude Performance - $OF_2/B_2H_6$ - AEDC Tests	74
34	Typical Simulated Altitude Data Trace (AEDC Data)	75
35	Nozzle Extension Pressure Distribution	77
36	Experimental Altitude Performance Corrected for $\lambda \cdot C_D \cdot C_V$ % c*	79



# ILLUSTRATIONS (cont)

Figure		Page
37	Performance at High $\xi$ for Candidate Space Propellants	81
38	2000-lb Thrust Ablative Chamber Design	84
39	Predicted Ablative Chamber Performance - $\text{OF}_2/\text{B}_2\text{H}_6$	85
40	Ablative Chamber Assembly	87
41	$\text{OF}_2$ Specific Heat Apparatus Schematic	89
42	$\text{OF}_2$ Specific Heat Laboratory Apparatus	90
43	Experimental Specific Heat of Liquid $\text{OF}_2$	94
44	Gas Film Coefficient Profile	100
45	Heat Transfer Variation of Dimensionless Nozzle Throat Convective Coefficient with Reynolds Number (Ref 17)	101
46	Chamber Geometry Heat Rejection Comparison for 30" L* Chamber	103
47	Physical Properties of Diborane - $\text{B}_2\text{H}_6$	104
48	Physical and Thermal Properties of Oxygen Difluoride - $\text{OF}_2$	105
49	Upper Limit of Nucleate Boiling Predictions - $\text{OF}_2$ - Bernath Correlation	107
50	Upper Limit of Nucleate Boiling Predictions - $\text{B}_2\text{H}_6$ - Bernath Correlation	108
51	Material Sample Pins Before and After Testing	109
52	Advanced Chamber Concepts - Torox, Voramic and Radiamic	114
53	Design Study Approach Diagram	117
54	2500-lb Space Thrust Radiamic Engine Design - $\text{OF}_2/\text{B}_2\text{H}_6$	119
55	Radiamic Thrust Chamber Assembly	120
56	Gas-Side Wall Throat Temperature - Radiamic Design	125

ILLUSTRATIONS (cont)

Figure		Page
57	Gas-Side Wall Chamber Temperature - Radiamic Design	126
58	Gas-Side Wall Temperature - Specific Impulse Tradeoff	129
59	OF <sub>2</sub> Bulk Temperature Rise as a Function of Operating Conditions - Radiamic Design	131
60	OF <sub>2</sub> Bulk Temperature Rise as a Function of L*, O/F	132
61	Radiamic Chamber Design - Throat Temperature Profile	133
62	Radiamic Chamber Design - Chamber Temperature Profile	134
63	Equilibrium Soak Temperature - Radiamic Design	135

TABLES

	Page
I Propellant-Cooled Injector Configurations	13
II Heat Sink Type Injector Configurations	20
III Mid-Diameter Vortex Propellant Cooled Injector -Test Data Summary	32
IV Heat Sink Mid-Diameter Vortex Injector -Test Data Summary	33
V Propellant-Cooled Vortex Oxidizer Injector Heat Flux Comparison	43
VI Heat Sink Oxidizer Injector Heat Transfer Summary	46
VII Oxidizer Injector Model Water Flow Test Summary	60
VIII $\text{OF}_2/\text{B}_2\text{H}_6$ Altitude Test Summary	72
IX Corrected Specific Impulse and Thrust Coefficient	78
X Experimental Data for Heat Capacity Determination of $\text{OF}_2$	92
XI $\text{OF}_2/\text{B}_2\text{H}_6$ Material Specimen Test Results	110
XII Material Thermal Properties	123
XIII Nominal Operating Conditions Radiamic Thrust Chamber	124
XIV List of Symbols	139



## I. INTRODUCTION

In order to fulfill the requirements of the long term deep space penetration missions contemplated for the future, propellant combinations offering high performance are a prerequisite and in addition, space storability and hypergolicity are desirable characteristics. For these missions, engines capable of operating with high reliability for long durations will be required. Experimental studies have shown that the  $\text{OF}_2 / \text{B}_2\text{H}_6$  propellant combination is hypergolic and provides high performance at sea level (References 1, 2). Space missions studies conducted by many Government contractors and agencies, including NASA (Reference 3), Martin (Reference 4), Bell Aerosystems (Reference 5), General Electric (Reference 6), and Thiokol-RMD (Reference 7) have shown that the  $\text{OF}_2 / \text{B}_2\text{H}_6$  propellant combination provides high payload capability (about equal to that deliverable with  $\text{F}_2 / \text{H}_2$  which is slightly better for short storage times only) as a result of high performance and high bulk density, long term space storability with low-loss storage capability (several orders of magnitude better than liquid hydrogen), and enhances space engine reliability as a result of its hypergolicity.

Many propellant combinations (e. g.,  $\text{F}_2 / \text{H}_2$ ,  $\text{O}_2 / \text{H}_2$ , Flox/Hydrocarbons,  $\text{OF}_2 / \text{MMH}$ ,  $\text{OF}_2 / \text{Hydrocarbons}$ ,  $\text{N}_2\text{O}_4 / \text{Hydrazine Base Fuels}$ ) were considered with respect to the three requirements listed above (high performance, space storability and hypergolicity). These characteristics all contribute, either directly or indirectly, to high mission reliability.

Initial experimental exploration of the space storable propellant combination, oxygen difluoride ( $\text{OF}_2$ ) and diborane ( $\text{B}_2\text{H}_6$ ), was initiated by Thiokol with Corporate funding in 1960. Several experimental rocket firings were made at the 150-pound thrust level which demonstrated hypergolic ignition and indicated high performance. Additional tests were also made at the 8000-pound thrust level with  $\text{OF}_2 / \text{MMH}$ . The success of these tests coupled with the results of continuing analytical studies led to an  $\text{OF}_2 / \text{B}_2\text{H}_6$  exploratory program with NASA commencing in 1962. Since June 1962, the development of the  $\text{OF}_2 / \text{B}_2\text{H}_6$  technology has been sponsored by the Office of Advanced Research and Technology, NASA Headquarters.

These exploratory investigations were continued and expanded under NASA Contract NAS-w-449. Under this program basic  $\text{OF}_2$  physical, thermodynamic, and materials compatibility properties were determined. Thrust chamber firings at the 150-pound thrust level demonstrated high performance over a wide range of mixture ratios, demonstrated hypergolic ignition at sea level and simulated space conditions, and provided heat transfer data for engine design. These investigations are described in detail in Thiokol-RMD Report 5507-F.

In 1963, the  $\text{OF}_2 / \text{B}_2\text{H}_6$  investigations were continued under NASA Contract NAS-3-2553, Supplemental Amendments Numbers 1 through 4, Tasks I and II. Evaluation of four types of injectors (mid-diameter vortex, full-diameter vortex, coaxial showerhead and impinging stream) demonstrated that high percentages of theoretical performance ( $c^*$ ) were achievable at the 2000-pound space thrust level; satisfactory ignition was attained over a wide range of operating conditions; and promising thrust chamber durability with present state-of-the-art ablative materials was demonstrated. These investigations are described in detail in Thiokol-RMD Report 6028-F.

The promising results obtained in these programs led to the next two logical steps in acquiring technology with the  $\text{OF}_2 / \text{B}_2\text{H}_6$  propellant combination; (1) Experimental demonstration of the space performance potential, and (2) Studies to determine and feasibility of long duration combustion containment.

In March 1964, the investigations of  $\text{OF}_2 / \text{B}_2\text{H}_6$  propellants were again expanded under NASA Contract NAS-3-2553, Supplemental Amendments Numbers 5 and 6, to assess space performance potential. In August 1964, a follow-on program directed towards containment studies was initiated under Supplemental Amendments Numbers 7 and 8. These investigations, the subject of this report, included:

- Injector test firings at the 2000-pound space thrust level to checkout hardware for the altitude performance phase of the program and to acquire design data.
- Altitude performance evaluation of  $\text{OF}_2 / \text{B}_2\text{H}_6$  at AEDC.

- Ablative chamber design studies.
- Experimental determination of the specific heat of liquid  $\text{OF}_2$ .
- Design studies of advanced thrust chamber cooling concepts for extending duration capability.

The following sections of this report describe, in detail, the effort conducted on these investigations during the period from March 1, 1964, to July 31, 1965.

## II. SUMMARY

The investigations of the space storable propellant combination  $\text{OF}_2 / \text{B}_2\text{H}_6$  were continued under Contract NAS-3-2553 in this program. This program extended the work conducted on the prior program under Tasks I and II (Reference 1) into the following five major areas of investigation under Tasks III through XVI of Contract NAS-3-2553, Supplemental Agreements Numbers 5, 6, 7 and 8.

### A. OBJECTIVES

1. Injector investigations at the 2000-pound space thrust level to evaluate performance and heat transfer to acquire design data and to provide hardware for the altitude performance phase of the program.
2. Altitude performance evaluation of  $\text{OF}_2 / \text{B}_2\text{H}_6$  utilizing an injector-combustion chamber tested at sea level in conjunction with a 40:1 area ratio conical nozzle extension.
3. Experimental determination of the specific heat of liquid  $\text{OF}_2$  over a range of temperatures ( $-180^\circ\text{C}$  to  $-57^\circ\text{C}$ ) and pressures (50 to 300 psia).
4. Design studies to determine the feasibility of advanced thrust chamber cooling concepts for long duration combustion containment of  $\text{OF}_2 / \text{B}_2\text{H}_6$ .
5. Test evaluation of a 2000-pound space thrust ablative chamber design based on prior ablative screening results obtained at the 150 pound thrust level.

The following sections summarize the program accomplishments.



## B. SEA LEVEL INJECTOR INVESTIGATIONS AT THE 2000-POUND SPACE THRUST LEVEL

An injector configuration was selected on the basis of test data obtained with four types of injectors in the prior program. These injectors were the mid-diameter vortex, full-diameter vortex, coaxial showerhead, and impinging stream. Based on the promising durability (one 19 second test) and performance (94% c\*), a 2000-pound space thrust mid-diameter propellant-cooled vortex injector design configuration was selected for use in the altitude test program. As a result of durability problems with the propellant-cooled injectors, heat sink type injector effort was undertaken to make additional hardware available for altitude performance testing and to provide design data.

Propellant-cooled and heat sink type vortex injectors were designed, fabricated and tested to provide hardware for the altitude test program and to establish baseline injector performance for comparison with altitude performance test results. The heat sink type injectors were heavily instrumented to provide injector heat transfer data. Seventeen test firings with propellant-cooled injectors and sixteen test firings with heat sink type injectors, each at a duration of 2-3 seconds, were accomplished with mixture ratio varied from 2.65 to 3.34.

The initial series of tests, which were conducted with propellant-cooled injectors, gave performance levels of 85.5% to 95.9% of theoretical c\*. Two propellant-cooled injectors completed acceptance testing and were utilized at AEDC for altitude testing. The performance levels for the heat sink type injectors were 91.5% to 98.8% of theoretical c\*. Five heat sink injectors were delivered to AEDC, three of which were tested in the altitude performance program.

During the course of the program, modifications, to reduce heat flux levels and to improve durability, were incorporated in the heat sink injector designs. Oxidizer injector heat flux levels were reduced from 16-18 Btu/sec-in<sup>2</sup>, a level obtained with a design configuration similar to the propellant-cooled versions, to 2.5-4 Btu/sec-in<sup>2</sup>. Based on propellant cooling correlations and the heat flux levels obtained (4 Btu/sec-in<sup>2</sup>), a long duration propellant cooled injector design appears feasible.

### C. ALTITUDE PERFORMANCE EVALUATION

Ten performance tests were conducted at simulated altitudes in excess of 125,000 feet at a nominal chamber pressure level of 150 psia over a mixture ratio range of 2.73 to 3.24. Useful data were obtained from seven tests. As a result of fuel runout during one run and injector feed problems during the last two tests, steady state operation was not achieved in three of the runs. The  $c^*$  efficiency varied between 87.3% and 94.5% for the five injectors utilized. Actual vacuum specific impulse values between 354 and 384 lbf-sec/lb<sub>m</sub> were obtained. The maximum vacuum specific impulse of 385 lbf-sec/lb<sub>m</sub> obtained at a  $c^*$  of 94.5% corresponds to 90.6% of theoretical shifting equilibrium. The experimental thrust coefficients were consistently on the order of 96% of theoretical shifting equilibrium values and are in excellent agreement with predicted values based on nozzle divergence and wall friction losses.

Comparisons of the test data with theoretical shifting and frozen equilibrium performance and predicted kinetic performance shows that  $\text{OF}_2 / \text{B}_2\text{H}_6$  did deliver high specific impulse. Allowing for nozzle divergence losses and combustion efficiency, 98% of theoretical vacuum shifting equilibrium was obtained. Based on these analyses negligible kinetic losses were obtained and the high space performance potential of  $\text{OF}_2 / \text{B}_2\text{H}_6$  has been demonstrated.

### D. SPECIFIC HEAT DETERMINATION OF $\text{OF}_2$

The specific heat of liquid  $\text{OF}_2$  was experimentally determined over a temperature range of -196 to -75°C and a pressure range of 10 psia to 300 psia. Values of 0.33 to 0.37 Cal/g-°C were obtained over the range of temperatures and pressures investigated.

### E. THRUST CHAMBER DESIGN STUDIES

Design studies of advanced thrust chamber cooling concepts for long duration combustion containment of  $\text{OF}_2 / \text{B}_2\text{H}_6$  were completed. Material screening tests in which specimens were exposed to an  $\text{OF}_2 / \text{B}_2\text{H}_6$  combustion environment were conducted to assess thrust chamber materials of construction. A tantalum-tungsten alloy and several high density graphites have shown the best compatibility results.

Analytical studies based on typical space storage propellant temperatures and pressure-fed systems (i. e.,  $P_{ch} \leq 150$  psia), indicates that a Thiokol-RMD concept (Radiamic) can provide adequate cooling without supplemental film or transpiration cooling for long duration, multiple restart applications.

This chamber concept which embodies low heat flux chamber radiation liner and low mass throat insert surrounded by a regenerative cooling jacket provides flexibility and growth potential through the integration of proven concepts. Utilization of boundary layer control, supplemental film or transpiration cooling, or combinations of these concepts could extend the operating range of this concept and also make it feasible to employ other cooling concepts (e. g., partial regenerative with ablative or high temperature insulation liners).

#### F. 2000-POUND SPACE THRUST ABLATIVE CHAMBER

Design and fabrication of a 2000-pound space thrust ablative chamber was completed. The ablative chamber utilizes a graphite phenolic material which demonstrated the lowest erosion rate in prior screening tests conducted at the 150 pound thrust level (Reference 1). Based on these screening tests, the performance of graphite phenolic with  $\text{OF}_2/\text{B}_2\text{H}_6$  is equivalent to that obtained with silica phenolic with  $\text{N}_2\text{O}_4/\text{MMH}$ . It appears then, that ablative technology has applicability for certain duty cycle requirements with  $\text{OF}_2/\text{B}_2\text{H}_6$ . As a result of the reallocation of funds to support additional injector effort (i. e., heat sink), test firings with the ablative chamber were not conducted.

### III. PROGRAM CONCLUSIONS AND RECOMMENDATIONS

On the basis of the  $\text{OF}_2 / \text{B}_2\text{H}_6$  investigations conducted during this program, the following conclusions are made:

1. The  $\text{OF}_2 / \text{B}_2\text{H}_6$  propellant combination delivers high specific impulse at sea level and simulated altitude conditions. Performance analysis show that for the altitude test conditions evaluated (i. e.,  $P_c = 150$  psia,  $\text{O/F} = 2.7-3.3$ ,  $\epsilon = 40:1$ ), kinetic losses were negligible. Thus, high space-performance potential of  $\text{OF}_2 / \text{B}_2\text{H}_6$  with high area ratio nozzles ( $> 40:1$ ) is available.
2. On the basis of the results of the injector investigations obtained in this program and analytical propellant cooling correlations, a long duration propellant cooled injector appears feasible. A series of injector design modifications, utilizing instrumented heat sink type injectors, were successful in reducing heat flux levels to values that can be accepted with propellant cooling.
3. Based on previous small scale testing (150 lb thrust) and analytical studies, ablative cooling with  $\text{OF}_2 / \text{B}_2\text{H}_6$  is feasible for certain duty cycles. A 2000-pound space thrust ablative chamber fabricated but not hot tested in this program has been designed for 300 seconds of operation with  $\text{OF}_2 / \text{B}_2\text{H}_6$ . Testing of this chamber would provide design data and determine the applicability of ablatives with  $\text{OF}_2 / \text{B}_2\text{H}_6$  at a practical thrust level.
4. Experimental specific heat values of liquid  $\text{OF}_2$ , which have been obtained, will permit more reliable thrust chamber cooling and space mission studies.
5. Long duration combustion containment with  $\text{OF}_2 / \text{B}_2\text{H}_6$  appears feasible. The most promising cooling concept to arise from the containment studies is a Radiamic combustion chamber concept in conjunction with a full-diameter vortex injector.

6. Based on Thiokol-RMD and AEDC experience,  $\text{OF}_2$  and  $\text{B}_2\text{H}_6$  can be handled safely with normal precautions. Established procedures have been developed for propellant storage, facilities operation and disposal of  $\text{OF}_2$  and  $\text{B}_2\text{H}_6$ . With proper selection and adequate cleanliness and passivation, materials compatibility and handling of  $\text{OF}_2$  and  $\text{B}_2\text{H}_6$  pose no significant problems.

As a result of the demonstrated high performance and promising combustion containment studies accomplished during this program, it is recommended that the following investigations of the  $\text{OF}_2 / \text{B}_2\text{H}_6$  propellant combination be continued at the 2000 pound space thrust level:

1. The test evaluation of several instrumented heat sink injector types (i. e., full-diameter vortex, coaxial showerhead and an impinging stream) should be continued to provide comparative design data for long duration, propellant cooled versions.
2. Propellant cooled versions of these injector types should be tested to determine the most compatible injector for use with the Radiamic combustion chamber concept.
3. Demonstration tests of the Radiamic combustion chamber concept should be conducted to establish the feasibility of long duration combustion containment with  $\text{OF}_2 / \text{B}_2\text{H}_6$ .
4. Definition of the cooling properties of  $\text{OF}_2$  and  $\text{B}_2\text{H}_6$  is required to permit more refined cooling studies for injectors and combustion chambers. Basic upper limit of nucleate boiling data of  $\text{OF}_2$  and  $\text{B}_2\text{H}_6$  are required as well as  $\text{B}_2\text{H}_6$  thermal decomposition data.
5. Testing of the available 2000-pound space thrust ablative chamber should be conducted. This evaluation will provide design data to define the limits of ablative cooling with  $\text{OF}_2 / \text{B}_2\text{H}_6$ .
6. Analytical and design studies should be continued to determine the feasibility of more advanced cooling techniques (i. e., transpiration, film cooling, etc.) to enhance and extend thrust chamber operating limits with  $\text{OF}_2 / \text{B}_2\text{H}_6$ . The feasibility of employing these techniques to extend the operating range of the Radiamic combustion chamber concept should be investigated.
7. Additional thrust chamber investigations are required to demonstrate long duration capability with  $\text{OF}_2 / \text{B}_2\text{H}_6$ . Several injector types, in addition to a full-diameter vortex, should be investigated, to determine the most compatible injector for feasibility testing of the Radiamic combustion chamber concept.

## IV. DISCUSSION

### A. SEA LEVEL INJECTOR INVESTIGATIONS

#### 1. Objective

The primary objective of this effort was to provide injector hardware for altitude performance evaluation of  $\text{OF}_2/\text{B}_2\text{H}_6$ . Injector tests at the 2000-pound space thrust level were made to determine sea level performance. Additional injector investigations, including heat transfer and model water flow studies with various vortex type configurations, were undertaken to provide injector design data. To accomplish these objectives, tests were conducted with both propellant cooled and heat sink injectors.

#### 2. Test Program

Thirty-three sea level test firings were conducted with propellant cooled and heat sink type injectors to evaluate performance and heat transfer. An uncooled, copper heat sink combustion chamber was utilized for these tests.

As originally planned, three propellant-cooled injectors were to be fabricated and tested to provide hardware for the altitude performance tests. The selection of a propellant cooled injector configuration was based on the test experience obtained with four types of injectors (the mid-diameter vortex, full diameter vortex, coaxial showerhead, and impinging stream) tested in a prior program. Based on the promising durability (19 second test) and the good performance (94% c\*) demonstrated by the propellant cooled mid-diameter vortex injector, this configuration was selected for use in this program. The demonstrated performance level was considered adequate to provide meaningful altitude performance data and evaluation of a 2000 lb. thrust ablative chamber.

Primary emphasis was placed on providing sufficient hardware to support the altitude performance program since durability problems were encountered with the propellant-cooled injectors during sea level testing. Consequently, an evaluation of instrumented, heat sink type injectors was undertaken. These injectors provided additional hardware for the altitude performance tests and provided injector-chamber heat transfer data. Two propellant-cooled and four heat sink type injectors tested at sea level were made available for altitude testing.

### 3. Test Hardware Design and Fabrication

#### a. Injector Design

Several basic vortex injector types were designed for the 2000-pound space thrust level and tested at sea level. In the vortex injector, fuel is injected tangentially through the large diameter of an annulus adjacent to the combustion chamber. The oxidizer is injected radially outward from the small diameter of the annulus and impinges on the swirling fuel. Both the propellants and the combustion products enter the chamber with a tangential and axial velocity component. In the mid-diameter vortex injector the fuel injector diameter is smaller than the adjacent chamber barrel diameter. All of the injectors utilized in this program consisted of a fuel injector and an oxidizer injector mechanically assembled to form a complete injector assembly.

(1) Propellant Cooled Design - The initial design, a propellant cooled mid-diameter injector, is shown in Figure 1. During the course of the program, several minor modifications were incorporated in the propellant cooled injector designs in an effort to improve oxidizer injector durability and still maintain performance. A series of design modifications including reduced injection pressure drops, increased oxidizer injector cooling velocity, increased oxidizer injector face thickness with a zirconia gas side coating and revised OF<sub>2</sub> cooling passage geometry at the entrance to the orifices were evaluated. Figure 2 shows an oxidizer injector configuration with an increased face thickness and a zirconia gas side coating. Figure 3 shows a full diameter vortex injector available from the prior program which was tested during this program. A summary of the propellant cooled injectors fabricated and tested during this program is presented in Table I.

All of the propellant-cooled injectors, except the full-diameter vortex, utilized the same injection pattern (two rows of twelve fuel orifices and one row of twelve oxidizer orifices) and combustion side geometry as an injector tested in the previous program. Since the injector used on the prior program was designed for a chamber pressure of 120 psia, it was necessary to modify the oxidizer injector cooling passage to provide adequate cooling velocity for operation at a chamber pressure level of 150 psia. A flow divider was added at the center of the oxidizer injector to provide improved cooling velocity since evidence of the injector face overheating at this location was experienced in the prior program. Chromium copper alloy was used for the combustion side injector components. This alloy will operate appreciably cooler than stainless steel, or even nickel, and is capable of being heat treated to a minimum yield strength of 38,000 psi. Previous studies have shown that this material was also suitable for flight type injectors.

Propellant - Cooled Injectors

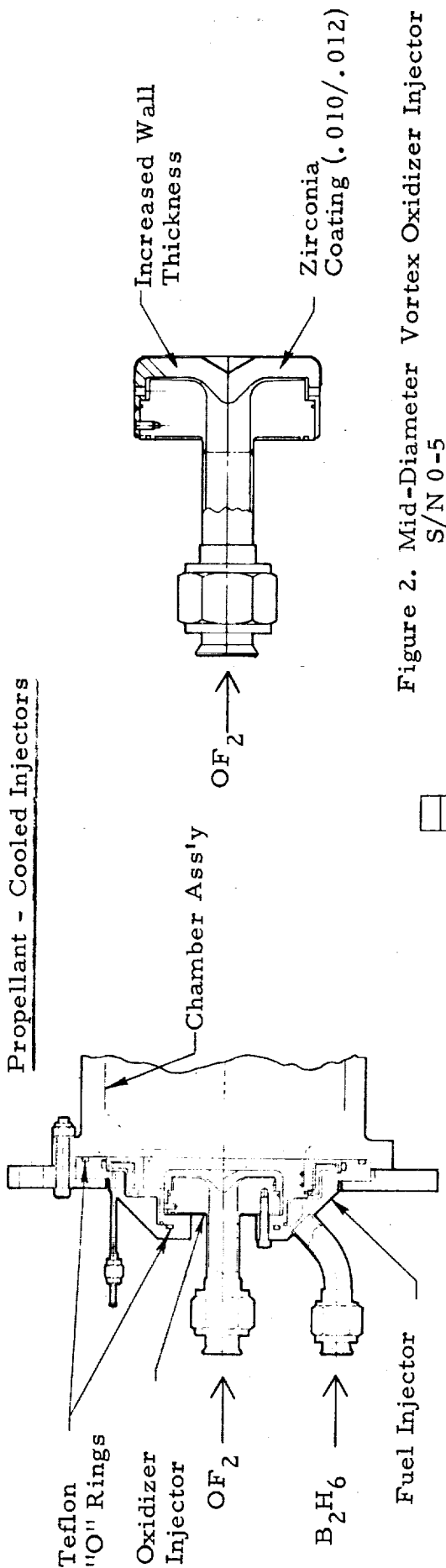


Figure 2. Mid-Diameter Vortex Oxidizer Injector  
S/N 0-5

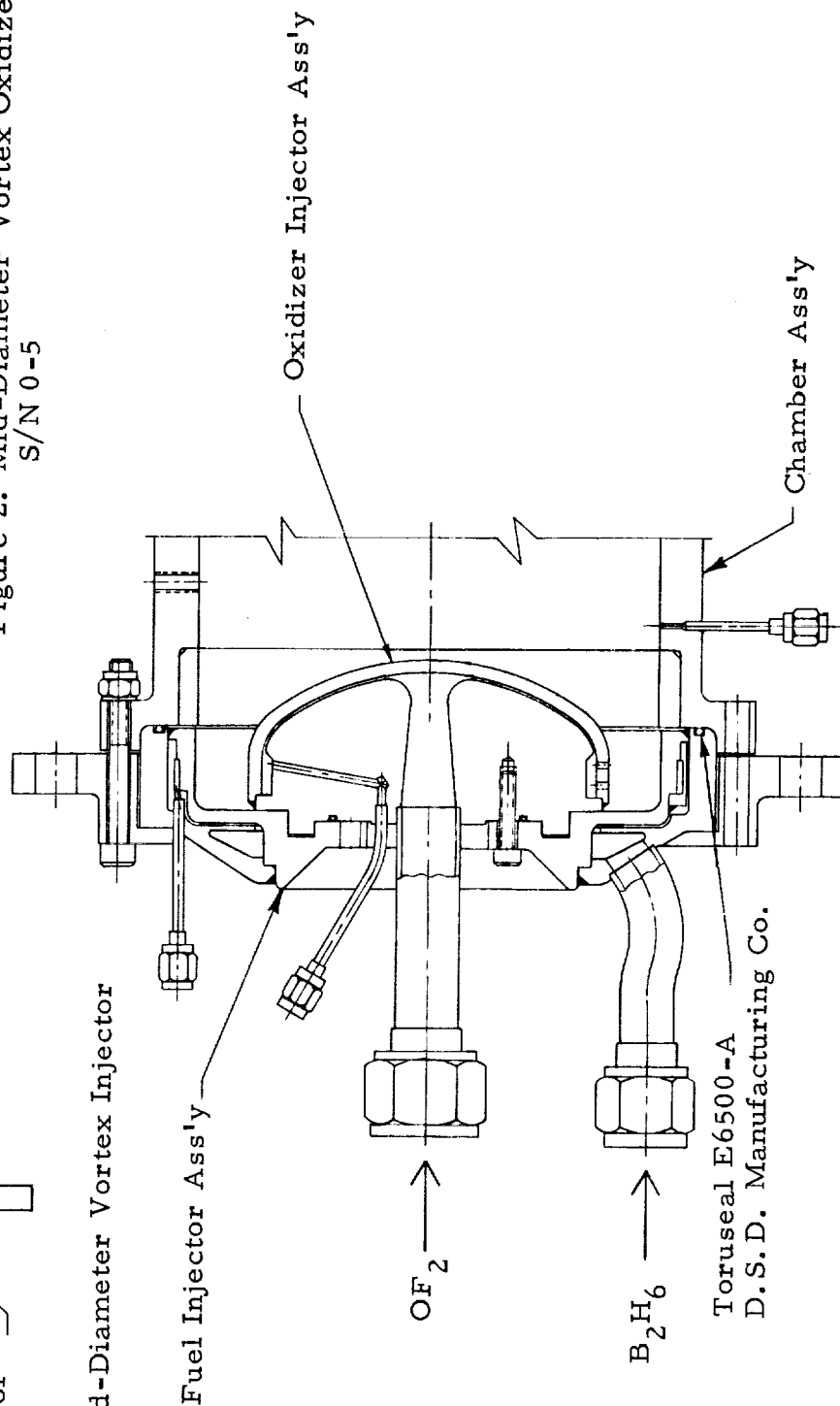


Figure 3. Full Diameter Vortex Injector Assembly



TABLE I  
PROPELLANT-COOLED INJECTOR CONFIGURATIONS

Injector Designation	Serial Number (1) Fuel-Oxidizer ( ) ( )	Configuration	Orifice Diameter (in) Fuel - Oxidizer	Combustion-Side Material Fuel - Oxidizer	Method of Ass'y	Run No.	Accumulated Run Time (sec)
X315445A, Mid-dia Vortex	1-1	Initial design Ref. Figure 1	.070	Cr-Cu	Fuel-mechanical seal, Teflon O- rings; Ox-B-70 braze	6CX1476	1.79 2.31 2.18 6.28
X315445B, Mid-dia Vortex	2-2	Same as S/N 1-1 except for orifice diameters	.078	Cr-Cu	"	6CX1479 6CX1480 6CX1481 6CX1485 RKO436-01 RKO436-03	3.28 3.20 3.23 2.20 2.13 2.10 16.14
53978, Mid-dia Vortex (Project 6028 type)	--	Similar to S/N 1-1 except no central ox flow divider; decreased ox orifice diameter	.070	Cr-Cu	"	6CX1482 6CX1483	3.25 2.00 5.25 (2)
X315445C Mid-dia Vortex	3-4	Same as 6028 type, except for central flow divider	.070	Cr-Cu	"	6CX1484	3.33
X315864 Mid-dia Vortex	3-5	Increased ox face thickness and increased OF <sub>2</sub> cooling velocity Ref. Figure 2	.070	Cr-Cu, .010" Rokide Z Coating on ox injector	"	6CX1486	2.00
X315445B, Mid-dia Vortex	1A-6	Similar to S/N 2-2 except improved OF <sub>2</sub> velocity	.078	Cr-Cu	"	6CX1487 6CX1488 6CX1489 6CX1490 RKO436-02	2.13 2.16 2.16 2.24 2.21 10.90 (3)
X315445B, Mid-dia Vortex	3-7	Ox injector same as S/N 0-6	.078	Cr-Cu	"	6CX1491	2.10 (4)
X315363, Full-dia Vortex	1-2	Ref. Figure 3	.070	"A" Nickel plus .010" Rokide A coating on ox injector	Welded	6CX1500	2.03 (5)

(1) Serialization code; 1-0 is fuel injector serial number and 0-1 is oxidizer injector serial number  
 (2) Total accumulated run time on 6028 type fuel injector, including previous program, is 45.6 sec  
 (3) Total accumulated run time on S/N 1A-0 fuel inj. is 17.2 sec  
 (4) Total accumulated run time on S/N 3-0 fuel inj. is 6.3 sec  
 (5) Injector available from prior program, total accumulated run time on fuel inj. is 10.2 sec.

Injector heat transfer and design analyses were performed utilizing the data obtained on previous  $\text{OF}_2/\text{B}_2\text{H}_6$  programs. The heat transfer analysis included radiation heat input from an ablative wall to the injector (since 2000 lb space thrust ablative chamber tests were planned) and the effects on coolant velocity due to thermal contraction and thermal-pressure stresses on the propellant cooling passage. Prior experimental heat transfer results based on measured  $\text{OF}_2$  injector and chamber bulk temperature rise data showed good agreement with analytical heat transfer predictions (Figure 4). The data spread noted for three of the tests with the 2000 lb thrust vortex injector is a result of operation over a wider mixture ratio range (3.0 - 4.0) and the fact that an insulation coating was utilized on this injector. The predicted injector heat flux levels are based on a mixture ratio of 3.0 at chamber pressure levels of 120 psia and 150 psia. These data were used as a basis for the injector cooling requirements.

Under nominal operating conditions (i. e.,  $P_c = 150$  psia,  $\text{O/F} = 3.0$  and a combustion efficiency of 98% c\*) the predicted convective heat flux to the injector is 3.29 Btu/sec-in.<sup>2</sup>; including a radiation heat flux from the ablative chamber wall of 0.22 Btu/sec/in.<sup>2</sup>. Since no experimental heat transfer upper limit of nucleate boiling data for  $\text{OF}_2$  or  $\text{B}_2\text{H}_6$  is available, calculations based on the method of Bernath (Reference 8) were employed to determine propellant cooling capability. To provide a theoretical heat transfer margin of safety of 25% under these conditions, the oxidizer injector cooling passage was designed to provide a nominal face coolant velocity of 67 ft/sec. The margin of 25% has been successfully employed in prior programs at Thiokol-RMD to account for non-uniformities in heat flux levels, inaccuracies in the propellant cooling correlations and operating transients. The effects of thermal and pressure stresses on cooling passage flow areas and hence cooling velocities were found to be negligible ( $< 1\%$ ). The method and data used for the injector heat transfer analysis is presented in detail in Appendix A.

(2) Heat Sink Designs - Several heat sink type vortex injector designs were evaluated during this program. These designs utilized heat sink oxidizer injectors in conjunction with propellant-cooled fuel injectors. The oxidizer injectors were fabricated from oxygen free high conductivity copper. The oxidizer injectors incorporated high response, foil type surface thermocouples (Figure 5) to obtain heat flux profiles across the combustion-side face of the injector.

The thermocouples recorded gas side wall temperature histories which are then utilized to calculate heat flux levels. Provisions were also made to incorporate similar probes with a thermocouple recessed .125" from the gas

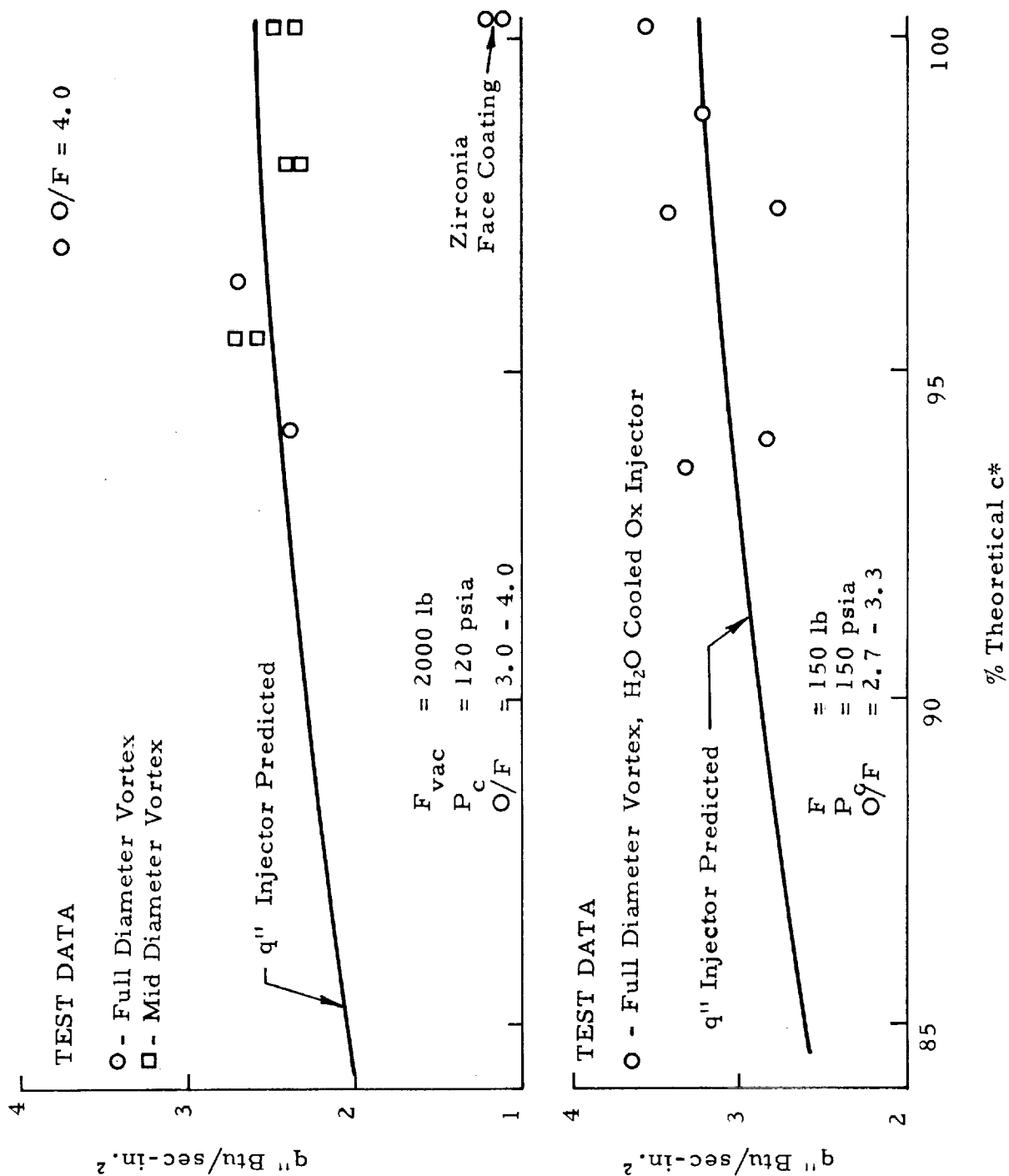


Figure 4. OF<sub>2</sub> Injector Heat Transfer Data

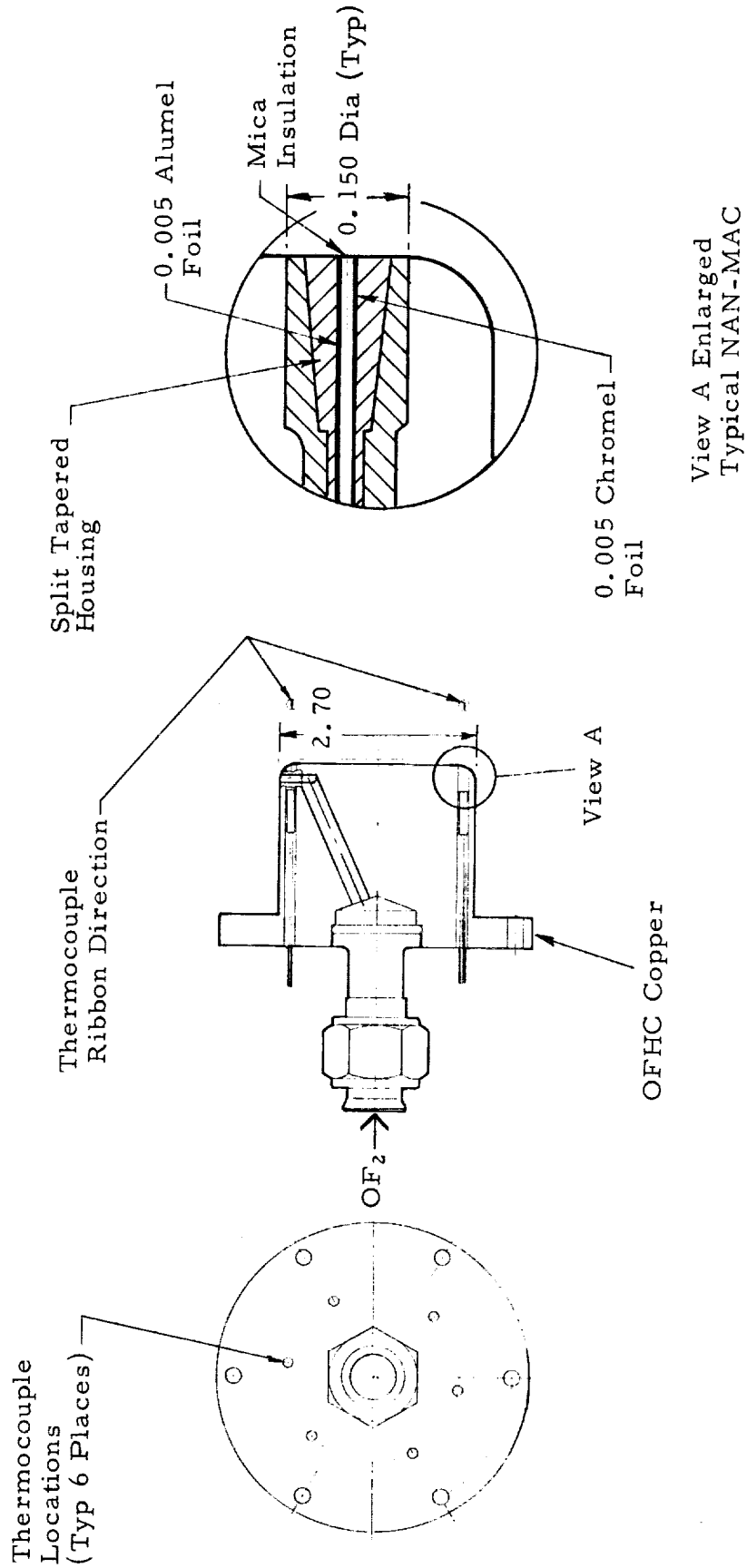


Figure 5. Typical Instrumented Heat Sink Oxidizer Injector Assembly

side face to obtain direct  $\Delta T$  measurements to provide additional heat flux data. The measured gas side wall temperature data is utilized to calculate heat flux levels by means of a computerized heat transfer program developed at Thiokol-RMD based on a method developed by P. R. Hill (Reference 9).

The initial heat sink design (Figure 6) retained the same injection pattern (two rows of fuel orifices and one row of oxidizer orifices) and gas side geometry as the propellant-cooled injectors to provide comparative heat transfer data. A backup design (Figure 7) utilizing an ablative cap over the face and between the orifices of the oxidizer injector was also evaluated. Chopped graphite phenolic cloth (Fiberite MX 4500) molded into discs was selected for the ablative caps. High response thermocouples were not used on this design due to the complexity of installing the units through the ablative cap. Severe erosion of the oxidizer injector was experienced with both of these designs.

Suitable durability for test purposes was obtained with the next two injector configurations evaluated. One design (Figure 8) utilized one row each of twenty fuel and oxidizer orifices and an increased fuel injector diameter which decreased the mass velocity (throughput) in the annular area between the fuel and oxidizer injector orifices from 1.3 to 1.0 lb/sec-in<sup>2</sup> (to correspond to the value utilized in the previous program at the 120 psia chamber pressure). The last design configuration evaluated, a modified mid-diameter vortex injector (Figure 9) utilized one row each of thirty fuel and oxidizer orifices and a further reduction in annular throughput to 0.44 lb/sec-in<sup>2</sup>.

A summary of the heat sink type injectors fabricated and tested during this program is presented in Table II.

#### b. Injector Fabrication

The propellant-cooled injectors utilized Teflon "O" rings to seal the fuel injector ring to the housing (Reference Figure 1). The oxidizer injector components were assembled by means of brazing to eliminate mechanical joints in contact with OF<sub>2</sub>. A sectioned oxidizer injector showing the braze joint and a photomicrograph showing the braze joint interface are presented in Figure 10. The braze employed is an Englehard Silvaloy B-70 alloy. This braze alloy provides excellent wetting of the chromium copper and permits braze temperatures (1825/1850F) which develop full heat treat strength in the chromium copper. The fuel and oxidizer injectors were mechanically assembled to form a complete unit and a metallic "O" ring was utilized to provide a combustion gas seal.

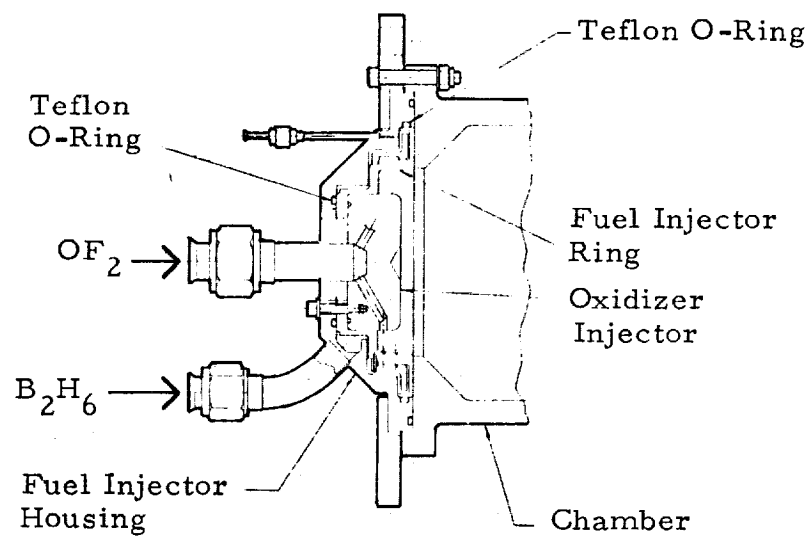


Figure 6. Two-on-One Heat Sink Type Injector

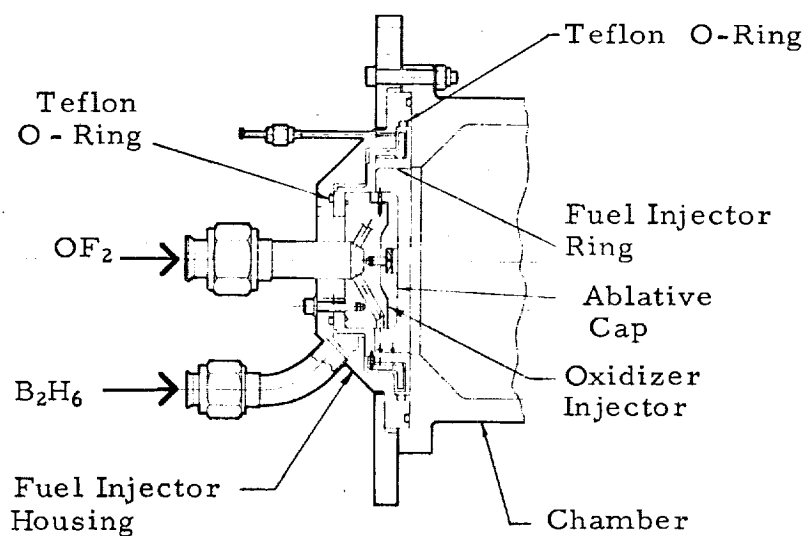


Figure 7. Two-on-One Heat Sink Type Injector Design Ablative Cap

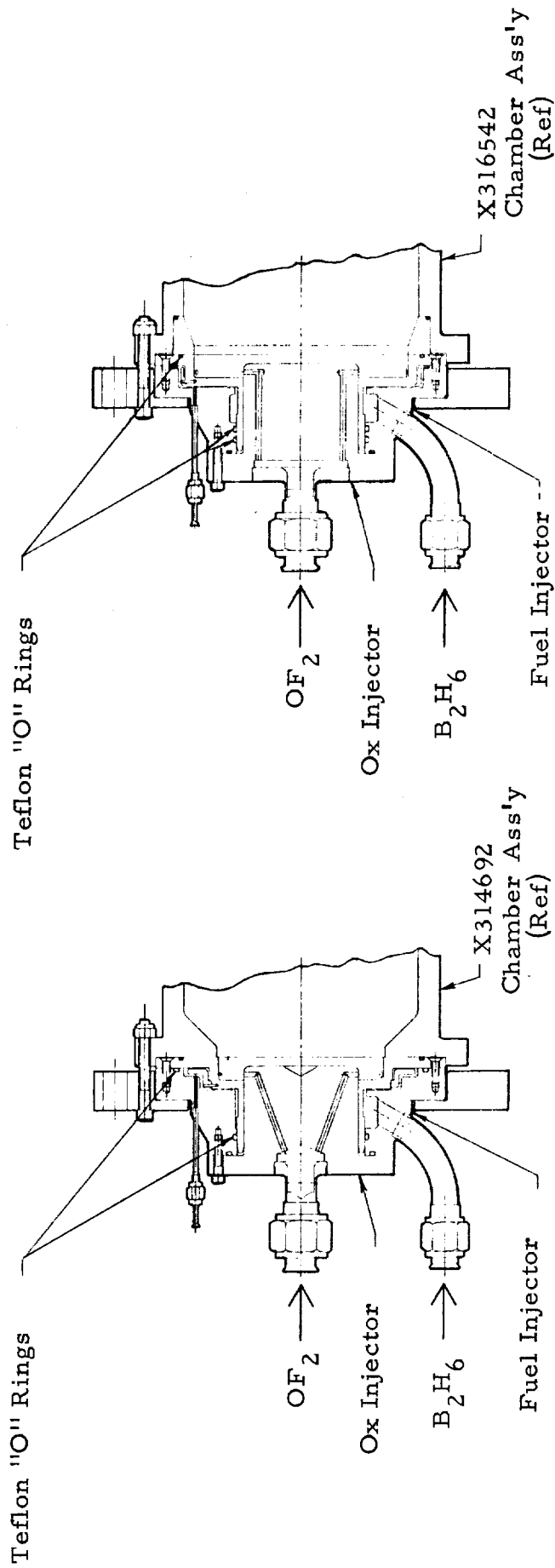


Figure 8. One-on-one Heat Sink Injector -  
20 Orifices

Figure 9. One-on-one Heat Sink Injector -  
30 Orifices

**TABLE II**  
**HEAT SINK TYPE INJECTOR CONFIGURATIONS**

Injector Designation	Serial Number Fuel - Oxidizer (1) (2)	No. Orifices Fuel - Oxidizer	Orifice Diameter (in) Fuel - Oxidizer	Combustion-Side Material Fuel - Oxidizer	Method of Assembly	Run No.	Accumulated Run Time (sec)
X316143, Mid-dia Vortex (Ref. Fig 6)	4-3 4-2	24 24	.136 .136	Gr-Cu Gr-Cu	Fuel-mechanical seal, Teflon O-rings Ox-solid	6CX1492 6CX1493	2.22 2.22
X316347, Mid-dia Vortex (Ref. Fig 7)	4-1	24	.136	Gr-Cu	OFHC copper with MX4500 graphite phenolic cap	6CX1494	2.18 (3)
X316357, Mid-dia Vortex (Ref Fig 8)	1-1	20	.100	Gr-Cu	OFHC copper	6CX1495 6CX1496 6CX1497 6CX1498 6CX1499 RKO436-04	1.60 1.59 2.10 2.10 1.23 2.15 10.77
X316357, Mid-dia Vortex (Ref Fig 8)	3-4	20	.100	Gr-Cu	OFHC copper plus 0.0005/0.001 nickel coating	6CX1501	2.05
X316357, Mid-dia Vortex (Ref Fig 8)	2-3	20	.100	Gr-Cu	"	6CX1503 6CX1504 RKO436-05 RKO436-06 RKO436-07 RKO436-08	2.05 2.13 2.14 2.16 2.15 2.15 12.78
X316357A, Mid-dia Vortex (Ref Fig 8) Increased ox L/D orifices	2-8	20	.100	Gr-Cu	Fuel-mechanical seal, Teflon coated metallic O-rings, ox-solid	6CX-1506 6CX-1507	2.17 2.14 4.31 (2)
X316540, Modified mid-dia vortex (Ref Fig 9)	4-5	30	.082	Gr-Cu	"	6CX1502 6CX1503 6CX1508 RKO436-09 RKO436-10	1.90 2.19 2.10 2.13 2.15 10.47

(1) Serialization Code

(2) All fuel injectors were propellant cooled

(3) Total accumulated run time on S/N 2-0 fuel injector is 17.09 sec

(4) Total accumulated run time on S/N 4-0 fuel injector is 6.72 sec

(5) RKO designation under run No. column indicates AEDC altitude tests.



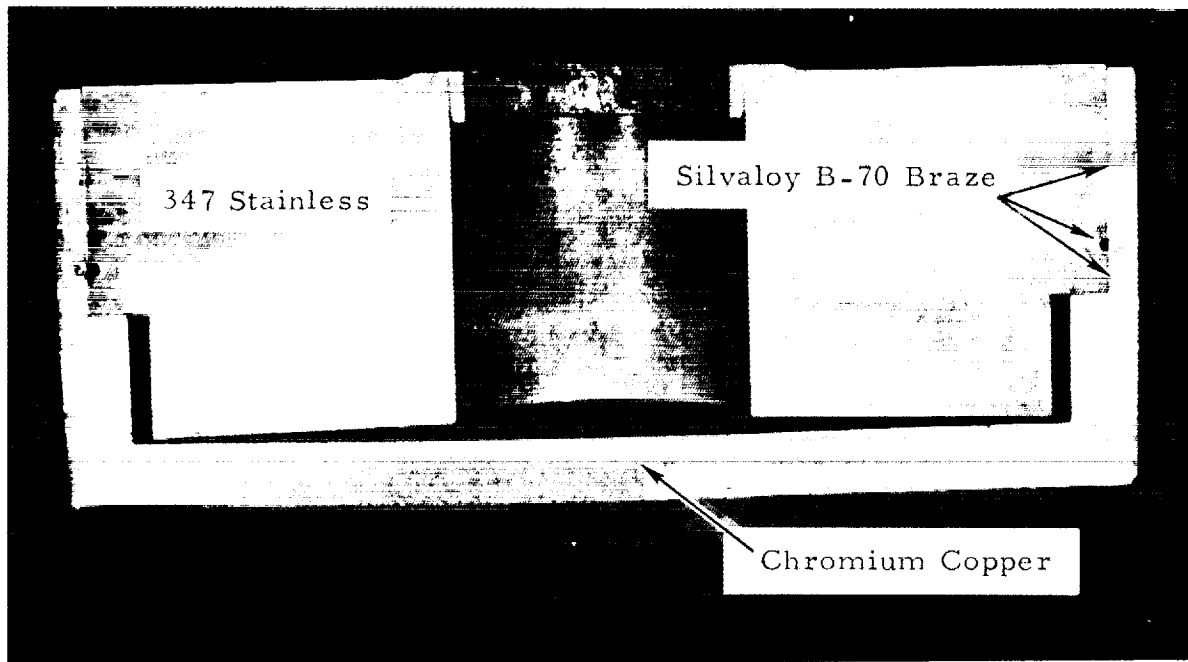


Figure 10-A

1.9 (Approx.)

H64169-1

Photomicrograph of a cross-section through a sample oxidizer injector. The braze joint between the chromium-copper cup and the 347 stainless steel plug can be seen along with the braze wire groove.

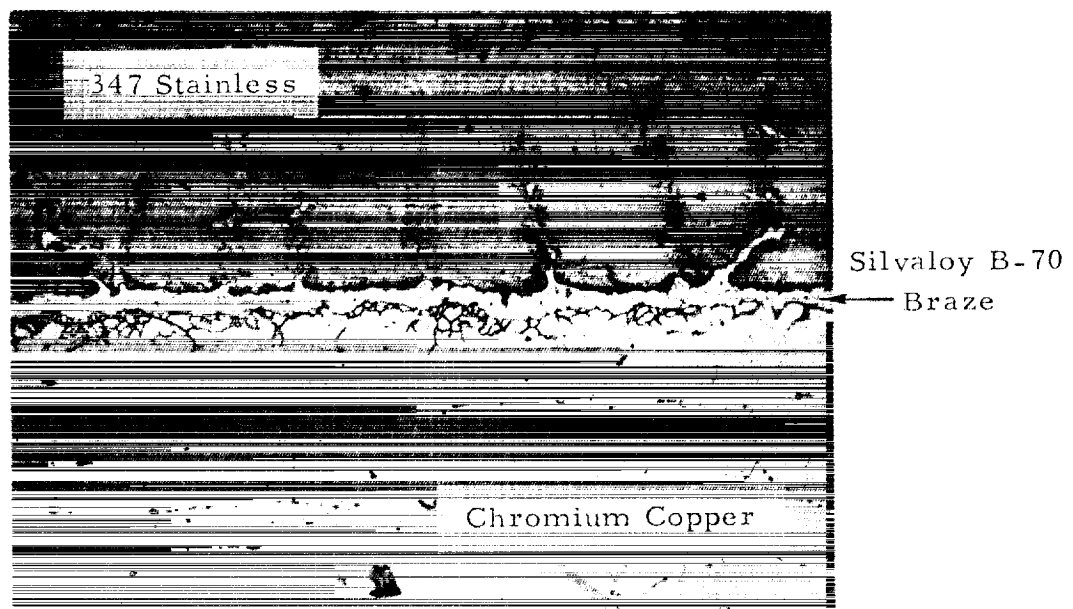


Figure 10-B

500X

H64169-2

Photomicrograph showing braze joint interface (Silvaloy B-70 Alloy) between chromium-copper and 347 stainless

Figure 10. Oxidizer Injector Braze Photographs

Each injector was subjected to a cold cycle-proof pressure test, water flow bench test and passivation in accordance with Thiokol-RMD established procedures and specifications prior to hot test firing.

Cold cycle-proof pressure tests were accomplished by flowing liquid nitrogen through the injector until the injector was chilled to -300F and proof pressure testing the injector at 250 psia. Three cold cycle-proof pressure tests were conducted to assure structural adequacy of the injector under operating pressures and temperature conditions experienced during an engine start.

Water flow bench tests were conducted with each injector to ensure that flow pressure drop characteristics were within design limits. Photographic monitoring of the injector flow was also accomplished in order to determine uniformity of orifice spray patterns.

All injector components were cleaned and fully passivated at the test facility. Passivation was accomplished by admitting fluorine gas through the oxidizer injector inlet to a pressure level of 15 psig and held for 5 minutes. The fluorine pressure was then increased in 50 psig increments up to 265 psig. The fluorine pressure was maintained for 5 minutes in the injector at each incremental level and for one hour at the maximum pressure level. No difficulty was experienced during the passivation cycle with any of the injectors in this program. The injector assembly was sealed in clean polyethylene bags until ready for use.

#### c. Combustion Chamber Design and Fabrication

Two types of chamber assemblies were designed and fabricated for the injector test program; (1) a heat-sink chromium copper chamber and nozzle assembly, and (2) a water-cooled chamber and nozzle assembly. The chamber assemblies are designed to operate at a chamber pressure of 150 psia at sea level. Design criteria are:  $L^* = 30$ ,  $A_c / A_t = 2.75$ ,  $A_t = 8.65 \text{ in}^2$ ,  $\alpha = 15^\circ$  and  $\xi = 2.56$ . Since two second duration tests were sufficient to obtain sea level and altitude performance data, the water-cooled chamber assembly was not required during this program.

The uncooled heat sink chamber and nozzle assembly which was fabricated from chromium-copper is shown in Figure 11. Chromium copper was selected because of its high thermal conductivity (80 - 90% of pure copper), high specific heat and high yield strength at elevated temperatures. The nozzle area ratio ( $\xi = 2.56$ ) was sized to provide optimum sea level expansion (i.e. 150 psia to 14.4 psia). The combustion chamber wall thickness was sufficient to permit 2 - 3 seconds operation and keep the combustion side wall temperatures below 1500F.

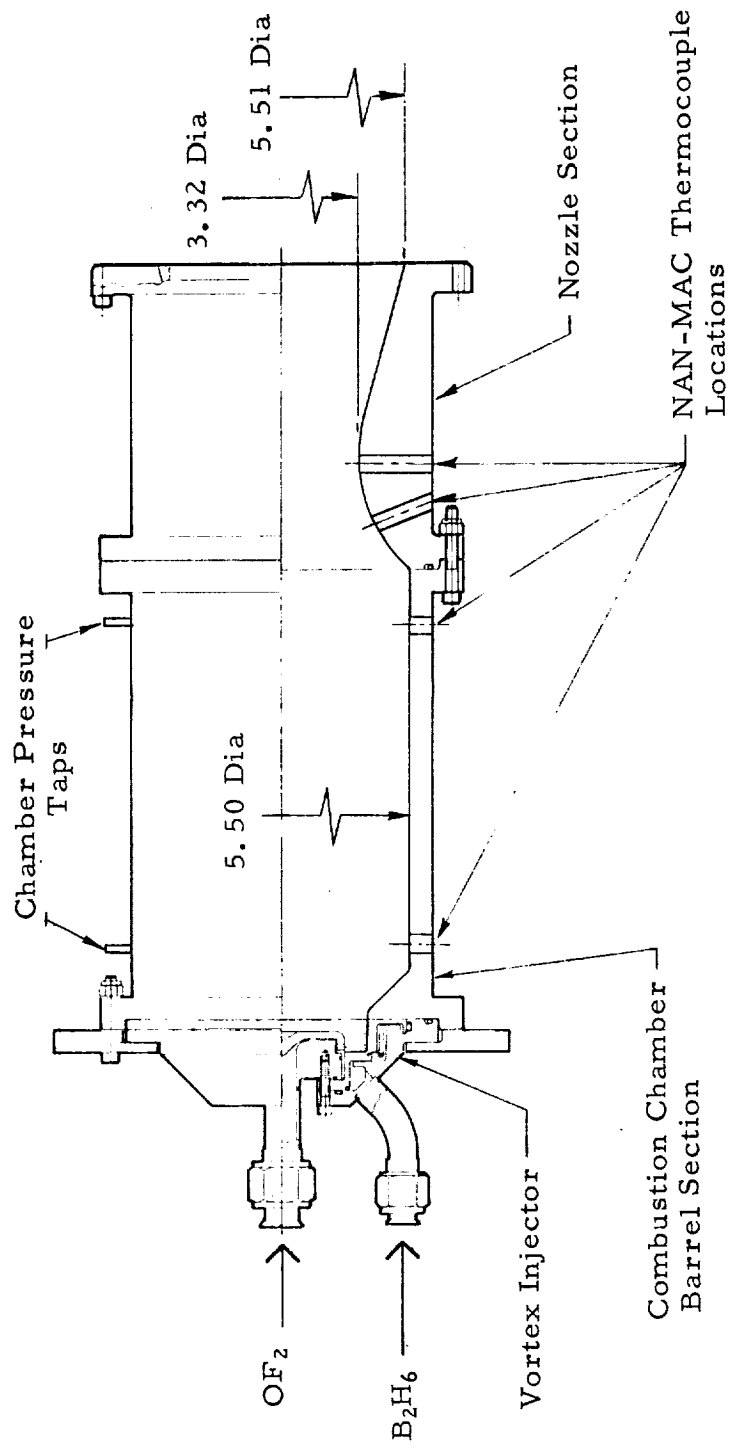


Figure 11. Uncooled Heat Sink Thrust Chamber Assembly X315863A

Two chamber pressure taps were employed; one near the injector and the other downstream, near the nozzle entrance. Thermocouple ports were also included in both the combustion chamber section and nozzle throat for installation of high response, foil-type surface thermocouples which were used as transient temperature transducers to determine heat flux levels. These units, which have been used at Thiokol-RMD on other programs, consist of a plug of the base material (chromium-copper) into which two, thermally-insulated, foil strips of thermocouple materials are imbedded. The plug is inserted into the chamber or nozzle so that the end is flush with the gas-side wall. The end of the plug is then abraded, thus forming the thermocouple junction.

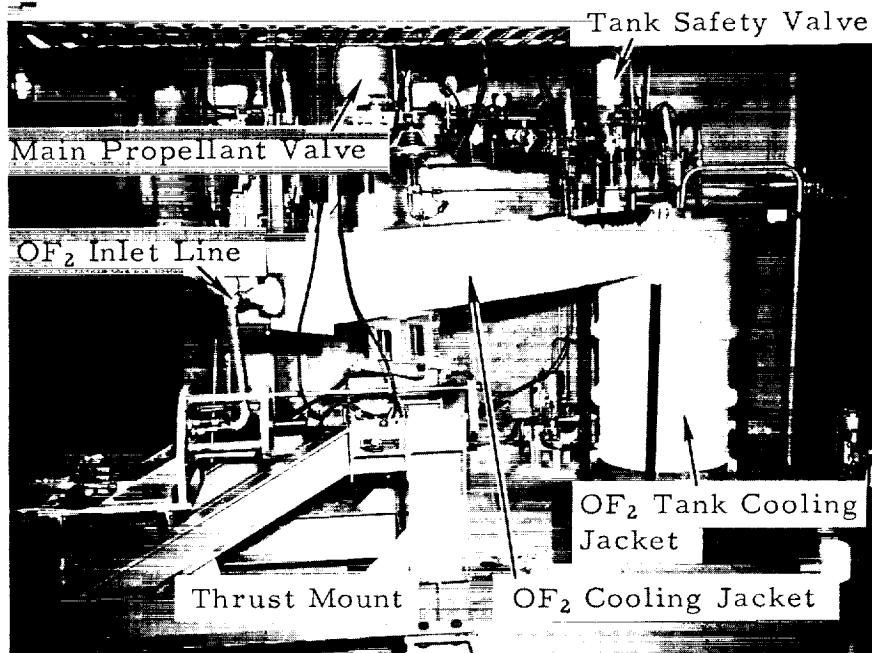
#### 4. Test Facility

All sea level test firings were conducted in Test Stand 6C, Thiokol-RMD's fluorinated oxidizer propellant rocket facility. The test facility installation is shown in Figure 12. Liquid oxygen difluoride and liquid diborane supplied from test facility tankage was used for all tests. The entire fuel and oxidizer propellant feed system from the run tanks to the main propellant valves were immersed in a cooling jacket to maintain the propellants in the liquid state. A dry ice/trichlorethylene mixture maintained the diborane temperature at  $100 \pm 10^\circ\text{F}$ . Liquid nitrogen was utilized in the oxidizer jacket to maintain an  $\text{OF}_2$  temperature of  $310 \pm 10^\circ\text{F}$ .

The liquid diborane was transferred from the shipping container directly to a 15 gallon run tank. Oxygen difluoride supplied from the vendor in the gaseous state was transferred from the shipping containers into a 20-gallon oxidizer run tank and then cooled down and condensed to the liquid state by the liquid nitrogen cooling jacket. Helium gas was employed to pressurize the propellant run tanks. Following a test firing, the liquid diborane was maintained in the run tank. The liquid nitrogen trough was drained and hot water was circulated around the  $\text{OF}_2$  propellant feed system gasifying the  $\text{OF}_2$ . The gaseous  $\text{OF}_2$  was then transferred back to storage tanks.

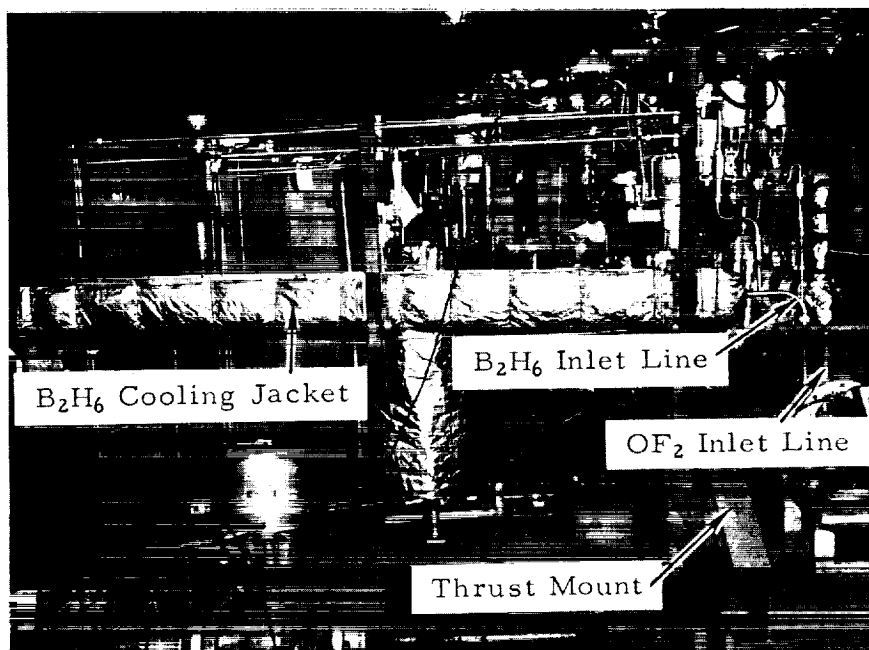
Test firings were conducted by automatic sequencing of the propellant control system and an automatic run timer. Injector precool using liquid nitrogen was utilized prior to each test to chill the hardware to propellant bulk temperature levels to minimize gaseous propellant starts.

The facility has data acquisition capability for 80 instrumentation channels. Recorded data included pressure, temperature, thrust and flow. Cavitating venturis were utilized to control and measure propellant flow. The data recording system consisted of a 60-channel system with high speed recording oscillographs, strip chart recorders and a 7-channel high speed tape recorder for high frequency measurements.



6028-20

Oxidizer Side



6028-230

Fuel Side

Figure 12.  $\text{OF}_2/\text{B}_2\text{H}_6$  Test Facility

5. Propellant-Cooled and Heat Sink Injector Performance and Heat Transfer Tests

a. Test Description

Thirty-three injector sea level performance tests, each of 2 to 3 seconds duration, were conducted with the 2000-pound space thrust uncooled hardware to evaluate injector performance and to obtain injector chamber heat transfer data. The uncooled chamber is shown mounted in the test facility in Figure 13. Seventeen tests were performed with propellant-cooled injectors and sixteen were performed with the heat sink type injectors. The nominal chamber pressure level was 150 psia except for two tests where the nominal level was 120 psia. Tests were conducted over a mixture ratio range of 2.65 to 3.34. The following sections describe the injector-combustion chamber performance and heat transfer test results obtained during this program.

b. Data Reduction

Performance data was calculated at 0.050 second intervals. These data samplings were used in determining average performance and heat transfer results over the stable portion of the test. For the propellant-cooled injectors, the data was averaged over a 1.0 to 1.5 second period. The heat-sink injector data was averaged over a 0.20 to 0.65 second period.

The injector performance is based on characteristic velocity and sea level thrust coefficient and specific impulse. The theoretical characteristic velocity, specific impulse and thrust coefficient, is based on shifting equilibrium. The experimental specific impulse and thrust coefficient data are compared to theoretical values which are based on maximum achievable sea level performance for the nozzle geometry (i. e.  $\xi$  and  $\mathcal{L}$ ) and the recorded test conditions (i. e.  $P_c$ ,  $F$ ,  $O/F$  and  $\dot{w}_t$ ).

The following is a list of symbols and subscripts utilized in the performance and heat transfer calculations.

6028-122

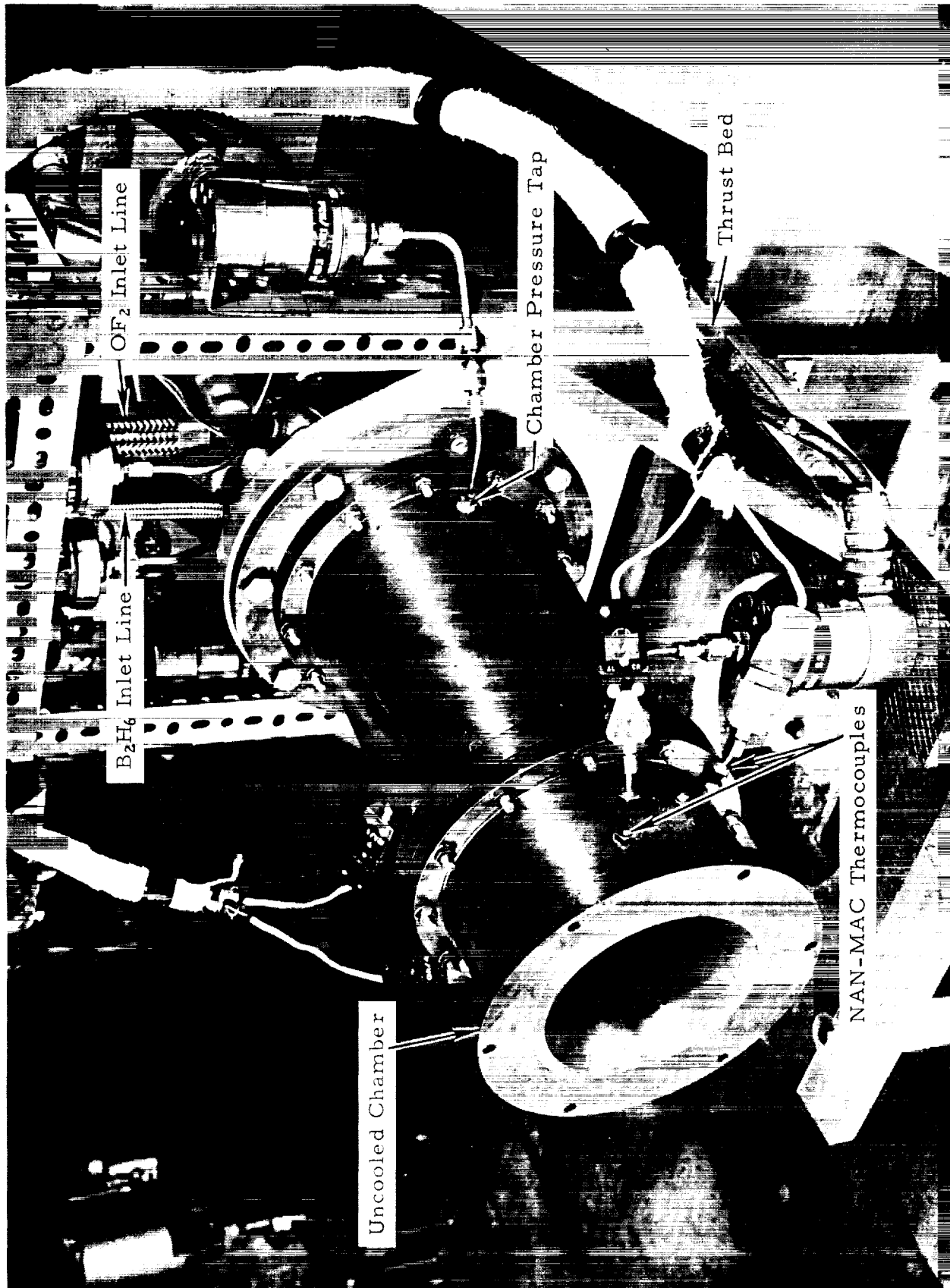


Figure 13. Uncooled Thrust Chamber Installed in Test Facility

$A_e$	Nozzle Exit area, in <sup>2</sup>
$A_t$	Throat area, in <sup>2</sup>
$A_s$	Oxidizer Injector Surface Area, in <sup>2</sup>
$C_F$	Sea Level Thrust Coefficient
$C_P$	Constant pressure specific heat, Btu/lb <sub>m</sub> -°R
$C_{map}$	Maximum Achievable Sea Level Thrust Coefficient
$c^*$	Characteristic Exhaust Velocity, ft/sec
$\xi_e$	Nozzle Exit to Throat Area Ratio, $A_e/A_t$
$F$	Thrust, lb
$G$	Vortex Injector Annulus Mass Velocity, lb <sub>m</sub> /sec-in <sup>2</sup>
$g_o$	Gravitational Constant - 32.174 lb <sub>m</sub> -ft/lb <sub>f</sub> -sec <sup>2</sup>
$I_{sl}$	Sea Level Specific Impulse, lb <sub>f</sub> -sec/lb <sub>m</sub>
$I_{map}$	Maximum achievable sea level Specific Impulse at $P_a, P_{ch}$ , O/F, lb <sub>f</sub> -sec/lb <sub>m</sub>
$q''$	Heat flux, Btu/sec-in <sup>2</sup>
$P_a$	Ambient pressure, psia
$P_{ch}$	Chamber Pressure, psia
O/F	Mixture ratio, (oxidizer/fuel)
$T$	Temperature, °F
$\dot{w}$	Flow rate, lb <sub>m</sub> /sec
$\eta$	Efficiency
$\Delta$	Indicates difference



' Indicates theoretical value

$\lambda$  Nozzle Divergence Loss

$C_d \cdot C_v$  Nozzle Friction Loss

Subscripts:

vac Value at  $P_a = 0$

(map) Corrected for nozzle friction and divergence losses ( $\lambda, C_d \cdot C_v$ )

o Oxidizer

f Fuel

Static chamber pressure measurements were taken at the injector end of the chamber and at the entrance to the nozzle. These chamber pressure measurements were consistently in close agreement with the theoretical pressure profile for this chamber geometry (i. e., based on Mach Number for  $A_c/A_t = 2.75$ ). The nozzle inlet total pressure,  $P_T$ , when calculated by correcting the measured combustion chamber pressure data obtained from the static pressure tap at the nozzle entrance for gas velocity was found to be in close agreement with the static pressure measured at the injector end. Consequently, the chamber pressure measured at the injector end of the combustion chamber was used to calculate experimental  $c^*$  and  $C_F$  for the sea level and altitude tests.

The thrust coefficient was calculated from test data as follows:

$$C_F = \frac{F}{A_t P_c} \quad (1)$$

The experimental thrust coefficient was compared to a maximum achievable value calculated as follows:

$$C_{F \text{ vac}} = \frac{I_{sp} g}{c^*} = (C_F(s_1)) + \frac{P_a \xi_e}{P_c} \quad (2)$$

where  $I_{sp}$  and  $c^*$  are based on thermochemical calculations for  $\xi_e \approx 2.56$  for

shifting equilibrium conditions and the range of mixture ratios and chamber pressures of interest. At the nominal conditions of  $P_c = 150$  psia and  $O/F = 3.0$  the theoretical value of  $C_{F \text{ vac}}$  is 1.536.

For the  $OF_2 / B_2H_6$  combination in the range of mixture ratios and chamber pressures of interest, the use of constant value of 1.536 for theoretical  $C_{F \text{ vac}}$  introduces negligible error. Thus, using  $P_a = 14.40$  psia, theoretical sea level thrust coefficients were calculated as follows:

$$C_F(s_1) = C_F(\text{vac}) - \frac{P_a \xi_e}{P_c} = 1.536 - \frac{36.87}{P_c} \quad (3)$$

The value of  $C_F(s_1)$  was corrected for nozzle friction and divergence losses through use of a calculated nozzle thrust coefficient efficiency,  $\eta_{CF}$ , to obtain a maximum achievable predicted sea level thrust coefficient ( $C_F \text{ map}$ ).

$$C_F(\text{map}) = \eta_{CF} C_F(1.536) - \frac{36.87}{P_c} \quad (4)$$

For nozzles with a 15 degree half angle and area ratio of 2.56,  $\eta_{CF}$  has been calculated to be 0.963. These calculations were based on nozzle divergence and wall friction losses. Based on past experience with the test nozzle geometry utilized in this program, a throat discharge and wall friction efficiency of 0.98 was employed.

$$C_F(\text{map}) = 1.479 - \frac{36.87}{P_c} \quad (5)$$

The values obtained by use of equation (5) for the measured test chamber pressure should correspond within instrumentation accuracy, to the calculated  $C_F$  values obtained by use of equation (1), hence comparison of  $C_F \text{ test}$  and  $C_F(\text{map})$  provides a check on the consistency of the thrust and chamber pressure measurements.

Characteristic exhaust velocity using an  $A_t = 8.65 \text{ in.}^2$ ; was calculated as follows:

$$c^* = \frac{A_t g_o P_{ch}}{w_p} = \frac{278.31 P_{ch}}{w_p} \quad (6)$$

The specific impulse was calculated from test data as follows:

$$I_{sp} = \frac{F}{P_{ch} A_t} \quad (7)$$

The experimental sea level specific impulse was compared to maximum achievable predicted values as follows:

$$I_{sp} (map) = \frac{c^* C_F (map)}{g} \quad (8)$$

thus the values obtained by use of equation 8 include nozzle friction and divergence losses and represents the maximum impulse obtainable under the test operating conditions.

Heat loss to the chamber walls were calculated from the gas side wall temperature measurements. The heat loss was found to be negligible ( $< 1\%$ ) and no heat loss corrections were made to the performance data.

The following efficiencies were then calculated:

$$\eta_{c^*} = \frac{c^*_{test}}{c^*}$$

$$\eta_{C_F} = \frac{C_{F test}}{C_F (map)}$$

$$\eta_{I_{sp}} = \frac{I_{sp test}}{I_{sp} (map)}$$

#### c. Test Performance

Table III presents the measured and calculated test performance data obtained with the propellant-cooled injectors. Table IV presents the measured and calculated test performance data obtained with the heat sink injectors.

The results of these tests have demonstrated that the  $OF_2 / B_2H_6$  propellant combination can deliver high sea level specific impulse. Allowing for nozzle throat discharge and friction losses (2%) and nozzle exit divergence losses (1.7%) of the test nozzle employed, values above 90% of predicted shifting equilibrium impulse

TABLE III  
MID-DIAMETER VORTEX PROPELLANT COOLED INJECTOR --- TEST DATA SUMMARY

Run No.	Injector	P <sub>ch</sub> (psia)	Thrust (lbs)	w <sub>t</sub> (lb/sec)	Mixture Ratio	Duration(1) (sec)	c* fps	% c*	C <sub>F</sub> (3) Test	% C <sub>F</sub> MAP	S. L. (3) I <sub>sp</sub> (sec)	% I <sub>sp</sub> MAP	Remarks
6 CX 1476	X315455, S/N 1-1	139.4	1452	6.202	2.87	1.79	6236	90.0	1.210	98.7	234.5	89.1	Good run - Hardware in excellent condition.
6 CX 1477	(Same as above)	134.9	1402	6.16	2.87	2.31	6070	87.5	1.210	99.3	227.5	87.0	Good run - Hardware in excellent condition.
6 CX 1478	(Same as above)	139.4	----	6.16	2.98	2.18	6260	90.5	----	----	----	----	Thrust load cell damaged in hard start. Oxidizer injector face and corner failure at 1.93 sec.
6 CX 1479	X315445B, S/N 2-2	135.4	1409	6.186	3.01	3.28	6080	87.8	1.207	99.0	228.0	87.0	Good run - Hardware in excellent condition.
6 CX 1480	(Same as above)	144.4	1519	6.63	2.72	3.20	6040	87.1	1.222	98.7	229.0	86.2	Good run - Hardware in excellent condition.
6 CX 1481	(Same as above)	139.8	1470	6.593	2.99	3.23	5920	85.5	1.214	99.0	223.5	84.5	Good run - Hardware in excellent condition.
6 CX 1482	53978-6028 Type	113.8	1050	4.90	2.95	3.25	6440	93.0	1.075(4)	103.3	214.5(4)	95.5	Good run - Hardware in excellent condition.
6 CX 1483	(Same as above)	157.0	1672	6.632	3.12	2.00	6550	94.6	1.240	98.6	252.5	93.2	Oxidizer injector face failure at 1.96 sec.
6 CX 1484	X315455C, S/N 3-4	120.0	1190	5.249	2.95	3.33	6350	91.7	1.152	97.5	227	89.0	Oxidizer injector face and corner failure at 3.0 sec.
6 CX 1485	X315455B, S/N 2-2	145.4	1568	6.684	3.22	2.20	6040	87.0	1.252	101.3	234.5	88.3	Good run - Hardware in excellent condition.
6 CX 1486	X315455B, S/N 3-5	154.4	1670	6.64	2.86	2.00	6460	92.8	1.251	99.8	252.0	93.4	Oxidizer injector corner failure at 1.67 sec.
6 CX 1487	X315445B, S/N 1A-6	156.3	1701	6.57	2.96	2.13	6570	94.1	1.267	100.9	259.0	95.6	Good run - Hardware in excellent condition.
6 CX 1488	(Same as above)	156.9	1700	6.688	2.70	2.16	6490	93.6	1.268	101.0	254.5	94.0	Good run - Hardware in excellent condition.
6 CX 1489	(Same as above)	157.4	1680	6.54	3.34	2.16	6650	95.9	1.242	98.9	256.5	94.7	Good run - Hardware in excellent condition.
6 CX 1490	(Same as above)	158(2)	1710	6.69	3.05	2.24	6540	94.0	1.260	100.2	256.0	94.5	Good run - Hardware in excellent condition.
6 CX 1491	X315455B, S/N 3-7	163.6	1760	6.93	3.08	2.10	6495	93.4	1.260	99.5	254.0	93.0	Oxidizer injector corner failure at 1.4 sec.
6 CX 1500	X315363, S/N 1-2(5) Full-Diameter Vortex	152.9	1632	6.28	2.65	2.03	6701	96.6	1.248	99.7	261.1	96.9	Oxidizer injector failure at 1.54 sec.

- (1) From Light-off  
(2) Tap Plugged: P<sub>ch</sub> from P<sub>ch</sub> vs Thrust Curve  
(3) Sea Level: 15° Half Angle Nozzle,  $\epsilon = 2.56$   
(4) Project 6028 Contoured Nozzle,  $\epsilon = 2.17$   
(5) Injector Available From Prior Program -  
Designed for Chamber Pressure of 120 psia

TABLE IV  
HEAT SINK MID-DIAMETER VORTEX INJECTOR --- TEST DATA SUMMARY

Run No.	Injector	P <sub>ch</sub> (psia)	Thrust (lbs)	W <sub>t</sub> (lb/sec)	Mixture Ratio	Duration(1) (sec)	c* (1) fps	% c*	CF(2) Test	% CF MAP	S. L. (2) I <sub>sp</sub> (sec)	% I <sub>sp</sub> MAP	Remarks
6 CX 1492	X316143, S/N 4-3	151.4	1560	6.445	3.07	2.22	6480	93.2	1.205	96.5	242.0	90.0	Oxidizer Injector erosion on corner in line with orifices.
6 CX 1493	X316143, S/N 4-2	154.4	1620	6.468	2.998	2.22	6570	94.5	1.23	98.0	250.5	92.6	Oxidizer Injector erosion on corner in line with orifices.
6 CX 1494	X316347, S/N 4-1	153.3	1612	6.35	2.92	2.176	6641	95.7	1.231	98.5	253.9	94.2	Oxidizer Injector erosion on corner in line with orifices. Loss of ablative cap during run.
6 CX 1495	X316357, S/N 1-1	165.8 (3)	1790 (3)	6.36	2.95	1.603	----	----	----	----	----	----	Run terminated due to fuel leak. Minor erosion on corner of 3 orifices at top of injector
6 CX 1496	(Same as above half of CX 1495 coated with .0005 Ni)	146.6	1509	6.34	2.93	1.59	6350	91.5	1.206	97.3	238.0	89.1	Good run - Hardware in good condition. No further erosion of oxidizer.
6 CX 1497	(Same as above)	154.9	1651	6.28	2.90	2.10	6776	97.5	1.249	99.7	262.9	97.3	Good run - Hardware in good condition.
6 CX 1498	(Same as above)	157.0	1656	6.34	2.66	2.10	6858	98.8	1.225	97.6	261.2	96.0	Good run - Hardware in good condition.
6 CX 1499	(Same as above)	159.6 (3)	1737 (3)	6.45	3.08	1.23	----	----	----	----	----	----	Run terminated due to fuel leak in test stand piping - Hardware in good condition.
6 CX 1501	X316357, S/N 3-4	151.6	1620	6.46	2.89	2.05	6470	93.5	1.250	98.9	251.0	92.5	Oxidizer Injector erosion on corner in line with orifices.
6 CX 1502	X316540, S/N 4-5	(4)	(4)	(4)	(4)	1.90	----	----	----	----	----	----	Run aborted at 1.9 seconds. Engine pulsing. Hardware in excellent condition.
6 CX 1503	X316357, S/N 2-3	157.8	1680	6.42	2.74	2.05	6767	97.5	1.245	98.8	262.0	96.5	Good run. Minor erosion of top corner of oxidizer.
6 CX 1504	(Same as above)	158.6	1710	6.54	3.11	2.13	6700	96.1	1.260	99.7	262.0	96.5	Good run. Erosion continued at top of oxidizer injector.
6 CX 1505	X316540, S/N 4-5	144 (4)	1200 (4)	6.25	3.00	2.19	----	----	----	----	----	----	P <sub>ch</sub> , F oscillations. Hardware in excellent condition.
6 CX 1506	X316357, S/N 7-8	154.4	1648	6.40	3.02	2.17	6695	96.5	1.242	99.0	257.0	95.2	Good run - Hardware in excellent condition.
6 CX 1507	(Same as above)	157.2	1668	6.42	2.69	2.14	6790	97.9	1.232	98.5	259.5	95.9	Oxidizer Injector erosion on corner in line with orifices.
6 CX 1508	X316540, S/N 4-5	151.4 (4)	1608 (4)	6.35	3.00	2.10	----	----	----	----	----	----	P <sub>ch</sub> , F oscillations. Hardware in excellent condition.

- (1) From Ignition  
(2) Sea Level  $\epsilon = 2.56$   
(3) Maximum P<sub>ch</sub> & Thrust at Shutdown - P<sub>ch</sub> Did Not Stabilize  
(4) P<sub>ch</sub> & Thrust Oscillations Throughout Run

were generally obtained. Good agreement between the measured test thrust coefficient and the predicted maximum achievable thrust coefficient was consistently obtained. Thus, a high level of confidence in the validity of the performance data was established.

(1) Propellant-Cooled Injectors - The first two injectors tested (S/N 1-1 and S/N 2-2) gave lower performance levels (4-7% c\*) than those obtained with similar injectors tested during the prior program. The lower c\* levels exhibited by these two injectors may have been due to a non-uniform oxidizer injector spray pattern observed during water flow calibration checks (described in detail in Section IV.5.1). Several orifice sprays exhibited an unsymmetrical conical pattern. Since the propellant-cooled injectors incorporated only 12 oxidizer orifices, it is possible that poor mixing even for one orifice could significantly affect performance. All of the subsequent propellant-cooled injectors exhibited more uniform spray patterns and yielded higher performance levels (92-96% c\*) than the first two injectors tested in this program.

The third injector tested was a configuration evaluated in the previous program (RMD Project 6028). A test conducted at a design chamber pressure of 120 psia for this injector confirmed the performance (93% c\*) previously obtained. A second test with this injector at a chamber pressure of 150 psia again confirmed attainable performance (94.6% c\*) with this type injector. Burnout of the oxidizer injector center face occurred on the second test. Since this injector did not incorporate a control flow divider, inadequate cooling was available at the 150 psia pressure level. The tests, however, confirmed attainable performance with this type injector and tended to substantiate that low performance obtained with the first two injectors resulted from non-uniform spray patterns observed from the oxidizer injector orifices during water flow calibration tests.

The fourth and fifth injectors, (S/N 3-4 and 3-5) injectors, tested incorporated modifications (outlined in Table I) intended to improve oxidizer injector durability. Although initial tests resulted in oxidizer injector erosion, high performance (92-93% c\*) was obtained with each injector.

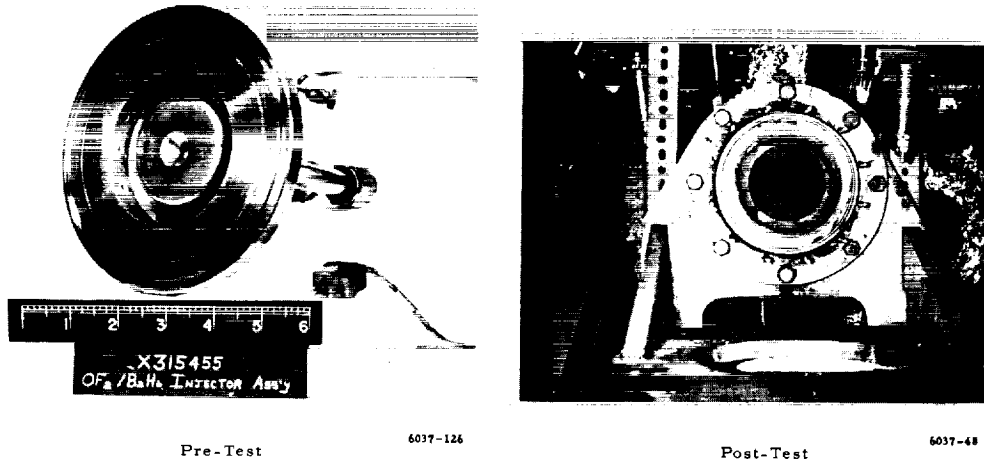
Four tests were conducted with the S/N 1A-6 injector. No hardware damage was experienced. The S/N 3-7 injector utilized an oxidizer injector fabricated to the same dimensions as the S/N 0-6 injector. The initial test with the S/N 3-7 injector gave high performance (93.4% c\*). However, erosion of the oxidizer injector was experienced.

The last propellant-cooled injector tested was a full-diameter vortex injector (Reference Figure 3) which, although never tested, was available from the previous program. Although the injector was designed to operate at a chamber pressure of 120 psia and although it exhibited high oxidizer cooling passage  $\Delta P$  during water flow checks, it was decided to test the injector at a chamber pressure of 150 psia. Since a similar full-diameter vortex injector previously tested gave high performance (94-100%  $c^*$ ), it was planned to utilize this injector as a backup to the S/N 2-2 and 1A-6 injectors for altitude testing at AEDC. The initial test with the full-diameter injector gave high performance (97%  $c^*$ ) but oxidizer injector erosion was experienced. The failure was probably due to cooling flow maldistribution as deduced from the abnormally high pressure drop noted during the water flow checks.

Four tests each were conducted with the S/N 2-2 and S/N 1A-6 injectors. The performance data for these injectors are presented on Figure 14. These injectors were subsequently tested at AEDC. The performance with the S/N 2-2 injector was 85.5% to 87.8% of theoretical  $c^*$ . The performance with the S/N 1A-6 injector (93.6% to 95.9%  $c^*$ ) corroborated performance obtained with this type injector in the prior program ( $c^*$  ave = 94.4%). Both injectors were of the same design. The variation in performance may have been due to the non-uniform oxidizer injector spray patterns discussed in the preceding paragraph. Both injectors were in excellent condition after each series of tests. Figure 14 shows pre-test and post-test photographs for the S/N 1A-6 injector.

The performance data for nine tests with the remaining propellant-cooled injectors are presented on Figure 15. Although durability problems were experienced with the oxidizer injectors in these tests, the performance data presented are taken prior to the failure and are considered valid. The performance levels for these injectors was 87% to 96%  $c^*$ . Also shown on Figure 16 are pre-test and post-test photographs of the S/N 3-7 injector. The post-test photograph indicates a typical oxidizer injector failure.

The oxidizer injector failures experienced with the mid-diameter vortex injector during this phase of the program were attributed to local heat fluxes much higher than predicted. In order to permit more accurate heat transfer analysis and to provide back-up hardware for altitude testing at AEDC, several heavily instrumented heat sink oxidizer injector designs were tested.



Mid-Diameter Vortex Injector Assembly,  
Propellant Cooled X315455B, S/N 1A-6

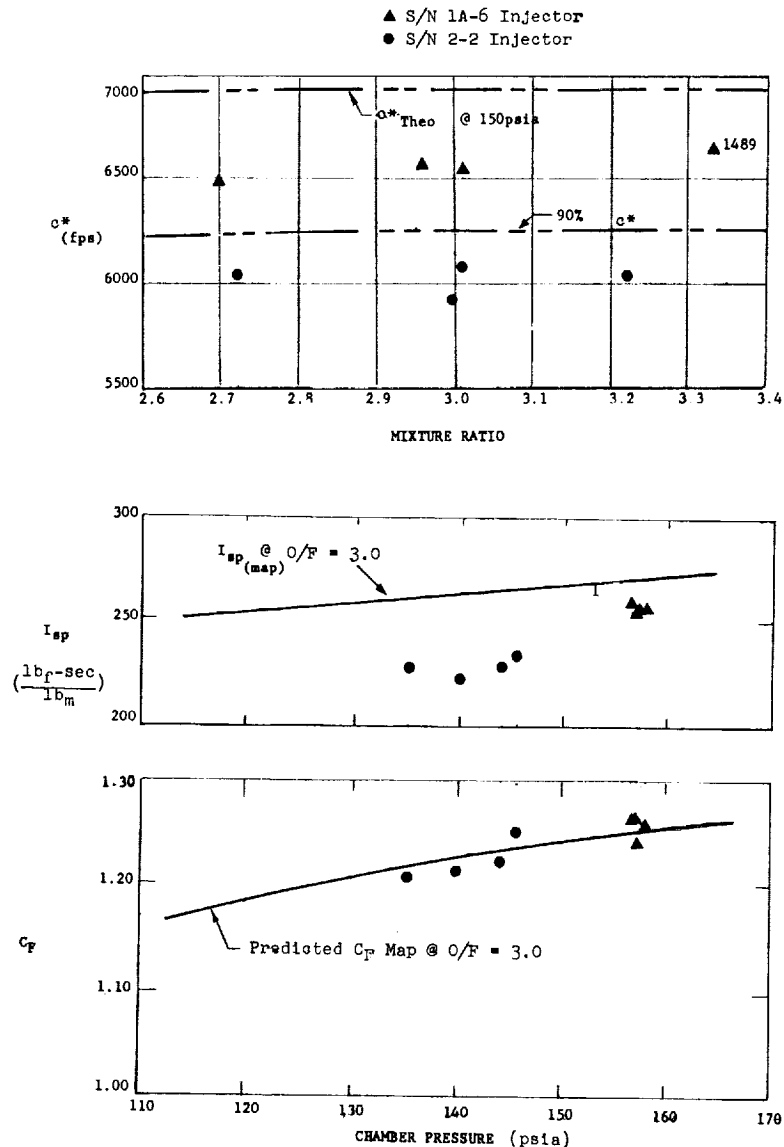
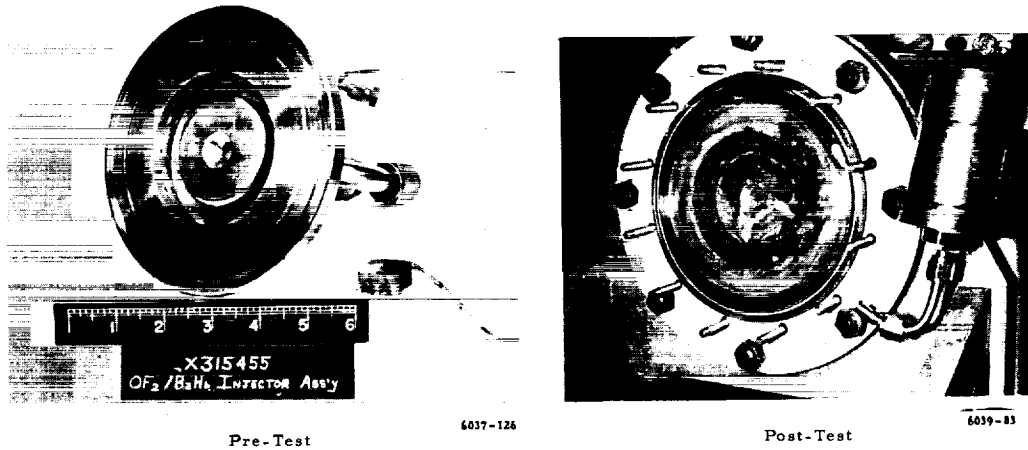


Figure 14. Propellant-Cooled Mid-Diameter Vortex Injector Sea Level Performance (Used at AEDC)





Mid-Diameter Vortex Injector Assembly,  
Propellant Cooled X315455B, S/N 3-7

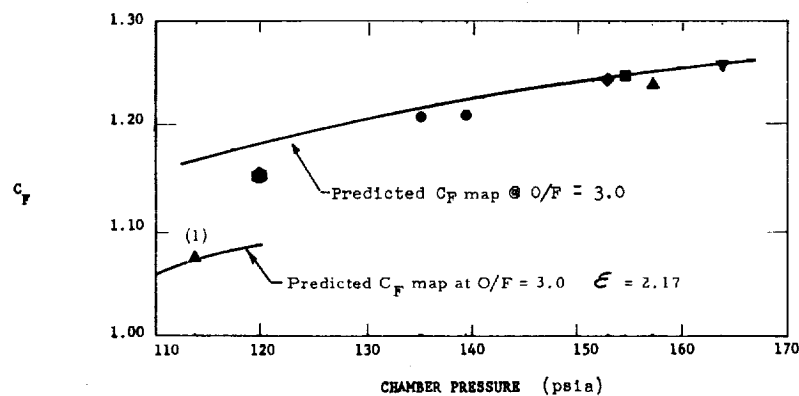
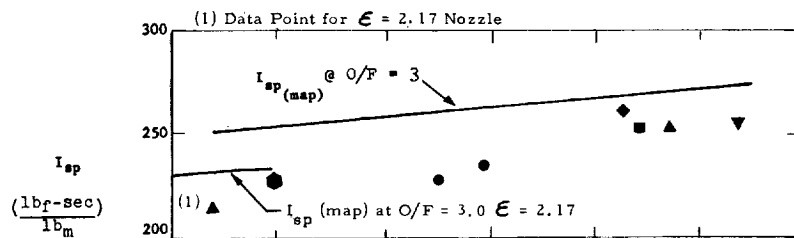
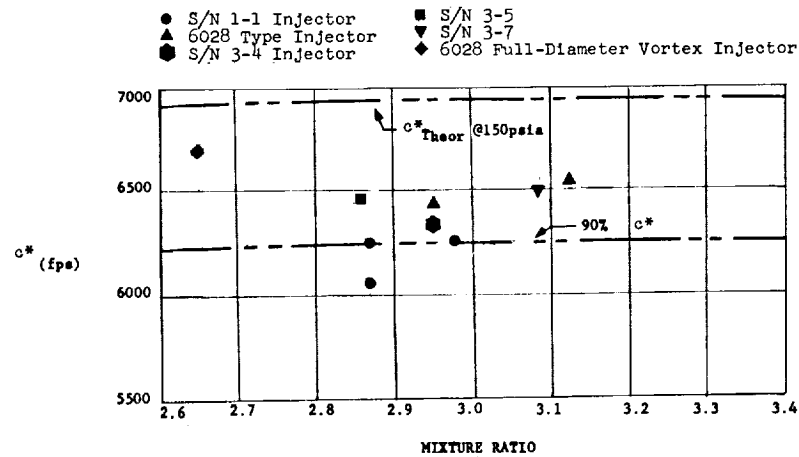
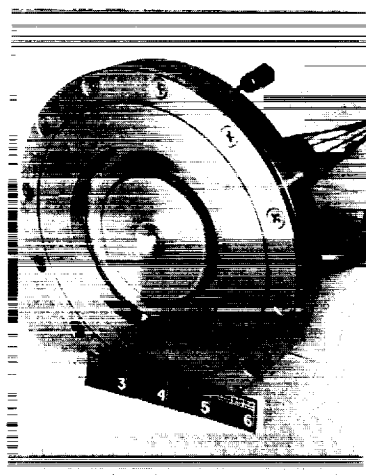
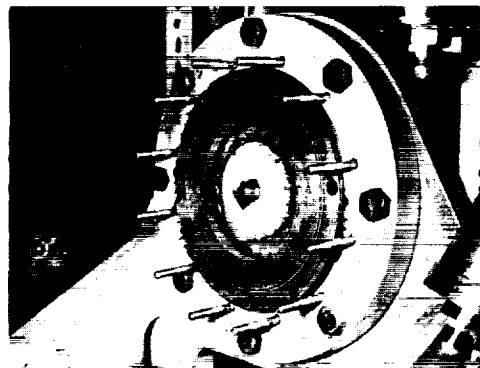


Figure 15. Propellant Cooled Mid-Diameter Vortex Injector Sea Level Performance



Pre-Test

6039-182



Post-Test

6039-227

One-On-One Heat Sink Type Vortex Injector Assembly,  
X315357, S/N 1-1

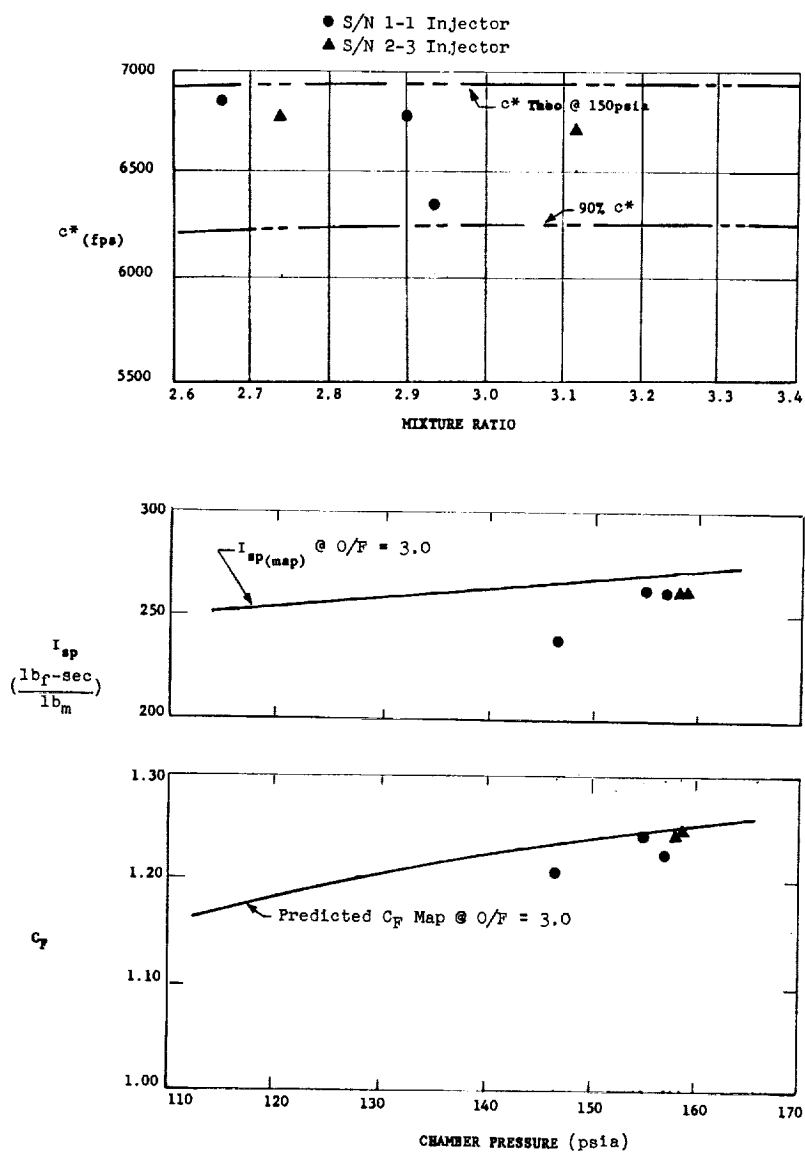


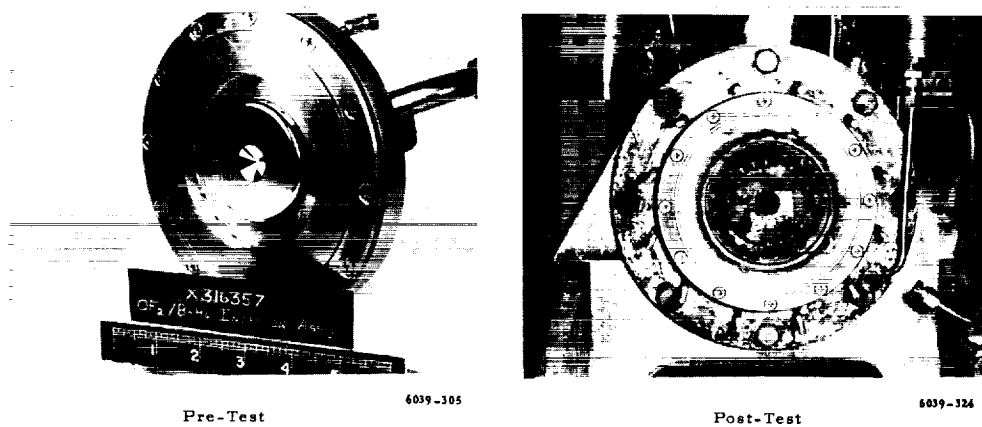
Figure 16. Heat Sink Vortex Injector Sea Level Performance (Used at AEDC)

(2) Heat Sink Injector Performance - Sixteen sea level tests were conducted with three types of heat sink injectors. Ten tests were conducted with injectors which were utilized in the altitude performance tests at AEDC. Performance data for two of these injectors (S/N 1-1, 2-3) are presented in Figure 16. Steady state operation was not achieved with the third injector (S/N 4-5) as a result of injector internal feed problems. During this phase of the program six tests were also conducted with five additional heat sink injectors. Performance data for these injectors are presented in Figure 17. Although oxidizer injector erosion was experienced in five of these tests, the performance data was obtained at steady state conditions prior to initiation of failure. Typical pre-test and post test photographs of the heat sink injectors are also shown on Figures 16 and 17.

Initial tests in this phase of the program were conducted with the S/N 4-3, S/N 4-2 and S/N 4-1 injectors. These injector designs maintained the same injection pattern and combustion side gas geometry as the mid-diameter vortex propellant-cooled injector design. One configuration S/N 4-1 incorporated an ablative cap over the oxidizer injector. The average performance level obtained in three tests with this configuration was 94.5% of theoretical  $c^*$  over a mixture ratio range of 2.92 to 3.07. Severe erosion of the oxidizer injector inline with each orifice was experienced with each of these injectors (Figure 18).

In order to provide durability, the heat sink design was modified. The modifications included 20 oxidizer and fuel orifices to provide more uniform mixing and to reduce the annular throughput in the vortex annulus from 1.3 to 1.0 lbs/sec-in<sup>2</sup> reduce heat transfer in the vortex annulus. Prior experience with vortex injectors, has shown improved durability with reduced throughputs. Eight tests using the one-on-one injection pattern, twenty orifice injector configuration were conducted with three injectors (S/N 1-1, S/N 2-3, S/N 3-4). An average performance level of 95.8% theoretical  $c^*$  was obtained over a mixture ratio of 2.66 to 3.11. During this series of tests, performance data from two tests with the S/N 1-1 injector were not obtained as a result of fuel leaks in the test system. Since only slight erosion on the oxidizer injector was noted on the S/N 1-1 and 2-5 injectors, the injectors were considered to have adequate durability for the 2-3 second duration altitude tests required at AEDC. The S/N 3-4 injector sustained more damage than the other two injectors but much less than the two-on-one heat sink type. Consequently, the S/N 3-4 injector was not considered for the AEDC program.

Heat transfer data acquired with the S/N 1-1 injector indicated a 50% reduction in heat flux when compared to the two-on-one configuration. This data corroborated the improved durability obtained with the one-on-one, 20 orifice injector (Section IV A.5 d describes the heat transfer results in detail).



Heat Sink Type Vortex Injector Assembly, S/N 3-4

- S/N 4-1, 4-2, 4-3
- ▲ S/N 2-8
- ◆ S/N 3-4

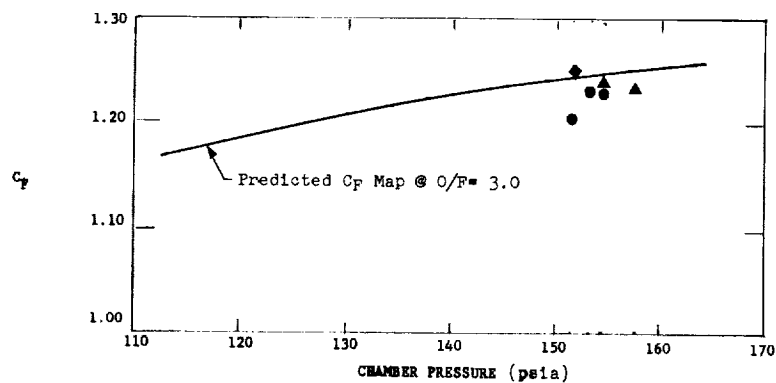
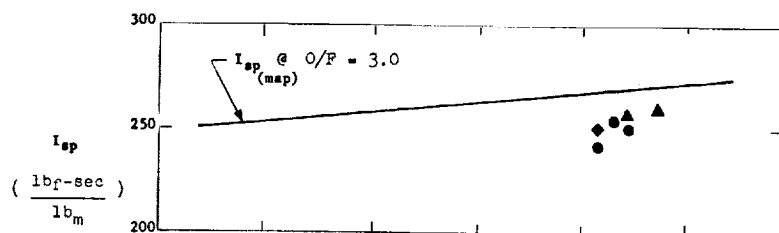
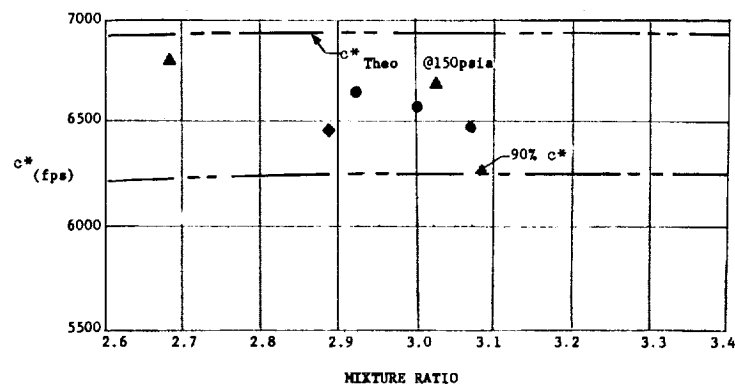
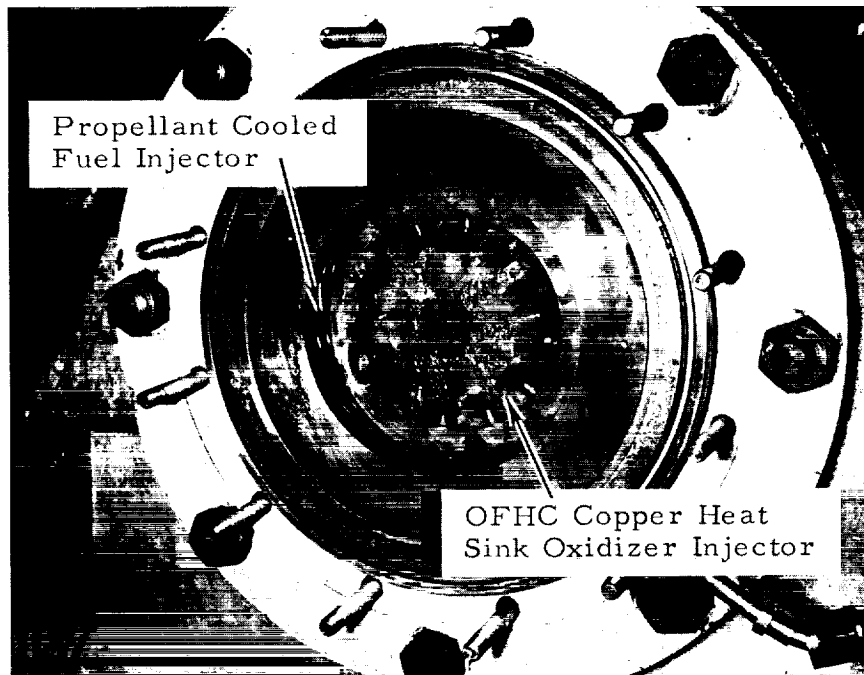
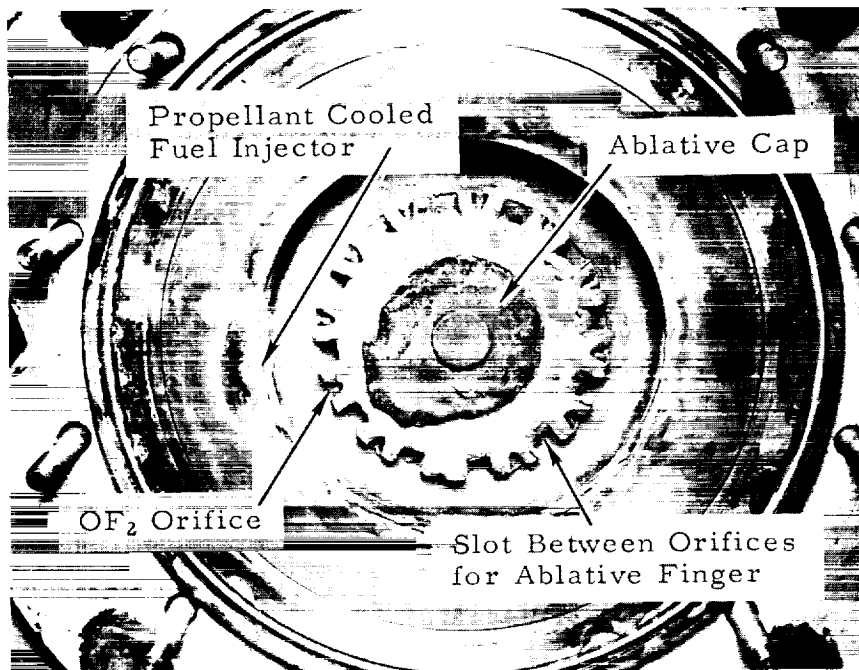


Figure 17. Heat Sink Injector Sea Level Performance



6039-136

S/N 4-3, Heat Sink Type



6039-185

S/N 4-1, Ablative Cap

Figure 18. Post-Test Photographs, Two-on-One Heat Sink Injectors

The erosion experienced with the heat sink oxidizer injectors also appeared to be related to the oxidizer rich environment in proximity to the orifices. In an effort to evaluate this possibility, an oxidizer injector incorporating increased orifice L/D (i. e., from 2 to 4) was tested. The increased orifice L/D should provide a more solid stream pattern which would in effect move the oxidizer away from the injector surface.

Two test firings were conducted with the S/N 2-8 which incorporated increased L/D oxidizer injector orifices. The average performance level obtained with this configuration was 97.2% of theoretical  $c^*$  over a mixture ratio from 2.69 to 3.02. No erosion was noted on the first test. The second test resulted in slight erosion of the oxidizer injector.

In an effort to provide increased injector durability and obtain injector heat fluxes compatible with a long duration propellant-cooled injector version, a third heat sink type injector was evaluated. This injector (S/N 4-5) incorporated 30 oxidizer and fuel orifices and an increased fuel injector diameter which gave a throughput of 0.444 lbs/sec-in<sup>2</sup>. Three tests were conducted using the S/N 4-5 one-on-one, low annular throughput, thirty orifice injector assembly. During the first test, engine pulsing was experienced and steady state operation was not achieved. Post-test examination of the injector revealed that the fuel injector deflected into the propellant passage, cutting off fuel flow to the engine. Modifications consisting of spacer wires and a shim in the fuel injector design eliminated this condition in subsequent tests. Two subsequent tests were made and although fuel flow was maintained, chamber pressure and thrust oscillations on the order of  $\pm 30\%$  of nominal values were experienced and steady state data was not obtained. However, it is significant to note that this injector has been tested five times with no evidence of erosion. The combustion oscillations probably are a result of a combination of low injection pressure drops (and hence low injection velocities) and longer stream lengths required for intimate propellant mixing. Based on past experience, increased injection pressure drops and optimization of stream length should provide smooth combustion.

#### d. Injector-Combustion Chamber Heat Transfer Results

Extensive injector-combustion chamber heat transfer analyses were conducted during the initial design phase and during the course of the program as test data became available. Heat transfer test data has been acquired to provide design data for extended duration thrust chamber containment with OF<sub>2</sub>/B<sub>2</sub>H<sub>6</sub>. The following sections describe the heat transfer analysis and test data obtained during this phase of the program and design approach leading to an extended duration propellant-cooled injector based on these results is also presented.

(1) Propellant-Cooled Injector Test Results - A total of eight propellant-cooled oxidizer injectors and five propellant-cooled fuel injectors were tested in this program. No durability problems were experienced with the fuel injectors. Oxidizer injector

burnout was experienced with five injectors. The failure with the S/N 1-1 injector which occurred on the third test was attributed to a hard start which collapsed the OF<sub>2</sub> cooling passage leading to insufficient cooling and burnout. The other five failures were typical heat transfer failures (i. e., erosion and burn through of the oxidizer injector combustion-side material into the cooling passage).

The propellant-cooled mid-diameter vortex oxidizer injectors were instrumented to obtain OF<sub>2</sub> bulk temperature rise so that overall heat flux data could be calculated. The experimental heat flux data obtained with the oxidizer injectors is presented in Table V. The predicted values are also shown in Table V to permit comparisons with experimental results. For injectors tested more than once, the range of heat flux values obtained is presented.

TABLE V

Propellant-Cooled Vortex Oxidizer Injector Heat Flux Comparison

Inj. S/N	No. Tests	c*(1) %	P <sub>ch</sub> (1) (psia)	O/F (1)	ΔT <sub>OF<sub>2</sub></sub> °F	Surface Area A <sub>s</sub> in. <sup>2</sup>	Pre- dicted	Heat Flux(3) Test (avg)
1-1	3	89.3	138	2.9	17-30	9.16	2.6	2.5-4.4
2-2	4	86.9	141	2.99	14-25	9.16	2.5	3.1-4.1
6028 Type Injector	1	93	114	2.95	47	9.16	2.4	6.1
6028 Type Injector	1(2)	94	157	3.12	54	9.16	3.2	7.5
3-4	1(2)	91.7	120	2.95	19	9.16	2.5	2.3
3-5	1(2)	93.2	145	2.86	24	10.5	2.03	2.9
1A-6	4	94.9	157	3.01	16.21	9.16	3.2	3.0-3.8
3-7	1(2)	93.4	165	3.08		9.16	3.00	4.7
Full Diameter	1(2)	96.6	153	2.65	--	--	--	--

(1) Average data for injectors tested more than once

(2) Oxidizer injector burn-out

(3)  $q''$  injector test =  $\frac{\dot{w}_{OF_2} \Delta T_{OF_2} C_p(OF_2)}{A_s}$ , Btu/sec-in.<sup>2</sup>

where:  $\dot{w}_{OF_2}$  = oxidizer flow, lbs/sec

$C_p (OF_2)$  = 0.30 btu/lb - °F used for these calculations

$\Delta T_{OF_2}$  = measured oxidizer injector bulk temp. rise, °F

$A_s$  = combustion-side surface area, in.<sup>2</sup>

In general, experimental heat flux values equal to or about 50% higher than the predicted values was obtained for most injectors except for the Project 6028 type injector. In this configuration heat fluxes two to three times higher than predicted were encountered during test. It is believed that incorrect propellant temperature measurements were obtained during the tests with the Project 6028 injector. On the basis of the comparative heat transfer data presented in Table V, it is apparent that; (1) average heat flux levels approximately 60% higher (S/N 2-2 injector) than those predicted have been experienced without burnout, (2) variations in heat flux on the order of 70% during otherwise apparently identical test conditions (S/N 1-1 injector) are evidenced.

The failure on the S/N 1-1 oxidizer injector which occurred on the third test was attributed to a hard start. The hard start, which was the only one ever experienced in over 150 test firings with  $OF_2/B_2H_6$  at Thiokol-RMD, was attributed to excessive ignition delay as a result of excessive fuel injector cooldown which resulted in an initial fuel inlet temperature of  $< -250$  F. It should be noted that hypergolicity tests (50) with  $OF_2/B_2H_6$  (Reference 1), did not result in hard starts with injector hardware pre-cooled as low as  $-320$  F.

Erosion of the Project 6028 oxidizer injector occurred during the second test with this injector. Failure occurred near the center face which did not have a central flow divider. In addition, it was operated at a chamber pressure level of 150 psia (design level was 120 psia) in an attempt to demonstrate durability at this level for possible use during testing at AEDC. It was concluded that insufficient face cooling was available at the 150 psia pressure level. All subsequent oxidizer injectors tested utilized a central flow divider to provide improved face cooling capability.

It was decided to test the full-diameter vortex injector at a chamber pressure of 150 psia. It was planned to utilize this injector, which was designed for a chamber pressure of 120 psia and was available from a prior program (RMD Project 6028), and as a possible backup injector for altitude testing at AEDC. The burnout experienced with the full-diameter vortex oxidizer injector was suspected to be due to cooling flow maldistribution. Water flow bench tests revealed an abnormally high injector pressure drop which may have been due to non-uniform cooling passage gaps (nominal gap was .005").



The S/N 0-4, 0-5 and 0-7 oxidizer injectors were all tested with the S/N 3-0 fuel injector. Since all three oxidizer injectors experienced erosion during the first test, a review of the S/N 3-0 fuel injector test data and water flow tests were conducted in an effort to determine if there was any evidence which could correlate injector characteristics with the failures. No apparent evidence could be found which could correlate S/N 3-0 fuel injector characteristics with the oxidizer injector failures.

During the course of the data analysis and after the S/N 1A-6 injector testing, a reassessment of the cooling capability of  $\text{OF}_2$  (i. e., upper limit of nucleate boiling), based on the method of Bernath was made with a more rigorous computer program in order to further define cooling capability. The more rigorous data predicted an  $\text{OF}_2$  upper limit of nucleate boiling capability 20% lower than the design values originally used. However, application of the Bernath correlation at Thiokol-RMD is accomplished through the use of a computer program in which a value of  $D_e = 0.232''$  is utilized since it represents the average of diameters forming the basis of the correlation. In the propellant-cooled injector design, equivalent diameters on the order of  $0.02''$  are present. Based on the Bernath correlation, it is reasonable to anticipate higher values of allowable heat flux for a  $D_e = 0.02''$  than for  $D_e = 0.232''$  but the application of current correlations does not extend to this range. However, the magnitude of the margin is unknown and unpredictable and certainly experimental data is required to determine the cooling capability limits of  $\text{OF}_2$  over a range of operating conditions (i. e., pressure, temperature, velocity).

On the basis of the oxidizer injector failures experienced during testing, it appears that locally injector heat flux levels much higher than predicted and much higher than cooling capability limits, were being experienced with the two-on-one injector configuration. In order to permit more accurate analysis, several heavily instrumented heat sink oxidizer injector designs were tested.

(2) Interim Heat Sink Injector Program Test Results - Several heat sink injector configurations were evaluated during the program. Injector geometrical changes resulted in reductions in localized heat flux level of the oxidizer injector from 16 - 18 Btu/sec-in<sup>2</sup>, obtained with configurations similar to the propellant cooled versions, to a value of 2.5 - 4 Btu/sec-in<sup>2</sup>. Table VI summarizes the oxidizer injector heat flux data obtained with the instrumented heat sink injector configurations in the order of testing. The heat transfer data was calculated by the method developed by P. R. Hill (Reference 9) utilizing a temperature data measured at the combustion side of the oxidizer injectors. The installation of the combustion side temperature probes is discussed in Section IV.A.3.a.

TABLE VI

Heat Sink Oxidizer Injector Heat Transfer Summary

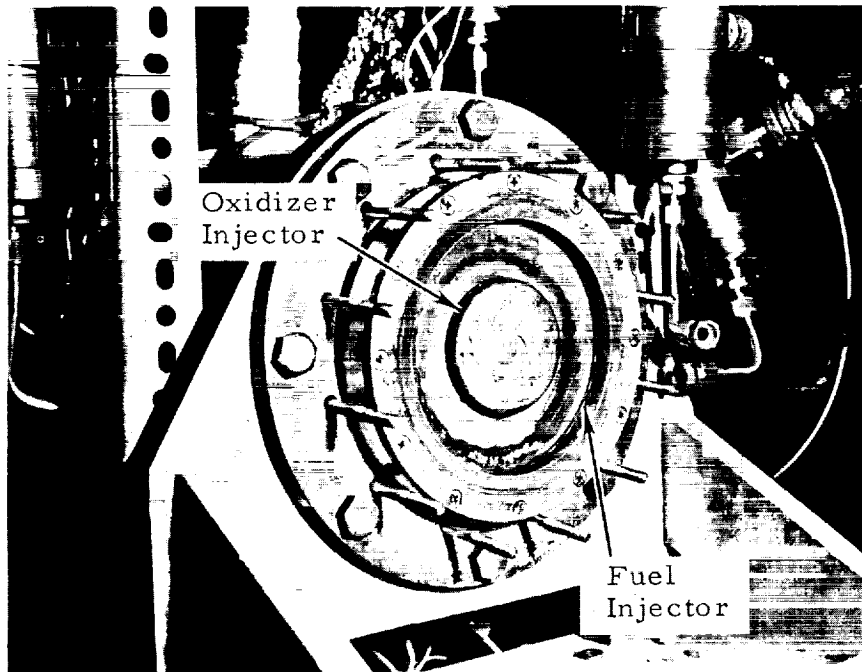
Injector	$G^{(1)}$ lb/sec-in <sup>2</sup>	No. Of Tests	$q''$ (Ave.), Btu/sec-in <sup>2</sup>
S/N 4-2, 4-3 Two-on-one (12 Orifice)	1.3	2	16 - 18
S/N - 1-1 One-on-one (20 Orifice)	1.0	5	11
S/N - 4-5 One-on-one (30 Orifice)	0.444	5	2.5 - 4

(1) G - Throughput; Vortex injector annulus mass velocity

A total of five propellant-cooled fuel injectors and eight heat sink oxidizer injectors were tested during this phase of the program. No durability problems were experienced with the propellant-cooled fuel injectors. Although oxidizer injector erosion was experienced with the initial designs, continuing design modifications resulted in a configuration (S/N 4-5) that did not show any evidence of erosion after five tests (Figure 19). Heat transfer instrumentation was only provided in the four injectors listed in Table VI because of the funding and scheduling limitations.

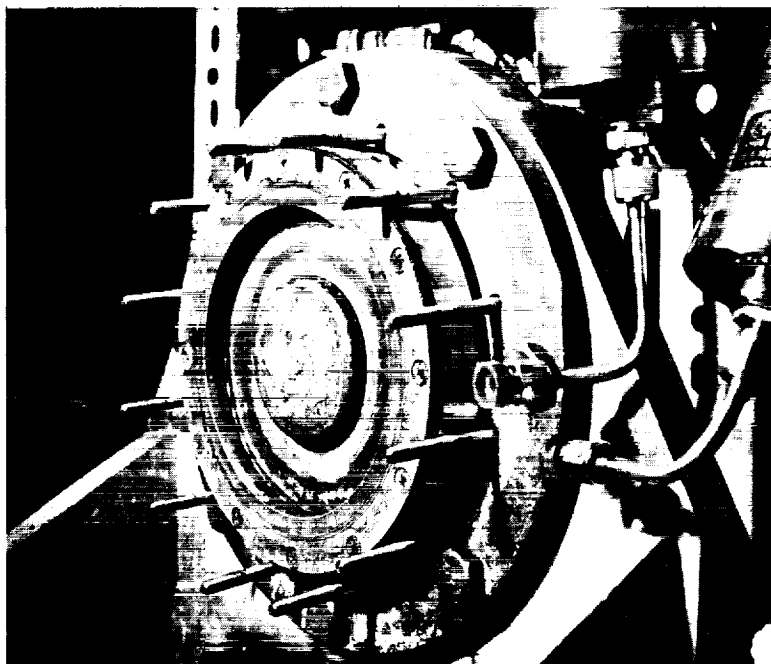
Initial tests were conducted with the X316143 (Figure 5) two-on-one injectors (S/N 4-3, 4-2). Heat transfer data were characterized by a peaking flux on the order of 16 - 18 Btu/sec-in<sup>2</sup> at about 0.7 seconds followed by a decrease in flux level to 10 - 13 Btu/sec-in<sup>2</sup> at about 1.2 seconds. Oxidizer erosion on the corner in line with each orifice appears to have begun at 1.2 seconds, as evidenced by the oscillation in all of the high response oxidizer injector surface temperatures. Figure 20 shows oxidizer injector combustion side temperature history data measured during testing with the S/N 4-3 injector. Figure 21 shows the corresponding calculated heat flux ( $q''$ ) data based on the temperature data.

In continuing the acquisition of heat transfer data, the next series of tests were conducted using the X316357 (Figure 7) one-on-one injector (S/N 1-1). In addition to increasing the number of orifices, the annular throughput was reduced



6039-407

View - Left Side



6039-408

View - Right Side

Figure 19. X316540 S/N 4-5 Heat Sink Injector After Five Tests

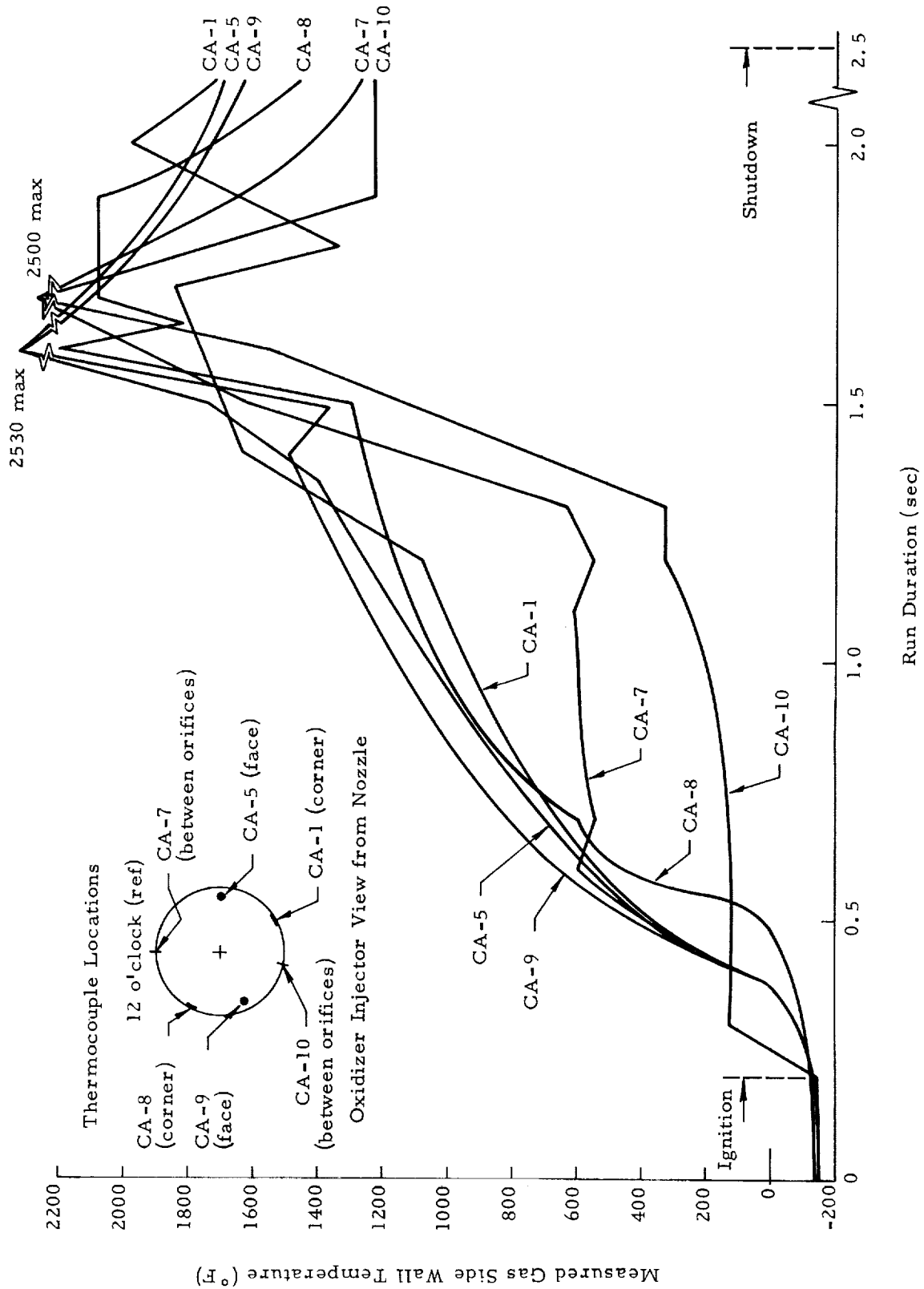


Figure 20. Gas Side Wall Temperature Data - S/N 4-3 Heat Sink Oxidizer Injector, Test Run 6CX1492

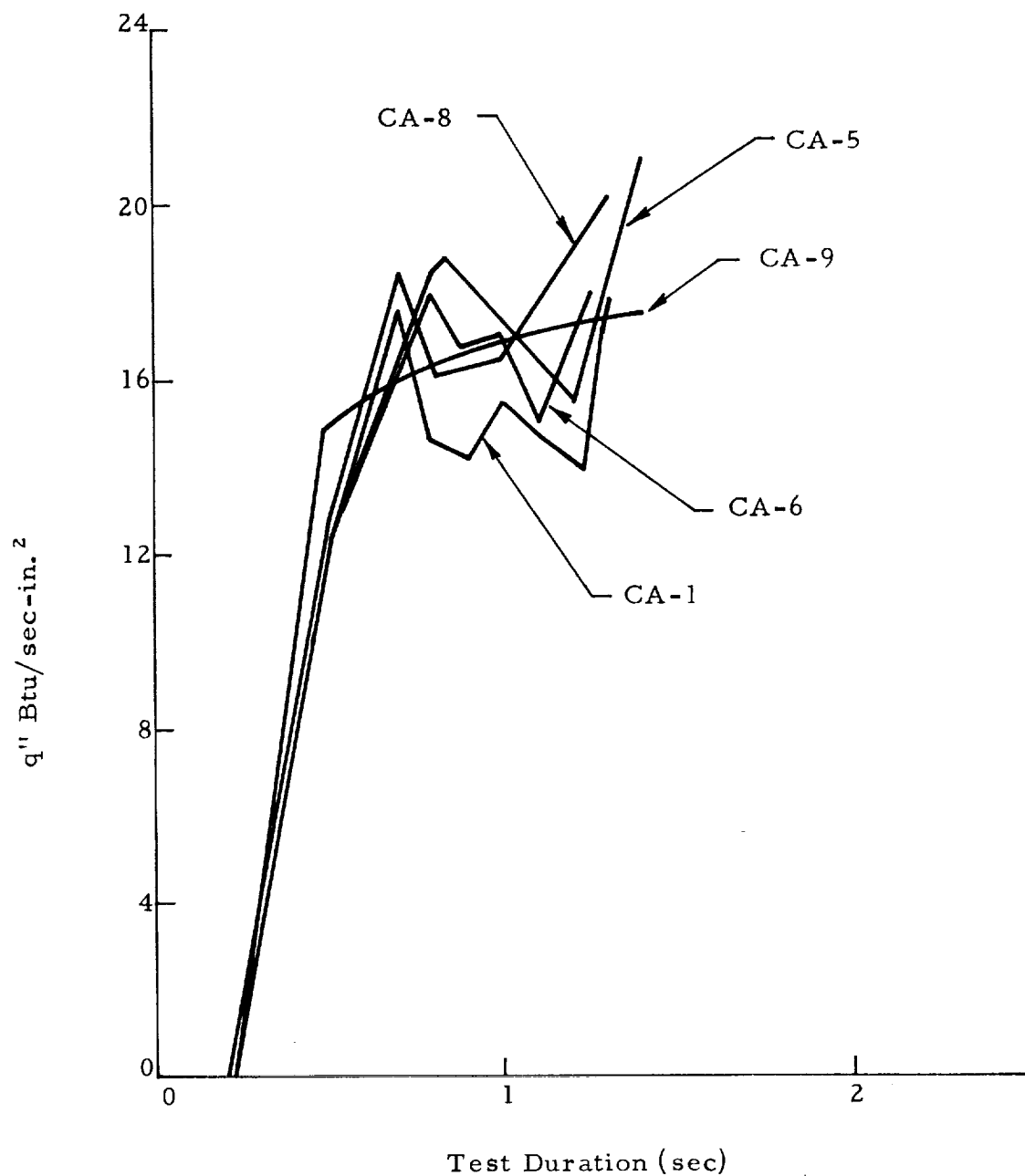


Figure 21. Oxidizer Injector Heat Flux S/N 4-3, Two-on-One Heat Sink  
Test Run 6CX1492

from 1.27 lb/sec-in<sup>2</sup> to 1.0 lb/sec-in<sup>2</sup>. Data acquired from five tests resulted in the heat flux levels of 11 - 13 Btu/sec-in<sup>2</sup> with no evidence of peaking fluxes exhibited by the two-on-one injector configuration. Figures 22 and 23 show typical combustion side wall measured temperature and calculated heat flux histories for this injector.

Continuing analysis of test data indicated that heat flux data could be correlated by the analytical gas film heat transfer function in the vortex annulus ( $G^{0.8}/D_e^{0.2}$ ) where:

$$G = \dot{w}/A$$

$\dot{w}$  = total propellant flow, lb/sec

$A$  = annular area between fuel and oxidizer injectors, in<sup>2</sup>

$D_e$  = hydraulic diameter of annulus between fuel and oxidizer injector diameters.

The effect of the gas film function on injector heat transfer is readily apparent from Figure 24 in which heat transfer data is plotted as a function of  $(G)^{0.8}/(D_e)^{0.2}$ . Since the gas film function is primarily related to mass velocity ( $G$ ), which corresponds to vortex injector annular throughput, an injector design approach based on reducing the injector throughput to 0.444 lb/sec-in<sup>2</sup> was evaluated. This injector (S/N 4-5) was the last configuration evaluated in this program.

Heat transfer data obtained from four test firings with the S/N 4-5 injector, including two tests made at AEDC, resulted in heat flux levels of 2.5 to 4.0 Btu/sec-in<sup>2</sup> which correlate very closely the value predicted by the prior analysis. The values of heat flux demonstrated with this configuration appear acceptable in an extended duration, propellant cooled injector design. The low heat flux results obtained with this injector are even more significant in view of the low frequency combustion pressure oscillations experienced with this injector which normally result in increased heat transfer levels.

(3) Improved Injector Durability - Throughout the development of the heat sink injector test program, injector designs were developed to improve durability through reduction of oxidizer injector heat flux levels.

To further verify these reduced injector heat flux levels, a full diameter heat sink type vortex injector was designed (Figure 25). The design was based on the same number of orifices and annular throughput as the S/N 4-5 injector. However, increased injection velocities and reduced stream lengths are incorporated in this injector to enhance combustion. In view of the improved durability

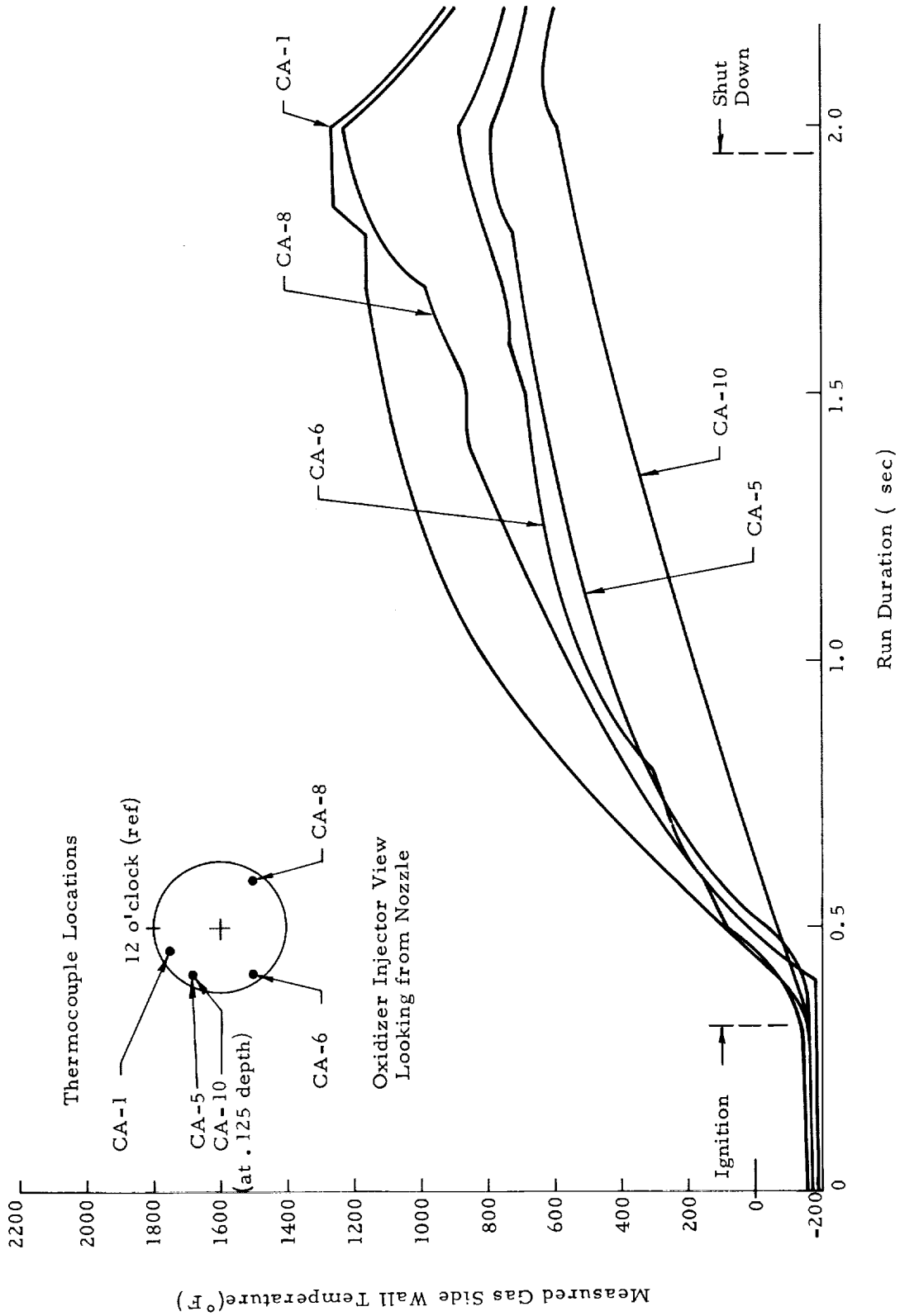


Figure 22. Gas Side Wall Temperature Data - S/N 1-1 Heat Sink Oxidizer Injector, Test Run 6CX1496

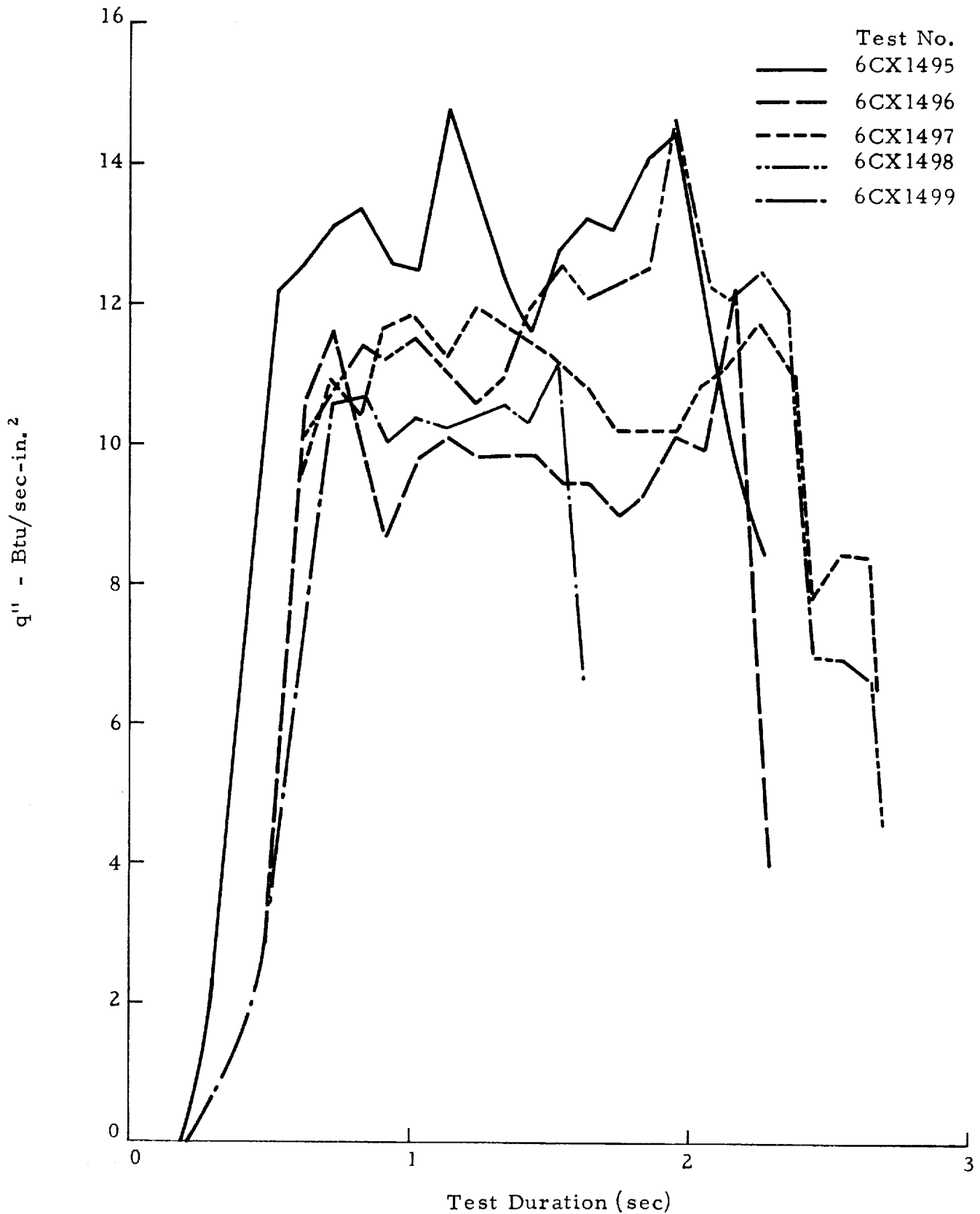


Figure 23. Average Oxidizer Injector Heat Flux S/N 1-1,  
One-on-One Injector



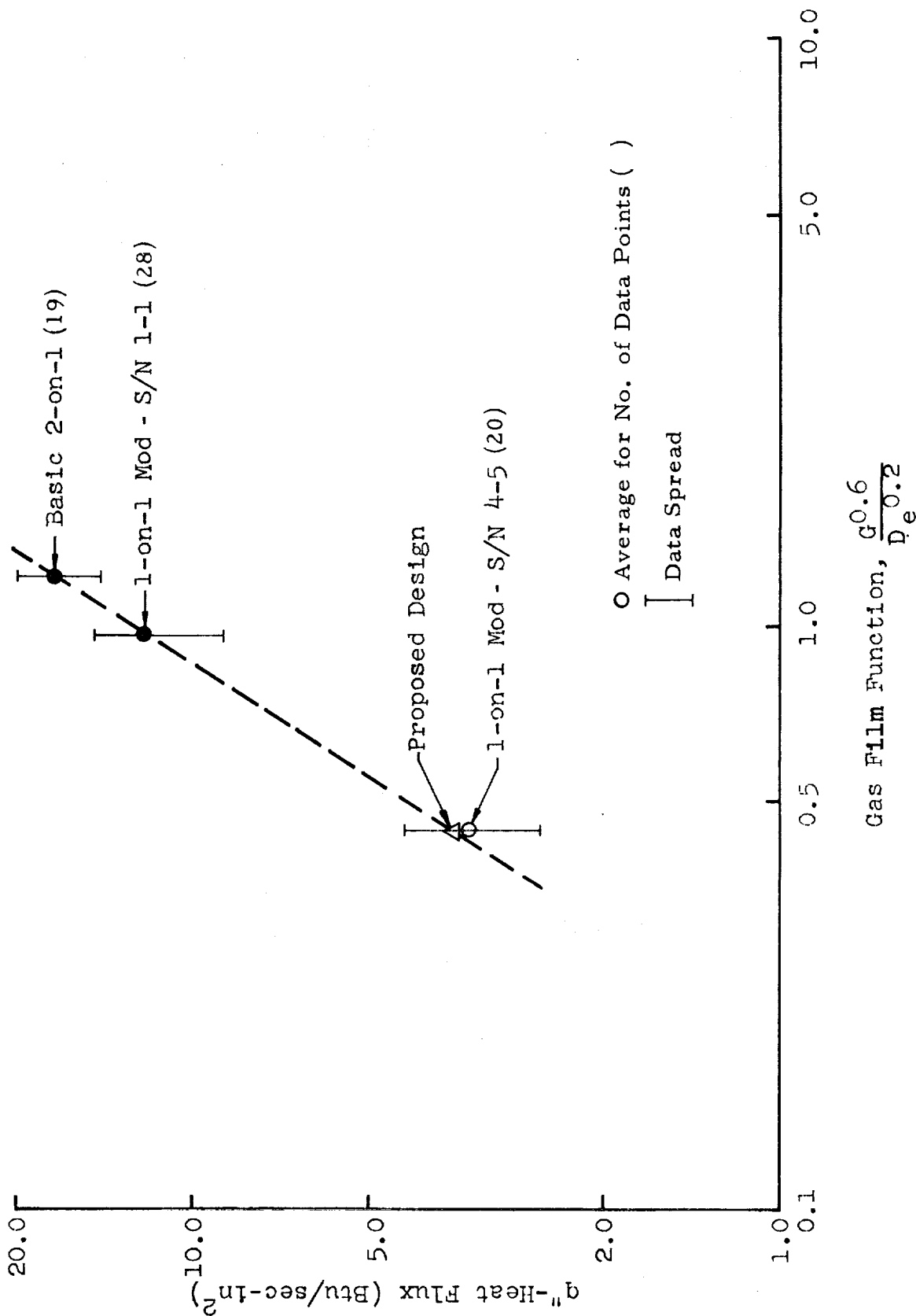


Figure 24. Heat Sink Oxidizer Injector Heat Flux vs Vortex Annulus Gas Film Parameter

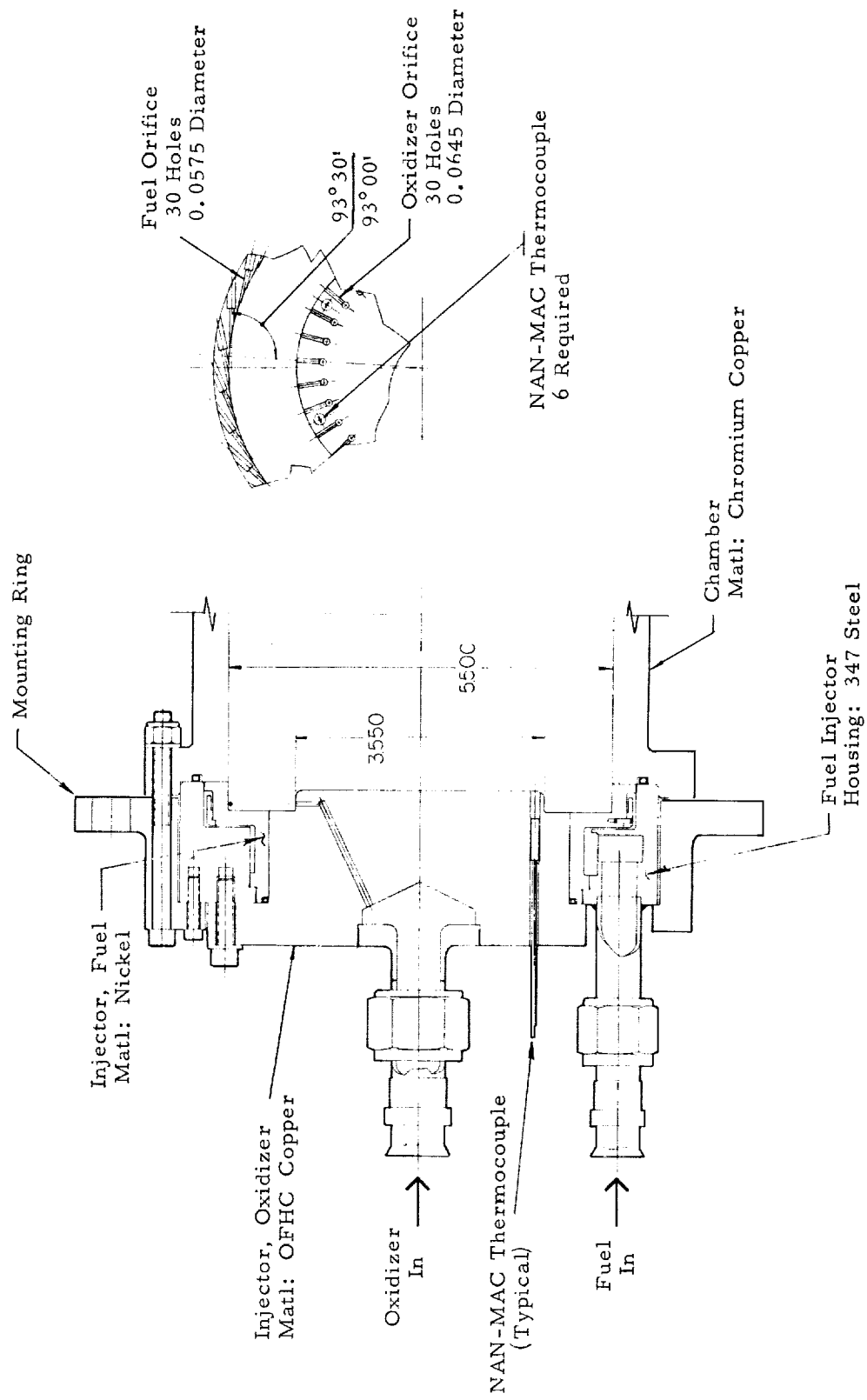


Figure 25. Heat Sink Full-Diameter Vortex Injector Design

demonstrated by the S/N 4-5 injector, it is believed that verification of low heat flux levels with this full-diameter heat sink design could lead to a reliable, long duration propellant-cooled injector. In addition, the full-diameter vortex injector can enhance combustion chamber durability through an effective film cooling environment along the chamber wall. Significant reductions in chamber and nozzle heat fluxes (on the order of 25% and 60% respectively in barrel and throat of that predicted by Bartz) has been demonstrated with the full-diameter vortex injector in other test programs with  $N_2O_4$ /MMH propellants and to an extent in this program (Section IV A. b. 4) with modified mid-diameter vortex injectors.

(4) Combustion Chamber and Nozzle Sea Level and Altitude Testing Heat Transfer Results - Heat transfer data were obtained in the chamber and nozzle by means of foil-type high response surface thermocouple probes located on the gas side wall in the chamber barrel and nozzle. Similar data obtained during the altitude performance tests conducted at AEDC (described in detail in Section IV. B) are presented in this section.

Figure 26 summarizes the heat transfer data acquired during sea level testing. The data are presented in terms of gas film heat transfer coefficients to permit comparisons with predicted values based on the method of Bartz (Reference 10). The range of experimental values are due primarily to the various injectors tested and variations in operating conditions (i. e., O/F,  $P_c$ ). Figure 27 summarizes the heat transfer data acquired during the altitude performance tests.

The results of these tests have shown that the experimental heat transfer gas film coefficients in the combustion chamber are lower than predicted by Bartz. This is in agreement with previous data acquired at Thiokol-RMD with vortex injectors. The experimental heat transfer gas film coefficients in the nozzle throat and nozzle extension are in good agreement with the values predicted by the method of Bartz. The results of these tests were utilized in the advanced chamber cooling study effort presented in Section IV. E.

#### e. Injector Design Data Investigations

During the course of the program, injector investigations in the areas of brazing, model water flow tests, and high frequency combustion pressure measurements were undertaken to provide additional design data for an extended duration injector design. The design data obtained from these studies have been utilized in the proposed injector design approach (Figure 25) discussed previously. The following sections discuss the results of these investigations.

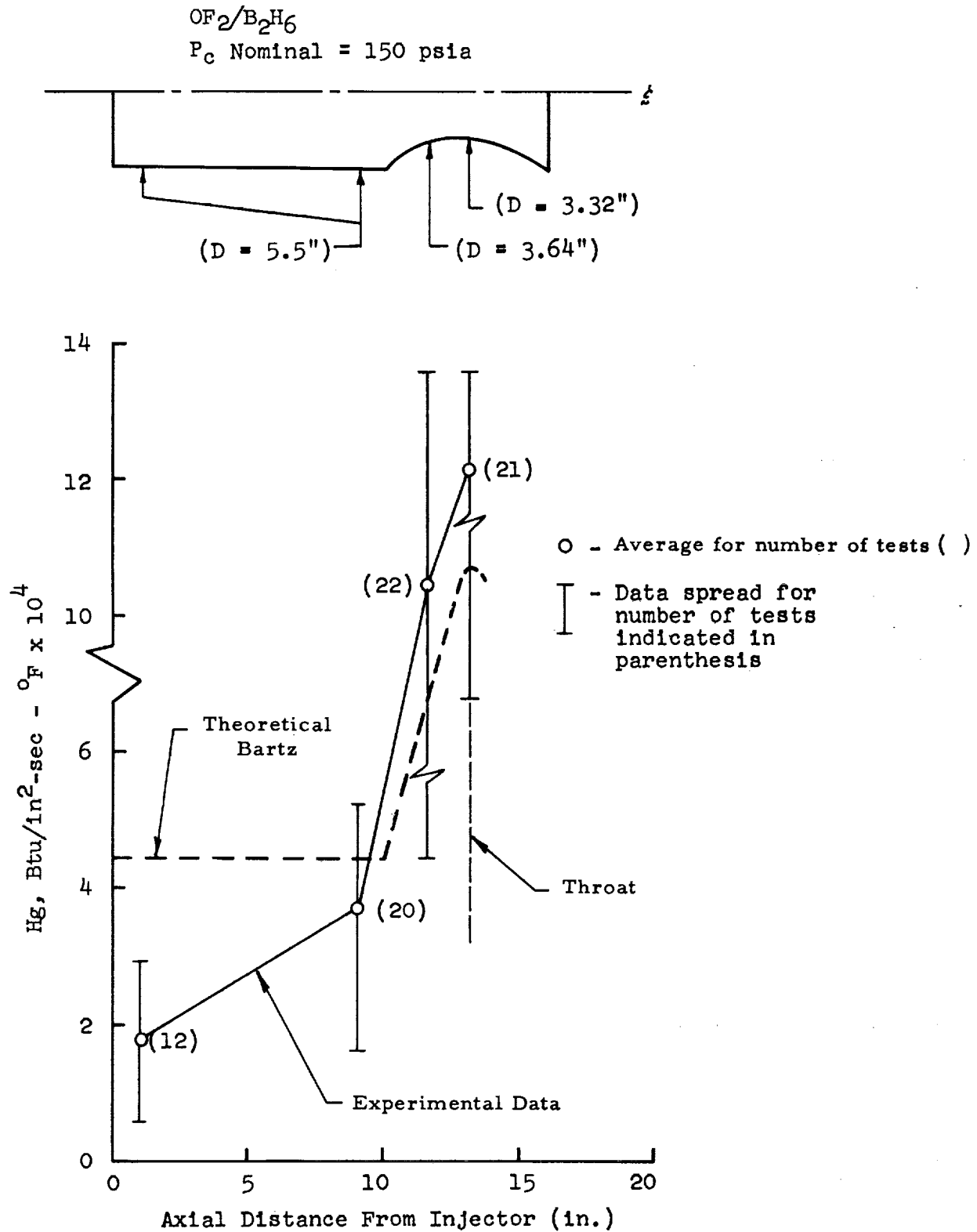


Figure 26. Gas Film Heat Transfer Coefficient vs Axial Location  
RMD Sea Level Test Data

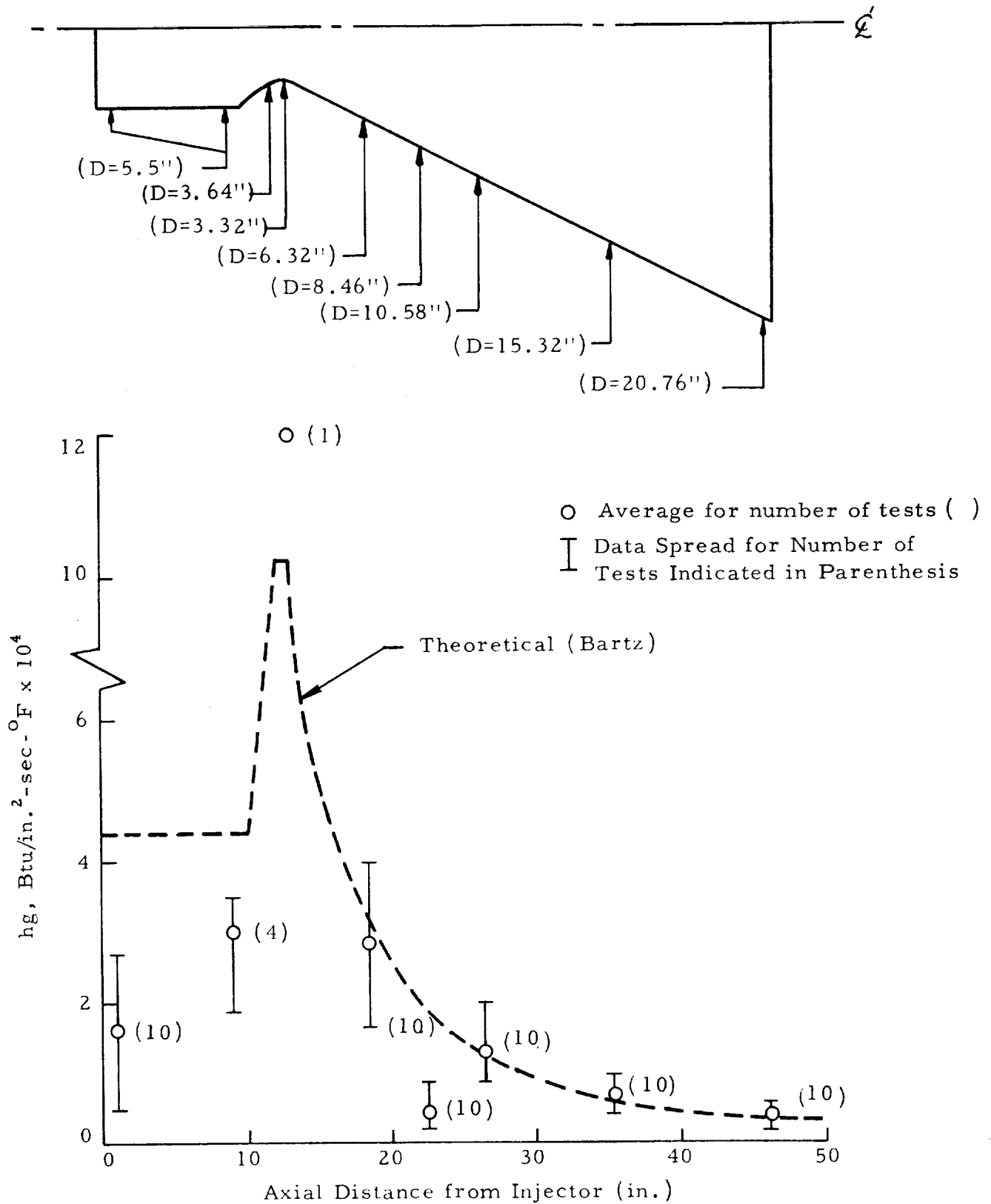


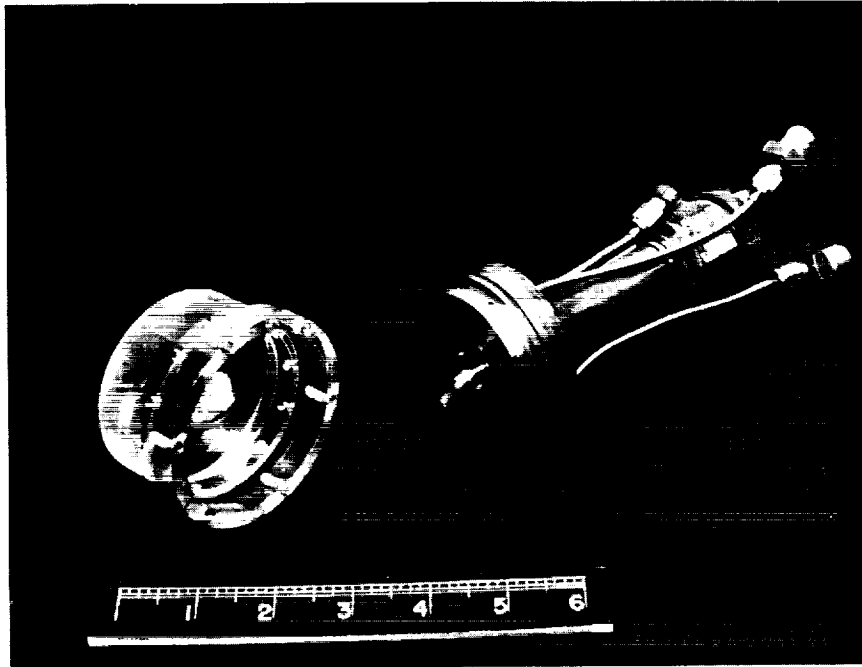
Figure 27. Gas Film Heat Transfer Coefficient vs Thermocouple Station - AEDC Data

(1) Oxidizer Injector Braze and Assembly Process - Braze joint failures in the prior program (RMD Project 6028) with oxidizer injectors utilizing a Lithobraz 925 braze alloy, necessitated the use of an alternate braze joint using Englehard B-70 alloy. The Lithobraz 925 alloy consists of 92.5% silver, 7.2% copper and 0.2% lithium with a recommended brazing temperature of 1720F. The Englehard Silvaloy B-70 alloy consists of 7% silver, 85% copper and 8% tin and has a brazing temperature of 1850F. The B-70 braze alloy allowed full heat treat strength in the chromium copper and produced a superior braze joint when compared to the Lithobraz 925. During the course of the program, two additional modifications were made to improve the braze process. The braze-heat cycle was changed to provide a faster quench cycle to develop full strength in the chromium copper, and the assembly process was modified to change the oxidizer injector cup shrink fit to a slip fit to eliminate the alignment problem encountered when assembling the chilled stainless steel to the chromium copper injector. No braze joint failures were experienced in this program.

(2) Oxidizer Injector Model Water Flow Studies - Oxidizer injector model water flow tests were undertaken in an effort to determine if a correlation existed between injection spray patterns and performance ( $c^*$ ) and to provide design data. The model utilized a steel plug with a plastic oxidizer face cap (Figure 28) in order to permit observation of internal flow disturbances or cavitation. The model was geometrically similar to the mid-diameter vortex propellant-cooled injector design and utilized 12 orifices. Oxidizer face flow passage gaps and orifice inlet geometry were varied to encompass the range of injector configurations tested. Corner face passage gaps of 0.006", 0.010" and 0.013" in conjunction with various orifice inlet configurations were studied. Water flow and pressure drop data were obtained over an inlet pressure range of 10 psig to 250 psig. Three equally spaced pressure taps were provided at the orifice inlet. Photographs of the orifice spray patterns were taken at the various pressure levels.

Several configurations were analyzed in regard to varying internal geometry of the injector, i.e., passage gaps and orifice inlet configurations and number of orifices. Table VII summarizes the results of seven configurations tested. It was found that decreasing passage gaps provided less uniformity of orifice injector spray, which could affect performance, and orifice discharge coefficients decreased as orifice cross velocity was increased. Figure 29 shows typical orifice spray patterns, as a function of passage gap, for an oxidizer model configuration similar to that employed in the propellant-cooled injectors.

During the course of the model tests, deliberate inclusion of foreign material in the face passages produced an erratic spray pattern at the orifice in line with the disturbance. This condition indicates that greater attention is required to ensure smooth passage surfaces (i.e., free of nicks, scratches, protuberances, steps, etc.) as smaller flow passage gaps are employed.



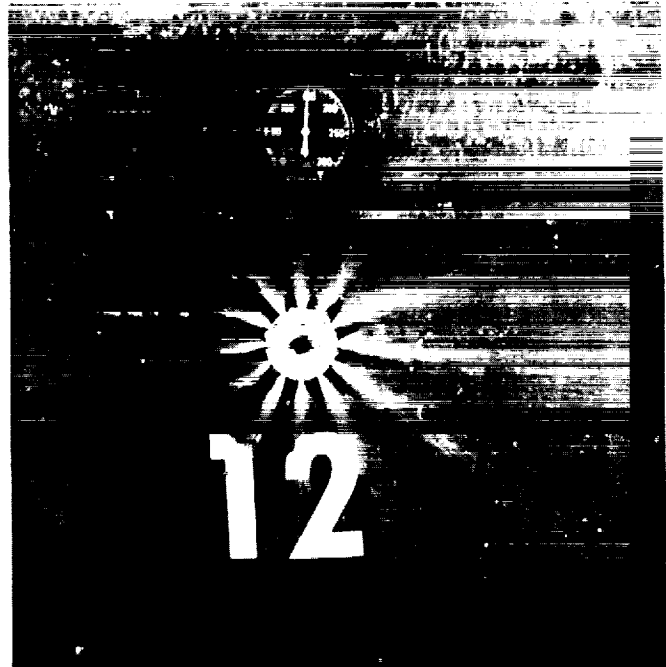
6039-34

Figure 28. Oxidizer Injector Water Flow Model



6037-232

0.006 in. Corner Face Gap

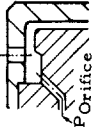
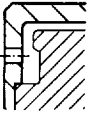
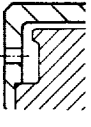
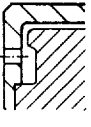
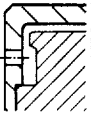
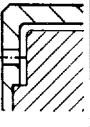
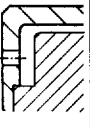


6037-220

0.0125 in. Corner Face Gap

Figure 29. Typical Oxidizer Injector Spray Pattern, S/N 0-6 Injector

TABLE VII  
OXIDIZER INJECTOR MODEL WATER FLOW TEST SUMMARY

Configuration (Typical Sections of OF <sub>2</sub> Injectors)	.066" Corner Face Gap			.010" Corner Face Gap			.013" Corner Face Gap		
	Pin-psig	P <sub>Orifice</sub> -psig <sup>(1)</sup>	C <sub>D</sub> (Orifice) <sup>(2)</sup>	Pin-psig	P <sub>Orifice</sub> -psig <sup>(1)</sup>	C <sub>D</sub> (Orifice) <sup>(2)</sup>	Pin-psig	P <sub>Orifice</sub> -psig <sup>(1)</sup>	C <sub>D</sub> (Orifice) <sup>(2)</sup>
1.  .022" Gap Lip Half-way across Orifices	98	15 - 25	.505	43	14 - 16	.55	36	14 - 17	.55
2.  .022" Gap Lip 1/64" Into Orifices	93	14 - 25	.51	50	17 - 20	.54	39	16 - 19	.55
3.  .022" Gap Lip 1/64" Away from Orifices	105	20 - 24	.47	36	19 - 22	.51	37	18 - 19	.53
4.  .010" Gap Lip In Line with Orifices	128	18 - 31	.41	118	30 - 31	.40	92	25 - 30	.43
5.  .015" Gap Lip In Line with Orifices	N O T T E S T E D			105	21 - 33	.48	58	22 - 24	.47
6.  .015" Gap	138	45 - 77	.34	87	50 - 60	.32	75	49 - 60	.31
7.  .039" Gap	130	25 - 34	.44	62	18 - 24	.50	48	19 - 23	.52

(1) Range of 3 Orifice Pressure Measurements

(2) Average Based on 3 Orifice Pressure Measurements



A second series of oxidizer injector model tests utilizing 20 orifices and shorter "pot" lengths (i. e. spud immersion depth into combustion zone) was conducted to provide design data for a propellant-cooled injector. For this configuration, the primary objective was to determine the effect on orifice spray pattern by locating the face cooling passage closer to the orifices. The shorter pot was considered desirable with regard to reducing injector surface area exposure in the combustion zone thereby improving injector durability. The increased number of orifices in a vortex injector should provide improved cooling distribution (i. e., reduce stagnant flow areas) and more uniform mixture ratio distribution. These tests revealed that a face cooling passage gap radially in-line with the orifices resulted in stable, solid streams (i. e., as opposed to fans or bushy streams).

Based on the results of the model flow tests and injector flow checks and performance results, improved injector durability and performance reproducibility may be accomplished by: (1) ensuring smooth cooling passage contours; (2) maintaining low orifice cross velocity (consistent with the heat transfer cooling requirements); (3) an increased number of orifices to provide better cooling distribution and more uniform mixture ratio distribution and (4) shortening the protrusion of the oxidizer injector into the combustion zone and still maintain the vortex concept.

(3) Combustion Stability - In order to investigate the possibility that unstable burning was a cause of the oxidizer injector durability problems, high frequency combustion pressure data was obtained during a series of eight tests with the heat sink injectors. Flush mounted, water-cooled Norwood pressure transducers (flat frequency response up to 15,000 cps) installed axially and longitudinally in the combustion chamber and recorded on high speed magnetic tape were used to obtain combustion pressure measurements.

Data obtained from the high frequency response chamber pressure measurements showed no evidence of combustion instability. No frequencies corresponding to the predicted fundamental combustion frequencies (i. e., 430 cps for cavity mode, 2300 cps for longitudinal mode, 5900 cps for transverse mode and 3200 cps for the tangential mode) were obtained. Some intermittent combustion pressure oscillations on the order of 600 cps with a maximum pressure amplitude of  $\pm 4\%$  of the nominal chamber pressure level were obtained followed by a damping of these frequencies to amplitudes of  $\pm 2\%$ . On the basis of these tests, it was concluded that destructive high frequency combustion instability was not the mode of failure of the vortex injectors.

Tests conducted with the last injector evaluated, the S/N 4-5 heat sink type, exhibited low frequency (80-200 cps) chamber pressure and fuel injector oscillations with pressure amplitudes of  $\pm 30\%$  of the nominal values. The low frequency combustion pressure oscillations were attributed to poor propellant mixing as a result of a combination of low oxidizer injection pressure drop (i. e., 20 psi) and oxidizer stream impingement length (i. e., increased throughput) for this injector configuration. Based on prior vortex injector experience in the main propellant combinations including  $\text{OF}_2/\text{B}_2\text{H}_6$  it is believed that with an increase in injection velocity and reduced stream impingement length (i. e., the annulus height), low frequency combustion pressure oscillations can be eliminated.

On the basis of the 2000-pound space thrust sea level injector tests, the following conclusions are made:

- The  $\text{OF}_2/\text{B}_2\text{H}_6$  propellant combination delivered high specific impulse over a mixture ratio of 2.7 to 3.3 at a chamber pressure level of 150 psia.
- Vortex injector design modifications, utilizing heat sink type injectors demonstrated reductions in heat flux levels to values that may be acceptable in an extended duration propellant cooled injector design. On the basis of these results (i. e., reduced erosion) obtained with heat sink type injectors, design criteria (i. e., injector pattern and geometry changes) have been developed that should enhance the durability of a propellant cooled injector.

## B. ALTITUDE PERFORMANCE EVALUATION OF $\text{OF}_2/\text{B}_2\text{H}_6$

### 1. Objectives

The objectives of the altitude test program were to obtain performance data at simulated altitude conditions with a 40:1 area ratio nozzle and to compare the experimental data with theoretical and predicted performance to determine the space performance potential of  $\text{OF}_2/\text{B}_2\text{H}_6$ .

### 2. Test Program

The altitude evaluation tests were conducted at U.S.A.F. Arnold Engineering Development Center Rocket Test Cell J-2, Arnold Air Force Station, Tennessee. Thiokol-RMD supplied the test article, support hardware, technical procedures for the test article and propellant facility requirements and engineering liaison. The NASA, Lewis Research Center was the contracting agency and AFRPL, at Edwards Air Force Base, California, sponsored the test program. ARO, Incorporated, the civilian contracting operator of the Center's Rocket Test Facility, performed the tests, data acquisition and data reduction. The corresponding AEDC project designation for this phase of the program was RK0436 and a report (AEDC TR-65-172) will be published by AEDC.

Ten performance tests, each of 2-3 seconds duration, were conducted at pressure altitudes in excess of 125,000 feet and at a nominal chamber pressure level of 150 psia over a mixture ratio range of 2.71 to 3.27. Useful data were obtained for seven tests. As a result of fuel exhaustion during one run and fuel injector feed problems with the S/N 4-5 injector, steady-state operation was not achieved in three of the runs.

### 3. Test Hardware

An uncooled, heat-sink, 2000 pound space thrust combustion chamber and nozzle extension assembly was utilized for the test program. The injector combustion chamber-nozzle extension assembly employed for the altitude performance tests is shown in Figure 30. Both propellant cooled and heat sink vortex injectors were utilized during the test program. The heat sink, copper combustion chamber configuration is discussed in detail in Section IV. A. 3. b.

Five vortex injectors were used in the altitude performance testing program. Two were propellant cooled (S/N 2-2 and S/N 1A-6) and the remainder were heat sink types (S/N 1-1, S/N 2-3, S/N 4-5). These injector configurations are discussed in more detail in Section IV. A. 3. a.

A chromium copper heat sink nozzle extension, with a fifteen degree half angle divergence was employed to provide an expansion ratio of 40:1 (Figure 30). A conical nozzle was chosen since the performance of the nozzle contour is well characterized. Static pressure taps were provided in the nozzle to determine the pressure distribution along the nozzle wall. High response, foil type thermocouples mounted flush with the combustion-side surface were also located along the nozzle extension wall to obtain heat transfer data.

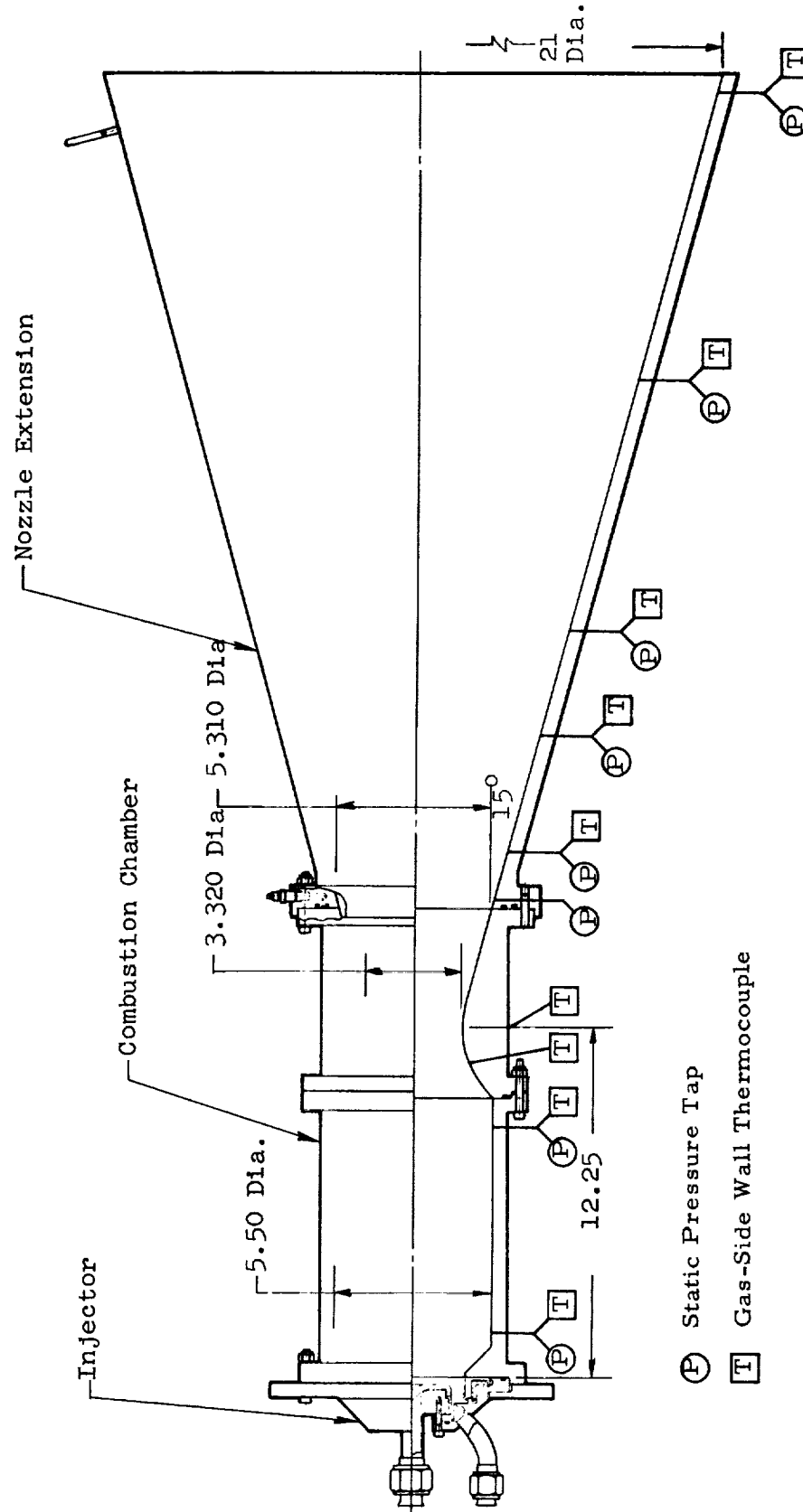


Figure 30. Altitude Evaluation Thrust Chamber and Nozzle Extension Assembly

#### 4. Test Facility

##### a. Description

The test article was installed in the J-2 Propulsion Engine Test Cell at AEDC (Figure 31). the J-2 facility is a horizontal test cell for testing rocket engines at simulated high altitudes. Axial thrust was transmitted through the thrust adaptor to a load cell mounted in a double-flexure column on the engine center line. A remotely operated thrust stand calibrator was used to obtain pre-fire and post-firing thrust system calibrations.

The propellant supply system included two cell mounted run tanks with a tankage capacity of five gallons of oxidizer and five gallons of fuel. A gaseous helium system was used to pressurize the propellants.

Propellants were supplied to the combustion chamber at a predetermined flow-rate and mixture ratio by controlling the gas pressure in the propellant tanks and flowing through cavitating venturis. The propellant tankage and lines up to the main propellant valves were jacketed to maintain propellant feed temperatures. Prior to testing, a high pressure passivation with gaseous fluorine was conducted on the OF<sub>2</sub> propellant system.

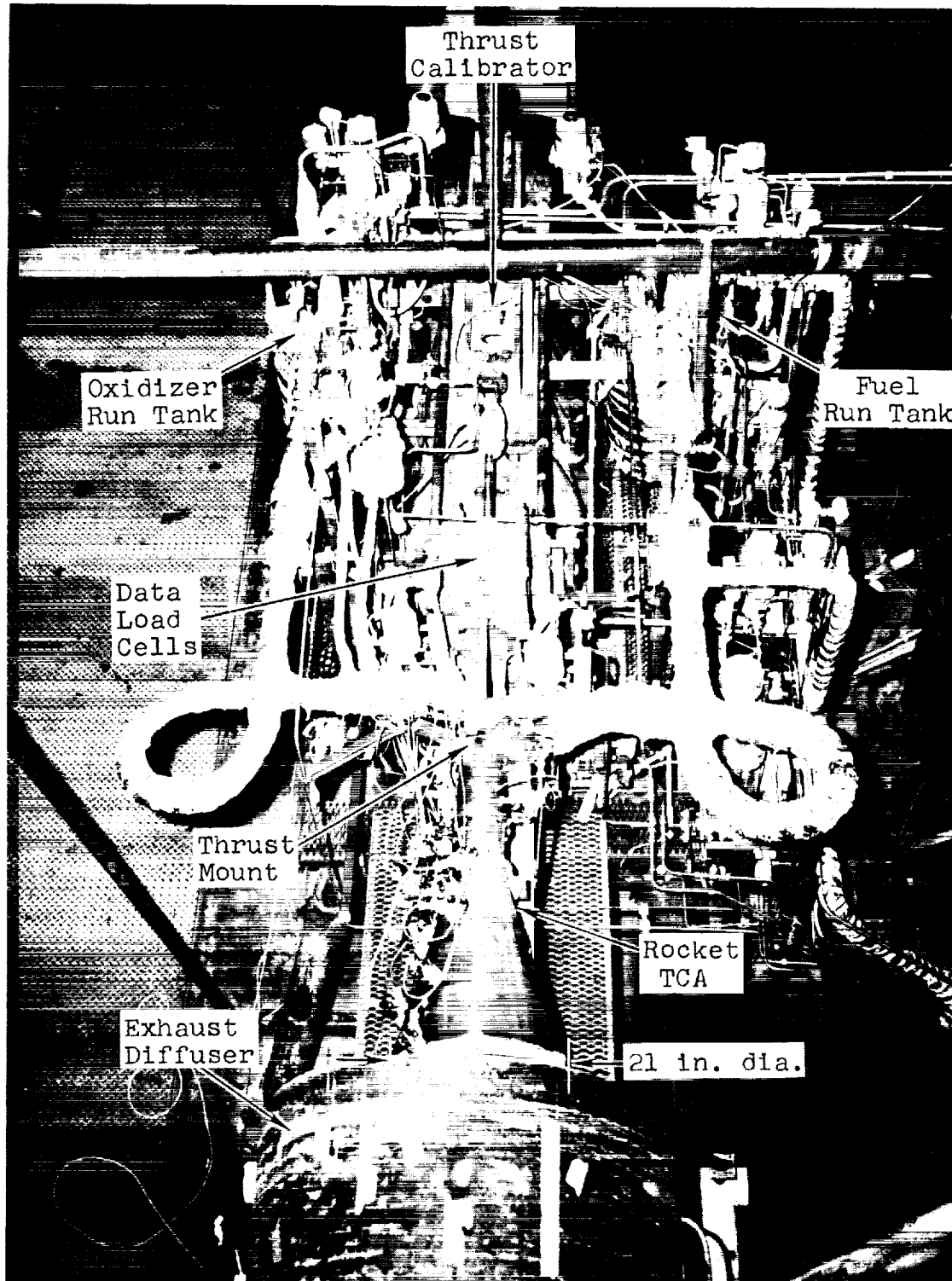
##### b. Data Acquisition

Instrumentation was provided to measure axial thrust, test cell pressure, combustion chamber pressure, propellant supply system pressure and temperatures, nozzle wall pressures and wall temperatures of the entire engine assembly. A schematic showing the relative location of test article instrumentation is shown in Figure 32. Extensive instrumentation was also provided to measure and monitor propellant transfer, pressurization and feed system parameters.

The thrust calibrator weights, thrust load cell, flowmeter and pressure transducers were laboratory calibrated prior to use in this program. After installation of the measuring devices in the test cell, all systems were calibrated at sea-level ambient conditions and again at simulated altitude conditions just before the engine firing. Following a test run, the systems were calibrated at simulated altitude.

Pertinent parameters were recorded on four basic systems (strip chart recorders, oscillograph, digital magnetic tape and magnetic tape). Primary data was recorded on magnetic tape. The transducer outputs were applied to analog-to-frequency converters, and the converter outputs were recorded on magnetic tape using a saturation-level pulse technique. Scan rate was sufficient to provide data reduction printout every 0.05 seconds for each channel.

The primary magnetic tape system was used, along with specific inputs from the secondary magnetic tape system, in a data reduction program to provide a printout of performance data parameters. All tape printouts were also automatically plotted versus time.



6039-410

Figure 31. Thrust Chamber Assembly Installation in Propulsion Engine Test Cell J-2 at Arnold Center



To provide control room preliminary performance and operating data, especially for the back-to-back test firings conducted during the same "air-on" period, pertinent parameters were displayed and recorded on null balance, potentiometer type strip charts and on two photographically recording, galvanometer-type oscillographs.

Test firings were visually monitored by a closed circuit television system. Permanent visual records were made using cell mounted, 16 mm, motion picture cameras.

### c. Test Procedure

A detailed test plan outlining test article assembly and disassembly, pressure checks, pre-run and post-run procedures, propellant handling and loading procedures, data acquisition and test operating conditions were prepared by Thiokol-RMD and transmitted to RTF-AEDC. Thiokol-RMD also provided engineering liaison at RTF-AEDC during facility installation, test program and test facility securing phases. ARO, Inc. performed the tests, data acquisitions and data reduction.

The system operating requirements such as propellant feed temperatures, main propellant valve timing, bleed cycles, injector precool cycle were closely monitored to ensure safe, reliable facility operations and performance in accordance with established practice.

After completion of pre-operational procedures in the test cell area, an electrical calibration of the instrumentation system was conducted at atmospheric conditions. The propellants were transferred into the run tank and manifolds. Following the atmospheric calibrations, the test cell was evacuated to approximately 0.4 psia using the facility exhaust compressors and was maintained at this level during altitude calibrations of the instrumentation systems. After the altitude calibration of the instrumentation systems, the test cell was further evacuated by the steam ejector to a pressure of 0.1 psia or less. The propellants were pressurized to the required levels and the test firing was accomplished.

Following engine shutdown, the steam ejector was shutdown, and postfiring calibrations were performed on the instrumentation systems. The test cell pressure was returned to atmospheric pressure for post-firing hardware and facility inspection.

The last six tests in the program were accomplished in a series of three back-to-back firings. After shutdown of the first test, post-run and pre-run calibrations were conducted at altitude conditions and a second firing was made before the test cell pressure was returned to atmospheric pressure. These tests were conducted in this manner in order to expedite the test program to avoid AEDC facility scheduling conflicts with other programs.

## 5. Data Reduction

Measurements of axial thrust, combustion chamber and test cell pressures, and propellant pressures, temperatures, and flow rates were recorded on magnetic tape as frequencies and translated into digital form. Average values of each parameter was computed at 0.05-sec intervals for each firing. These average values were then



used in determining the calculated performance parameters and efficiencies over the stable portion of each test.

The following is a list of symbols and subscripts utilized in the altitude performance calculations.

$A_e$	Nozzle exit area, in. <sup>2</sup>
$A_t$	Throat area, in. <sup>2</sup>
$C_F$	Thrust coefficient
$C^*$	characteristic exhaust velocity, ft/sec
$\xi$	Nozzle area ratio, $A_e/A_t$
$F$	Thrust, lb.
$G_o$	Gravitational constant, -32.174 lb <sub>m</sub> - ft/lb <sub>f</sub> -sec <sup>2</sup>
$I_{sp}$	Specific impulse, lb <sub>f</sub> -sec/lb <sub>m</sub>
$I_{vac}$	Specific impulse at $P_a = 0$ , lb <sub>f</sub> -sec/lb <sub>m</sub>
$P_a$	Altitude pressure, psia
$P_{ch}$	Chamber pressure, psia
$O/F$	Mixture ratio, (oxidizer/fuel)
$\dot{w}$	Flow rate, lb <sub>m</sub> /sec
$\eta$	Efficiency, %
$\lambda$	Non-axial momentum nozzle loss
$C_D$	Nozzle throat loss
$C_V$	Nozzle frictional drag loss (not including nozzle extension)
'	Indicates theoretical value

Subscripts:

vac	Value at $P_a = 0$
(cor)	Corrected for momentum loss, friction loss and heat loss

subscripts (continued):

o	oxidizer
f	fuel
t	total

Static chamber pressure measurements were taken at the injector end of the chamber and at the entrance to the nozzle. Since theoretical corrections made to the nozzle inlet static pressure for combustion gas velocity in the chamber agreed with the measured injector end static pressure, this measurement was utilized for the performance calculations.

Test performance data were calculated as follows:

$$CF = \frac{F}{A_t P_c} \quad (1)$$

$$I_{sp} = \frac{F}{\dot{w}_t} \quad (2)$$

$$C^* = \frac{P_c A_t}{\dot{w}_t} g \quad (3)$$

for these tests  $A_t = 8.65 \text{ in.}^2$  and

$$\dot{w}_t = \dot{w}_o + \dot{w}_f \quad (4)$$

Vacuum thrust, vacuum specific impulse and vacuum thrust coefficient were calculated by the following equations:

$$F_{vac} = F + P_a A_e \quad (5)$$

$$I_{s_{vac}} = F_{vac} / \dot{w}_t \quad (6)$$

$$C_{F_{vac}} = F_{vac} / P_{ch} A_t \quad (7)$$

where  $P_a$  is the measured test cell altitude pressure and  $A_e = 346.28 \text{ in.}^2$

To provide a better comparison of test vacuum specific impulse and vacuum thrust coefficient data with theoretical values, the calculated vacuum performance data presented in this report were corrected for the nonaxial momentum resulting from exhaust flow divergence of a 15-deg half-angle conical nozzle, nozzle throat discharge and friction losses and combustion efficiency ( $\eta_{c^*}$ ). These corrections were calculated using the formulas:

$$C_{F \text{ vac}(\text{cor})} = C_{F \text{ vac}} / C_D \cdot C_V \cdot \lambda \quad (8)$$

$$I_{sp \text{ vac}(\text{cor})} = \frac{I_{sp \text{ vac}}}{\eta_{c^*} \cdot C_D \cdot C_V \cdot \lambda} \quad (9)$$

where  $\lambda = 1/2 (1 + \cos 15^\circ) = 0.983$

$C_D C_V = 0.98$  (value used for sea level tests - does not include nozzle extension friction losses)

Theoretical data were obtained from the Thiokol-RMD aerothermochemical one-dimensional isentropic flow computer program. Heat of formation values for the propellants were based on feed temperatures of -300F and -100F for the  $\text{OF}_2$  and  $\text{B}_2\text{H}_6$  respectively. The following efficiencies were then calculated:

$$\eta_{c^*} = \frac{c^*_{\text{test}}}{c^*_{\text{theor}}} \quad (10)$$

$$\eta_{C_F} = \frac{C_{F \text{ vac}(\text{cor})}}{C_{F'}}$$

(11)

$$\eta_{I_{sp}} = \frac{I_{sp \text{ vac}(\text{cor})}}{I_{sp'}}$$

(12)

## 6. Test Results

### a. Performance

Ten performance tests were conducted in the altitude performance evaluation program. Useful performance data were obtained from seven tests and are summarized in Table VIII. These results demonstrated the extremely high performance potential

TABLE VIII  
OF<sub>2</sub>/B<sub>2</sub>H<sub>6</sub> ALTITUDE TEST SUMMARY

			Measured Data			Calculated Performance							Remarks			
Injector	AEDC Test No.	Date	P <sub>a</sub> (psia)	Pressure Altitude (ft)	Thrust (lb)	W <sub>t</sub> lb/sec	P <sub>ch</sub> (psia)	O/F	C* Test (lps)	I <sub>sp</sub> vac lb-sec lbm	C <sub>F</sub> vac	% c <sup>2</sup> Shifting		Vacuum Thrust (lb)	I <sub>sp</sub> vac Corrected lb-sec lbm	C <sub>F</sub> vac Corrected
X315455B S/N 2-2 Propellant Cooled	1	4/2/65	.050	127,700	2197	6.26	138.3	3.11	6154	354	1.851	87.9	2214	409	1.883	Good run
	3	4/4/65	.0477	129,600	2307	6.32	138.7	2.71	6104	356	1.880	87.3	2252	415	1.913	Good run
X315455B S/N 1A-6 Propellant Cooled	2	4/9/65	.0404	133,200	2238	6.32	143.2	2.98	6311	368	1.876	90.1	2324	415	1.908	Oxidizer Injector Burnout at 1.6 sec due to Fuel Injector leak
X316357 S/N 1-1 Heat Sink	4	4/23/65	.0471	129,180	2263	6.31	141.3	2.96	6216	361	1.871	88.8	2279	414	1.903	Good run Slight Test Stand and Fuel Injector leak
X316357 S/N 2-3 Heat Sink	5	4/29/65	.0427	131,680	2256	6.31	140.9	2.97	6210	360	1.866	88.7	2271	413	1.898	Good run
	7	4/30/65	.0389	134,480	2308	6.295	143.4	2.73	6343	369	1.872	90.7	2322	414	1.904	Good run
	8	4/30/65	.0375	135,000	2408	6.30	149.8	3.27	6623	384	1.868	94.5	2421	414	1.900	Good run - Injector Operating Shift

$$(1) \text{ Thrust (vac)} = \text{Thrust}_{(\text{meas})} + P_a A_e$$

$$(2) I_{sp \text{ vac}} \text{ corrected} = \frac{I_{sp \text{ vac}} (\text{test})}{\left( \frac{P_a}{P_{a \text{ test}}} \right) \left( \frac{\lambda}{\lambda_{\text{test}}} \right)}$$

$$(3) C_{F \text{ vac}} \text{ corrected} = \frac{C_{F \text{ vac}} (\text{test})}{\lambda}$$

$$\lambda = 0.983$$

under altitude conditions. The maximum vacuum specific impulse of 384  $\text{lb}_f/\text{lb}_m$  obtained at a  $c^*$  of 94.5% corresponds to 90.6% of theoretical shifting equilibrium. The measured thrust coefficients consistently gave values on the order of 96% of theoretical shifting equilibrium values.

Figure 33 presents a plot of the performance parameters (characteristic exhaust velocity, specific impulse, and thrust coefficient) versus mixture ratios. For reference, the theoretical curves of one hundred percent and ninety percent characteristic exhaust velocity are shown. In the case of specific impulse and thrust coefficient the theoretical curves shown are for shifting and frozen equilibrium.

Two test firings (Runs 1 and 3) employed the S/N 2-2 propellant-cooled injector. The performance for these two tests gave specific impulse values of 351 and 354  $\text{lb}_f\text{-sec}/\text{lb}_m$  at  $c^*$  values of 88-89% respectively of theoretical shifting performance. Data obtained from a typical firing are shown in Figure 34. The injector was in excellent condition after these two tests. This injector has accumulated 16.1 seconds of operation over six test firings with no evidence of deterioration.

One test (Run 2) was made with the S/N 1-A6 propellant cooled injector. During this test, a fuel leak was observed at the fuel injector. Post test inspection revealed an oxidizer injector burnout. Stable engine operation was obtained up to a duration of 1.6 seconds at which time oxidizer injector erosion appears to have begun as evidenced by a decay in engine parameters. Injector failure is attributed to off mixture operation as a result of the fuel injector leak at a Teflon O-ring seal. Attachment bolts at this seal had loosened either during injector cooldown prior to start or during operation. Prior to the AEDC test this injector had completed four sea level firings with no difficulty. Data obtained during the stable portion of the test indicated a specific impulse of 365  $\text{lb}_f\text{-sec}/\text{lb}_m$  and a  $c^*$  of 90.1%. The test thrust coefficient was 96.7% of the theoretical vacuum shifting equilibrium value. Thus, although the  $c^*$  value was lower ( $\approx 5\%$ ) than that obtained during sea level testing, probably as a result of the fuel leak, the high percentage of  $C_F$  obtained indicates the high performance potential of  $\text{OF}_2/\text{B}_2\text{H}_6$ .

Test 4 was conducted using the S/N 1-1 heat sink injector. After approximately 1.75 seconds, a fuel leak was observed at the test stand fuel check valve, located in the fuel purge system. Post fire inspection also revealed a pinhole leak on the back face of the oxidizer injector. Performance data obtained prior to indication of a fuel leak gave specific impulse of 359  $\text{lb}_f\text{-sec}/\text{lb}_m$  at a  $c^*$  of 88.8%. Again, the  $c^*$  value was lower than that obtained during sea level testing but a high  $C_F$  ( $\eta C_F = 96.4\%$ ) was obtained.

Tests 5 and 6 were made in the same "air on" period using the S/N 2-3 heat sink injector. Test 5 was successfully completed and preliminary data reviewed. All parameters appeared normal and Test 6 was made. However, because of faulty fuel loading indications, the engine ran out of fuel after 0.5 seconds. Post-fire inspection revealed only slight erosion on the oxidizer injector. Tests 7 and 8 were also made in the same "air on" period with the S/N 2-3 injector. Specific impulse values of 358 to 382  $\text{lb}_f\text{-sec}/\text{lb}_m$  were obtained at  $c^*$  values of 88.7 to 94.5% of theoretical values for

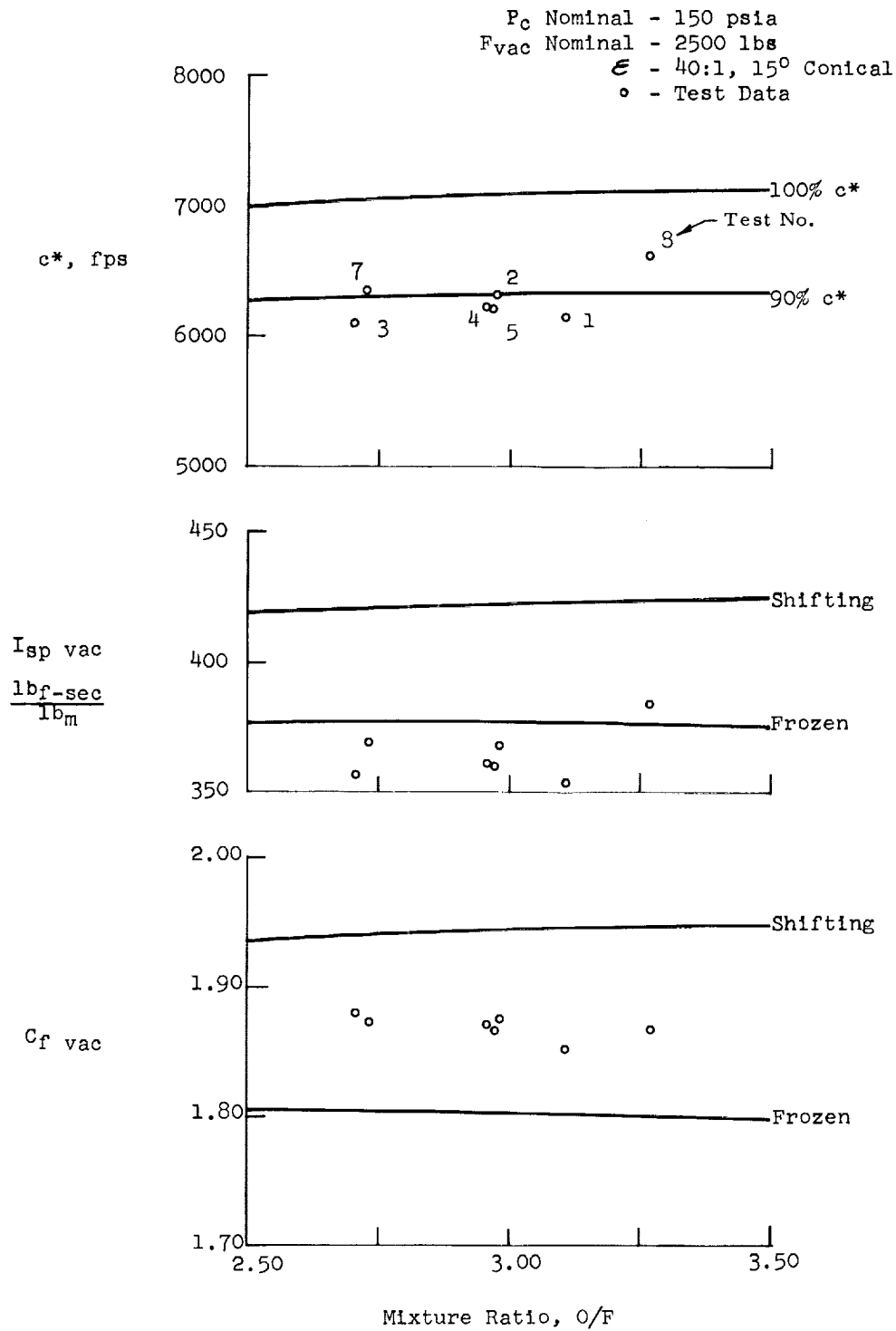


Figure 33. Experimental Altitude Performance -  $OF_2/B_2H_6$  - AEDC Tests

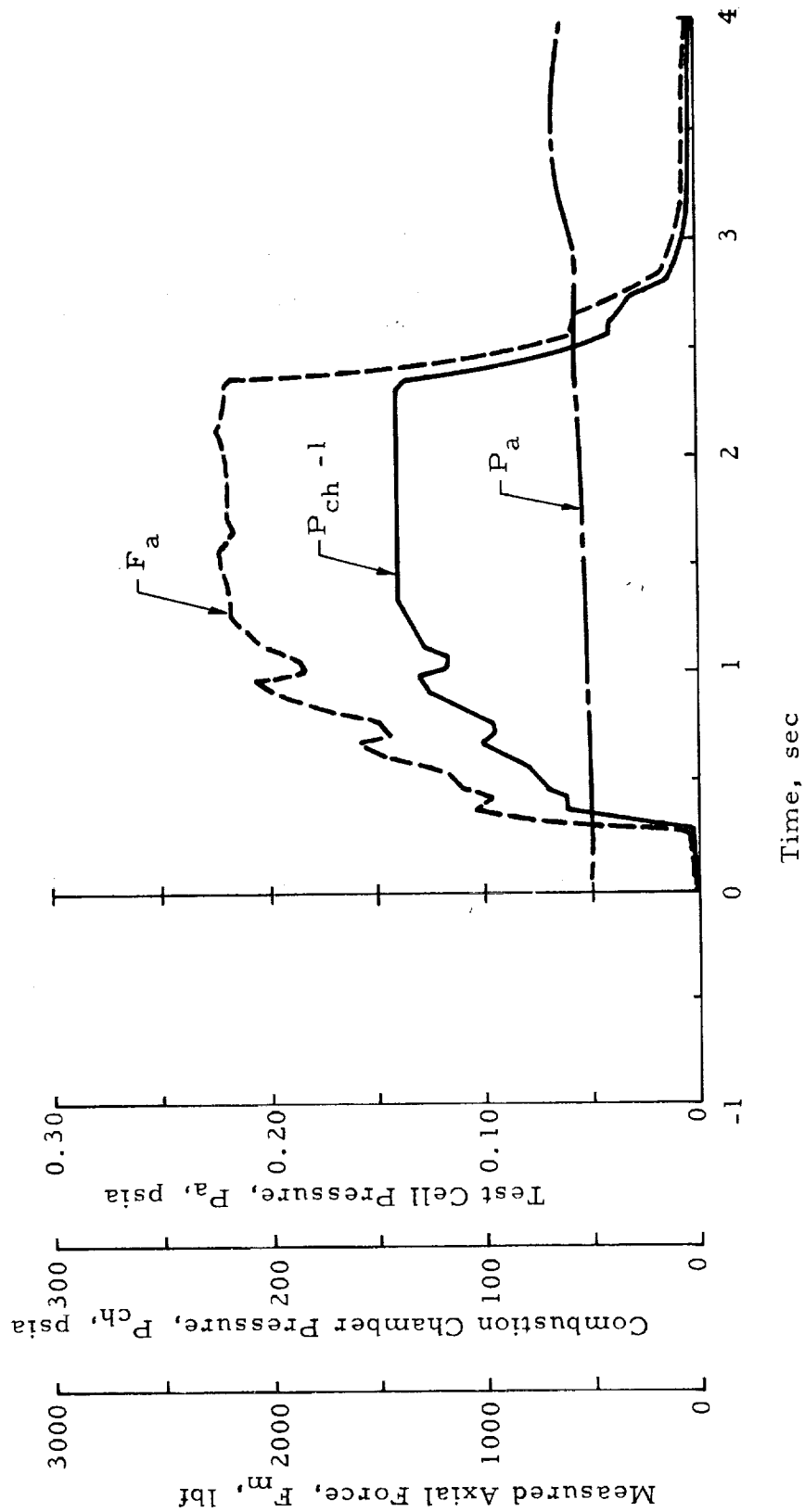


Figure 34. Typical Simulated Altitude Data Trace (AEDC Data)

the three tests. Tests 5 and 7 demonstrated steady state operation during the entire run. During test run 8, a downward operating shift in all engine parameters occurred at 1.68 seconds. Performance data presented for this run are taken over a steady state period of 0.63 seconds prior to this operating shift. The performance variation exhibited by the S/N 2-3 injector during test 8 is attributed to an oxidizer injector spray pattern change as a result of a shift in the orifice discharge coefficient. This condition in the oxidizer orifices had been observed during water flow calibration. It is believed that the increased oxidizer flow for this test to obtain an O/F of 3.3 was sufficient to cause the injector to operate in this critical regime.

The last two tests (Runs 9 and 10) were conducted with the S/N 4-5 heat sink injector in the same "air on" period. Although scheduling did not permit complete sea level evaluation of this injector prior to the AEDC tests, it was believed that this injector would provide high performance levels. The test runs exhibited large amplitude ( $\approx \pm 30\%$ ) 80 cps oscillations in chamber pressure, thrust, and fuel injector pressure. Consequently, no valid performance data was acquired during these two tests. This injector incorporating fuel manifold spacers was later tested at sea level at Thiokol-RMD. In these tests (described in Section IV A.5.c.3) chamber pressure oscillations were reduced but not eliminated.

#### b. Nozzle Pressure

Nozzle wall static pressure measurements were obtained at six axial stations along the nozzle extension wall (Ref. Figure 32). Figure 35 is a plot of the ratio of measured nozzle pressure to injector end chamber pressure versus the nozzle area ratio. Test data presented represent an average of two pressure readings taken  $90^\circ$  apart at each station. For comparison, the theoretical frozen and shifting equilibrium values are shown on Figure 35. The measured nozzle pressure data show good agreement with the theoretical shifting equilibrium values.

Calculations using the measured static wall pressures in the nozzle and injector end chamber pressure corrected to total pressure to obtain thrust, show agreement within one-half of one percent of the measured thrust for the altitude tests. These calculations provide corroboration of the experimentally measured thrust values and calculated nozzle thrust coefficients.

#### c. Performance Comparisons

Since the primary purpose of the AEDC experimental runs was to determine the performance of  $\text{OF}_2 / \text{B}_2\text{H}_6$  using a high area ratio nozzle ( $\epsilon = 40:1$ ), an evaluation of the  $\text{OF}_2 / \text{B}_2\text{H}_6$  altitude performance data has been made. This evaluation was made in order to compare the test data with theoretical and predicted performance allowing for combustion losses and nozzle expansion losses including kinetic losses.



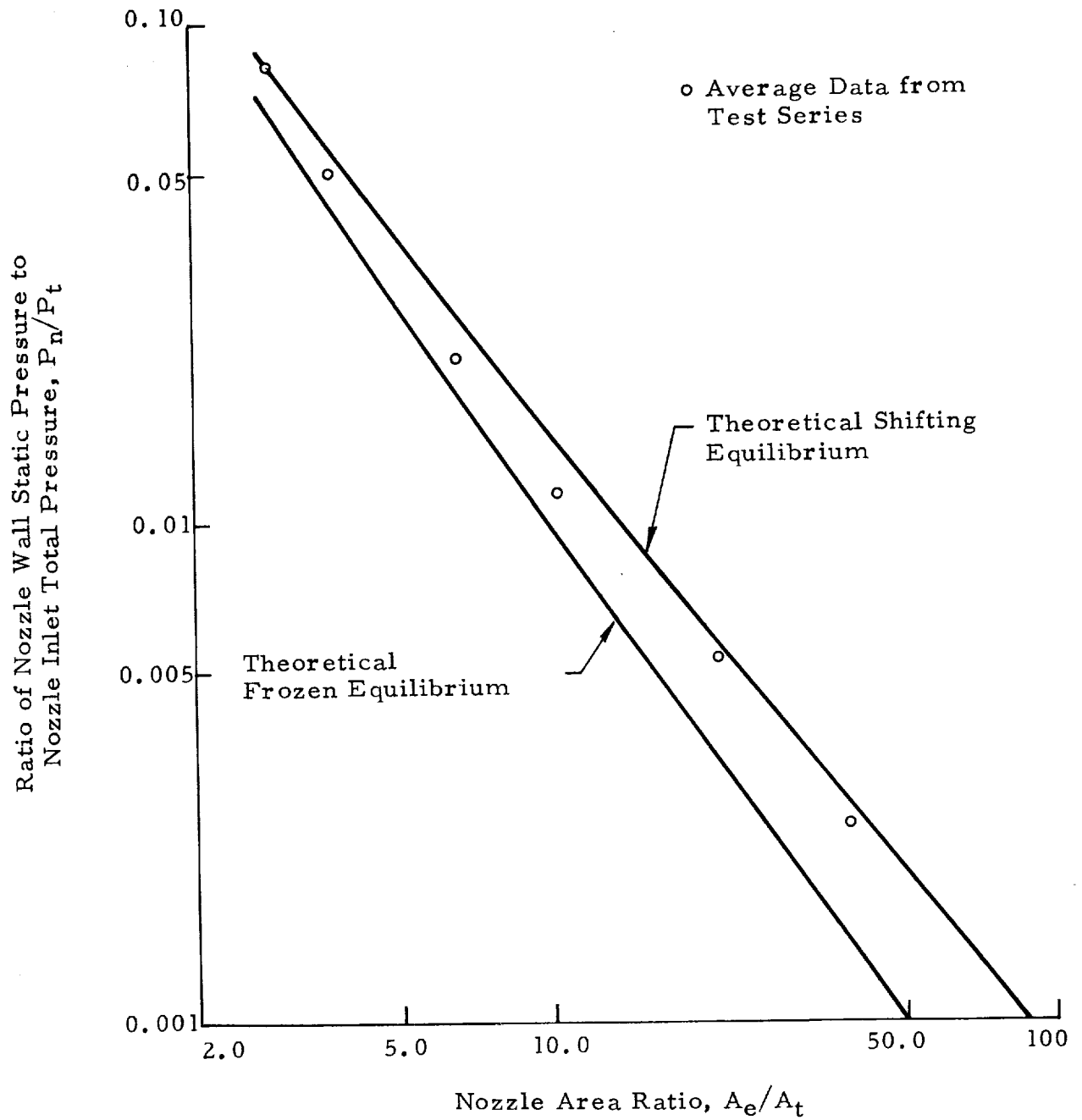


Figure 35. Nozzle Extension Pressure Distribution

Conventionally when comparing measured rocket performance with theory, two primary losses are usually considered. These losses are combustion efficiency losses and expansion nozzle losses. Combustion losses normally considered are those associated with combustion upstream of the sonic point or throat and assume burning is completed prior to throat entry. The expansion nozzle losses normally considered are comprised of geometrical losses (divergence  $\lambda$ , and throat discharge,  $C_D$ ), drag losses (friction,  $C_V$ ).

The performance comparisons presented in this section are based on combustion efficiency losses, nozzle divergence losses and nozzle throat and expansion (not including nozzle extension) frictional losses previously discussed in section IV.B.5. Table IX shows the corrections made for each experimental data point and presents a comparison of the corrected data with theoretical shifting equilibrium data.

Figure 36 shows the theoretical shifting and frozen specific impulse and thrust coefficient curves with superimposed test data, adjusted for  $c^*$  efficiency, nozzle friction ( $C_D \cdot C_V$ ) and divergent ( $\lambda$ ) losses. It is apparent from this figure that the corrected experimental impulse and thrust coefficient values are essentially equal to the theoretical shifting values.

TABLE IX

Corrected Specific Impulse and Thrust Coefficient

Run No.	Vacuum Test Data						
	(1) $C_F$	$I_{sp} \text{ lb}_f \text{ sec}/\text{lb}_m$	(1) $\eta_{c^*}$	(2) $C_{Fvac}(\text{cor})$	(3) $I_{spvac}(\text{cor})$	$\eta_{CF}$	$\eta_{Isp}$
1	1.851	353.7	87.9	1.921	417.7	.988	.983
2	1.876	367.6	90.1	1.947	423.6	1.002	.999
3	1.880	356.4	87.3	1.952	423.8	1.006	1.004
4	1.871	361.2	88.8	1.942	422.1	.999	.996
5	1.866	359.9	88.7	1.937	421.1	.996	.993
7	1.872	368.8	90.7	1.943	422.1	1.002	1.000
8	1.868	384.3	94.5	1.939	422.1	.997	.993

(1) Test data corrected for  $P_a A_e$

(2) Vacuum  $C_F$  corrected for ( $\lambda$ ), ( $C_d \cdot C_v$ )

(3) Vacuum impulse corrected for  $\lambda$ ,  $C_d \cdot C_v$ ,  $\eta_{c^*}$

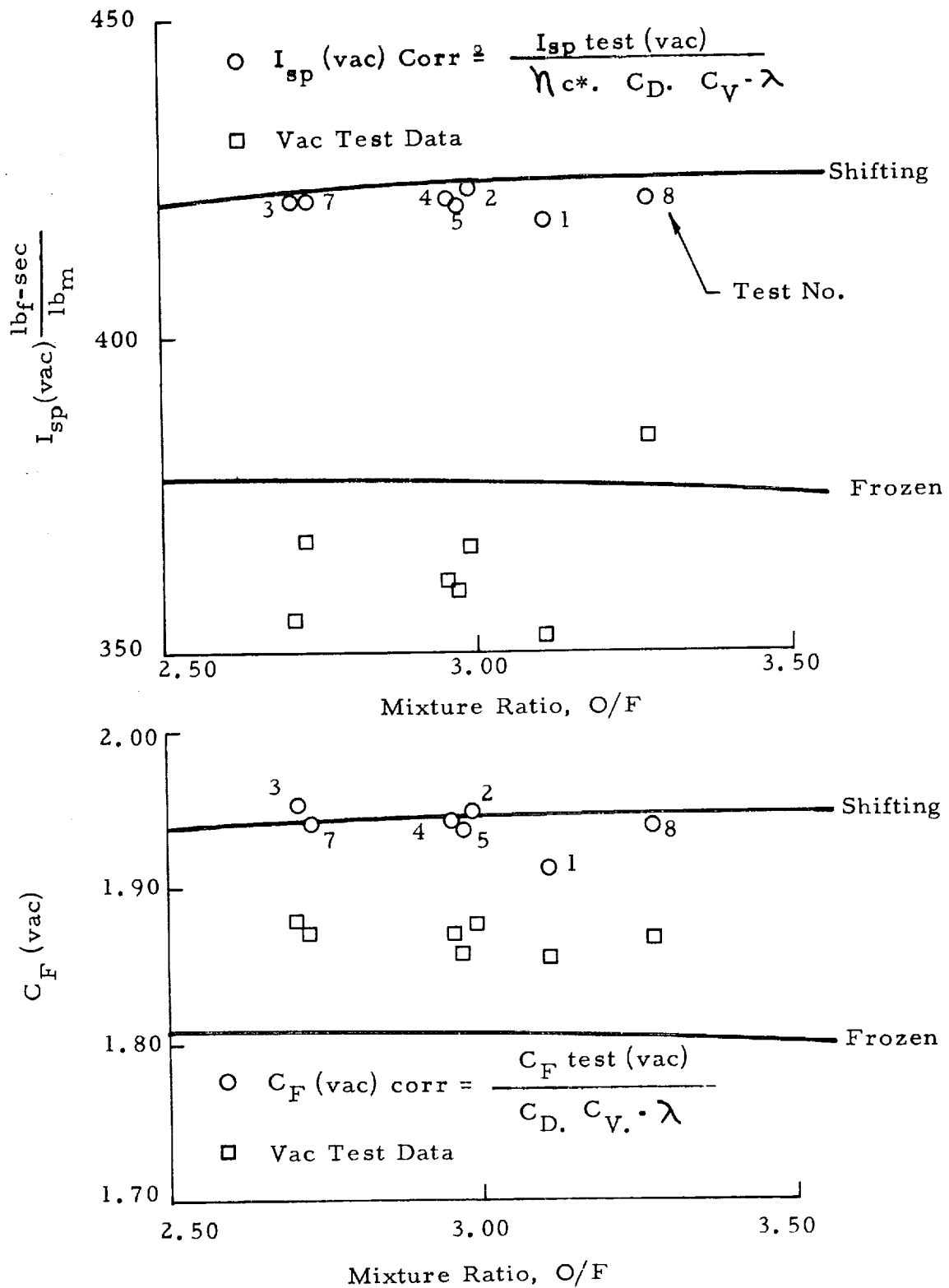


Figure 36. Experimental Altitude Performance Corrected for  $\lambda$ ,  $C_D \cdot C_V$ , %  $c^*$

The results indicate that  $\text{OF}_2/\text{B}_2\text{H}_6$  can deliver high performance with a 40:1 area ratio nozzle. It is significant to note that a maximum experimental specific impulse of  $384 \text{ lb}_f\text{-sec}/\text{lb}_m$  was obtained, which corresponds to 91% of theoretical shifting equilibrium. The experimental specific impulse data reflect a direct correlation with the experimental  $c^*$  data (i.e., lower  $I_{sp}$  corresponds to lower  $c^*$  and higher  $I_{sp}$  corresponds to higher  $c^*$ ). However, the thrust coefficient which is not significantly affected by  $c^*$ , shows consistently high experimental values over the range of  $c^*$  values obtained during this test program. Experimental vacuum thrust coefficients on the order of 96% of theoretical shifting equilibrium values were obtained on all tests. These high efficiencies were especially significant, in that they provide excellent agreement with predicted values based on conventional nozzle performance corrections (i.e.,  $\lambda = 0.983$  and  $C_D \cdot C_V = 0.98$ ). Thus, an indication high level of confidence in the high space performance potential of  $\text{OF}_2/\text{B}_2\text{H}_6$  has been demonstrated.

The corrected vacuum specific impulse and thrust coefficient data presented in Table IX shows that for the test conditions evaluated (i.e.,  $\xi = 40:1$ ,  $P_c = 150 \text{ psia}$  and  $\text{O}/\text{F} = 2.7 - 3.3$ ),  $\text{OF}_2/\text{B}_2\text{H}_6$  performance approaches theoretical shifting equilibrium. These comparisons reveal that negligible kinetic losses were obtained in this program, and it appears that high space performance with  $\text{OF}_2/\text{B}_2\text{H}_6$  is feasible with high area ratio nozzles (i.e.,  $>>40:1$ ).

Figure 37 presents theoretical shifting specific impulse as a function of high nozzle area ratios for several space storable propellant combinations. It can be seen from Figure 37 that  $\text{OF}_2/\text{B}_2\text{H}_6$  offers essentially the same space performance potential as the  $\text{O}_2/\text{H}_2$  propellant combination. Another characteristic contributing to the high performance of  $\text{OF}_2/\text{B}_2\text{H}_6$  is the comparatively low gamma (ratio of specific heats) of the exhaust gases as contrasted to that of such propellant combinations as  $\text{F}_2/\text{H}_2$  and  $\text{O}_2/\text{H}_2$ . This results in more significant increases in space specific impulse as nozzle expansion area ratio is increased. Coupled with the encouraging altitude performance results and mission studies,  $\text{OF}_2/\text{B}_2\text{H}_6$  offers promise as a high performance, space storable propellant combination.

In an effort to provide a more rigorous comparison of test performance with theoretical values, corrections to the vacuum performance data for nozzle extension wall friction losses and chamber-nozzle extension heat losses were also made. These corrections which were based on theoretical nozzle drag losses and averaged heat total heat transfer loss determined from calculated heat flux profiles are presented in detail in Appendix B. Also presented in Appendix B is a discussion of predicted kinetic performance.

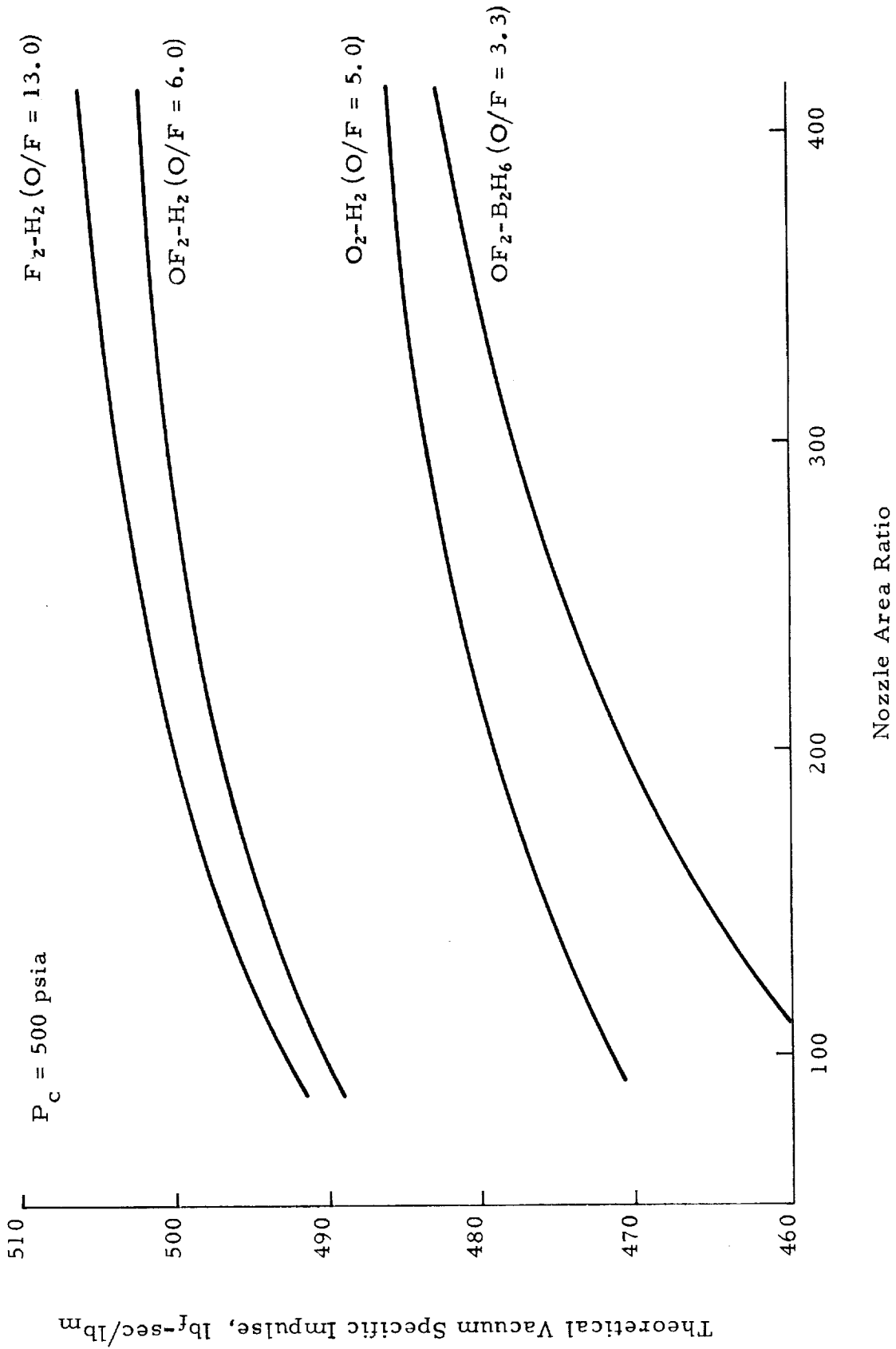


Figure 37. Performance at High  $\epsilon$  for Candidate Space Propellants

The results of this more rigorous performance analysis indicated that the corrected experimental vacuum specific impulse data is about 2.5% above theoretical shifting equilibrium values. A theory (i.e. supersonic combustion) postulating this apparent inconsistency is presented and discussed. Suffice to say, the theory may lead to a more accurate determination of engine performance and merits serious consideration for future investigations in the areas of propellant performance and high area ratio nozzles.

Based on the altitude performance results and the subsequent performance analysis, the following conclusions have been drawn.

- Allowing for combustion losses and nozzle divergence losses, 98% of theoretical shifting equilibrium impulse was obtained.
- Experimental thrust coefficients which were consistently within 96% of theoretical shifting equilibrium values indicate that for the test conditions evaluated, negligible kinetic losses were obtained. Thus, high space performance potential of  $\text{OF}_2/\text{B}_2\text{H}_6$  with high area ratio nozzles ( $>40:1$ ) appears feasible.
- Testing experience at the AEDC facility again has demonstrated that  $\text{OF}_2$  and  $\text{B}_2\text{H}_6$  can be handled safely with normal precautions. This is especially significant in view of the fact that these propellants have never been handled before by AEDC facilities personnel and the fact that AEDC operations are rather confined and not isolated as most rocket test facilities.

## C. 2000-POUND THRUST ABLATIVE COMBUSTION CHAMBER

### 1. Objectives

The objectives of this phase of the program were to design, fabricate and test a 2000-pound thrust ablative chamber to provide ablative design data. These data were to be utilized to determine the applicability and operating limits of ablatives with  $\text{OF}_2/\text{B}_2\text{H}_6$ . Design and fabrication of the unit was completed. However, as a result of reallocation of funds to another phase of the program, testing of the ablative chamber was not conducted.

### 2. Design and Fabrication

The ablative material selection was based on the results of screening tests and analytical studies conducted at the 150-pound thrust level in the previous program. In that program, Fiberite MX-4500 graphite-phenolic gave the lowest experimental erosion rate corroborating the prior analytical ablative predictions that graphite reinforced materials would yield the lowest erosion rate with  $\text{OF}_2/\text{B}_2\text{H}_6$ .

The ablative combustion chamber design shown in Figure 38 embodies a monolithic MX 4500 graphite-phenolic liner, Thiokol-RMD Type 1A Ablatalite passive insulation and a structural shell of 7178 aluminum alloy. The design is based on ten 30 second duration tests (limited by test stand tankage) operating at an initial chamber pressure of 150 psia, a mixture ratio of 3.0, a combustion efficiency of 98% (corresponding to a predicted combustion temperature of 6270F) and a maximum external structural shell temperature of 400F, which is considered as a reasonable limit for spacecraft requirements.

The material thicknesses were sized by a Thiokol-RMD analytical ablative prediction program (Reference 11). This program, made available for use in this design, predicts erosion, char depths, and temperature profiles for an ablative chamber design operating under any given set of conditions. Conversely, the prediction program also permits determination of the required material properties to maintain a predetermined level of performance for a given set of operating conditions. The design criteria (erosion, char, temperature gradients) were confirmed by test results obtained in the previous program. Figure 39 shows the predicted performance (i. e. throat erosion) for this design based on the analytical evaluation.

The Thiokol-RMD Type 1A Ablatalite is a low density, low conductivity, castable passive insulation which minimizes heat soak into the structural shell. The use of Ablatalite insulation has been successfully demonstrated with ablative chamber designs

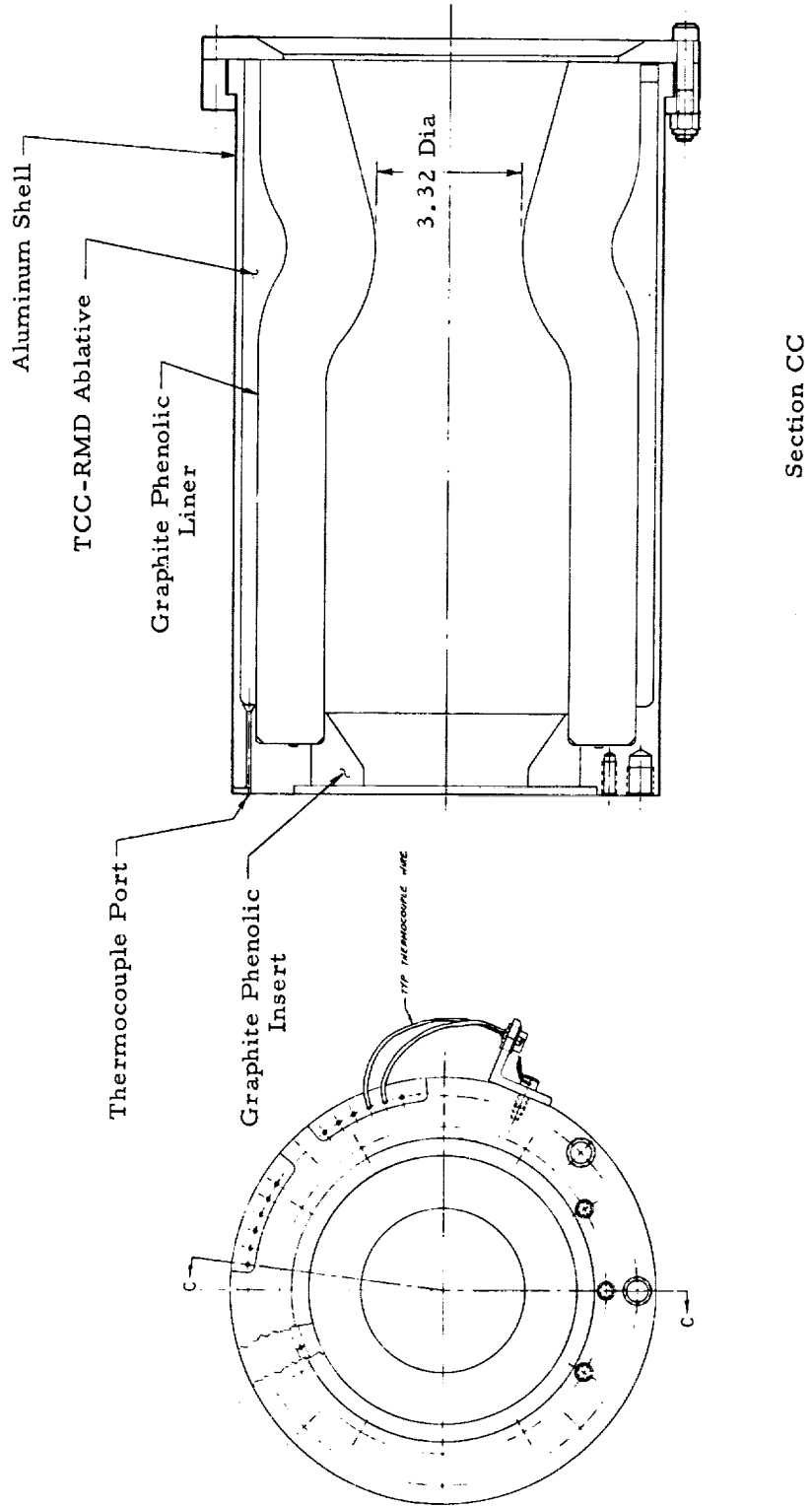


Figure 38. 2000-lb Thrust Ablative Chamber Design



F = 1610 lb (Sea Level)

c\* = 98%

O/F = 3.0

Duty Cycle = Four, 30 sec tests

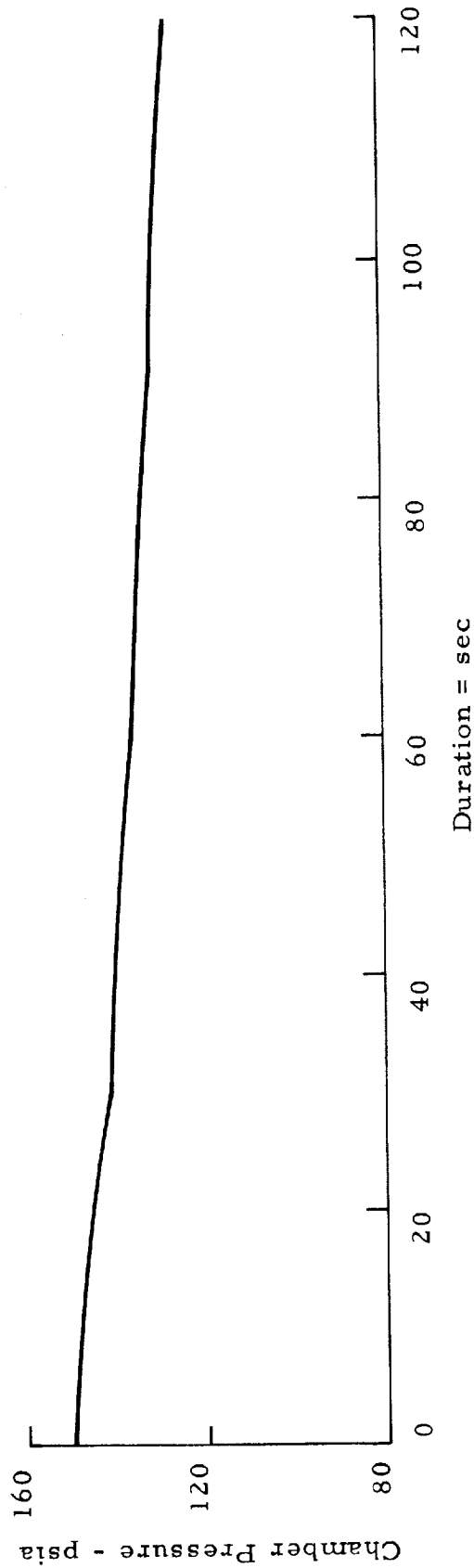


Figure 39. Predicted Ablative Chamber Performance -  $\text{OF}_2/\text{B}_2\text{H}_6$

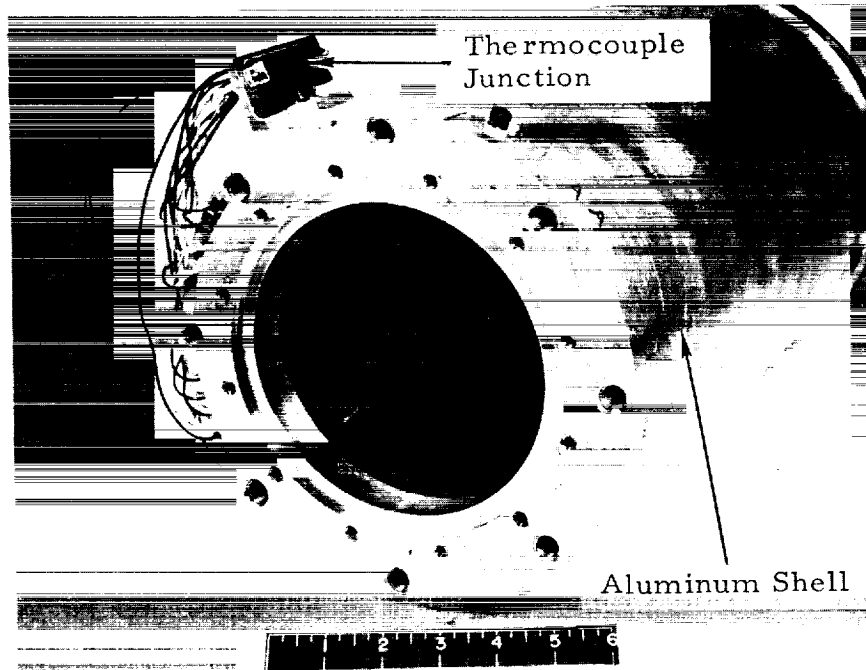
tested up to the 10,000-pound-space thrust level during Corporate funded test programs.

The structural shell, 7178 aluminum alloy, has a mounting flange for the injector. In addition, it furnishes support for the ablative liner and backup insulation. The Ablatalite insulation is cast and cured in place between the aluminum shell and ablative liner.

As part of the design requirements, a detailed process specification (Thiokol-RMD Specification No. 7548) was prepared to provide quality assurance provisions for the fabrication and assembly of the ablative combustion chamber. In addition, the ablative liner is instrumented at various depths with high temperature thermocouple probes in the chamber barrel and nozzle throat plane to provide design data on ablative wall temperatures.

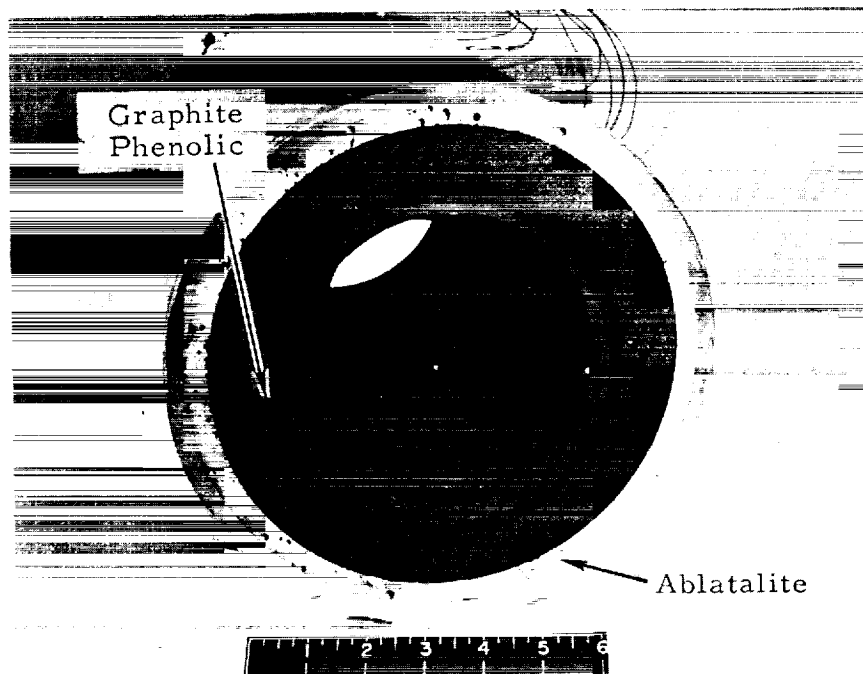
Fabrication of the ablative combustion chamber assembly was completed (Figure 40). As a result of technical direction during the course of the program, funding for the ablative chamber test phase was allocated to support the altitude performance program (i. e. heat sink injector effort).

Based on other hot test results at Thiokol-RMD it is estimated that the graphite-phenolic ablative material will provide durability with  $\text{OF}_2 / \text{B}_2\text{H}_6$ , which is approximately equivalent to that obtained with silica reinforced ablatives with  $\text{N}_2\text{O}_4 / 50-50$ . The significance of this equivalence in ablative performance indicates that propulsion performance upgrading can be achieved within acceptable throat erosion limits for certain limited duty cycle missions.



6037-353

Injector End



6037-352

Nozzle End

Figure 40. Ablative Chamber Assembly

## D. SPECIFIC HEAT DETERMINATION OF LIQUID OF<sub>2</sub>

### 1. Object

The objective of this task was to experimentally determine the specific heat of liquid OF<sub>2</sub> over a temperature range of -196 to -95°C, and a pressure range of 50 psia to 300 psia. These experiments were undertaken to provide design data for the thrust chamber cooling study phase of the program. This effort was undertaken since various estimates of specific heat values from 0.20 Cal/g-°C to 0.35 Cal/g-°C have been reported in the literature(Ref.12,13) and reliable experimental data was not available.

### 2. Test Program

A total of 26 specific heat determinations were made over a temperature range of -196 to -75°C and a pressure range of 10 psia to 300 psia. No variation of specific heat capacity for the pressure range investigated was observed.

In order to obtain accurate data, calorimeter calibrations were performed employing liquid oxygen and liquid propane to encompass the required temperature range for the OF<sub>2</sub> experiments. A total of 20 test runs were made over a temperature range of -190 to -40°C to obtain the calorimeter calibration.

The OF<sub>2</sub>, which is commercially available at a purity of 97%, was distilled to a purity of 99.5% for use in these experiments. The purity of the calibrating fluids (liquid oxygen and liquid propane) was 99.9%.

### 3. Test Apparatus

The calorimeter employed in these studies is a modification of that described by Johnston et al (Reference 14). A diagram of the apparatus is shown in Figure 41. Figure 42 shows the apparatus installed in the laboratory for leakage tests.

The OF<sub>2</sub> container was constructed of copper tubing. Radial fins running longitudinally were press fitted into the sample container. The fins were included to promote thermal transfer. The container was wound with reference grade platinum wire which served as a temperature sensing element and a heating element.

The OF<sub>2</sub> container is housed within two concentric copper cylinders which served as constant temperature jackets. The inner jacket is wound with nichrome wire which is utilized to control temperature in the calorimeter. The space between

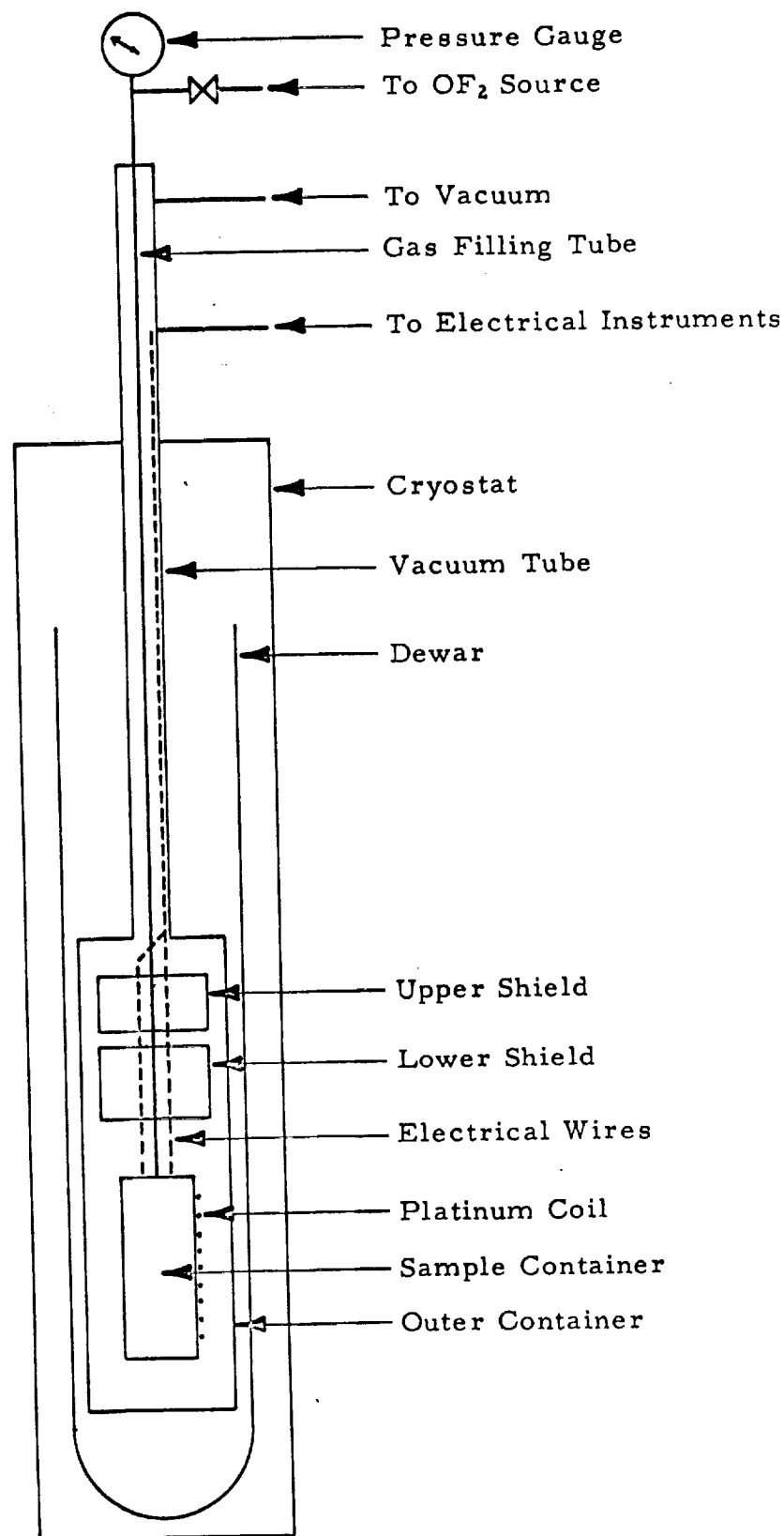
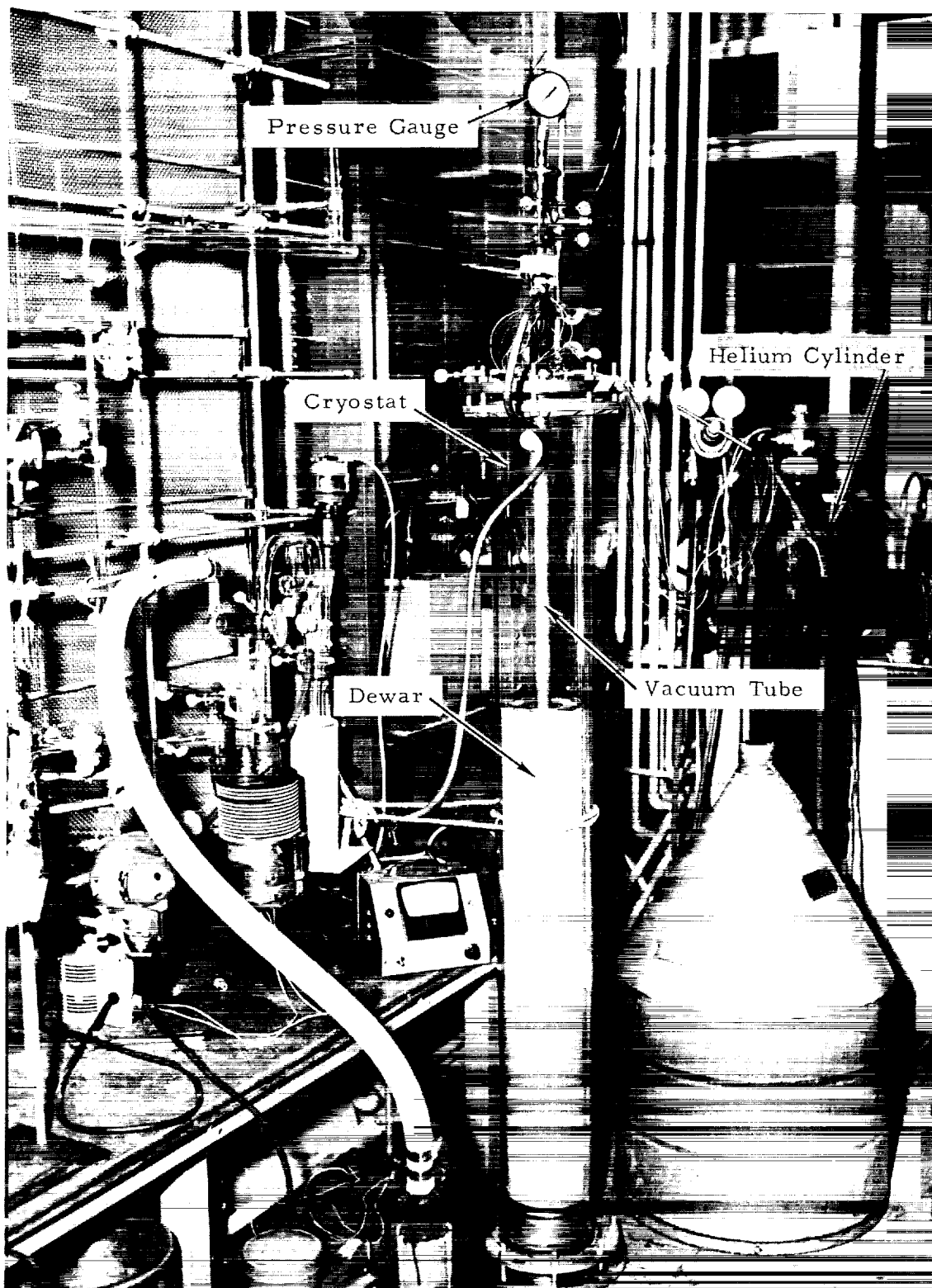


Figure 41.  $\text{OF}_2$  Specific Heat Apparatus Schematic



6039-102

Figure 42.  $\text{OF}_2$  Specific Heat Laboratory Apparatus

the inner and outer jacket serves as a thermal barrier for the calorimeter when it is evacuated. However, when the calorimeter is being charged, this cavity is filled with helium to promote thermal transfer. A detailed description of the apparatus is presented in Appendix C.

#### 4. Apparatus Calibrations and Test Procedures

Prior to the  $\text{OF}_2$  specific heat measurements, apparatus calibrations were conducted to provide the necessary data and to permit accurate specific heat measurements. Calibrations were conducted to determine characteristics of the platinum temperature sensing element and to determine the heat leak rate to the associated components as a function of temperature.

##### a. Calibrations

The platinum resistance wire which was used as the temperature sensing element was calibrated to determine the resistance change as a function of temperature. The calibration was accomplished by obtaining resistance measurements at various temperatures corresponding to the vapor pressure of liquid oxygen which was admitted into the sample container.

The calorimeter constant (i. e., heat leak rate) for the apparatus was obtained by actual measurements of the temperature rise of a known mass of liquid oxygen and liquid propane for a known amount of heat input. Both liquid oxygen and liquid propane were utilized in order to cover the temperature range ( $-190^\circ\text{C}$  to  $-45^\circ\text{C}$ ) required for the liquid  $\text{OF}_2$  experiments. In addition, the properties (i. e.,  $C_p$ , vapor pressure) of these fluids are well characterized.

The calibration techniques employed and the test results obtained are described in detail in Appendix C.

##### b. Test Procedure

The test procedure for the  $\text{OF}_2$  specific heat determination consisted basically of transferring gaseous  $\text{OF}_2$  into the apparatus condensing the  $\text{OF}_2$  and stabilizing the  $\text{OF}_2$  temperature, energizing the platinum heating element and after stabilization, taking the necessary measurements. The test procedure and the technique employed to determine the specific heat of liquid  $\text{OF}_2$  is presented in detail in Appendix C.

#### 5. Test Results

Heat capacity measurements on  $\text{OF}_2$  were conducted over a temperature range of  $-196^\circ\text{C}$  to  $-75^\circ\text{C}$ . These data are presented in Table IX and plotted as a function of

TABLE X

EXPERIMENTAL DATA FOR HEAT CAPACITY DETERMINATION OF  $\text{OF}_2$

Temperature ( $^{\circ}\text{C}$ )	$\xi_1$ (cal)	$\Delta t$ ( $^{\circ}\text{C}$ )	$C_p$ (cal/g $^{\circ}\text{C}$ )
-191.1	127.1	2.964	0.330
-191.0	148.0	3.487	0.324
-191.0	128.1	3.016	0.327
-191.3	*	3.188	--
-191.4	*	3.190	--
-189.3	244.7	5.686	0.327
-170.3	126.2	2.593	0.335
-171.4	129.3	2.663	0.336
-171.5	146.3	3.033	0.332
-173.2	126.8	2.632	0.335
-154.9	*	2.376	--
-155.0	128.5	2.373	0.340
-155.8	126.4	2.476	0.337
-156.1	120.3	2.357	0.337
-146.4	*	2.354	--
-146.7	128.5	2.244	0.343
-147.1	240.2	4.534	0.347
-147.5	120.3	2.294	0.341
-148.3	115.4	2.190	0.345
-130.1	115.2	2.111	0.345
-132.3	110.5	2.026	0.347
-134.0	200.6	3.678	0.349
-134.7	210.4	3.881	0.346
-110.1	110.9	1.938	0.357
-112.3	*	3.760	--
-112.9	116.0	2.026	0.360
-114.0	230.3	4.070	0.353
-75.3	145.3	2.396	0.373
-76.1	142.2	2.355	0.370
-77.3	148.7	2.467	0.369
-78.0	140.8	2.345	0.367

\*Data rejected because of non-uniform heat leakage during these runs.



temperature in Figure 43. As can be seen, the change of heat capacity with temperature is linear and can be expressed by the following expression.

$$C_p = 0.395 + 3.545 \times 10^{-4} T \quad (-196 \text{ to } -75^\circ\text{C})$$

where:

$C_p$  = heat capacity (cal/g $^\circ$ C)

$T$  = temperature ( $^\circ$ C)

Data for a typical experiment are presented in Appendix C.

It can be expected that this linear relationship will not hold as the temperature approaches that of the critical temperature of  $\text{OF}_2$  ( $-45^\circ\text{C}$ ). This is primarily due to the non-linear variation of the density of liquid  $\text{OF}_2$  as it approaches the critical temperature.

Several experiments to determine the effect of pressure on the heat capacity of  $\text{OF}_2$  were conducted. The pressure range covered was from 10 to 300 psia using helium as a pressurizing medium. The effect of pressure on the heat capacity could not be detected with the apparatus employed. This can be explained as follows. The heat capacity as a function of pressure for a substance at a given temperature can be expressed by the following relationship:

$$(C_p)_p = C_p^\circ - T/J \int_{P^\circ}^P \left( \frac{\gamma}{\gamma T^2} \frac{\partial V}{\partial T} \right)_P \gamma P$$

where:

$C_p^\circ$  = reference specific heat at  $P^\circ$  (cal/g- $^\circ$ C)

$T$  = temperature ( $^\circ$ C)

$P$  = pressure (psia)

$V$  = volume

$J$  = constant

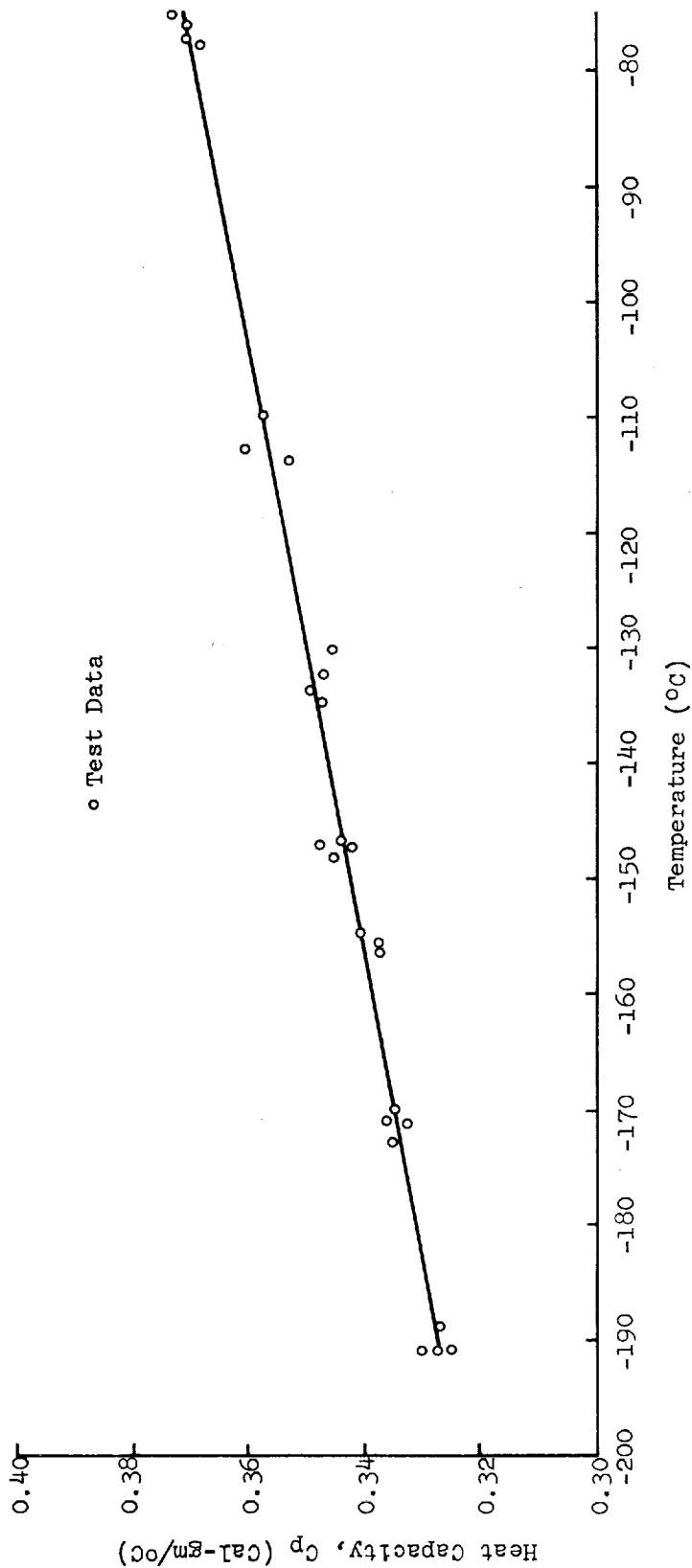


Figure 43. Experimental Specific Heat of Liquid  $OF_2$

The integral can be evaluated if the coefficient of thermal expansion,  $\alpha$ , is known as a function of temperature and pressure.

$$\alpha = 1/V \left( \frac{\gamma V}{\gamma T} \right)_p$$

Since for most liquids,  $\text{OF}_2$  included,  $\alpha$  is very small, the value of the integral in the above equation is negligible when compared to the actual heat capacity value. Therefore, these minute changes were not detected by the apparatus and technique employed.

It is estimated that the prevision in each specific heat measurements is approximately 1% and the plotted data (Figure 43) representing the heat capacity equation is reliable to within  $\pm 5\%$ . This is based on an error analysis of the measured parameters taking into account resistance, voltage, sample weight and time measurements.

Based on the results of this phase of the program the following conclusions are drawn:

- A more optimistic value for the cooling capability over that previously predicted can be obtained with  $\text{OF}_2$ . Previous studies at Thiokol-RMD utilized a specific heat value for  $\text{OF}_2$  of  $0.3 \text{ Cal/g-}^\circ\text{C}$ . Values reported in the literature (Refs. 12 and 13) ranged from  $.20$  to  $\text{Cal/g-}^\circ\text{C}$  to  $.35 \text{ Cal/g-}^\circ\text{C}$  for liquid temperatures at the boiling point (i.e.,  $-230^\circ\text{F}$ ). Experimental results obtained in this program have given values of  $0.327$  to  $0.37 \text{ Cal/g-}^\circ\text{C}$ .
- Based on test results covering a wide range of temperatures and pressures, an empirical expression for  $\text{OF}_2$  heat capacity has been developed. The expression will permit more reliable space mission and thrust chamber cooling studies for the ranges of temperatures and pressures evaluated in this program.

## E. $\text{OF}_2 / \text{B}_2\text{H}_6$ COMBUSTION CONTAINMENT DESIGN STUDIES

### 1. Objective

The objective of this task was to perform design studies to determine the feasibility of reliable thrust chamber concepts capable of extended firing durations with  $\text{OF}_2 / \text{B}_2\text{H}_6$ . Thrust chambers operating up to 2500 pounds space thrust and chamber pressures up to 150 psia were considered. In order to accomplish this task, analytical evaluations of state-of-the-art cooling technology were extended to include advanced cooling concepts. Investigations of promising materials of construction were also conducted.

### 2. Design Studies

#### a. Design Considerations

For future potential space missions, such as planetary orbiters, planetary landers, and lunar vehicles, propulsion systems offering high performance, hypergolic ignition space storability and capable of extended firing durations over many cycles of operation are desirable. Mission studies have indicated that the total duration capability should be in the range of 1000 to 2000 seconds. A target duration of 1800 seconds was used for the feasibility studies performed during this program. The design criteria assumed a variable duty cycle with any combination of single durations totaling 1800 seconds.

The single, major deterrent to the advancement of  $\text{OF}_2 / \text{B}_2\text{H}_6$  technology is that of injector-thrust chamber durability for the missions described above. Under Task I of NASA Contract NAS 3-2553 (Reference 1) the behavior of ablative materials was investigated with  $\text{OF}_2 / \text{B}_2\text{H}_6$ . Analytical predictions were developed for the thermal characteristics and erosive resistance of various ablative materials which were later confirmed by test at the 150 pound thrust level. This program established that the graphite phenolic type of ablative was by far more erosion resistant than other materials with this propellant combination. Comparison of the results obtained on other programs at Thiokol-RMD with  $\text{N}_2\text{O}_4 / 50\%$  hydrazine 50% UDMH indicated that erosion rates were quite similar. However, the erosion rates being currently experienced with  $\text{N}_2\text{O}_4$ -50/50 (and hence also those of  $\text{OF}_2 / \text{B}_2\text{H}_6$ ) restrict the type of mission in which ablative chambers can be used. Consequently, the investigation of other methods of thrust chamber cooling which can provide greatly extended duration capability were undertaken.

During this program the problem of containment of the oxygen difluoride-diborane propellant combination has been explored in detail to arrive at a plan for the acquisition of the necessary technology to provide a long duration thrust chamber capability. The basic containment problems encountered with  $\text{OF}_2/\text{B}_2\text{H}_6$  are in most cases similar to those associated with many other high energy propellant combinations; (1) high flame temperatures, and (2) unknown or poor exhaust product compatibility with materials at elevated temperatures. Analysis to establish the applicability of the present state-of-the-art methods of cooling and material technology were undertaken. These analyses were extended and emphasis directed towards advanced cooling concepts.

The effect of chamber pressure, O/F, %c\*, propellant temperature and combustion chamber geometry on cooling capability were investigated to define operating limits for reliable combustion chamber cooling. The cooling evaluation undertaken considered two basic approaches:

1. Regenerative and radiation cooling systems
2. Mass addition cooling systems
  - Transpiration
  - Liquid or gaseous film cooling

b. Thrust Chamber Cooling Considerations

The specific cooling requirement imposed on the propellants was determined by predicting the total heat rejection to the thrust chamber walls and cooling medium. The influence of variations in the shape of the combustion chamber and nozzle on total heat transfer was considered. Regenerative cooling in conjunction with insulation appears to be the most feasible approach. Two ways of providing insulation were considered: (1) the standard approach of using low conductivity materials, and (2) a radiation gap. To further support the design definition, analytical stress considerations of the designs and a materials literature search-screening effort was undertaken.

(1) Gas Film Heat Transfer Coefficients - The heat rate absorbed by the thrust chamber walls was predicted for various surface wall temperatures using the relationship:

$$Q = (q'') (A_s), \text{ Btu/sec; where } q'' = h_g (t_g - t_{gw}), \text{ Btu/sec-in}^2$$

$$A_s = \text{combustion side chamber surface area, in}^2$$

$h_g$  = gas film heat transfer coefficient, Btu/hr-ft<sup>2</sup> - °F

$t_g$  = combustion gas temperature, °F

$t_{gw}$  = combustion side chamber wall temperature, °F

The predicted gas film coefficient,  $h_g$ , was obtained by means of the Bartz correlation and the property function correction listed below:

$$h_g = .026 \left( \frac{\mu^{0.2} C_p}{Pr^{0.6}} \right) \left( \frac{P_c}{c^*} \right)^{0.8} \left( \frac{De}{r_c} \right)^{0.1} \left( \frac{A^*}{A} \right)^{0.9} \quad \sigma \quad (1)$$

where  $\sigma$  is the boundary layer temperature correction and is calculated by the following expression:

$$\sigma = \frac{1}{\left[ \frac{1}{2} \frac{T_w}{T_o} (1 + \frac{\gamma-1}{2} M^2) + \frac{1}{2} \right]^{.68} \left[ 1 + \frac{\gamma-1}{2} M^2 \right]^{(.12)}} \quad (2)$$

The experimental heat transfer data obtained from the transient thermocouple probes installed in the uncooled, heat sink chambers during sea level and altitude testing were adjusted for the gas film property differences between the relatively low (< 1500F) measured heat sink chamber wall temperatures and the predicted wall temperatures (i. e. 2000 - 4000F) for each concept evaluated. OF<sub>2</sub>/B<sub>2</sub>H<sub>6</sub> heat transfer data obtained during this program (Section IV. A. d) and previous programs were utilized in the analysis to develop analytical correlations for the design concepts studied. Prior OF<sub>2</sub>/B<sub>2</sub>H<sub>6</sub> heat transfer data obtained with water cooled chambers and high response foil-type thermocouples (References 1 and 2) showed good agreement with predicted values based on the Bartz correlation. More recent data obtained during this program and during Corporate sponsored programs with N<sub>2</sub>O<sub>4</sub>/MMH propellants have shown heat transfer coefficients equal to or lower than theoretical predictions based on the Bartz method.

In addition to these OF<sub>2</sub>/B<sub>2</sub>H<sub>6</sub> data, recent tests with N<sub>2</sub>O<sub>4</sub>/MMH propellants have revealed significant reductions in heat transfer coefficients in the throat and chamber (Reference 15) has been demonstrated with engines employing the full diameter vortex injector. The heat transfer coefficients associated with the full-diameter vortex injector were experimentally measured in a series of tests with an uncooled copper heat sink chamber by means of high response, foil-type thermocouples (Reference 16). The firings were conducted with N<sub>2</sub>O<sub>4</sub>-MMH at a chamber pressure

of 100 psia and a thrust level of 100 lb. The average values of heat transfer coefficients for these conditions were 104 Btu/hr-ft<sup>2</sup>-°F and 152 Btu/hr-ft<sup>2</sup>-°F for the chamber and throat respectively. These values were adjusted to account for the gas property differences between the cold walls of the copper thrust chamber and the Radiamic liner temperatures by using the Bartz equation and the property function correction listed previously (equations 1 and 2). Figure 44 shows the comparison between predicted Bartz coefficients, the OF<sub>2</sub>/B<sub>2</sub>H<sub>6</sub> experimental gas film coefficients and the coefficients based on the N<sub>2</sub>O<sub>4</sub>/MMH tests. The coefficients based on the N<sub>2</sub>O<sub>4</sub>/MMH tests at a chamber pressure of 100 psia and adjusted for various chamber pressures (i. e. 150 and 50 psia) were utilized in the thrust chamber cooling studies.

The film coefficients in the chamber barrel obtained from the OF<sub>2</sub>/B<sub>2</sub>H<sub>6</sub> tests is in good agreement with the N<sub>2</sub>O<sub>4</sub>/MMH data. The throat section film coefficients based on OF<sub>2</sub>/B<sub>2</sub>H<sub>6</sub> data is equal to or higher than the predicted Bartz coefficients.

The relatively higher OF<sub>2</sub>/B<sub>2</sub>H<sub>6</sub> throat coefficients are attributed to use of a mid-diameter vortex injector in conjunction with a combustion chamber utilizing an L\* of 30 in. Test experience on other programs with N<sub>2</sub>O<sub>4</sub>/MMH have shown significant reductions in nozzle throat film coefficients between operation with a mid-diameter vortex injector and a full-diameter vortex injector.

The low measured film coefficients obtained in the throat during N<sub>2</sub>O<sub>4</sub>/MMH testing use of a full diameter vortex injector and low L\* (10) chamber. Low throat coefficients have also been measured by other investigators (Reference 17). The conclusions is that they are a result of a laminar or transition boundary layer occurring in the throat region. The results presented in Reference 17 indicate that heat transfer and flow regions of laminar boundary layer, turbulent boundary layer or transition between the two can occur at the throat of the nozzle depending upon its design, upstream flow conditions and operating conditions.

Figure 45 based on data obtained from Reference 17 indicates that at Reynolds number of  $1.6 \times 10^5$  (equivalent to that for the 100 lb thrust engine with N<sub>2</sub>O<sub>4</sub>/MMH) the ratio of a laminar coefficient to that of a turbulent (Bartz) would be 0.38. It is considered significant that this ratio when converted to a heat transfer coefficient agrees with the measured values of film coefficients obtained at the throat with low L\* chambers and a full diameter vortex injector (Figure 44). On the basis of these data, it is concluded that a full diameter vortex injector and low L\* chamber will provide film coefficients lower than those predicted by the Bartz and hence less severe cooling requirements for thrust chambers utilizing OF<sub>2</sub>/B<sub>2</sub>H<sub>6</sub> propellants.

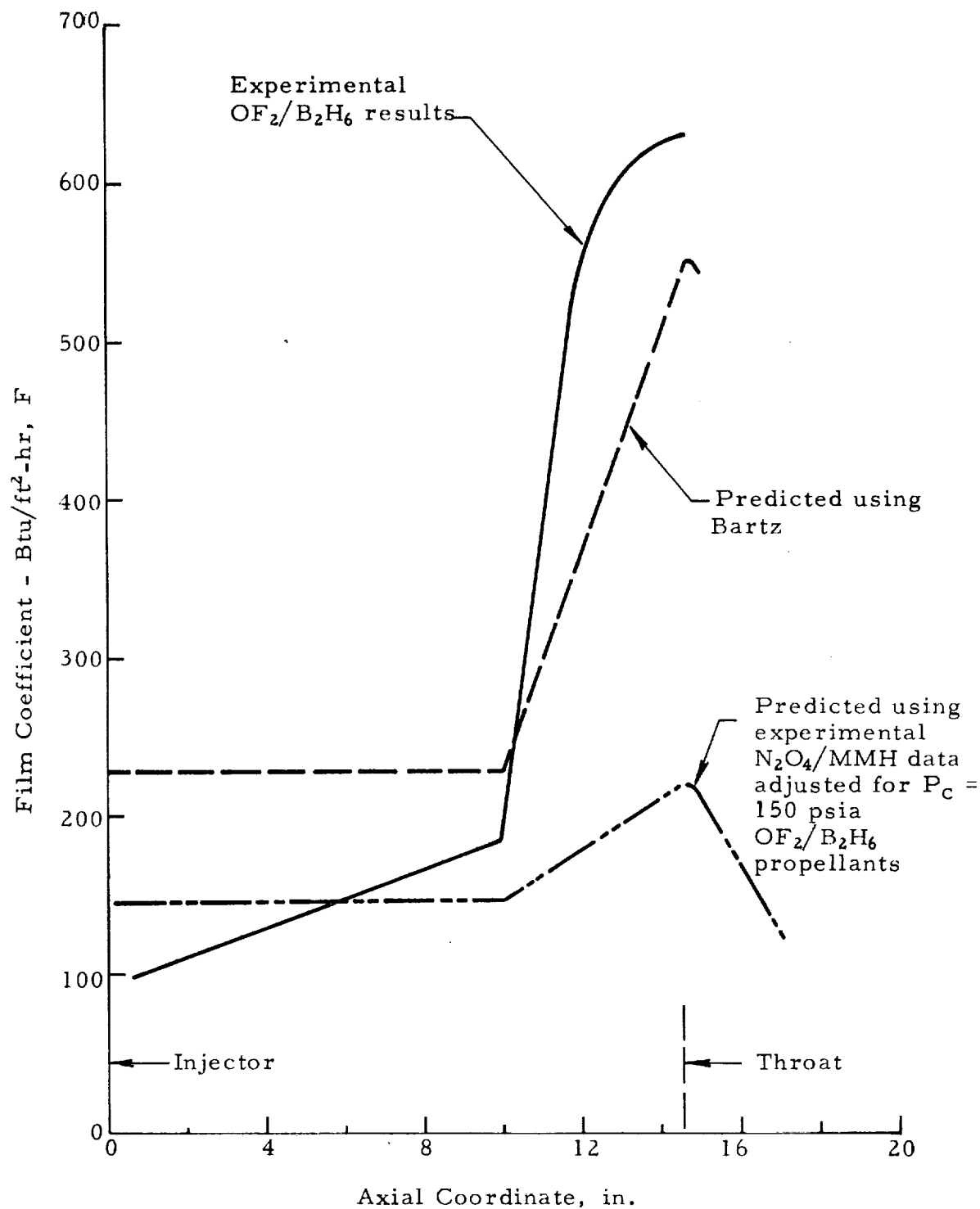


Figure 44. Gas Film Coefficient Profile



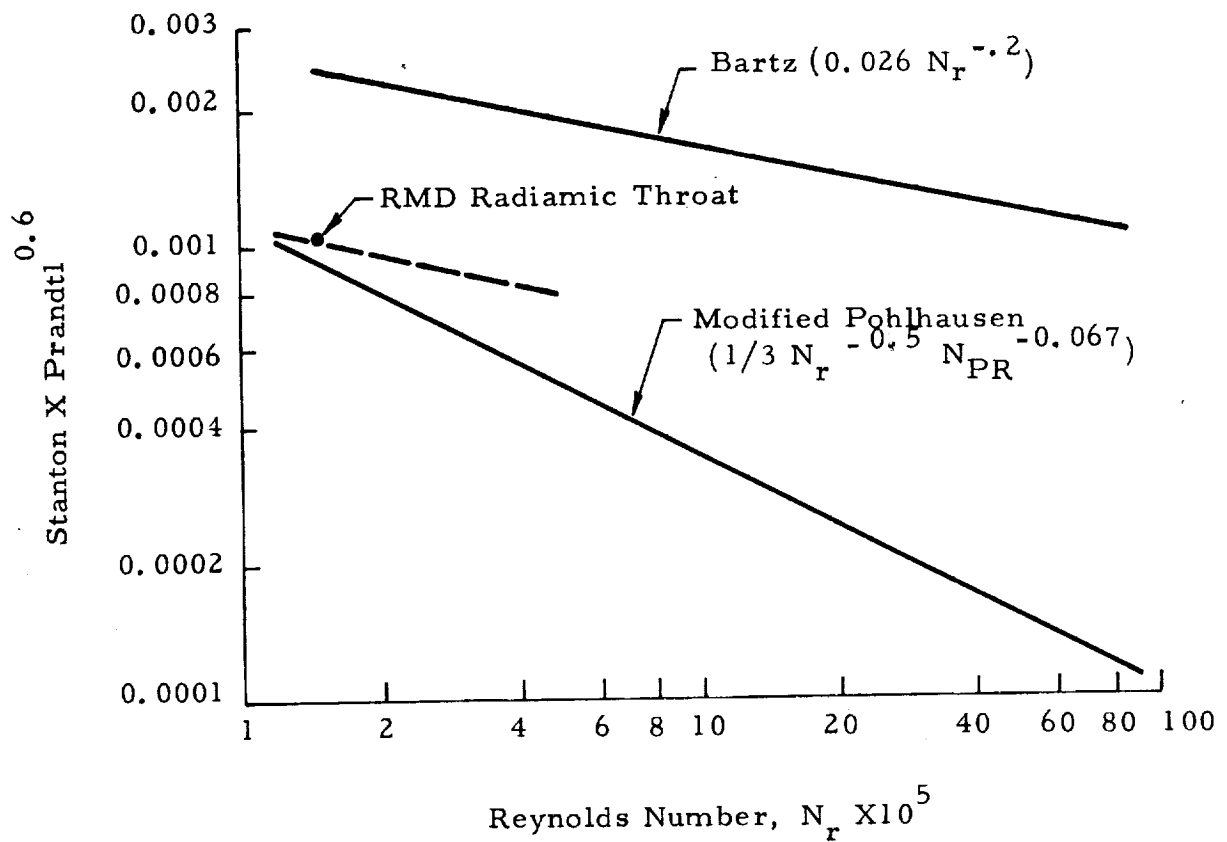


Figure 45. Variation of Dimensionless Nozzle Throat Convective Heat Transfer Coefficient with Reynolds Number (Ref 17)

(2) Combustion gas radiation heat transfer - The contributions of heat transfer from gaseous radiation of the  $\text{OF}_2 / \text{B}_2\text{H}_6$  combustion products in the chamber walls was investigated. Based on emissivity data available for 65% (by partial pressure) of the combustion products, a radiation heat flux of  $0.16 \text{ Btu/in.}^2\text{-sec}$  to the thrust chamber walls was calculated. Emissivity data for the remaining 35% of the combustion specie could not be found. However, for this portion to be significant, a gas emissivity equal to that of water vapor (the most emissive gas) is required. Since the combustion species of  $\text{OF}_2 / \text{B}_2\text{H}_6$  contain only 2% water (by wt) the assumption was made that gaseous radiation can be neglected.

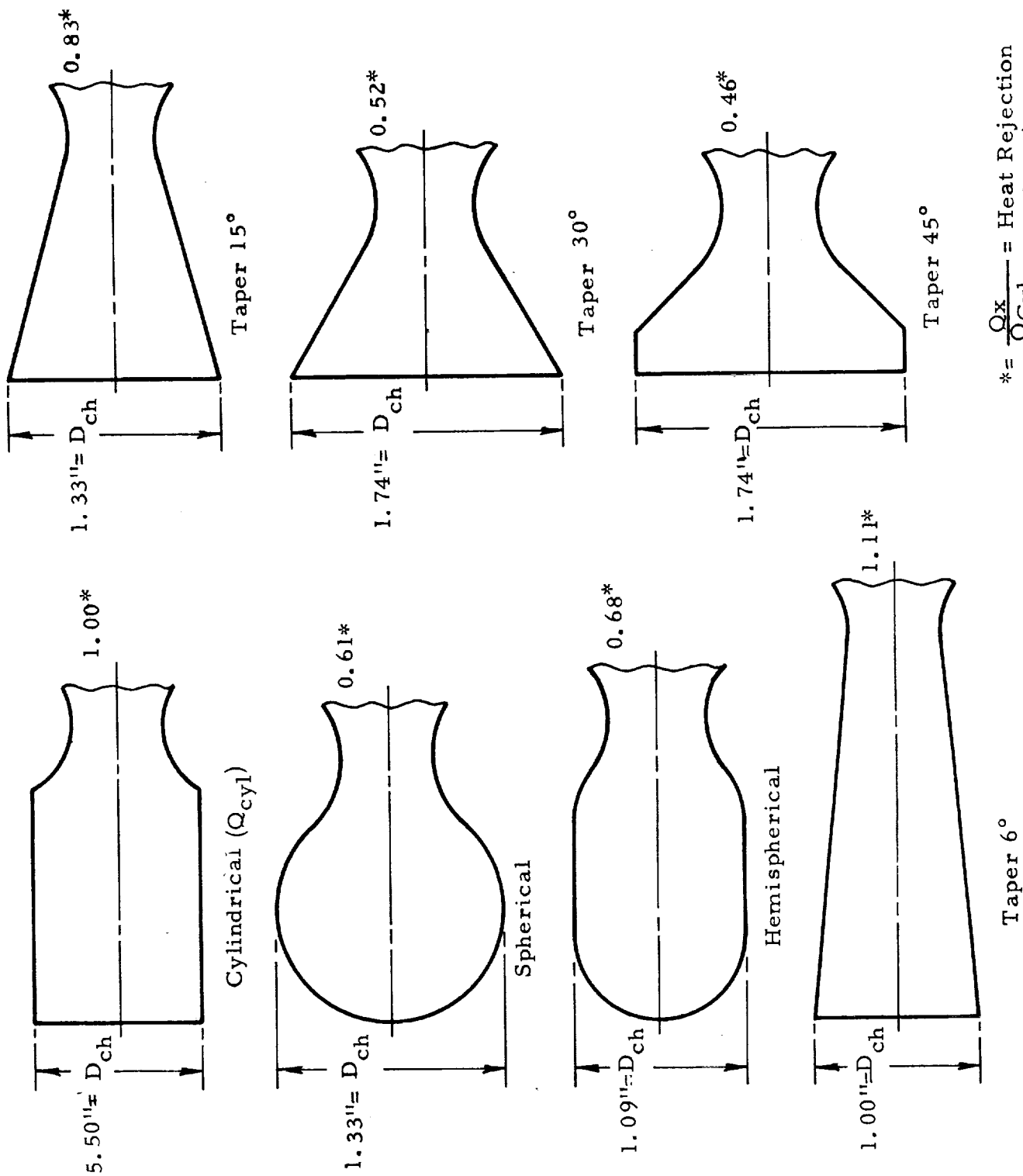
(3) Combustion Chamber Geometry - As a part of the heat transfer analysis, a comparison was made between a number of possible combustion chamber shapes (i.e. up to the throat plane) to determine which would provide the minimum heat rejection at a constant  $L^*$  of 30" and a thrust level of 2500 lbs. In general, large contraction ratios reduce heat transfer to the thrust chamber walls. A comparison of the heat transfer/geometry conditions resulting from this study is shown in Figure 46. The relative cooling ratio of the various chamber configurations is presented in terms of overall heat rejection,  $Q(\text{Btu/sec})$ , compared to the heat rejection for a conventional chamber (i.e. cylindrical, conventional throat) such as that employed for sea level and altitude testing during other phases of this program.

The minimum total heat rejection is obtained with a tapered thrust chamber which has an injector end diameter approximately 1.75 times the diameter utilized during this program. However, there are a number of additional design considerations (e.g., effect of chamber geometry on  $c^*$ , larger injector surfaces exposed to heat transfer, total pressure losses, increased structural loads, etc.) associated with the tapered chamber approach. Consequently, the conventional chamber geometry employed during this program (i.e., cylindrical  $\epsilon_c = 2.75$ , conventional throat) was utilized in the thrust chamber cooling analysis, since: (1) heat transfer and design analysis indicated that adequate cooling could be accomplished with this geometry, and (2) performance with this type geometry is well characterized.

#### c. Propellant Cooling Capabilities

During the course of this program, the specific heat of liquid  $\text{OF}_2$  was experimentally determined (Section IV.D.). The values obtained (0.33 to 0.37  $\text{Cal/g-}^\circ\text{C}$ ) were utilized in this effort. Figures 47 and 48 present the propellant physical property data utilized during the cooling studies.

Although  $\text{OF}_2$  and  $\text{B}_2\text{H}_6$  have limited cooling capability it has been assumed that they are capable of operating at nucleate boiling temperatures (i.e.,  $t_{\text{sat}} + 40\text{F}$ )



$$* = \frac{Q_x}{Q_{Cyl}} = \text{Heat Rejection Fraction}$$

Figure 46. Chamber Geometry Heat Rejection Comparison for 30" L\* Chamber

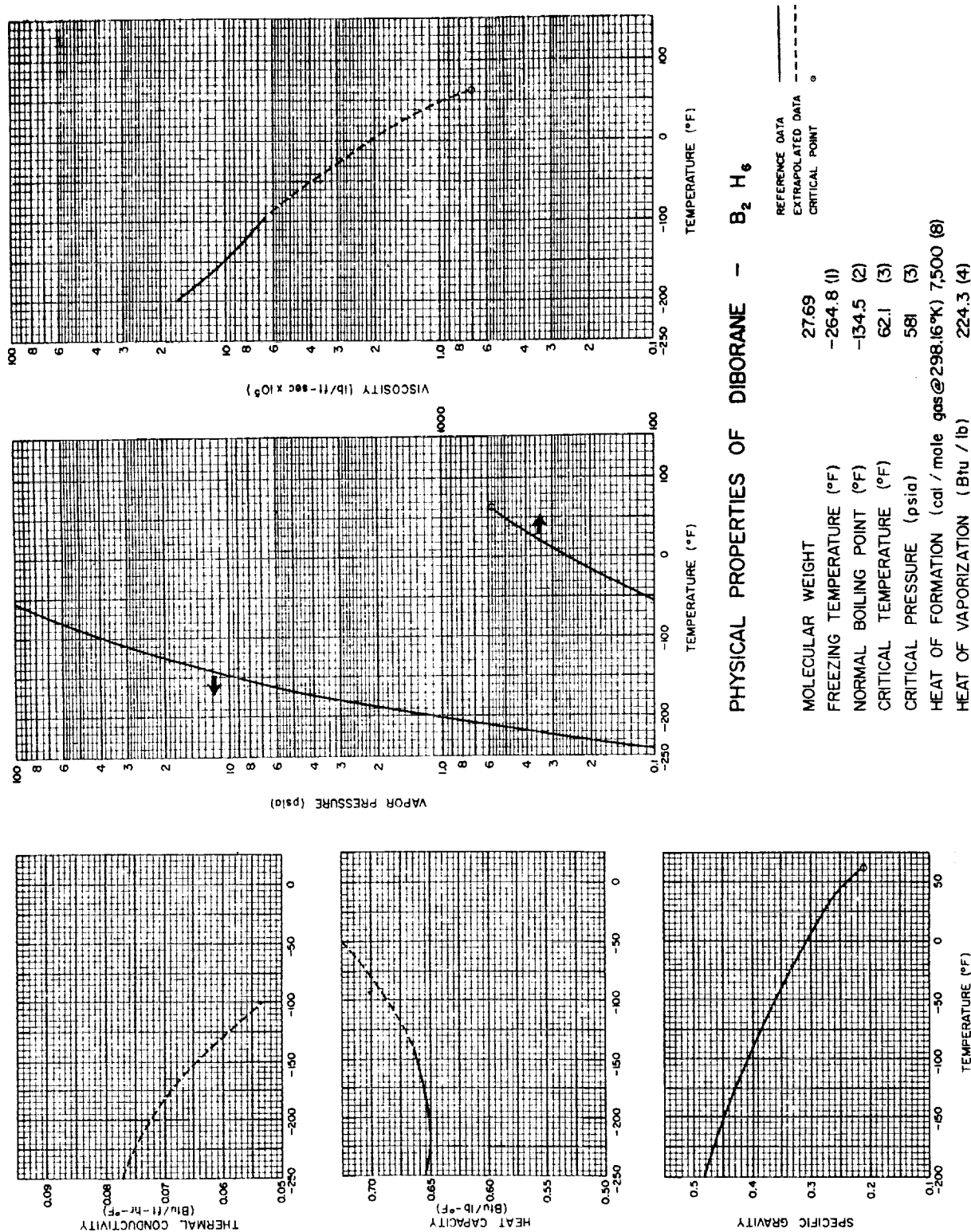


Figure 47. Physical Properties of Diborane -  $B_2H_6$  (Refer to Aerojet General Corporation Report No. LRP 178)

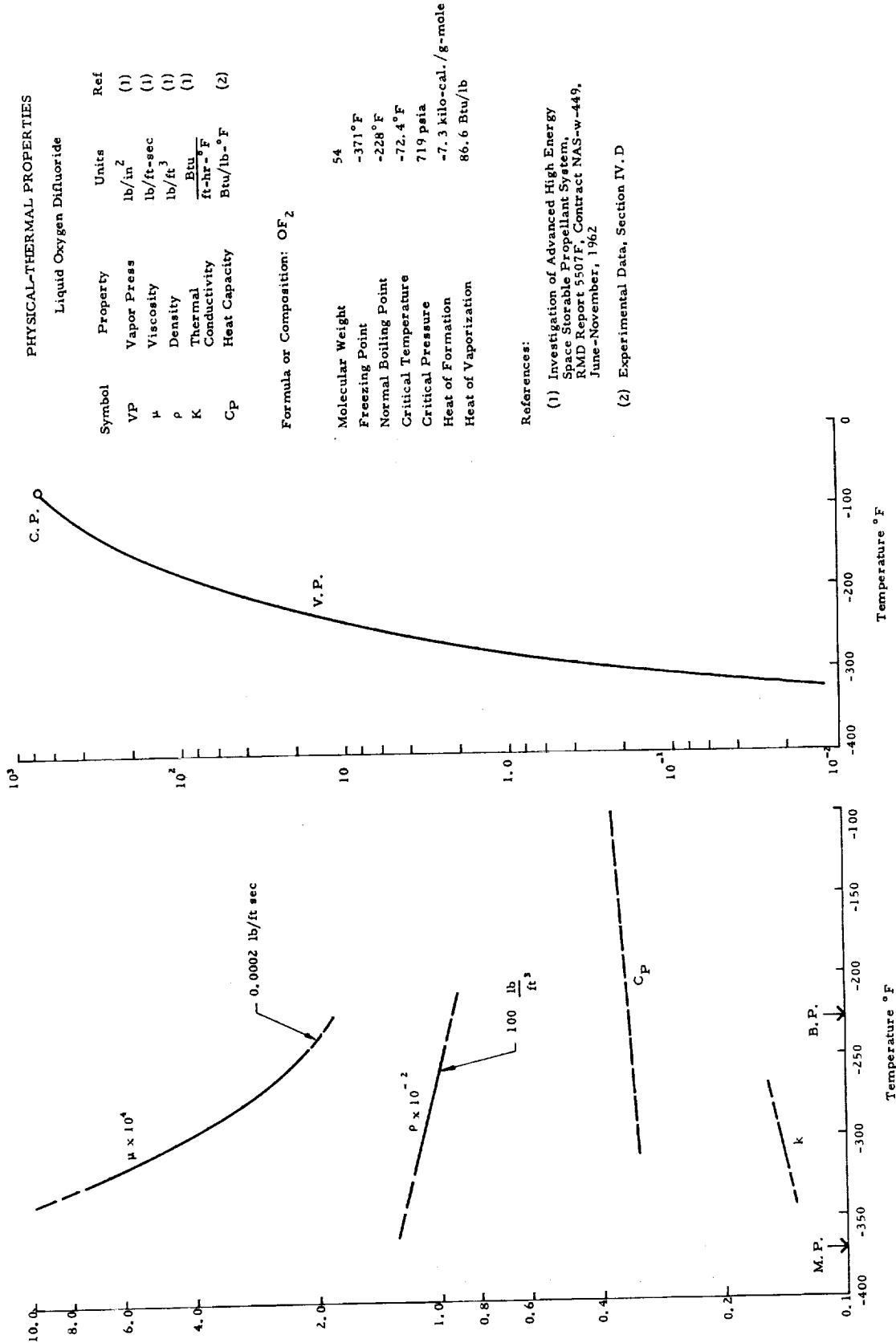


Figure 48. Physical and Thermal Properties of Oxygen-Difluoride -  $\text{OF}_2$

and will have the upper limit capabilities as predicted by the Bernath correlation (Reference 8 ). Figures 49 and 50 present the upper limit of nucleate boiling ( $q''_{UL}$ ) predictions based on the Bernath correlation which were utilized for the cooling studies. A discussion of the method for calculating  $q''_{UL}$  is presented in detail in Appendix A.

The thermal stability of  $B_2H_6$  in nucleate boiling is considered good. Thermal stability studies (Reference 18) show very slow diborane decomposition (measured in days) at the temperatures considered for the cooling studies (-200F to -10F).

#### d. Combustion-Side Material Compatibility

The compatibility of materials at high temperatures with the  $OF_2 / B_2H_6$  combustion specie was investigated to provide design recommendations for a long duration thrust chamber. A literature search for applicable test data uncovered no results with comparable products of combustion. However, a partially applicable analytical prediction for the reactions of various gases with refractory metals and oxides (Reference 19) did give some indication of promising materials. Twelve candidate materials were selected to determine their relative compatibility in an  $OF_2 / B_2H_6$  combustion environment.

The relative screening consisted of immersing material sample pins into the combustion zone ( $\approx 0.5$  inch) during the sea level injector tests described in Section IV A. 5. The samples were .250 inch diameter pins installed at the entrance to the nozzle (Figure 51). Thirty-two sample tests were conducted during the injector performance test phase of the program (Section IV. A. 5). Figure 53 also shows a set of material specimens before and after a test firing.

In addition, candidate specimens of injector materials were screened during one test. These materials were chromium copper, OFHC copper, A nickel and stainless steel. The OFHC copper and chromium copper specimens were in excellent condition. The 347 stainless steel and A nickel specimens were severely eroded.

The material specimens were measured and weighed before and after a test firing to determine material loss. Metallurgical examination of the material specimens was conducted to determine grain growth, recrystallization, hardness, fractures and any evidence of a reaction between the material and the combustion products.

Table XI presents the test results of the material specimens in the order of compatibility. On the basis of material loss and metallurgical examination, the tantalum-tungsten alloy (T-111) showed the best compatibility results, followed in order by Graphitite G and JTA graphite.

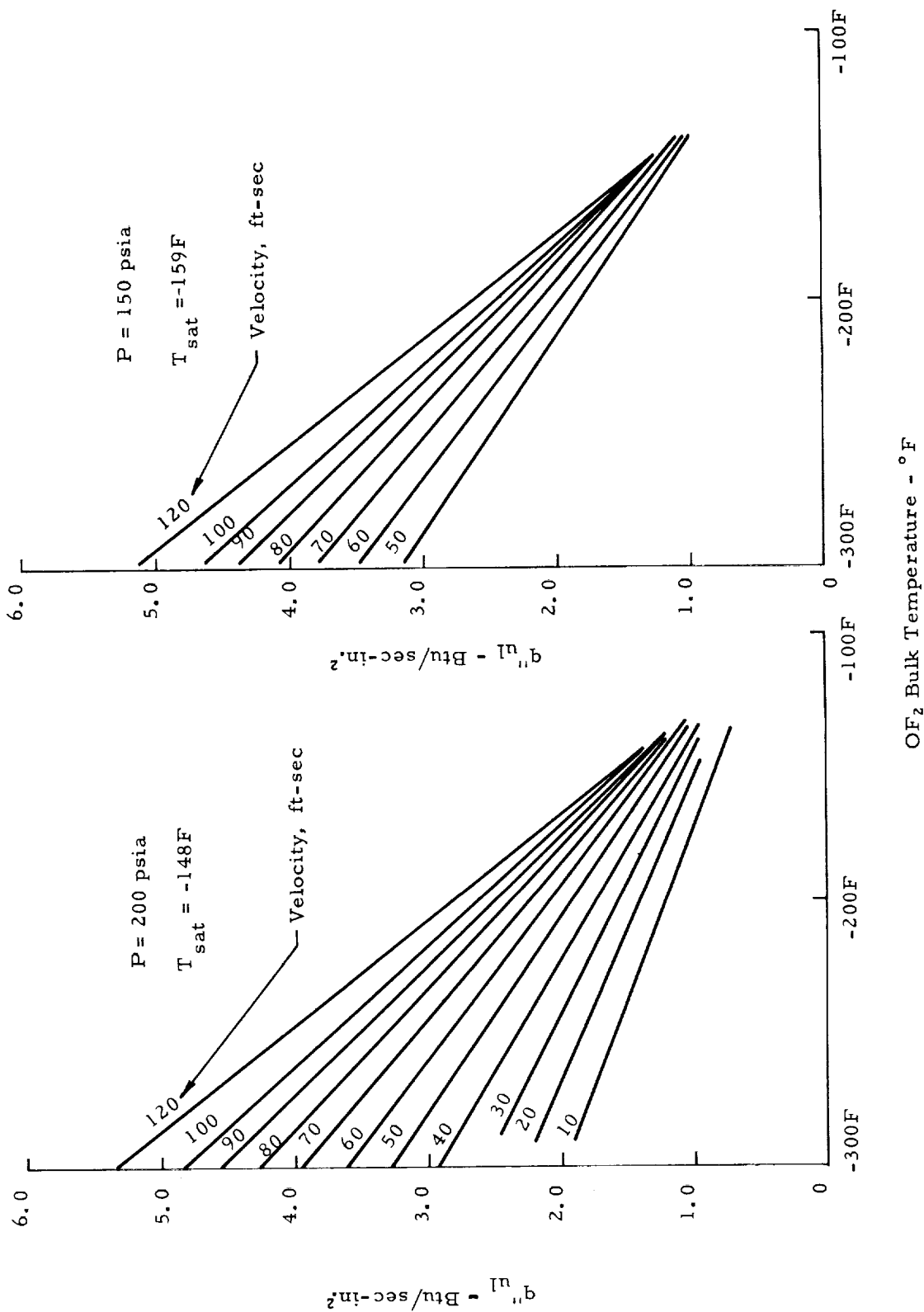


Figure 49. Upper Limit of Nucleate Boiling Predictions -  $\text{OF}_2$  - Bernath Correlation

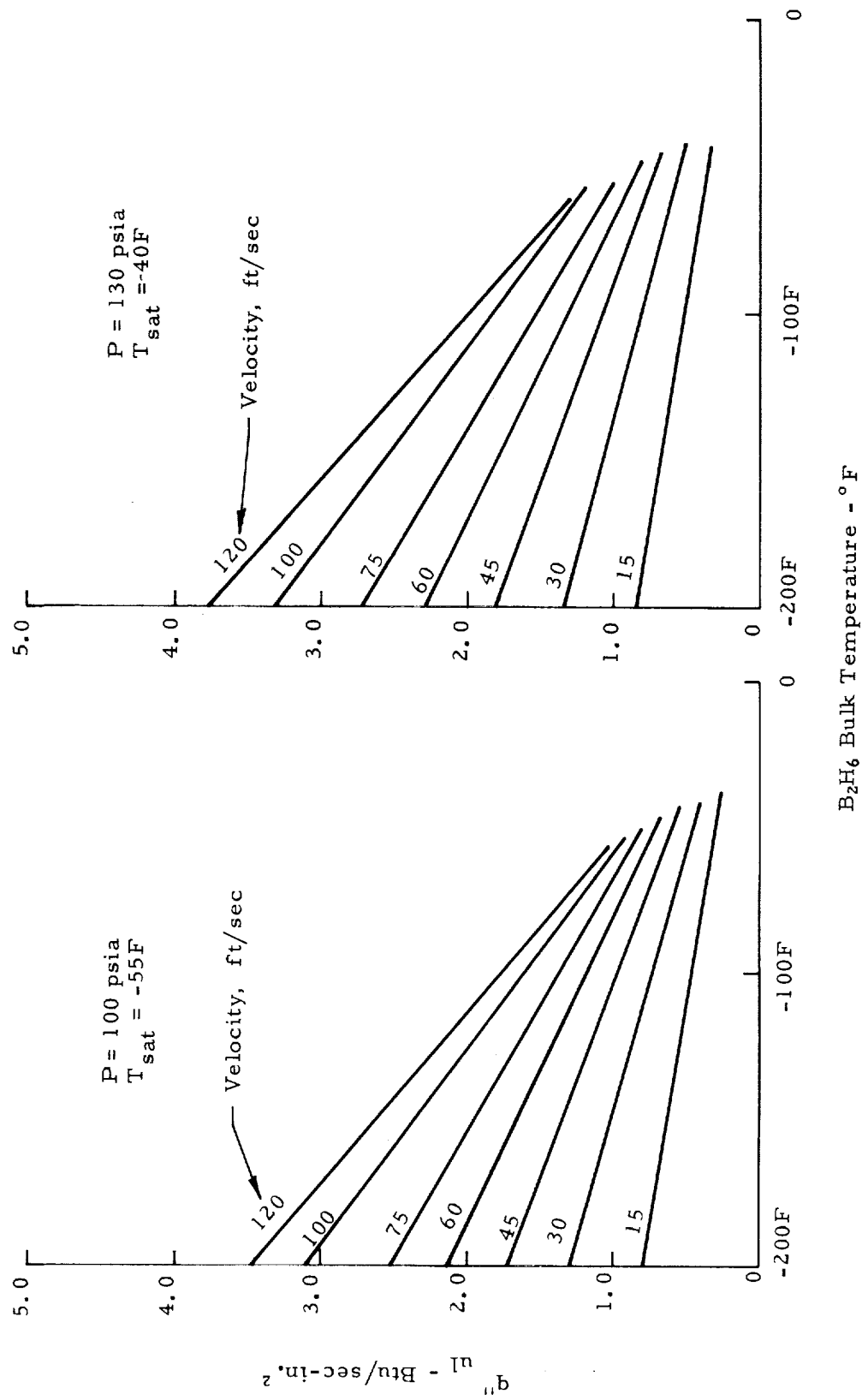
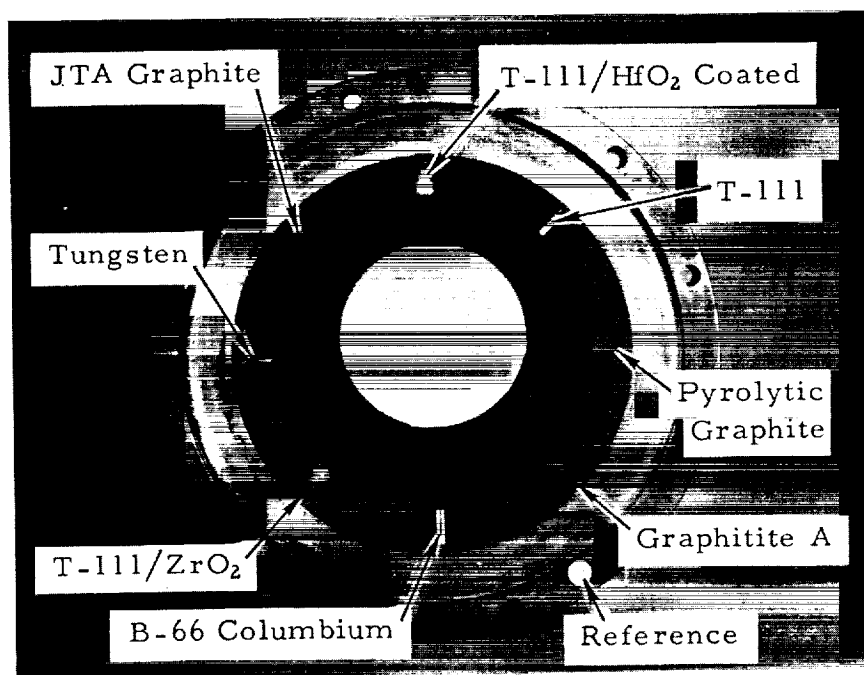


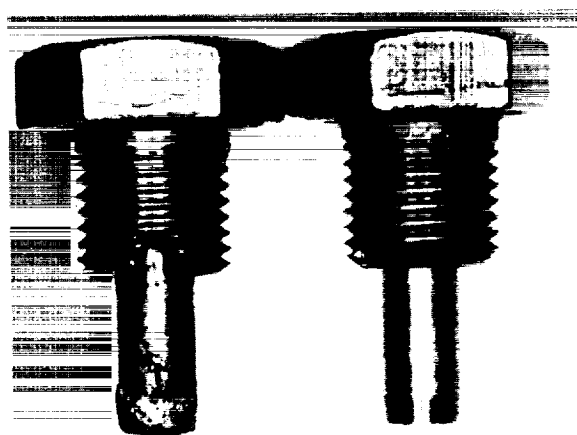
Figure 50. Upper Limit of Nucleate Boiling Predictions -  $B_2H_6$  - Bernath Correlation





6039-88

Uncooled Chamber-Looking Forward

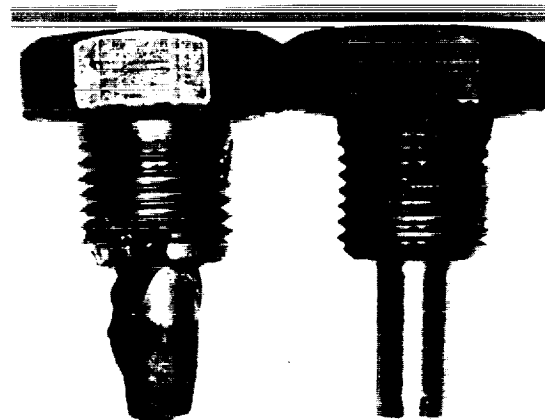


64165-12

Post Test

Pre Test

T-111 Tantalum



64165-12

Post Test

Pre Test

Tungsten

Figure 51. Material Sample Pins Before And After Testing

TABLE XI

OF<sub>2</sub>/B<sub>2</sub>H<sub>6</sub> Material Specimen Test Results

Material	No. Tests	Ave. Material Loss % Volume - (1)
T-111 Tantalum	6	1.5
T-111 Tantalum Coated Zr <sub>2</sub> BO <sub>3</sub>	2	2.0
T-111 Tantalum Coated HFO <sub>2</sub>	2	2.5
T-111 Tantalum Coated ZrO <sub>2</sub>	2	3.5
Graphitite G	6	(2)
JTA Graphite	6	(2)
Tungsten (unalloyed)	2	9.3
Pyrolytic Graphite	2	28.0
B-66 Columbium	2	45
B-66 Columbium Coated Zr <sub>2</sub> BO <sub>3</sub>	2	(3)

$$(1) \% \text{ Volume loss (cc)} = \frac{\text{Weight loss (grams)} / \rho \text{ (g/cc)}}{\text{Vol initial}} \times 100\%$$

(2) Slight weight gain, but slight dimensional change at tip

(3) Slight weight gain (.03-.05 grams) probably due to oxidation formation; but severe tip erosion occurred.

Although the combustion temperature of  $\text{N}_2\text{O}_4/\text{MMH}$  is lower than that of  $\text{OF}_2/\text{B}_2\text{H}_6$  (i.e., 5300 vs 6500F), the measured combustion side material temperatures obtained during extensive materials screening test results with  $\text{N}_2\text{O}_4/\text{MMH}$  were used as the design limits for the  $\text{OF}_2/\text{B}_2\text{H}_6$  cooling studies. Combustion chamber gas-side liners and nozzle throat components fabricated from refractory materials have been evaluated during 100 lb thrust chamber test firings with  $\text{N}_2\text{O}_4/\text{MMH}$  propellants. During these tests, measured combustion-side wall temperatures on the order of 2500-3290F in the chamber barrel and 2500F in the nozzle throat region were obtained. The most promising material evaluated during  $\text{N}_2\text{O}_4/\text{MMH}$  testing was 90% tantalum - 10% tungsten alloy with a Silicide combustion-side coating during which one component accumulated 6128 seconds of operation. It is believed that a material such as this would provide improved durability with  $\text{OF}_2/\text{B}_2\text{H}_6$  since the oxidizing environment (i.e.,  $\text{O}_2$ , O,  $\text{H}_2\text{O}$  gas species) of  $\text{N}_2\text{O}_4/\text{MMH}$  is considerably more severe than that of  $\text{OF}_2/\text{B}_2\text{H}_6$  for similar operating temperatures (i.e., 2000-3500F).

The results of these tests demonstrate a reasonably high level of confidence in the ability of present state-of-the-art materials to provide compatibility with the  $\text{OF}_2/\text{B}_2\text{H}_6$  combustion environment. Although test evaluation of these materials over long durations is required to provide an optimized design, a promising thrust chamber materials technology base has been established.

### 3. Cooling Concept Evaluation

In order to evaluate the approaches and to arrive at a thrust chamber design which makes the best use of the propellant cooling capabilities, design concepts were evaluated and analyzed with the objective of evolving a concept having the capability of long duration operation at high performance levels.

The basic cooling concepts investigated during the course of this study were:

- Regenerative - Propellant cooling jacket
- Radiation - Monolithic combustion liner radiating to space
- Torox - Ablative chamber incorporating a propellant-cooled throat section

- Voramic - Combustion side insulation liner and hard throat insert surrounded by a propellant-cooling jacket
- Radiamic - Monolithic combustion liner incorporating a low mass throat insert all surrounded by a regenerative cooling jacket
- Augmented Radiamic - Transpiration and Film Cooling with Radiamic chambers

Based on the analytical studies and state-of-the-art materials technology, the Radiamic thrust chamber concept is feasible and offers the most promise for long duration capability with  $\text{OF}_2/\text{B}_2\text{H}_6$ . Although transpiration or film cooling techniques appear feasible, further studies and design data are required to fully assess these concepts.

The following sections summarize the results of the cooling concepts considered in this study.

(1) Regenerative - Regenerative cooling is limited from several standpoints. Utilization of either  $\text{OF}_2$  or  $\text{B}_2\text{H}_6$  would result in a coolant bulk rise sufficient to cause bulk boiling problems. The throat heat fluxes associated with a thin wall chamber will be on the order of 2 to 5 Btu/sec-in.<sup>2</sup> (for chamber pressures of 150 psia) depending on the type of injector. To accommodate these fluxes at bulk temperatures approaching coolant saturation temperatures, cooling velocities in the range of 50 to 80 ft/second would be required and only local cooling is feasible. The problem then, for thin wall regenerative chambers, is excessive heat input into the coolant. However, regenerative cooling can be employed if a sufficient amount of heat blockage either through insulation or boundary layer control can be accomplished.

(2) Radiantly Cooled Thrust Chamber - The radiantly cooled thrust chamber is simple, involving only a monolithic shell of refractory material. Since the only heat transfer path to the propellants is via the injection head, thermal soak problems are minimized. However, application is limited by the environment in which it is placed. It cannot, therefore, be considered a universal type design since it must be related to vehicle installation and cannot be buried. A basic problem with radiation cooled thrust chambers is the selection of a suitable material for the shell. Although there are a large number of refractory materials which theoretically might be used, many of these are still laboratory curiosities beyond the present state of the art. Material technology currently limits the use of radiation cooled thrust chambers to chamber pressure levels of approximately 100 psia or less. High heat transfer rates, especially at the throat region, accompanying operation at higher pressures, increases the equilibrium wall temperatures and necessitates material technology advancements before these pressure levels can be used.

Although a radiation cooled thrust chamber could be used for certain specific mission requirements, it requires augmentation such as film cooling and does not possess the capability of providing high performance and reliable operation for extended duty cycles.

(3) Torox Thrust Chamber (Figure 52) - In recognition of the limited cooling capability of the propellants, a design concept was evolved to maintain throat integrity by using these capabilities to maximum advantage. In the Torox thrust chamber, the throat region is formed from a toroidal, tubular coolant passage through which the oxidizer is passed (hence the name Tor-ox). The remainder of the thrust chamber utilizes ablative cooling. This concept may be applicable to the  $\text{OF}_2/\text{B}_2\text{H}_6$  propellant combination provided that sufficient insulation can be provided on the combustion side surface of the throat region to limit the heat flux into the  $\text{OF}_2$ . However, ablatively cooled sections are duty cycle limited. Because of the high temperature and fluxes associated with  $\text{OF}_2/\text{B}_2\text{H}_6$  combustion and the large area requiring cooling and because of the limitations of ablative cooling, Torox application with these propellants was found to be limited. With the incorporation of the required insulation materials on the gas side to limit the heat flux to the coolant, the concept evolves into the Voramix thrust chamber, discussed below.

(4) Voramix Thrust Chamber (Figure 52) - The Voramix Thrust Chamber embodies a combustion side liner of high temperature refractory material which is reliably maintained at a satisfactory design operating temperature by the application of propellant cooling to its outer surface. This type of design has been successfully applied at lower combustion temperatures such as those used in the RMD TD-283, YLR48, and the NASA Surveyor Vernier Rocket Engines. A limitation of this concept is the thermal storage capacity of the throat insert which creates a problem of heat soak on down-throttling or restarts. To provide a configuration capable of wider operating limits with the oxygen difluoride/diborane propellants, a configuration for minimizing the heat storage limitations was sought.

(5) Radiamix Thrust Chamber (Figure 52) - The Radiamix thrust chamber concept is unique in that it combines the advantages of both radiation and regeneratively cooled designs. This design employs a chamber liner which is completely separated from the cooled jacket by an annular passage. Thus, the heat transferred from the liner to the cooled jacket is primarily by radiation, which results in low heat fluxes to the coolant. Augmented by a gas boundary layer control (such as provided by the full-diameter vortex injector), heat flux is further substantially reduced. The liner is continued through the nozzle region where it is backed up by a refractory insert of low conductivity and low mass material. This concept provides a controlled gas side wall temperature distribution and it also provides the lowest possible heat flux to the coolant jacket.

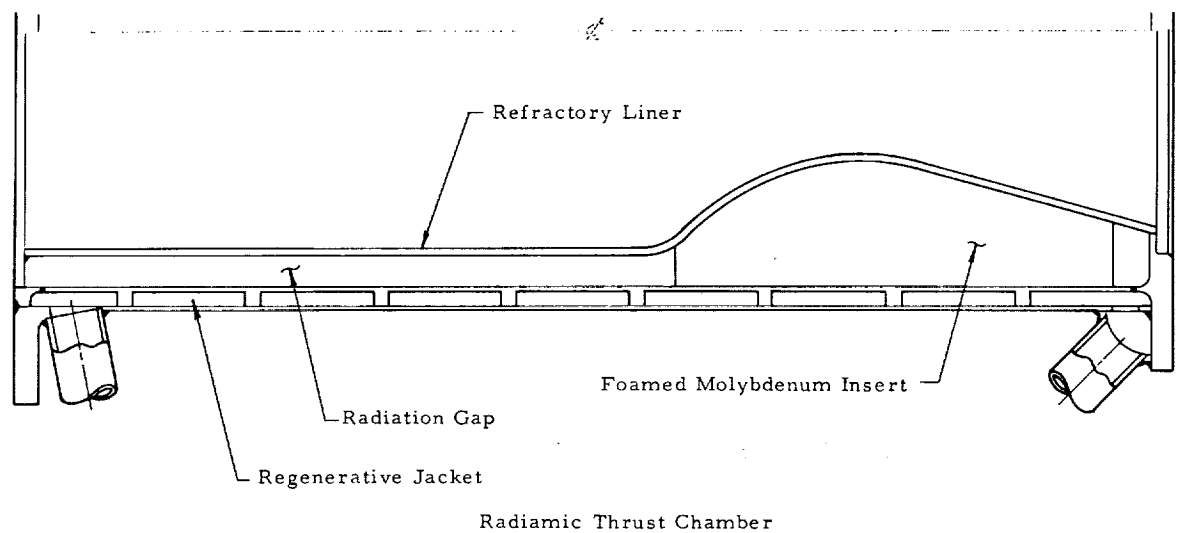
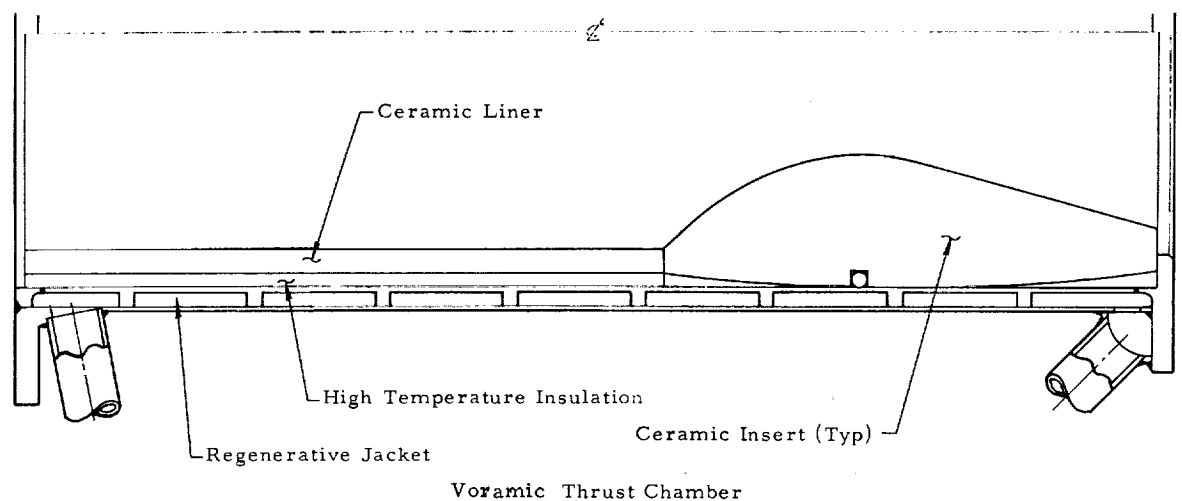
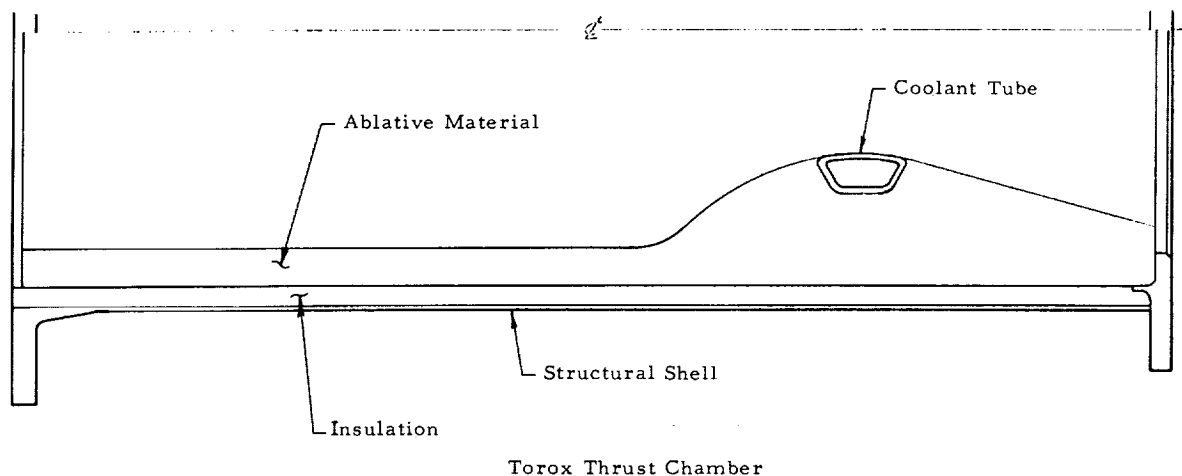


Figure 52. Advanced Chamber Concepts - Torox, Voramic and Radiamic

A radiation gap in the combustion chamber and a low density foamed molybdenum insert in the nozzle minimizes the heat stored by the internal parts of the thrust chamber. A secondary liquid propellant jacket is used to provide a mass of cold material which will absorb the heat stored. Sufficient propellant coolant mass is provided to maintain the transient and equilibrium liquid temperatures below the saturation or decomposition point. Low supply temperatures, typical of a vehicle in deep space, which are available minimize the size and weight of the outer jacket arrangement.

The heat stored within the thrust chamber controls the transient temperatures after shutdown and the final equilibrium temperature. These temperature levels are influenced by the shutdown temperature gradient, volumes and specific heats of the materials used. Low temperatures are desirable to minimize the possibility of boiling and/or decomposition of the liquid propellant coolants.

The Radiamic approach combines all of the features required to maintain low liquid coolant temperatures.

- Low heat input with the use of a full diameter vortex injector which has been demonstrated with  $N_2O_4$  /MMH propellants. Other injector types that would provide low heat inputs to the chamber wall could also be employed.
- Low heat storage materials inside the combustion chamber
- A large cold mass of liquid propellant surrounding the thrust chamber

(6) Augmented Radiamic - Transpiration and Film Cooling - The Radiamic thrust chamber, with its controlled thermal environment for the inner liner can also be employed with other types of augmentation techniques in addition to the full diameter vortex injector. The establishment of a cool mass along the wall of the combustor can provide both a reduction in heat flux to the wall and an appreciable lowering of the gas side surface temperature. Since this approach has the potential for allowing  $OF_2 / B_2 H_6$  chamber technology to proceed with state of the art materials, it was given serious consideration. The examination of two approaches was undertaken, transpiration and film cooling.

To establish the analytical feasibility of these concepts the extensive, prior work in related fields was reviewed, the applicability to the design study assessed, and a computer program developed for the computerized analysis of transpiration and film cooled rocket engines. This program permits the rapid comparison and evaluation of the various analytical approaches to transpiration, liquid film and vapor film cooled thrust

chambers. The efforts developed under prior NASA technology programs at both Marquardt (Reference 20 ) and Rocketdyne (Reference 21 ) were included as well as work from Purdue, University of Michigan, and JPL. The program is comprised of nine independent methods, viz two for transpiration cooling, four for liquid film cooling, and three for vapor film cooling.

The results of the analysis indicate that supplemental film or transpiration cooling utilizing  $\text{OF}_2$  or  $\text{B}_2\text{H}_6$  is feasible. However, further study and design data are required to permit optimization from a heat transfer and performance standpoint of these techniques. It is expected that the results of this design application will provide an excellent backup for the primary approach of the boundary layer control vortex injector with a Radiamic thrust chamber.

Based on the analytical studies and material screening results, the Radiamic concept offers the most promise for long duration combustion containment with  $\text{OF}_2 / \text{B}_2\text{H}_6$  since it provides low heat flux levels into the coolant while maintaining combustion side wall temperatures at tolerable levels and it is capable of restarts. The following section describes the Radiamic thrust chamber and the analytical results of the design study.

#### 4. Radiamic Thrust Chamber Design Analysis

##### a. Approach

A logic diagram of the approach used to verify the design of a Radiamic thrust chamber with  $\text{OF}_2 / \text{B}_2\text{H}_6$  is shown in Figure 53. An analytical thermal model was made of an existing Thiokol-RMD Radiamic engine which has been operated for many thousands of seconds at 100 psia and 100 lb thrust with  $\text{N}_2\text{O}_4 / \text{MMH}$ . This analytical model was then compared to the test data which included measurements of coolant bulk temperature rise, liquid side wall temperatures at various stations during firing and heat soak, and interface wall temperatures in the throat region and barrel radiation section. Heat transfer gas film coefficients calculated from transient temperature measurements in an uncooled copper chamber were employed to revise the heat transfer model to give the closest possible approximation to the actual measured conditions. The revised analytical model was then applied to two  $\text{OF}_2 / \text{B}_2\text{H}_6$  Radiamic engines operating at 100 lb thrust and 2000 pounds space thrust to define the operation conditions such as wall temperatures, coolant bulk rise, and heat soak temperature. A final  $\text{OF}_2 / \text{B}_2\text{H}_6$  thermal model was obtained and the conditions for satisfactory operation of a Radiamic thrust chamber at the 2000-pound space thrust level were then defined. Parametric tradeoffs of performance, mixture ratio and chamber pressure against suitable materials, wall temperatures, coolant bulk rise



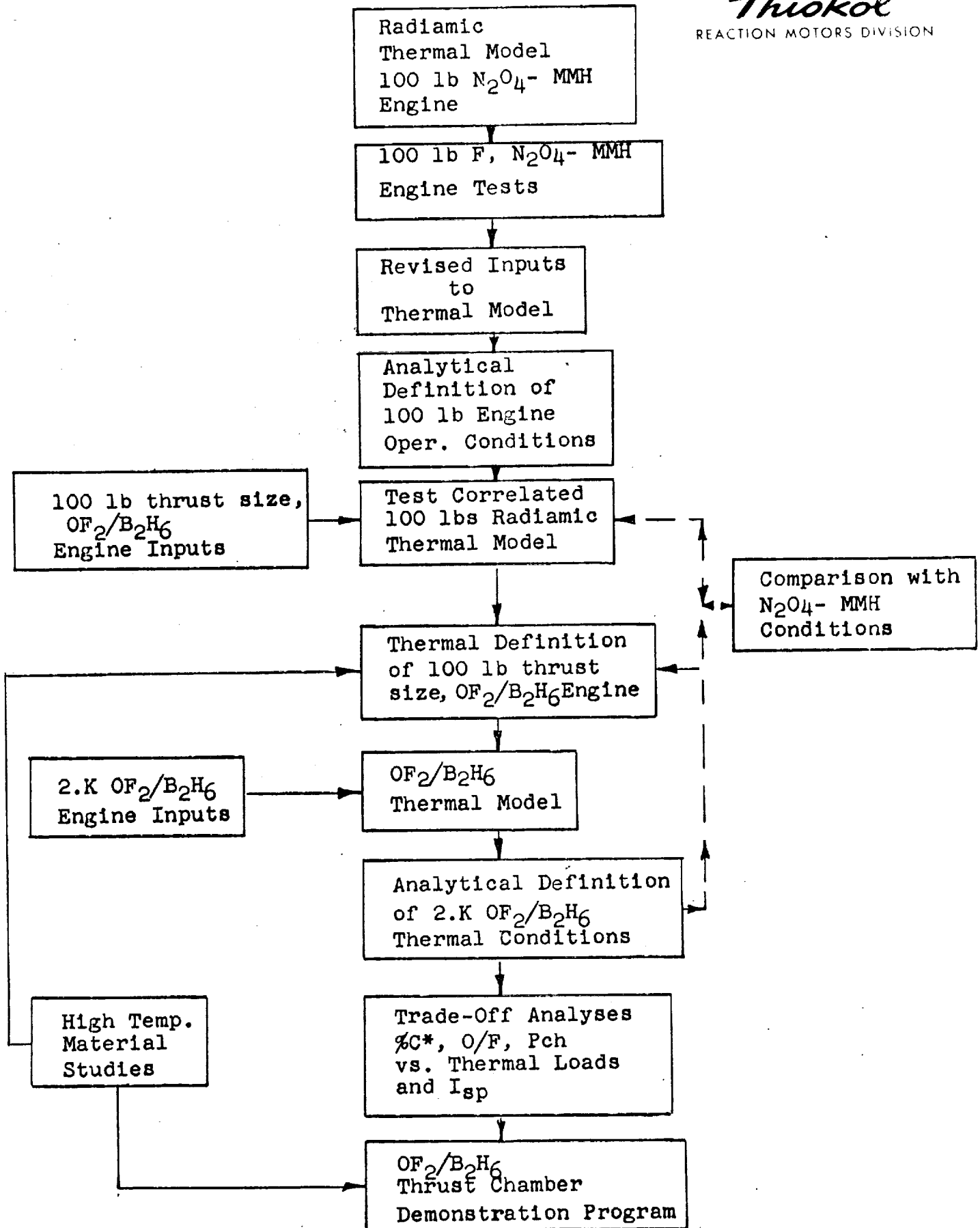


Figure 53. Design Study Approach Diagram

and soak temperatures were conducted. Material compatibility data from the  $\text{OF}_2/\text{B}_2\text{H}_6$  screening tests and from Corporate sponsored high temperature materials study programs for advanced space engines was utilized in the tradeoff studies.

b. Radiamic Concept

The results of the advanced chamber design study have been applied to a 2500 lb thrust space engine as shown in Figure 54. This design shows the embodiment of the study results in a realistic, flight type, thrust chamber. Oxidizer cooling is used in the nozzle and for a portion of the combustion chamber. The forward end of the combustion chamber is fuel cooled. A full diameter vortex injector is used to provide the low heat transfer coefficients.

Initially, it was planned to fabricate and test the most promising thrust chamber concept evolved during this program. To demonstrate the capabilities of the Radiamic design for  $\text{OF}_2/\text{B}_2\text{H}_6$  service a design was prepared targeted toward a technology design which would provide a maximum amount of data with a minimum of program risk. As a result of reallocation of funding to support the heat sink injector effort (Ref. Section IV.A.3), fabrication and testing of this concept was not undertaken.

Figure 55 shows the design layout of a 2000-pound space thrust  $\text{OF}_2/\text{B}_2\text{H}_6$  Radiamic combustion chamber that was planned to be utilized for test evaluation. The layout shows a 15 L\* and 30 L\* geometry. It is a double-jacketed, regeneratively cooled engine. The throat region contains a liner and a refractory throat substrate backed by a copper ring, all surrounded by a double, helical passage cooling jacket. The throat liner extends through the chamber barrel section. In this section there is a radiation gap between the liner and the double cooling jacket.

The outer jacket provides the required heat sink capacity after shutdown to reduce the transient and equilibrium soak temperature of the coolant. In this manner the liquid coolant is maintained below its saturation temperature during heat soak period. The fins in the jacket are aligned to provide a radial thermal bypass path for the heat from the inner jacket wall and the coolant to the outer jacket wall where it is dissipated. The main advantage of the aligned fin occurs during heat soak where the heat is funneled into the cooler outer jacket thus reducing the transient coolant temperature peaks. The temperature restrictions on the coolant jacket material are not limiting. Therefore, a lightweight, high thermal conductivity material such as aluminum is the obvious candidate for the coolant jacket and helical fins.



## Design Conditions

Thrust (vac)	2500 psia
Chamber Pressure	150 psia
Mixture Ratio (O/F)	3.0
Nozzle Expansion Area Ratio	40
Design Specific Impulse	390 sec
Engine Weight	56 lb

Figure 54. 2500-lb Space Thrust Radiamic Engine Design -  $\text{OF}_2/\text{B}_2\text{H}_6$

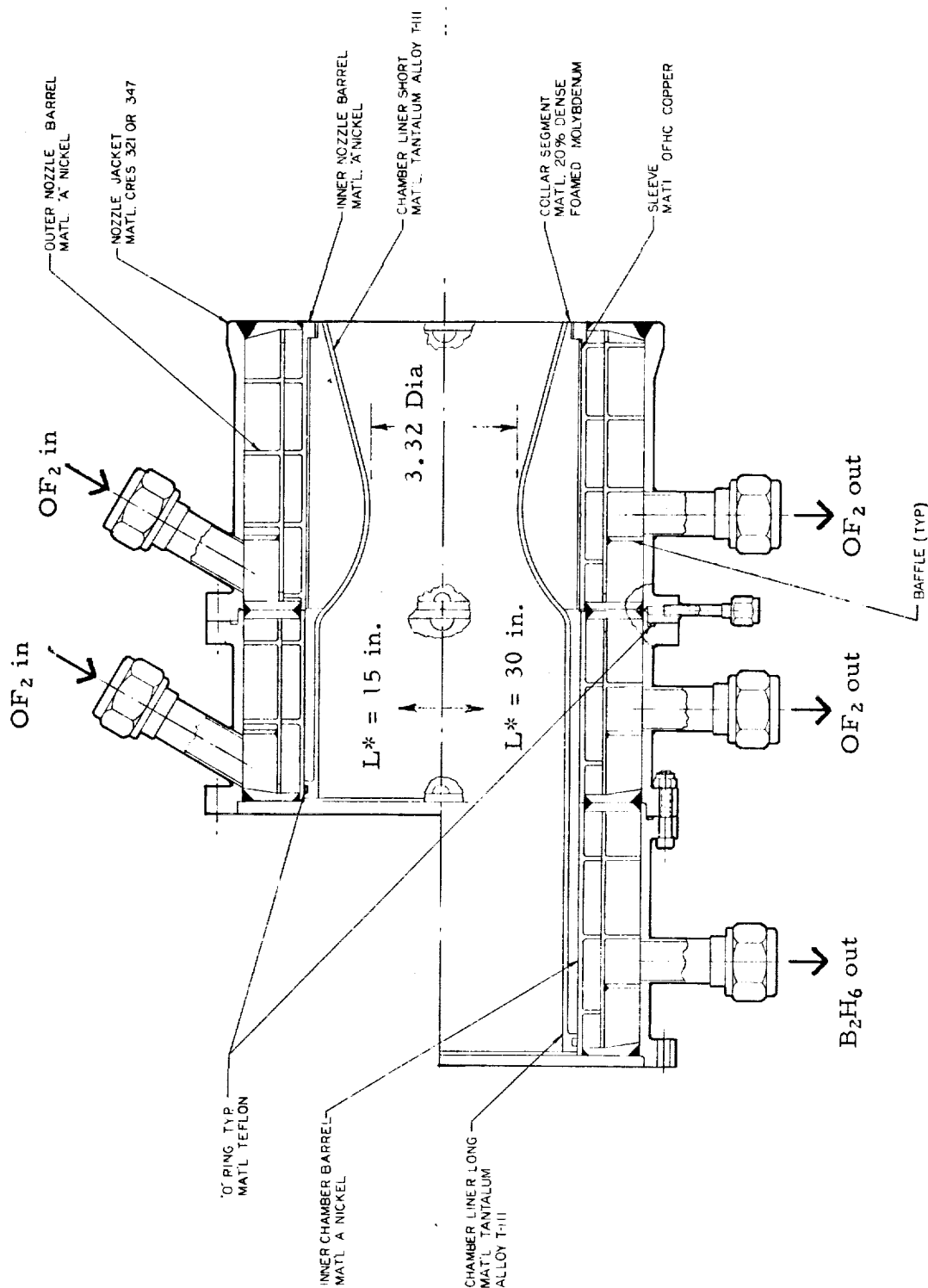


Figure 55. Radiamic Thrust Chamber Assembly

The Radiamic advantages lie in a combination of engineering design and materials usage to solve the problem of confining the combustion heat to a small mass on a surface away from the coolant and outer structure. Throttling and pulsing mode operation can have wide variations without causing coolant bulk rise problems or high outside structure heat leaks to surrounding systems. Since the Radiamic concept minimizes the heat input into the coolant, the coolant velocity requirements on a Radiamic engine would be extremely low; 10-20 ft/second in the throat region and 2-10 ft/second in the radiation chamber section. This design concept would make the use of  $\text{OF}_2$  or  $\text{B}_2\text{H}_6$  as coolants more attractive. The gas side surface temperatures of this type of combustion chamber will be high; necessitating combustion-side liners utilizing advanced materials.

(1) Radiamic Nozzle Section - The nozzle section would employ a coated liner consisting of a layer of  $\text{HfO}_2$  (.025-.035) on a 90Ta-10W alloy. The low conductivity of the  $\text{HfO}_2$  provides oxidation and erosion resistance for the 90Ta-10W structural liner. Adherence of the  $\text{HfO}_2$  by surface conditioning has been achieved at Thiokol-RMD. The refractory substrate material is a foamed molybdenum (FoMo); 25% the density of solid molybdenum with 12.5% of its thermal conductivity. FoMo is an ideal high temperature material for blocking heat to the coolant while keeping the heat storage in the insert to a minimum. A copper ring surrounding the FoMo insert is used to minimize axial thermal gradients.

(2) Chamber Region - The chamber barrel would consist of the same coated liner as the throat region. A radiation gap separates the liner from the cooling jacket and limits the heat input into the coolant during operation. Heat storage is confined in the thin low mass radiation liner. The radiation barrier also limits the rate at which this stored heat is released to the coolant during heat soak. During steady state operation, the radiation barrier limits the heat input to the coolant to such an extent that low jacket coolant velocities are possible, permitting a low heat capacity coolant such as  $\text{OF}_2$  to absorb the heating rate without difficulty. The double coolant jacket provides a means of limiting the propellant temperature rise during heat soak.

(3) Injector - The injector is a full diameter vortex. This injector concept has provided a significant reduction in throat heat transfer coefficients due to boundary layer effects with  $\text{N}_2\text{O}_4$ /MMH propellants (Ref. Section IV.A.5). The heat blockage concept of the Radiamic chamber has associated with it high combustion side wall temperatures. With a high flame temperature combination such as  $\text{OF}_2$  /  $\text{B}_2\text{H}_6$  it is desirable to have an injector that provides low heat transfer coefficients in the critical regions. It is believed that the utilization of a full-diameter vortex injector with  $\text{OF}_2$  /  $\text{B}_2\text{H}_6$  would provide low heat transfer film coefficients similar to those obtained during  $\text{N}_2\text{O}_4$ /MMH testing.

c. Analytical Approach

(1)  $\text{OF}_2/\text{B}_2\text{H}_6$  Thrust Chamber Model Configuration - The dimensional representation made in the  $\text{OF}_2/\text{B}_2\text{H}_6$  heat transfer model for the design shown on Figure 57, consists of 10 axial stations, five in the chamber and five in the nozzle. Similar analyses were also performed for a thrust level of 100 lb. As described earlier, the liner consists of a  $\text{H}_2\text{O}_2$  coated shell consisting of  $\text{HfTa}$  and 90 Ta-10w base material. The throat substrate is a 25% theoretical density foamed molybdenum (FoMo) backed by a copper ring and surrounded by a double cooling jacket of either nickel or aluminum. The chamber consists of the coated liner, a radiation gap and the double cooling jacket. Table XII lists the materials and their thermal properties (as a function of temperature) used in this analysis.

(2) Heat Transfer Analysis Technique - A Thiokol-RMD computer program based on a steady state one-dimensional, radial heat transfer mode was used to determine radial wall temperature distribution and coolant bulk rise and equilibrium heat soak temperatures.

A previous study, using the measured heat transfer data and adapting the computer program to conform to these results, indicated that a contact resistance between the liner and the foamed molybdenum was necessary to obtain agreement between predicted steady state and transient liquid wall temperatures and steady state liquid bulk temperature with that of the measured test data. The contact resistance is simulated by use of a fin in the program in which an effective fin coefficient  $h_f$  is used. The combustion chamber heat transfer gas film coefficients for the 2000-pound space thrust design presented in Figure 44 were utilized in this. The heat transfer coefficients were based upon data correlations described previously.

Table XIII lists the nominal baseline operating conditions for the thrust chamber designs analyzed during the study.

(3) Parametric Study Conditions - The thrust chamber designs were analyzed for conditions of chamber pressures of 50, 100, 150 psia, mixture ratios of 1.5, 2.0, 2.5, 3.0 and % c\* of 98, 96, 94, 92, and 90. The analytical results of the 2000-pound space thrust design are presented in the following section.

d. Analytical Results - 2000-Pound Space Thrust Radiamic Design

(1) Gas Side Wall Temperatures - Figure 56 shows the throat gas side wall temperatures as a function of chamber pressure, mixture ratio and % c\*. Figure 57 shows the gas side wall temperature of the coated radiation liner in the chamber barrel section. The operating temperature limits for 90Ta-10w alloy

TABLE XII  
MATERIAL THERMAL PROPERTIES

Material	1000°F			500°F		
	K	$\rho$	C <sub>P</sub>	K	$\rho$	C <sub>P</sub>
Hafnium Oxide (H <sub>f</sub> O <sub>2</sub> )	1.5	500	.12	1.5	500	.123
Haftan (H <sub>f</sub> - 20 Ta)	20	815	.035	20	815	.035
Tantalum-Tungsten (90Ta-10W)	34	1045	.045	34	1045	.045
Formed Molybdenum (FoMo)	10.1	172	.06	8.15	172	.06
Copper	225	495	.09	225	495	.09
Nickel	35	550	.13	33	550	.13

Note: Thermal Conductivity (K) - Btu/hr-ft<sup>2</sup> - °F/ft  
Density ( $\rho$ ) - lb/ft<sup>3</sup>  
Specific Heat (C<sub>P</sub>) - Btu/lb - °F

TABLE XIII  
NOMINAL OPERATING CONDITIONS  
RADIAMIC THRUST CHAMBER

		N <sub>2</sub> O <sub>4</sub> -MMH (Actual)	OF <sub>2</sub> -B <sub>2</sub> H <sub>6</sub> (Predicted)	OF <sub>2</sub> -B <sub>2</sub> H <sub>6</sub> (Predicted)
Pch	psia	100	150	150
F (Thrust)	lb	100	150	2000
O/F		1.6	3.0	3.0
c*	ft/sec	5700	7010	7010
Tg, Gas Temperature	°F	4925	6535	6535
Coolant		MMH	OF <sub>2</sub>	OF <sub>2</sub>
Coolant Inlet Temperature	°F	60-130	-325	-325
Coolant Throat Velocity	ft/sec	20	24.8	15
Coolant Chamber Velocity	ft/sec	7	8.8	10



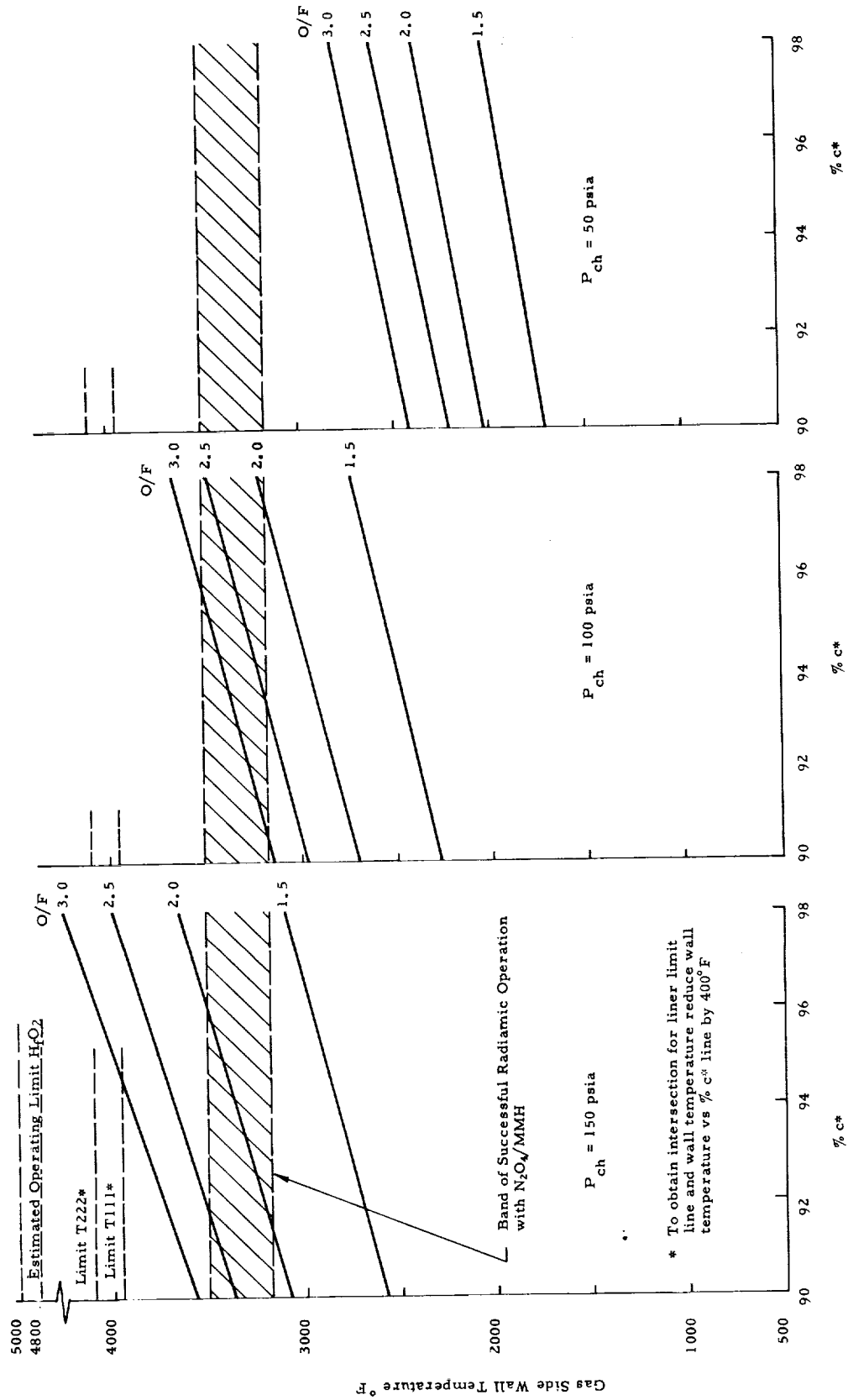


Figure 56. Gas Side Wall Throat Temperature - Radiamic Design

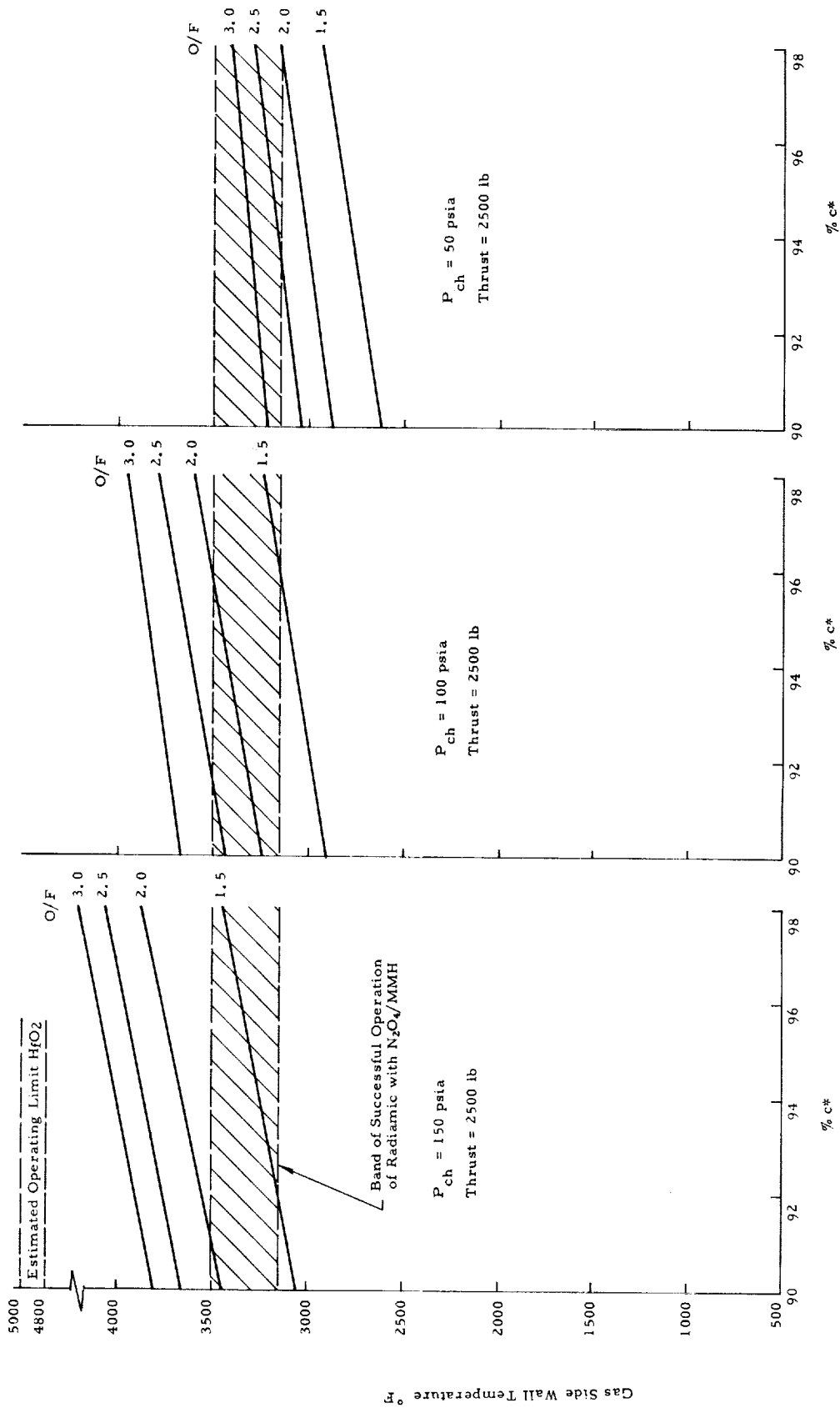


Figure 57. Gas-Side Wall Chamber Temperature - Radiamic Design

and more advanced materials (T-111 and T-222) are superimposed on Figures 56 and 57. The limiting temperature of the  $\text{HfO}_2$  is estimated to be 4800 to 5000°F. The estimated temperature limit of the 90Ta-10W alloy is 3500°F. The T-222 and T-111 alloys have operating limits ranging between 3800-4200°F.

The  $\text{HfO}_2$  coating provided oxidation and erosion resistance with  $\text{N}_2\text{O}_4$ /MMH propellants. Theoretically the  $\text{HfO}_2$  coating should be able to operate at these chamber pressure and mixture ratio ranges with  $\text{OF}_2$ / $\text{B}_2\text{H}_6$  without difficulty. It should be noted that the gas-side liner temperature limits are conservative limits since there is a temperature drop (440°F) across the  $\text{HfO}_2$  coating which is not reflected on Figures 56 and 57.

Superimposed on Figures 56 and 57 is a band representing gas side wall temperatures to which these coatings and materials have been successfully operated for durations between 300 and 4000 seconds with  $\text{N}_2\text{O}_4$ /MMH propellants. With this band as a starting point, and using a full diameter vortex injector with a chamber  $L^*$  of 10 to 15 inches, successful throat operation is predicted at a chamber pressure of 100 psia, and O/F of 2.5 and a performance level of 98%  $c^*$ . Successful operation could be achieved with other combinations of chamber pressure  $P_c$ , O/F and  $c^*$ . The limiting condition is the radiation gas side surface in the chamber section where temperatures are higher than in the throat plane. This is due to heat blockage of the radiation gap. The band representing radiamic operating conditions indicates that the chamber region is feasible at a chamber pressure of 100 psia, a mixture ratio of 2.5 and a performance level 91.8% of theoretical  $c^*$  (or any combination of those conditions giving similar temperature levels). As seen from Figures 56 and 57, the main limitation is the operating temperature regime demonstrated with refractory materials using  $\text{N}_2\text{O}_4$ /MMH propellants. Indications are that with the  $\text{HfO}_2$  coating operating temperatures up to 4800°F can be obtained. Figure 56 shows that at the throat section the 90Ta-10W liner could operate at an O/F of 3.0 and 95%  $c^*$  at 100 psia.

There are many operating conditions which comply with a maximum wall temperature limit of 3500°F. A range of operating conditions are feasible depending on mission requirements (i. e., on the basis of specific impulse, propellant tank size and weight). For feasibility demonstration, it is recommended that, initially, test evaluations should be made at an O/F of 2.5, a chamber pressure of 100 psia and  $c^*$  of 91.8%.

For the entire range of operating conditions studied, the foamed moly throat substrate is maintained below its limiting temperature of about 3500°F.

Operation can be extended beyond the range set in this study if the more advanced alloys, hafnia coated T-111 and T-222 are used. These are well along

in feasibility demonstrations being conducted at Thiokol-RMD. These tests are being conducted with  $\text{N}_2\text{O}_4/\text{MMH}$  propellants at a chamber pressure level of 100 psia. The hafnia coating has shown excellent performance at measured gas side liner temperatures on the order of 3500F. The hafnia ( $\text{HfO}_2$ ) coating application has been developed to a degree where it protected a 347 stainless steel liner for 70 seconds; whereas an uncoated stainless steel liner burned out after 10 seconds. Based on this data, operation with  $\text{OF}_2/\text{B}_2\text{H}_6$  at conditions providing the same combustion liner surface temperatures (i. e. 3150-3500F) as those obtained with  $\text{N}_2\text{O}_4/\text{MMH}$  will provide successful long duration chamber capability. The results of the  $\text{OF}_2/\text{B}_2\text{H}_6$  material screening tests and corporate sponsored studies have shown that the most promising material appears to be the T-111 tantalum (coated with  $\text{HfO}_2$  and uncoated). The use of the tantalum tungsten alloys with a  $\text{HfO}_2$  coating in a Radiamic concept should provide adequate protection for long duration containment of  $\text{OF}_2/\text{B}_2\text{H}_6$ .

(2) Specific Impulse - Gas Side Wall Temperature Tradeoff - During the course of the studies, a parametric tradeoff on the effects of chamber pressure, mixture ratio and combustion efficiency on vacuum specific impulse was made. The minimum operating conditions of 100 psia chamber pressure, a mixture ratio of 2.5 and combustion efficiency of 91.8%  $c^*$  are based strictly on heat transfer (i. e., combustion side wall temperature of 3500F). An interesting effect occurs when specific impulse is considered. This is shown in Figure 58. This figure shows the gas side wall temperature as a function of chamber pressure,  $\%c^*$ , and mixture ratio for the chamber radiation section with values of constant specific impulse superimposed. Examination of Figure 58 shows that equivalent specific impulse can be obtained by operating at lower mixture ratios and higher  $\%c^*$ , or operating at reduced chamber pressure for a given mixture ratio and  $\%c^*$ , with a significant reduction in the gas side wall temperature. For example, the performance at the minimum design operating conditions ( $\text{O/F} = 2.5$ , 91.8%  $c^*$ ,  $T_{\text{wg}} = 3500^\circ\text{F}$ ) is 382 seconds. This value of specific impulse can also be obtained at an  $\text{O/F}$  of 1.5 and  $c^*$  of 98%. The resulting wall temperature for these conditions is  $3200^\circ\text{F}$ , a much more desirable situation, of course, from the standpoint of heat transfer and durability. The significance of this tradeoff shows that it would be easier to obtain duration durability by reducing chamber pressure and/or mixture ratio and increasing  $\%c^*$  once an acceptable operating temperature level is selected. Based on a selection of  $3500^\circ\text{F}$  as the limiting wall temperature and upon past radiamic performance, the highest specific obtainable is 397 seconds at a mixture ratio of about 1.8 and  $\%c^*$  of 98% for a chamber pressure of 100 psia. The recommended selection for initial feasibility testing (i. e., an  $\text{O/F}$  of 2.5 and a  $c^*$  of 91.8%) might be more advantageous from the standpoint of typical space mission propellant and tank storage weights and sizes. Many tradeoffs can be made but the final selection of operating parameters would be dependent upon specific mission requirements.

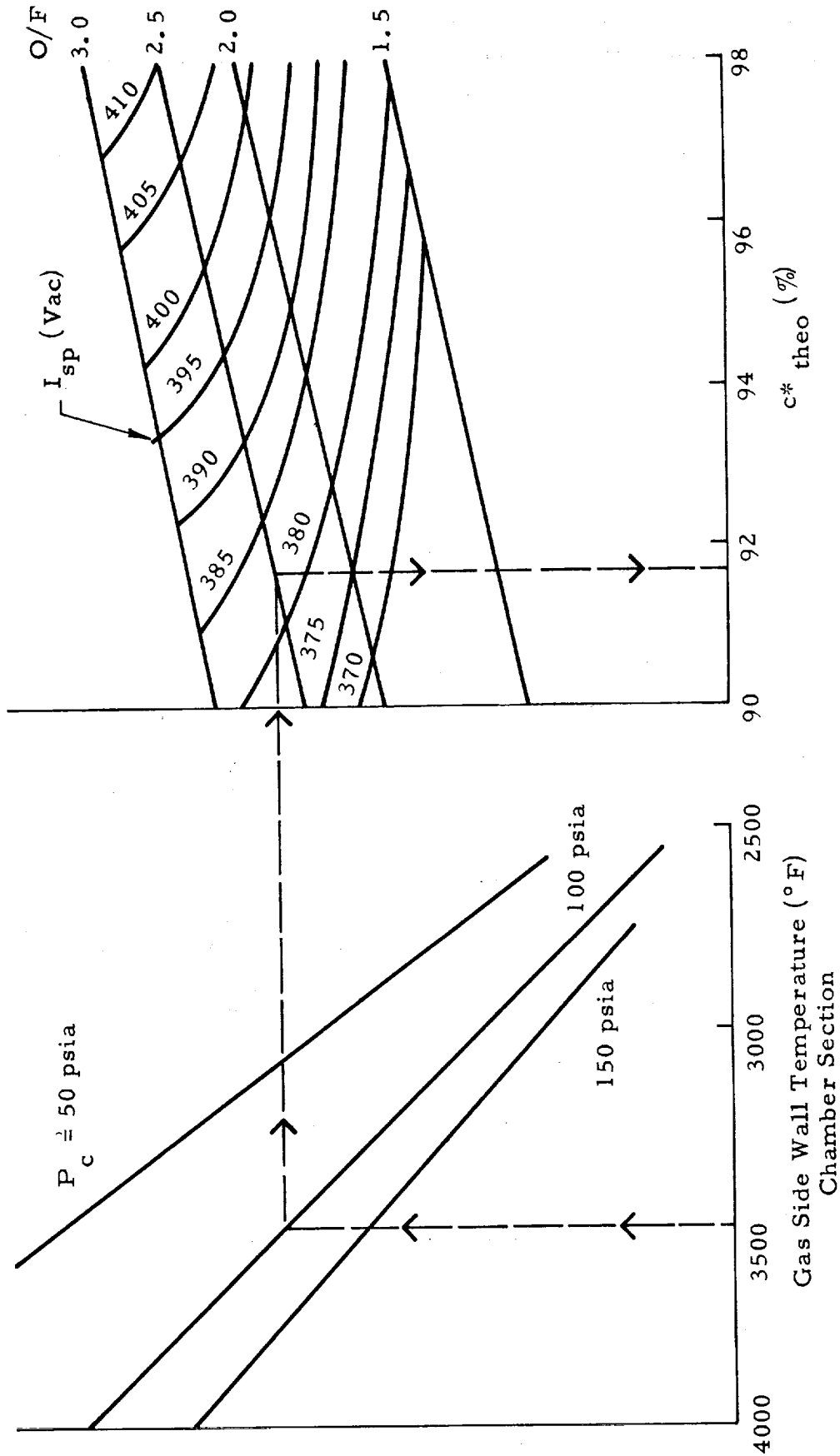


Figure 58. Gas-Side Wall Temperature - Specific Impulse Tradeoff

(3) Coolant Bulk Rise - For the 2000 pound space thrust  $\text{OF}_2/\text{B}_2\text{H}_6$  design, cooling can be accomplished with  $\text{OF}_2$  and coolant bulk temperature rise is not a problem. The bulk rise for a range of chamber pressures is shown on Figure 59. The limit of the bulk rise is reached when bulk boiling occurs (i. e., when the coolant reaches its saturation temperature). It is seen that in all cases considered, the coolant bulk rise is not a problem and that  $\text{OF}_2$  should be satisfactory as a coolant for steady state operation with an inlet temperature of  $320^\circ\text{F}$ . For warmer  $\text{OF}_2$  inlet temperatures, it would be necessary to consider  $\text{B}_2\text{H}_6$  and  $\text{OF}_2$  as dual coolants. Conversely, for higher thrust levels (i. e.  $> 2000$  lb) correspondingly lower coolant bulk temperature rise would occur permitting operation with warmer propellants.

Figure 60 shows the effect of  $L^*$  and mixture ratio on  $\text{OF}_2$  bulk rise. Although bulk rise is acceptable for an  $L^*$  of 30, the  $L^*$  of 15 provides the enhancement effect on throat boundary conditions as discussed previously. For both  $L^*$  conditions and operation over a mixture ratio range of 1.5 to 3.0, the  $\text{OF}_2$  bulk temperatures are well below the saturation temperature.

(4) Coolant Velocity and Liquid Side Wall Temperature - The  $\text{OF}_2$  jacket cooling velocities are 10 ft/sec and 15 ft/sec in the chamber and nozzle sections, respectively. The predicted fluxes in the throat and chamber are on the order of .36 and .40 Btu/sec-in.<sup>2</sup>, respectively. At these low flux levels, the liquid side wall temperatures are well below the range where nucleate boiling occurs. Figures 61 and 62 show typical  $\text{OF}_2$  liquid side wall temperatures in the throat and radiation barrel region.

(5) Equilibrium Soak Temperature - The average equilibrium soak temperature of the combustion chamber provides an indication of the heat soak to the coolant after shutdown. For restart conditions, boiling of the coolant in the jacket is to be avoided because of resultant injection and control problems. Liquid side wall temperatures and bulk temperatures can have transient peaks above equilibrium soak temperature and these must be restudied for a particular design. Figure 63 shows the equilibrium soak temperature for the 2000 pound space thrust design operating at a chamber pressure of 150 psia. The total heat capacity of the thrust chamber design can be adjusted to reduce the heat soak to the coolant during shutdown to obtain values below the saturation temperature limit ( $-155^\circ\text{F}$ ) of  $\text{OF}_2$  at a chamber pressure of 150 psia. For a chamber pressure level of 100 psia, heat soak is not a problem.

Based on the results of the analytical design studies, the following conclusions are drawn:

- Through the combination of a small  $L^*$  (10-15) engine, a full diameter vortex injector and the current state-of-the-art materials technology, the Radiamic thrust chamber concept is feasible with  $\text{OF}_2/\text{B}_2\text{H}_6$  to provide a thrust chamber with durability for long firing durations and restart capability.

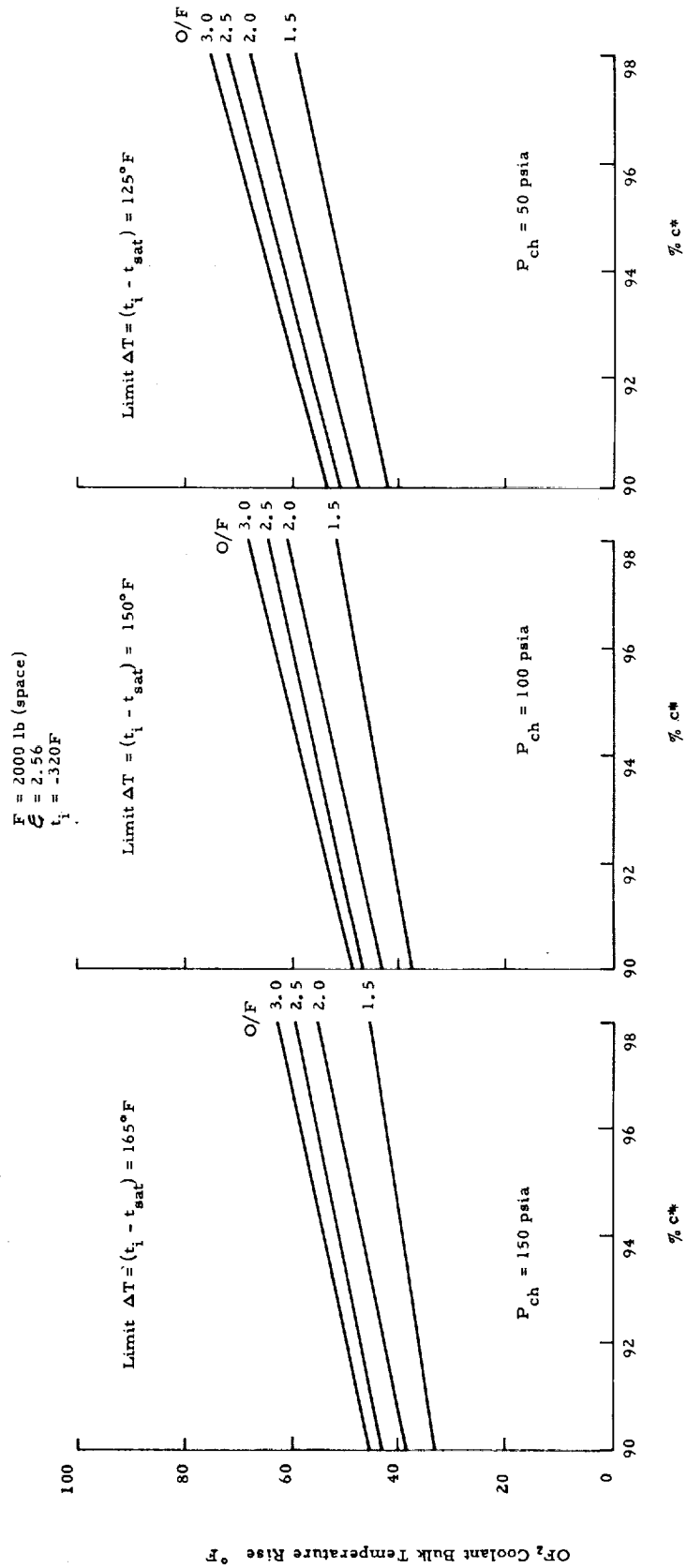


Figure 59.  $\text{OF}_2$  Bulk Temperature Rise as a Function of Operating Conditions-Radiamic Design

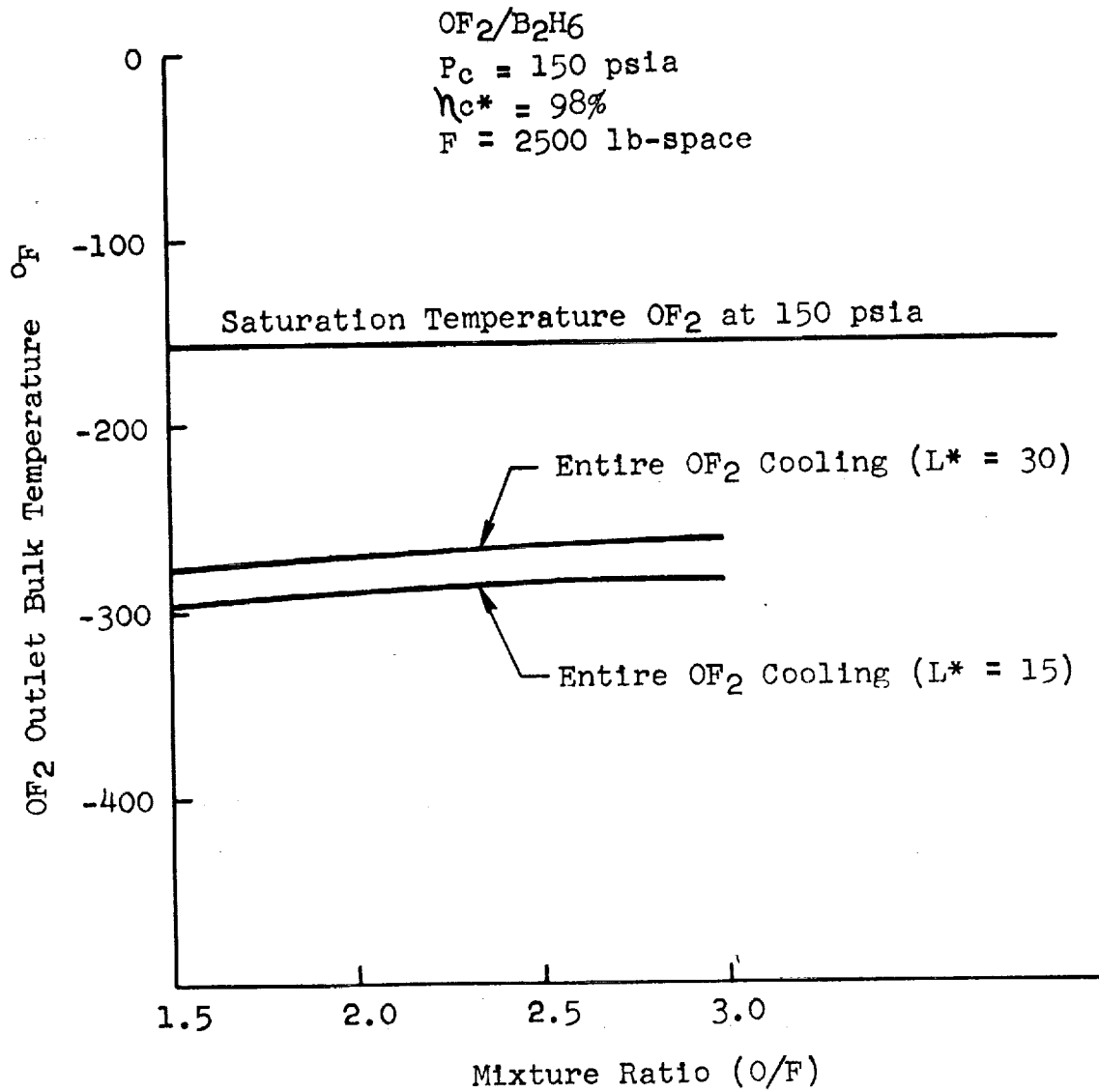


Figure 60. OF<sub>2</sub> Bulk Temperature Rise as a Function of  $L^*$ , O/F



OF<sub>2</sub>/B<sub>2</sub>H<sub>6</sub>  
P<sub>c</sub> = 150 psia  
O/F = 3.0  
F = 2500 lb-space  
OF<sub>2</sub> Jacket Velocity=15 Ft/Sec

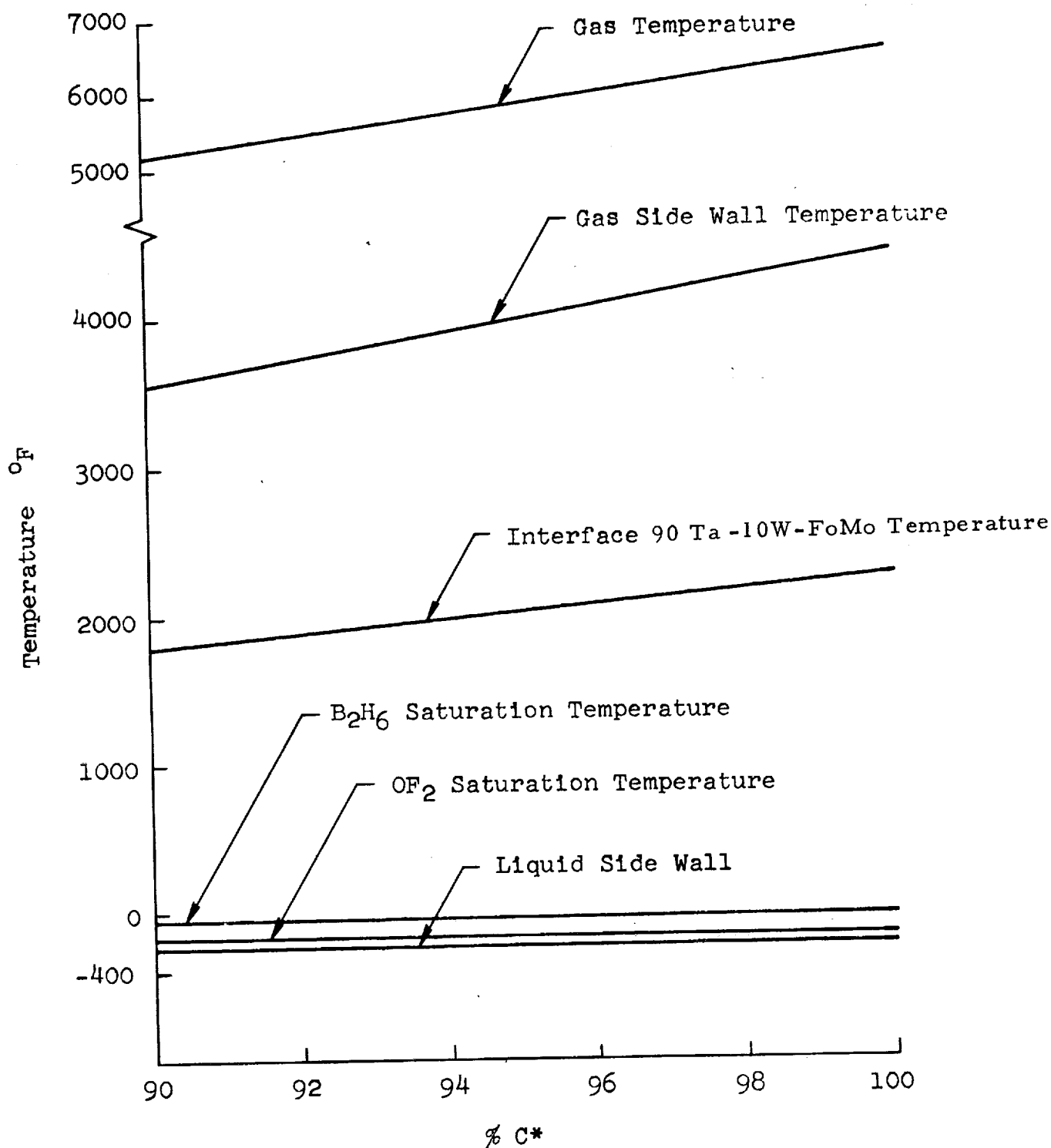


Figure 61. Radiamic Chamber Design-Throat Temperature Profile

$\text{OF}_2/\text{B}_2\text{H}_6$   
 $P_c = 150 \text{ psia}$   
 $\text{O/F} = 3.0$   
 $F = 2500 \text{ lb-space}$   
 $\text{OF}_2 \text{ Jacket Velocity} = 10 \text{ Ft/Sec}$

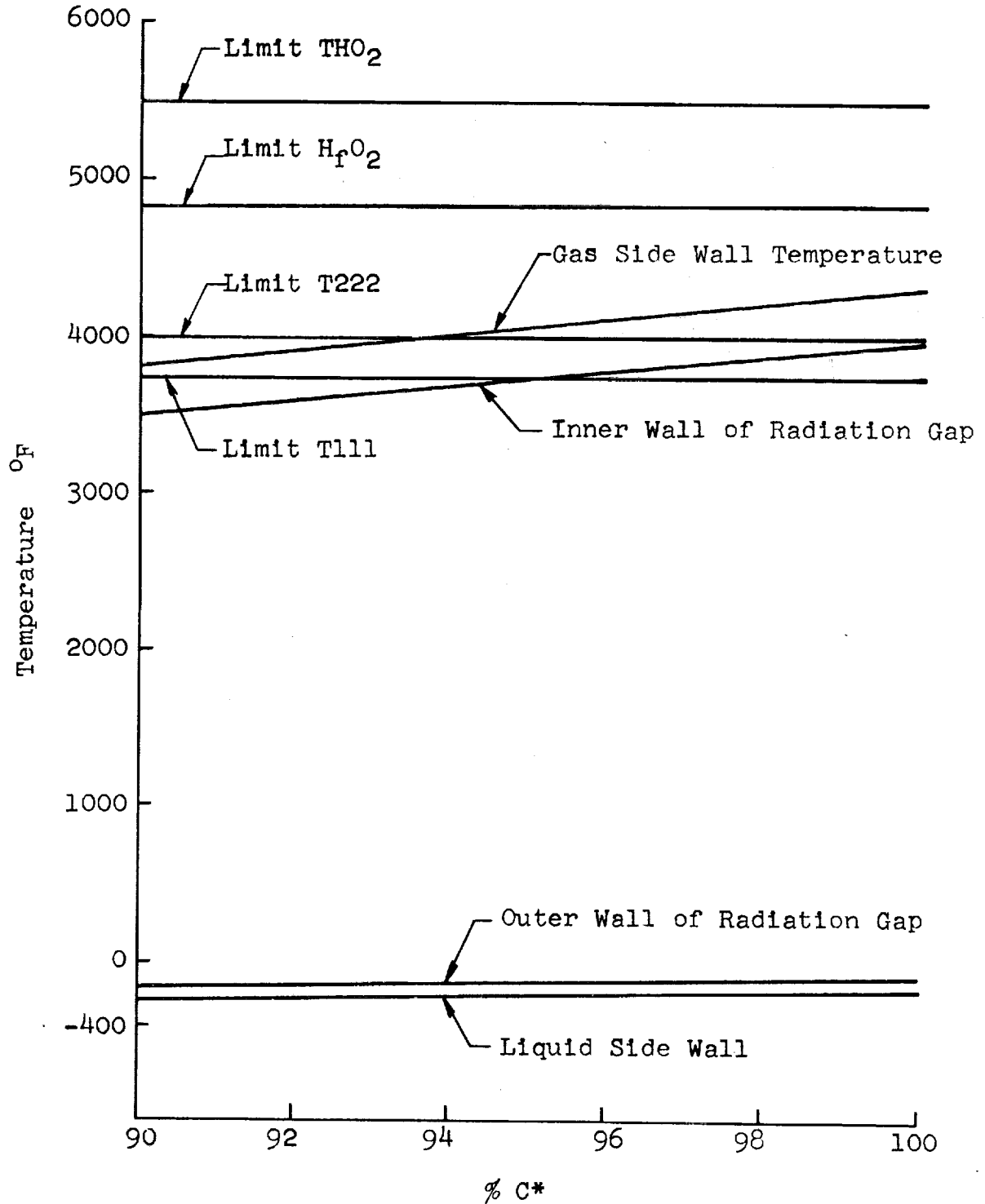


Figure 62. Radiamic Chamber Design-Chamber Temperature Profile

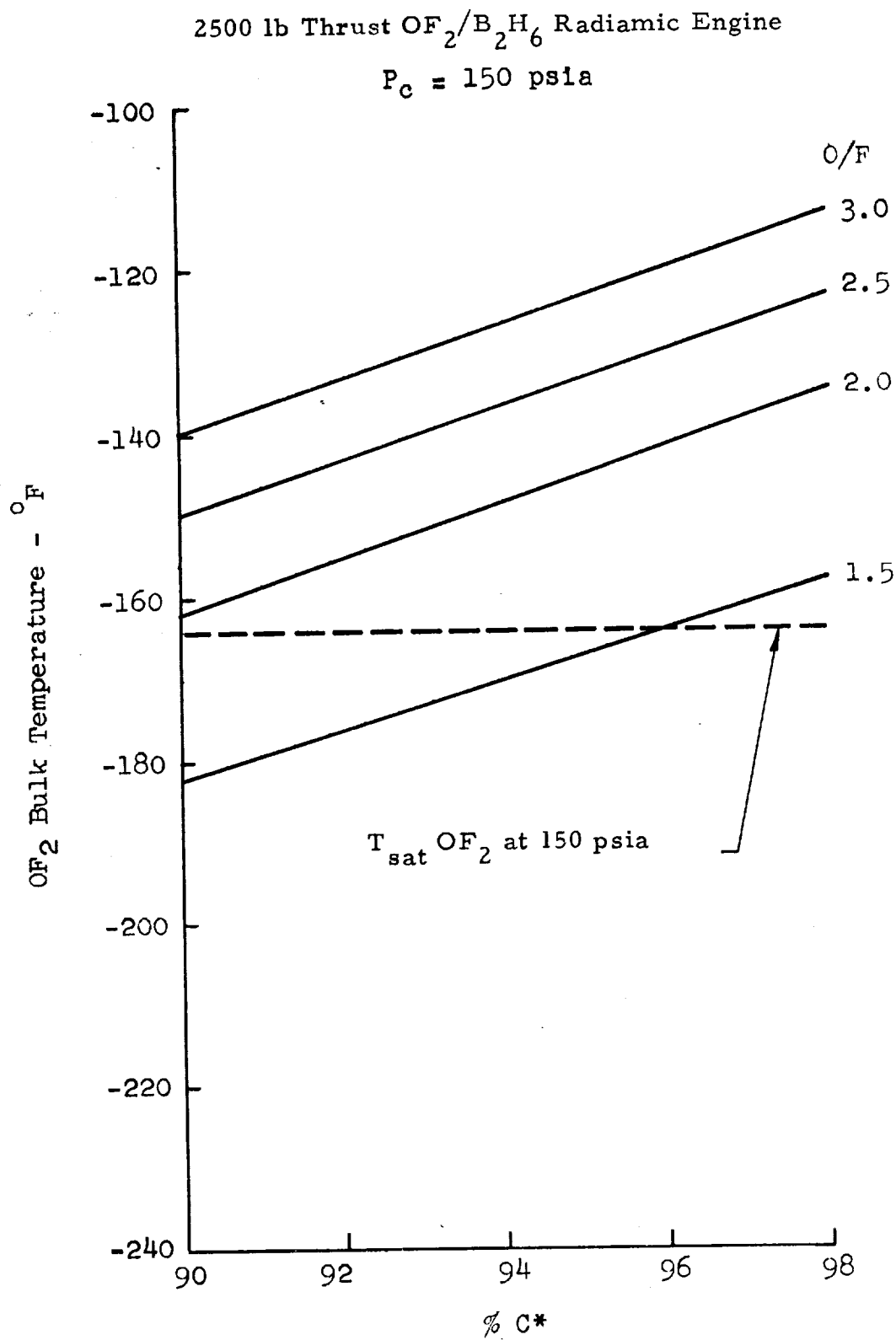


Figure 63. Equilibrium Soak Temperature - Radiamic Design

- The Voramic chamber concept can provide duration capability for missions not requiring restarts.
- For engines operating at higher thrust levels (i. e.  $> 2000$  lbs) or lower chamber pressures (i. e.  $< 100$  psia), partial regenerative cooling with a Voramic chamber appear feasible of providing long duration, restart capability.

## REFERENCES

1. Thiokol-RMD, "Investigations of Space Storable Propellants", Final Report 6028-F under Contract NAS 3-2553, January 1964.
2. Thiokol-RMD, "Investigation of Advanced High Energy Space Storable Propellant System", Final Report 5507-F under Contract NAS-w-449, November 1962.
3. Hunter, M. W., II, "Future Unmanned Exploration of the Solar System", Astronautics and Aeronautics, Vol. 2, No. 5, May 1964.
4. Martin Company, "Spacecraft Propulsion Systems for Manned Mars and Venus Missions", Final Report under Contract NAS-w-1053, July 1965.
5. Carey, L., "Pressure-Fed Liquid Rocket Payload Potential", AIAA Paper No. 64-268, Presented at the 1st AIAA Annual Meeting, Washington D.C., 29 June - 2 July 1964.
6. General Electric, "Propellant Storability in Space", Technical Documentary Report No. RPL-TDR-64-75, June 1964.
7. Smith, D. S., Mann, D. J., "OF<sub>2</sub> Looks Promising As A Space Storable Propellant", Space Aeronautics, January 1963.
8. Bernath, L. "A Theory of Local Boiling Burnout and Its Application to Existing Data". "Heat Transfer", Chemical Engineering Progress Symposium Series No. 30, Vol. 56, 1960, A.I.C.H.E.
9. Hill, P. R., "A Method of Calculating the Transient Temperatures of Thick Walls", NASA Report 1372, 1958.
10. Bartz, D. R., "A Simple Equation for Rapid Estimation of Rocket Nozzle Convective Heat Transfer Coefficients", Jet Propulsion, Volume 27, January 1957, pp. 49-51.

11. Tick, S. J., Huson, G. R., Griese, R., "Design of Ablative Thrust Chambers and Their Materials", AIAA Paper No. 64-261, Presented at the First AIAA Annual Meeting, Washington, D. C., June 29 - July 2, 1964.
12. JANAF Thermochemical Data, 1961
13. Liquid Propellants Handbook Battelle Memorial Institute
14. H. L. Johnson, G. T. Clarke, E. B. Rifkin and E. C. Kerr., J. Am. Chem. Cos., 72 393 (1950)
15. Thiokol Chemical Corporation Project D-64-302, RMD Project 9058, Summary Report, "Spacecraft Propulsion Advanced Combustion Chamber Development", 31 December 1964
16. "Project Definition Phase - Radiamic C-1 Engine Program", RMD Summary Report 6200-G3, 18 June 1965.
17. Brinswade, A. F., and Desman, L. G., "Hypothesis for Correlating Rocket Nozzle Throat Convective Heat Transfer", Ai Che Reprint 25, 9 August 1964.
18. Yaffe, B. S., "Diborane, Space Storable Fuel", Callery Chemical Corporation, January 1962.
19. Peters, D. L., "Chemical Corrosion of Rocket Liner Materials and Propellant Performance Studies", Ford Motor Company, Aeronutronic Division Publication No. U-2384, Final Report Volume I, 15 December 1963
20. "Thrust Chamber Cooling Techniques for Spacecraft Engines", Marquardt Report No. 5981, Vol. II-70, Contract NAS 7-103.
21. "Investigation of Cooling Problems at High Chamber Pressures, (Final Report", Rocketdyne Report R-3999, Contract NAS 8-4011.

TABLE XIV  
LIST OF SYMBOLS

<u>Symbol</u>	<u>Description</u>	<u>Units</u>
G	Throughput Vortex Annulus Mass Velocity ( $\dot{w}/A$ )	$\text{lb}_m/\text{sec-in}^2$
$\dot{w}$	Propellant Flow rate	$\text{lb}_m/\text{sec}$
A	Annular Area Between Vortex Fuel and Oxidizer Injectors - combustion zone	$\text{in}^2$
$c^*$	Characteristic exhaust velocity	$\text{ft/sec}$
$\xi_e$	Nozzle exit to throat area ratio, $A_e/A_t$	
F	Thrust	$\text{lb}_f$
$P_{ch}$	Chamber pressure	$\text{psia}$
$C_F(\text{map})$	Maximum achievable sea level nozzle thrust coefficient, corrected for $\lambda, C_D, C_V$	
$I_{sp}(\text{map})$	Maximum achievable sea level specific impulse corrected for $\lambda, C_D, C_V$	$\text{lb}_f\text{-sec}/\text{lb}_m$
$C_F \text{ vac}$	Nozzle thrust coefficient at $P_a = 0$	
$I_{sp} \text{ vac}$	Specific impulse at $P_a = 0$	$\text{lb}_f\text{-sec}/\text{lb}_m$
$\Delta P$	Injector pressure drop	$\text{psi}$
T	Temperature	$^{\circ}\text{F}$
O/F	Mixture ratio (oxidizer-to-fuel) by weight	
$q''$	Heat transfer rate	$\text{btu}/\text{sec-in}^2$
$h_g$	Gas film heat transfer coefficient	$\text{btu}/\text{sec-in}^2\text{-}^{\circ}\text{F}$
Q	Total chamber heat rejection rate	$\text{btu}/\text{sec}$
$\eta$	Efficiency	
$\lambda$	Nozzle divergence loss	
$C_D \cdot C_V$	Nozzle throat discharge and friction loss	
<u>Subscripts</u>		
f	fuel	
o	oxidizer	
inj	injector	





APPENDIX A  
HEAT TRANSFER CALCULATIONS

## APPENDIX A

### HEAT TRANSFER CALCULATIONS

#### I. BERNATH CORRELATIONS - UPPER LIMIT OF NUCLEATE BOILING

##### 1.0 INTRODUCTION

To provide capability for the design of regeneratively cooled rocket engines, the upper limit of nucleate boiling of the liquid coolants as a function of pressure, bulk temperature, and velocity is needed. Experimental data for  $\text{OF}_2$  and  $\text{B}_2\text{H}_6$  are not available. To pursue this need the boiling burnout correlations that are available in the literature were investigated. The correlation presented here is the Bernath correlation (Reference 1). It has been programmed on the G-20 computer to facilitate the determination of cooling limits over ranges of coolant and operating parameters. In the following paragraphs, the equation will be presented and the use of the computer program will be explained.

##### 2.0 PROGRAM DESCRIPTION

##### 2.1 Nucleate Boiling Process and Burnout

In nucleate boiling, heat is transferred from the heated surface through the boiling, discontinuous film into the subcooled bulk coolant. The boiling locale is characterized by vigorous mixing of the two phases: the vapor in the form of bubbles leaves the surface and flows counter to discrete streams of subcooled liquid. This liquid partially quenches the bubbles while flowing toward the metal surface. The liquid then impinges on the surface in the wakes of the departing bubbles. The thickness of this boiling film is a function of the physical properties of the coolant, the heat flux, and the velocity and subcooling of the coolant. This determines the wall superheat or, the excess of temperature of the surface above saturation temperature of the coolant. When the heat flux approaches the maximum, both bubble frequency and diameter increase rapidly, resulting in the formation of patches of vapor on the surface. The heat generated in that region cannot be completely conducted away through the vapor film and, therefore, it is stored in the metal, raising

its temperature rapidly. The theory presented by Bernath (reference 1) in his correlation is as follows:

At the heat flux corresponding to the incipient burnout condition, the coolant adjacent to the heated surface is highly turbulent and despite the presence of bubbles and clusters of bubbles, the two phases are so well mixed that the coolant in this region may be considered homogeneous. Therefore, the transport of heat normal to the heated surface may be viewed as a conduction process, in which the conductance of the turbulent two phase layer to the surface is given by the ratio ( $k_{eff}/\Delta x$ ) of effective thermal conductivity and the thickness of the boundary layer. The driving force is taken as the difference in temperature between the heated surface ( $t_w$ ) and the bulk coolant ( $t_b$ ). This relationship may be written in the form conventionally used for heat conduction problems:

$$\ddot{q}_{BO} = \left( \frac{k_{eff}}{\Delta x} \right)_{BO} (t_w - t_b)_{bo} \frac{\text{Btu}}{\text{Sec-in}^2} \quad (1)$$

Since neither  $k_{eff}$  nor  $\Delta x$  can be readily measured or computed, the conductance of the boiling layer at incipient burnout can be written as a film coefficient as is customary in describing convective heat transfer. The equation is:

$$\ddot{q}_{BO} = h_{BO} (t_w - t_b)_{bo} \frac{\text{Btu}}{\text{sec-in}^2} \quad (2)$$

where:  $h_{BO}$  = burnout film coefficient, Btu/sec-in<sup>2</sup>-°F  
 $t_{wbo}$  = wall temperature at burnout, °F

Therefore, if an empirical correlation can be obtained for  $t_{wbo}$  and  $h_{BO}$  as a function of pressure velocity and type of fluid, the upper limit of nucleate boiling could be estimated. This is essentially what the Bernath correlation accomplishes.

## 2.2 Burnout Equations

The wall superheat at burnout has been generalized by applying the principles of the law of corresponding states (Reference 1). The equation is as follows:

$$t_{wBO} = \left[ 57 \ln \frac{P_{sat}}{H_2O} - 54 \left( \frac{P_{sat}}{H_2O} + 15 \right) - \frac{V}{4} \right] \times 1.8 + 32 (^\circ F) \quad (3)$$

This equation represents wall superheat at burnout for water at discrete pressure levels. This pressure level  $P_{sat}$  is obtained from the saturation temperature of the coolant.

A reduced temperature of the coolant is first computed.

$$\frac{T_r}{Coolant} = \left( \frac{t_{(sat\ Coolant)} + 460}{t_{(Critical\ Coolant)} + 460} \right) \quad (4)$$

The equivalent saturation temperature of water is then obtained by equation (5).

$$\frac{t_{sat}}{H_2O} = \left( \frac{T_r}{Coolant} \right) \left( \frac{T_{Critical}}{H_2O} \right) - 460 \quad (^\circ F) \quad (5)$$

The saturation pressure of  $H_2O$  at this temperature is obtained from the Keenan and Keyes steam tables (reference 2) from the following equation:

$$\log \frac{P_{Crit}}{P_{sat}} = \frac{\chi}{\frac{T_{sat}}{H_2O}} \frac{a + b \chi + c \chi^3 + d \chi^4}{1 + d \chi} \quad (6)$$

where:  $P_{sat}$  = vapor pressure of  $H_2O$ , psia  
 $P_{crit}$  = critical pressure of  $H_2O$ , psia  
 $\chi$  =  $(T_{critical} - T_{sat\ H_2O})$ ,  $^\circ R$

$\frac{T_{sat}}{H_2O}$  = saturation temperature  $H_2O$ ,  $^\circ R$

The value of the constants a, b, c and d are given in reference 2.

Equation 3 for the wall superheat, although obtained for water, is applicable to all liquids. It is based upon the assumption that a universal relationship exists between the maximum wall superheat (that can be sustained by any liquid) and the corresponding reduced temperature. The burnout heat transfer coefficient  $h_{bo}$  is obtained from equation (7).

$$h_{bo} = (5445) (1.8) \left( \frac{k_{H_2O}}{k_{coolant}} \right) \left( \frac{\alpha_{H_2O}}{\alpha_{coolant}} \right)^{0.5} \left( \frac{V_{coolant}}{V_{H_2O}} \right)^{0.4} + \frac{48}{De} \times$$

$$\left( \frac{P_{crit} H_2O}{P_{crit. Coolant}} \right) \text{ Btu/hr-ft}^2\text{-}^\circ\text{F} \quad (7)$$

where:

$k$	=	thermal conductivity
$\alpha$	=	thermal diffusivity
$\mu$	=	kinematic viscosity
$De$	=	equivalent diameter
$P_{crit}$	=	critical pressure
$V$	=	velocity

The physical and thermal properties of liquid  $OF_2$  and  $B_2H_6$  are presented in Figures A-1 and A-2. The upper limit of nucleate boiling predictions based on the  $h_{bo}$  calculations for  $OF_2$  and  $B_2H_6$  are presented in Figures A-3 and A-4.

## II. INJECTOR HEAT TRANSFER CALCULATIONS

The method used to calculate the predicted injector heat flux of the propellant cooled injectors is based on a nucleate boiling heat transfer mode and employs the following formula:

$$q'' \text{ injector} = \frac{T_g - (T_{sat} + 40)}{R_g + R_w} \quad (\text{Btu/sec-in}^2)$$

where:

$q''$	=	injector heat flux ( $\text{Btu/sec-in}^2$ )
$T_g$	=	actual chamber gas temperature ( $^\circ\text{F}$ )
$T_{sat}$	=	saturation temperature of coolant corresponding to operating pressure and bulk temperature ( $^\circ\text{F}$ )
$R_g$	=	gas film resistance ( $\text{sec-in}^2\text{-}^\circ\text{F/Btu}$ )
$R_w$	=	metal wall resistance ( $\text{sec-in}^2\text{-}^\circ\text{F/Btu}$ )
$T_g$	=	$(\eta_{c*})^2(T_{g\text{theo}})$

The gas film resistance  $R_g$  is obtained from the following formula:

$$R_g = \left( \frac{10^4}{1.21 \phi_g} \right) \frac{(D_{ch})^{1.8}}{(\dot{w}_t)^{0.8}} \quad (\text{sec-in}^2\text{-}^\circ\text{F/Btu})$$

where:

$\phi_g$	=	$0.029 C_P \mu^{0.2}$ , gas film property function
$C_P$	=	specific heat ( $\text{Btu/lb-}^\circ\text{F}$ )
$\mu$	=	viscosity ( $\text{lb/in-sec}$ )
$\phi_g$	=	$20.4 \times 10^{-4}$ ( $\text{Btu/in-sec-}^\circ\text{F}$ for $OF_2/B_2H_6$ )
$D_{ch}$	=	diameter chamber (inches)
$\dot{w}_t$	=	total propellant flowrate ( $\text{lb/sec}$ )

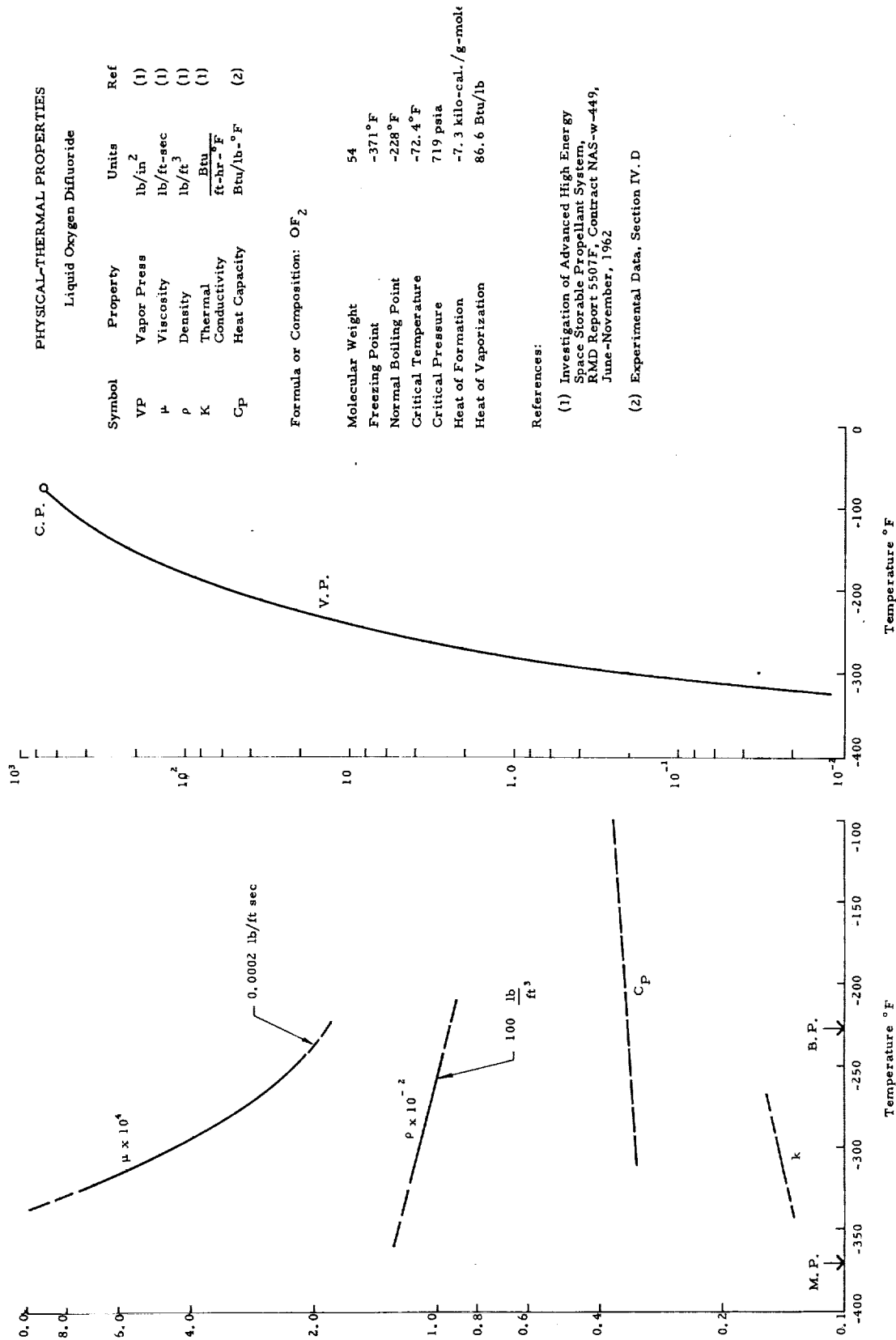


Figure A-1. Physical and Thermal Properties of Oxygen-Difluoride - OF<sub>2</sub>

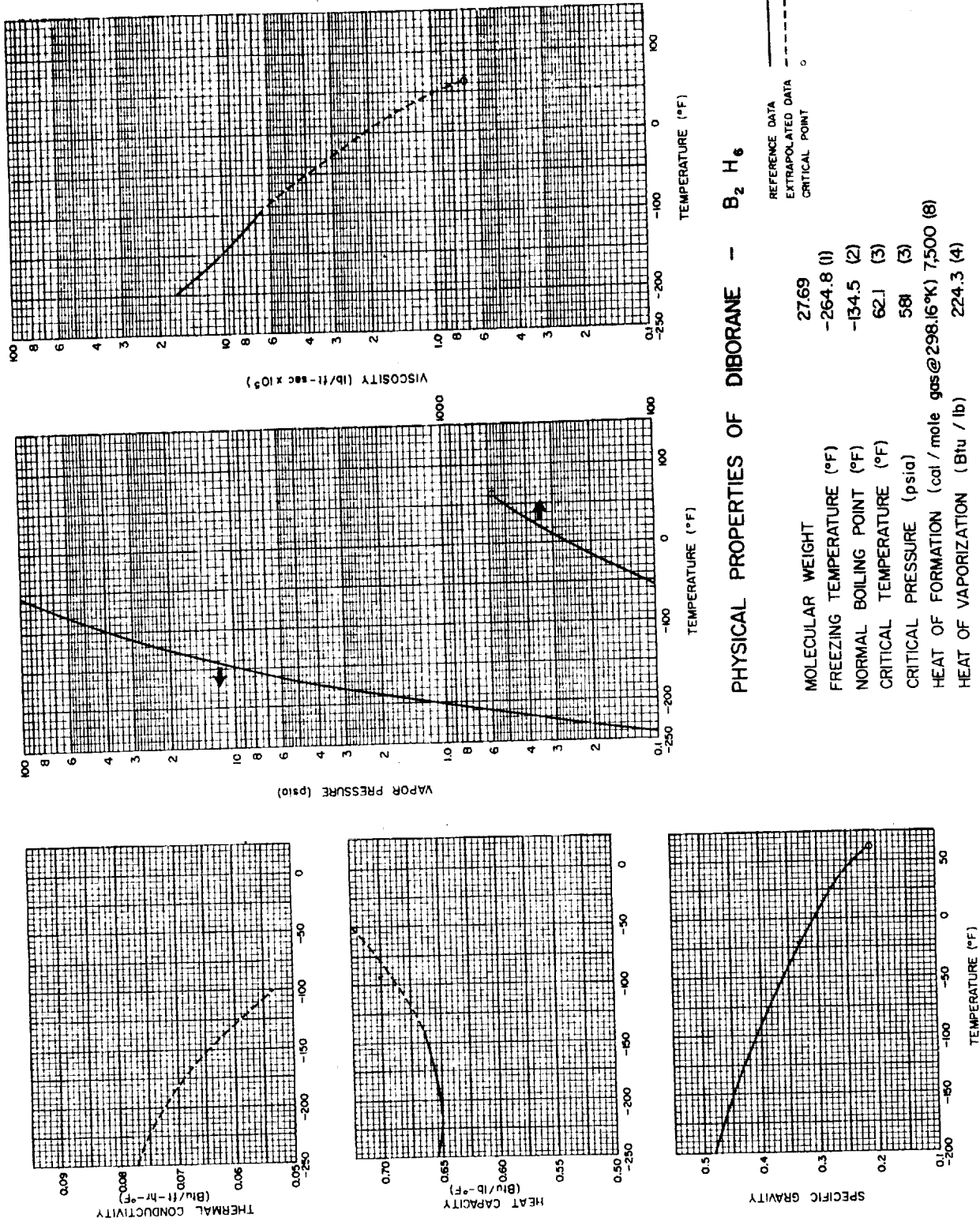


Figure A-2. Physical Properties of Diborane -  $B_2H_6$  (Refer to Aerojet General Corporation Report No. LRP 178)

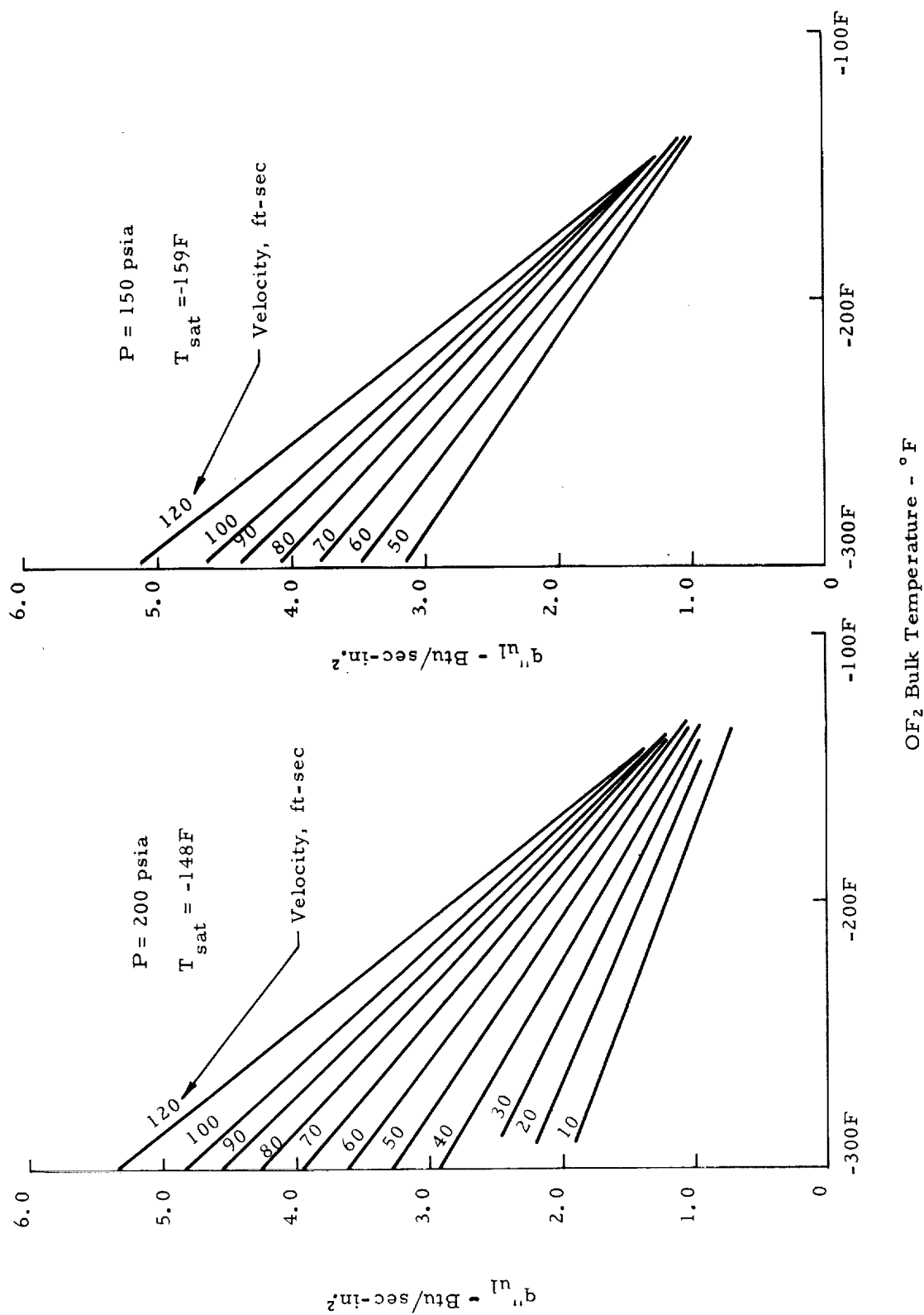


Figure A-3. Upper Limit of Nucleate Boiling Predictions - OF<sub>2</sub> - Berneath Correlation



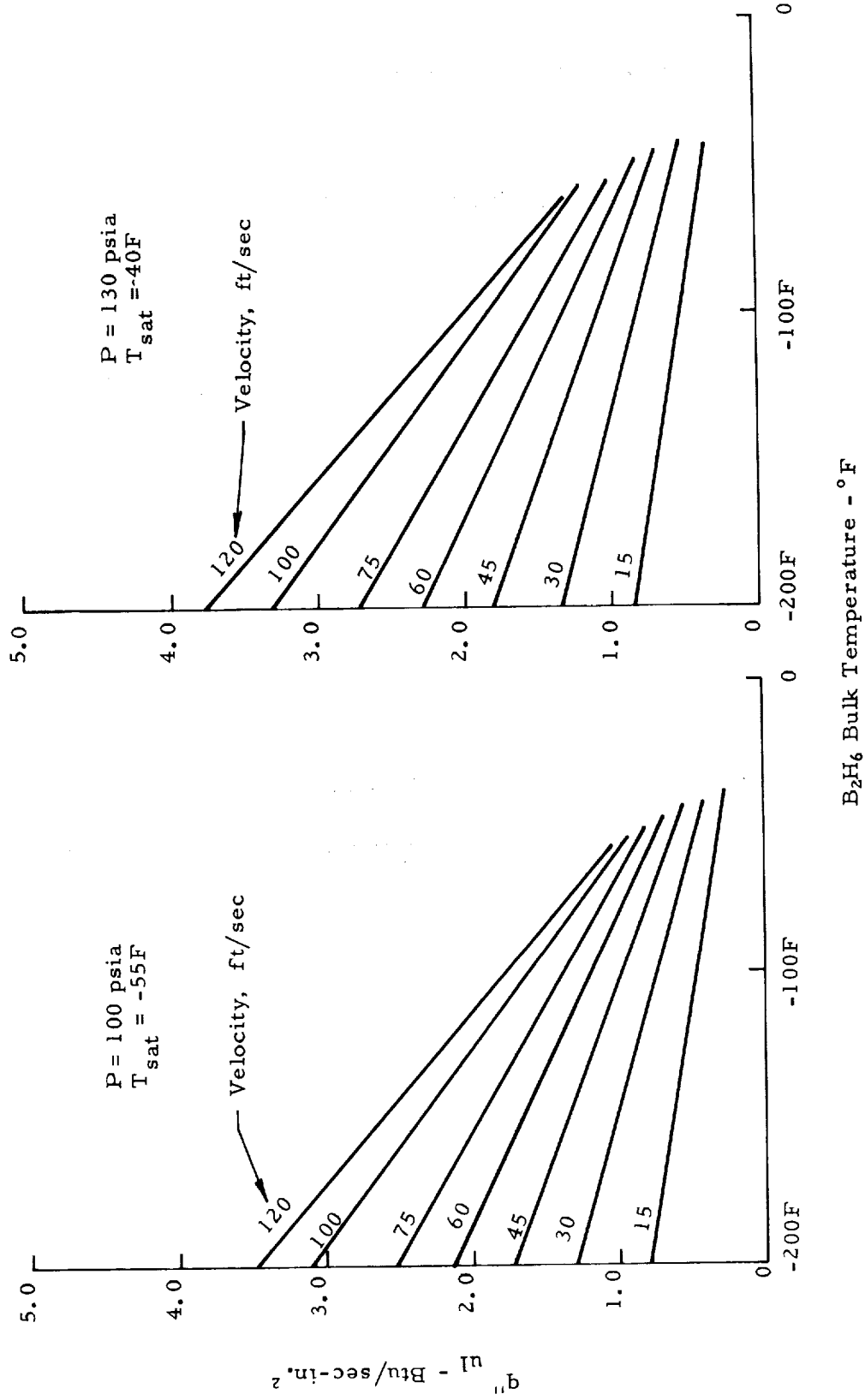


Figure A-4. Upper Limit of Nucleate Boiling Predictions -  $B_2H_6$  - Bernath Correlation

The metal wall resistance is obtained from the relationship:

$$R_w = t_w/k$$

where:  $t_w$  = thickness of wall (in.)  
 $k$  = conductivity of wall material (Btu-in/sec-in<sup>2</sup>-°F)

To determine the measured heat flux obtained from experimental data the following relationship was used:

$$q''_{\text{injector}} = \frac{(\dot{w}_{\text{oxidizer}})(C_P)(\Delta T)}{A_s} \quad (\text{Btu/sec-in}^2)$$

where:  $\dot{w}$  = oxidizer flowrate (lb/sec)  
 $C_P$  = specific heat of oxidizer (Btu/lb-°F), 0.30 Btu/lb-°F used in calculations  
 $\Delta T$  = measured bulk temperature rise (°F)  
 $A_s$  = surface area of injector (in<sup>2</sup>)

#### REFERENCES

1. Bernath, L., Chem. Eng. Prop. Symposium, Serial #18, 52, 1956
2. Keenan & Keyes, Thermodynamic Properties of Steam, John Wiley & Son, 1949

APPENDIX B  
THERMOCHEMICAL AND KINETIC  
PERFORMANCE ANALYSIS

## THERMOCHEMICAL AND KINETIC PERFORMANCE ANALYSIS

Since the primary purpose of the AEDC experimental runs was to determine the performance of  $\text{OF}_2/\text{B}_2\text{H}_6$  using a high area ratio nozzle ( $\epsilon = 40:1$ ), an evaluation of the  $\text{OF}_2/\text{B}_2\text{H}_6$  altitude performance data has been made. This evaluation was made in order to compare the test data with theoretical and predicted performance allowing for combustion losses and nozzle expansion losses including kinetic losses. A detailed discussion of the thermochemical and kinetic methods used in the performance calculations and performance of comparisons are presented in this section.

### 1.0 THEORETICAL THERMODYNAMIC PERFORMANCE CALCULATION

#### 1.1 Equilibrium (Shifting) Performance Calculation

The equilibrium performance of a nozzle is based upon the energy equation:

$$U_e = \sqrt{2 gJ \Delta H + U_c^2} \quad (1.1)$$

where velocity of the gas in the chamber ( $U_c$ ) is assumed to be zero. The exit velocity ( $U_e$ ) can, therefore, be computed, based upon the change in enthalpy ( $\Delta H$ ) between the chamber and the exit plane. The change-in-enthalpy calculation begins with the computation of the specie molal concentration and temperature in the combustion chamber. This calculation requires the use of a mass balance, a pressure balance, several equilibrium conditions and an energy balance equation; solved by the use of simultaneous equations. Since molal species, temperature; and pressure in the chamber have been determined, both enthalpy and entropy can be determined. The enthalpy at the exit must then be determined. This is accomplished by using a mass balance, Gibbs free energy law, and the assumption of constant entropy. By simultaneously solving these equations, the exit temperature and specie concentrations may be obtained, which will enable the enthalpy of the mixture to be computed. The specific impulse can be next obtained by the use of the equation:

$$I_{sp} = \frac{U_e}{g} \quad (1.2)$$

$U_e$  is computed from equation 1.1. The basic assumption used in computing the shifting impulse is that equilibrium exists throughout the nozzle, implying that all chemical reactions in the expansion processes occur at infinite rates. A sample computer print-out calculation is shown on Figure B-1.

PAGE 1 OF 2  
SAS NO.

FILE: 92H6-100F

REACTION MOTORS DIVISION

SAS NO.

PROJ. NO. 67-37-24-3106

NAME OR SYMBOL	EMPIRICAL FORMULA		FEED T DEG. K	DENS. G/CC	MOL. WT. G/MOLE	DELTA H/F KCAL/MOLE
B2H6-100F	82. H <sub>6</sub> .	(L)	200.00	0.437	27.688	2.340
OF2-300F	01. F <sub>2</sub> .	(L)	88.56	1.525	54.	-7.840

COMPOSITION WEIGHTS GRAMS:

0/F	3.000
B2H <sub>6</sub> -10nF	25.000
0F2-300F	75.000

## ELEMENTS IN PROPELLANT, GRAM ATOMS

B	1.80584
H	5.41751
O	1.38989
F	2.77778

THEMAL DATA AND PERFORMANCE PARAMETERS:

(CP)C EQUIL.	36.42	36.42	36.42	36.42	36.42
GAMMA BAR	1.111	1.112	1.113	1.114	1.116
ENTROPY	3.396	3.396	3.396	3.396	3.396
CF,VAC	1.894	1.925	1.931	1.939	1.967
AE/AT	25.32	33.18	35.14	38.8	49.80
CF, IDEAL	1.776	1.814	1.822	1.833	1.868
12 RHO/BULK	0.940	0.940	0.940	0.940	0.940
11 C*, TH	7009.5	7009.5	7009.5	7009.5	7009.5
10 ISP, IDEAL	386.84	395.21	396.92	399.31	406.86
9 ISP, RHO/R	363.61	371.48	373.08	375.33	382.43
8 ISP, SPACE	412.59	419.31	420.65	422.54	428.56
EQUILIBRIUM,	SHIFTING	SHIFTING	SHIFTING	SHIFTING	SHIFTING
	CHAMBER	EXHAUST	EXHAUST	EXHAUST	EXHAUST
5 PRES., PSIA	150.00	0.75	0.50	0.46	0.30
4 PRES., ATM	10.207	0.048	0.034	0.032	0.020
3 TEMP., K	3984.2	2279.3	2189.9	2168.0	2042.0
2 TEMP., F	6535.5	3642.5	3482.1	3442.7	3266.0
1 MOLE WT.	17.566	10.794	19.891	19.998	20.005

Figure B-1. Propellant Performance Report

## 1.2 Frozen Performance Calculation

The same thermodynamic calculation which determines chamber combustion temperature and specie concentration in the shifting performance calculation can also be applied in the frozen calculation. In the frozen expansion process, the specie concentration is assumed to be constant and the temperature at the exit may be obtained by assuming constant entropy stepped down to the given exit pressure. Since pressure, temperature, and specie concentration are known in the change, the exit enthalpy may be determined by assuming constant entropy, and consequently the total change in enthalpy can be calculated to give the frozen specific impulse. The important assumption of assuming constant concentration means that all chemical reaction rate constants are zero. A sample computer print-out calculation is shown on Figure B-2.

## 2.0 KINETIC PERFORMANCE CALCULATION

The calculation of shifting performance assumes infinite reaction rate constants whereas frozen performance assumes zero reaction rate constants. Since the actual reaction rate constants lie somewhere between zero and infinity, it would appear that the actual thermodynamic performance should lie somewhere between shifting and frozen performance. The results of calculations involving finite reaction rates are classified as "kinetic" performance. The kinetic performance calculation is quite lengthy. There are many chemical species, each of which may be involved in a number of different reactions for which reaction rate constants must be determined.

At the present time, kinetic calculations follow two basic approaches: one is an exact method using a finite difference integration, and the other is the Bray-method (Reference 1) which tests for equilibrium at various area ratios. The two methods are discussed in the following sections.

### 2.1 "Exact" Calculation Method

The exact method of computing the thermodynamic performance of a nozzle (specific impulse) is the more rigorous of the two above-mentioned methods. The basic method for determining the specific performance of an engine is accomplished by integrating the chemical equations with the aid of the reaction rate constants. The fundamental problem of this method of solution, however, is that the number species and chemical equations are considerable when normal rocket propellants are used. Westenberg and Favin (Reference 2) made some exact calculations on  $H_2$ ,  $H_2O$ ,  $CO$ ,  $CO_2$ ,  $H$ ,  $OH$  and  $H_2$ ,  $H_2O$ ,  $O_2$ ,  $H$ ,  $OH$ ,  $O$  systems.

Reference 3 discusses the combination of finite kinetics and the method of characteristics. Combining chemical kinetics and the method of characteristics gives a two-dimensional finite kinetic performance, as opposed to one-dimensional finite kinetic performance. The results of using the two-dimensional program showed that the two-dimensional performance could be considerably greater than the one-dimensional performance. It should be noted, however, that the chemical system analyzed was fairly simple.

FILE: R2H6-100F	THIOKOL CHEMICAL CORPORATION REACTION MOTORS DIVISION	PAGE 1 OF 2 SAS NO.
-----------------	--	------------------------

INGREDIENTS INFORMATION	PROJ. NO. 6 37-24-3186
-------------------------	------------------------

NAME OR SYMBOL	EMPIRICAL FORMULA	FEED T DEG. K	DENS. G/CC	MOL. WT. G/MOLF	DELTA H/F KCAL/MOLE
R2H6-100F	R2.H6.	(L) 200.40	0.437	27.688	2.340
OF2-300F	01.F2.	(L) 88.56	1.525	54.	-7.840

COMPOSITION WEIGHTS GRAMS:

O/F	3.000
R2H6-100F	25.000
OF2-300F	75.000

HAND STOCK FORM NO. 11113

ELEMENTS IN PROPELLANT, GRAM ATOMS	
B	1.80584
H	5.41751
O	1.38889
F	2.77778

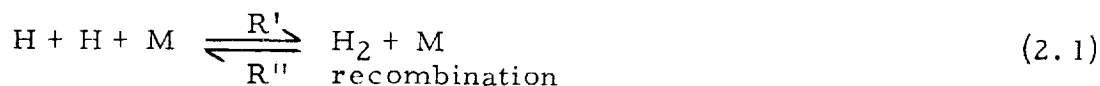
THERMAL DATA AND PERFORMANCE PARAMETERS:						
(C <sub>P</sub> ) <sub>C</sub> EQUIL.	36.42	36.42	36.42	36.42	36.42	36.42
GAMMA BAR	1.292	1.293	1.294	1.296	1.297	1.297
ENTROPY	3.396	3.396	3.396	3.396	3.396	3.396
CF, VAC	1.762	1.773	1.787	1.795	1.804	1.804
AE/AT	21.60	25.34	31.15	35.46	41.66	41.66
CF, IDEAL	1.690	1.706	1.724	1.736	1.748	1.748
RHO/BULK	0.940	0.940	0.940	0.940	0.940	0.940
C*, TH	6731.4	6731.4	6731.4	6731.4	6731.4	6731.4
ISP, IDEAL	353.65	356.89	360.77	363.13	365.75	365.75
ISP, RHO/R	332.41	335.46	339.11	341.32	343.79	343.79
ISP, SPACE	348.71	371.03	373.81	375.49	377.38	377.38
EQUILIBRIUM,	FROZEN	FROZEN	FROZEN	FROZEN	FROZEN	FROZEN
	CHAMBER	EXHAUST	EXHAUST	EXHAUST	EXHAUST	EXHAUST
PRES., PSIA	150.00	0.50	0.40	0.30	0.25	0.20
PRES., ATM	10.207	0.034	0.027	0.020	0.017	0.014
TEMP., K	3884.2	182.2	124.7	954.9	912.0	863.2
TEMP., F	6535.5	1484.0	1384.8	1259.2	1181.9	1094.1
MOLF WT.	17.566	17.566	17.566	17.566	17.566	17.566

Figure B-2. Propellant Performance Report

## 2.2 Bray "Freezing Criteria" Method

Bray (Reference 1) found the kinetic performance could be determined with reasonable accuracy by assuming that the reactants shift all the way down to some calculated "freezing point" and that the flow is frozen from there on. Bray also developed a method for determining a freezing point. Wegener (Reference 4) used this method for comparison with the experimental flow of  $N_2 + N_2O \rightleftharpoons N_2 + NO_2$  and found reasonably good agreement. The above work was used on very simple systems; when the Bray criteria is extended to more complex systems, the chemistry becomes more involved.

Bray's method can be illustrated by the following example: After the propellants undergo combustion in the chamber, some diatomic species ( $H_2$ ) dissociate at the high temperature in the chamber into the corresponding atomic species ( $H$ ). As these dissociated species pass through the nozzle, the gas expands adiabatically, thereby reducing the temperature. This reduction in temperature will cause the atomic species to recombine and form the diatomic molecule,  $H_2$ . This process of recombination involves an exothermic reaction and therefore the sole mode of recombination is to have a third body ( $M$ ), collide with the two diatomic species at the same instant, so that the energy may be removed. This process can be shown by the equation:



The recombination reaction rate,  $R'$ , is defined as the rate at which the monatomic species  $H$  recombines to form diatomic molecules. This  $R'$  represents the maximum rate that the monotomic species can be made to form  $H_2$ . It will be shown later that  $R'$  will be a function of specie concentration, third body, and reaction rate constant.

If one were to compute specie concentration of  $H$  using the RMD shifting expansion program, it would be possible to calculate the rate of which  $H$  must disappear in order to maintain equilibrium. This rate could be called the minimum rate at which the specie concentration ( $H$ ) must disappear in order to maintain equilibrium. It is quite obvious that if the required rate ( $R$ ) is much less than the actual rate, equilibrium must exist. However, if the required rate is much greater than the actual rate, then one would expect non-equilibrium flow. Bray shows that if it was assumed that the flow would freeze when the required rate equals the actual rate, the flow will, indeed, "freeze".

For example, suppose, as noted before, that the freezing location is equal to the area ratio at which the required and actual rates are equal.

$$\left( \frac{dH}{dt} \right)_j = R_e^* \quad (2.2)$$



The term on the right represents the rate at which H can be removed kinetically. For a simple system of H and H<sub>2</sub>, the chemical equation can be reduced to the following:



where  $kH$  is the rate constant and  $M$  is known as the third body. The term on the left hand side of equation 2.2 can be changed to the following, by use of the chain rule.

$$\frac{dH}{dt} = \frac{dH}{d(rj/r_{th})} \cdot \frac{d(rj/r_{th})}{dx} \cdot \frac{dx}{dt} = \frac{dH}{d(rj/r_{th})} \frac{d(rj/r_{th})}{dx} u_j \quad (2.4)$$

If this is substituted into equation 2.2 and solved for  $d(rj/r_{th})/dx$ , the propellant freezing coefficient ( $\omega$ ), then,

$$\omega = \frac{d(rj/r_{th})}{dx} = \frac{R_e}{u_j} \left[ \frac{dH}{d(rj/r_{th})} \right] \quad (2.5)$$

This equation holds at one location in a nozzle. The term  $u_j$  represents the local velocity, and the term  $dH/d(rj/r_{th})$  represents the local rate of removal of H required for equilibrium. This term is obtained by solving the mole concentrations of H (from the theoretical shifting calculations) at various area ratios and taking the derivative of that at some given area ratio. If the propellant freezing coefficient,  $\omega$ , is plotted as a function of area ratio, the plot would represent the maximum tangent that can exist at a given area ratio necessary to maintain equilibrium at that point.

If the slope of the nozzle contour as a function of length,  $\sigma$ , (termed the nozzle freezing coefficient) is plotted against area ratio on the curve, the area ratio beyond which the kinetic reactions can no longer keep up with the expansion process can be established. This area ratio is the point where the two curves intersect. The intersection is termed the freezing area ratio.

The performance of such a system is obtained by calculating the change in enthalpy for shifting equilibrium from the chamber to the freezing area ratio, and the change in enthalpy for frozen conditions from the freezing area ratio to the exit. These enthalpy terms can then be added and the exit velocity can be determined.

This example merely explains the basic concept of Bray's method. In actual chemical rockets the number of dissociated species and their corresponding recombination chemical equations are usually much greater in number than those

of simple illustration. Because of this added complexity, a number of alternative models have been developed. Westenberg and Favin (Reference 2) show that for a complex system, using the complicated exact analysis, the dissociated species will freeze at various area ratios. It is desirable, for the sake of simplification, to freeze all species simultaneously. Consequently, a method must be devised for obtaining some "effective" freezing area ratio that will produce the same impulse as freezing all the species at their respective freezing locations. The analytical models that have been used to accomplish this are as follows:

#### 2.2.1 Lezberg and Franciscus Method

Lezberg and Franciscus (Reference 5) have developed a method for determining the freezing point by considering all species. They have performed a considerable amount of testing with ramjets and found that their model was quite successful in determining performance. This method involves the use of the Bray equation 2.5 where the  $H$  in the  $d_H/d(r_j/r_{th})$  term is composed of all species. The  $R_e$  term is also changed to include all recombination reactions involving a third body. Once the ratio of the slope to the throat radius is obtained a nozzle contour plot can be superimposed and the freezing area ratio can be determined.

2.2.2 W. G. Courtney of TCC-RMD has also devised a method for determining the freezing area ratio (Reference 6). This method is very similar to the method of Lezberg and Franciscus, except that the  $H$  in the  $d_H/d(r_j/r_{th})$  term includes only the dissociated species. This method has been used for the evaluation of flames but has not yet been used to evaluate the experimental firings of rockets.

#### 2.2.3 Kushida and Koppang Method

The Kushida and Koppang method (References 7, 8) takes each specie and freezes it as in the Bray analysis. The area ratio at which the last specie freezes is used as the "effective freezing area ratio".

#### 2.2.4 Comparison of Results

As illustrative of the similarity of results obtained by the various methods Table I shows the results of three of the chemical kinetic impulse calculation methods for a 8000 pound thrust engine for a chamber pressure of 100 psia and an area ratio of 40/1. The propellant combination in this case is  $N_2O_4$  - 50% UDMH-50%  $N_2O_4$  at a mixture ratio of 2.0. The total variation between minimum and maximum estimates is 9.7 seconds for the four approaches. Although there is a relatively large total variation, the percentage variance about the average of these estimates is small,  $\pm 1-1/2\%$ . The only method with substantial experimental back-up is the Lezberg procedure. These data, however, are for ramjet engines at flame temperature much lower than those encountered in rocket engines.

TABLE I

Similarity of Recombination Predictions

Equilibrium Specific Impulse 337.8 sec.

$\epsilon = 40:1$ ,  $P_c = 100$  psia,  $O/F = 2.0:1$ ,  $N_2 O_4/50-50$

<u>Method</u>	<u>Kushida Koppang</u>	<u>Courtney</u>	<u>Lezberg Franciscus</u>
Reference	7,8	6	5
Loss from Recombination	9.1 sec	12.3	18.8
Theoretical $I_{sp}$ (recombination kinetics considered)	328.7	325.5	319

### 2.3 Computer Program

RMD has available a previously developed computer program for three different methods described above to determine the propellant freezing coefficient  $\omega$  at specified area ratios. This program is a subroutine to the RMD specific impulse program and provides the needed specie concentrations at various area ratios. The basic equation that must be solved for is:

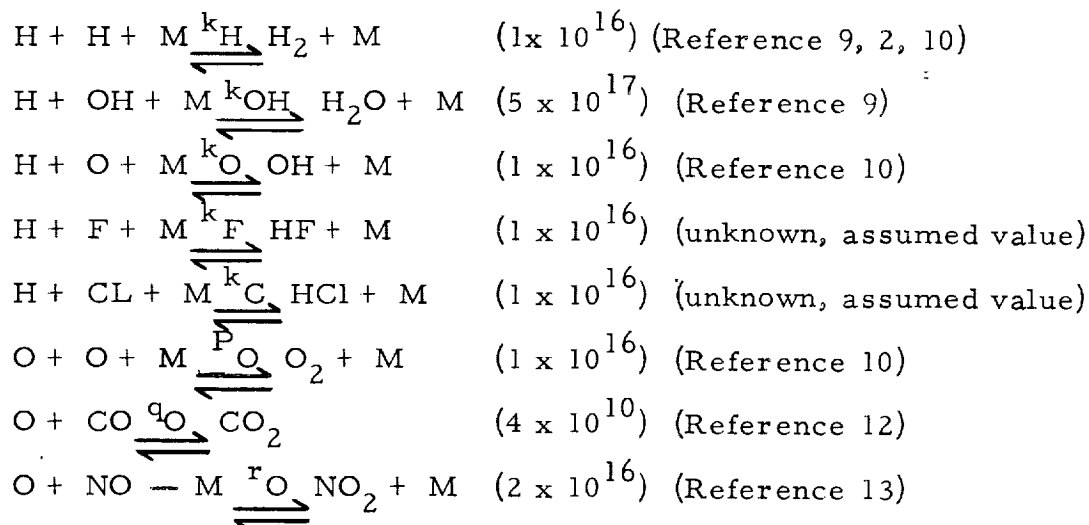
$$\omega = \frac{d(r_j/r_{th})}{d_x} = \frac{R_e}{u_j \left[ \frac{d_H}{d(r_j/r_{th})} \right]} \quad (2.6)$$

The term  $u_j \frac{d_H}{d(r_j/r_{th})}$  represents the change in the product of the dissociated species local velocity with radius ratio. The term is obtained by adding the dissociated specie concentrations and multiply this by the local velocity at each station. Then by using a curve fitting technique the change of  $u_j d_H$  can be determined.

The  $R_e$  term in equation 2.6 can be expressed in terms of

$$R_e = (2 k_H C_{H_2} + 2 k_{OH} C_H C_{OH} + 2 k_{O^k_H} C_O \\ 2 k_f C_H C_F + 4 p_O C_{CO_2} + 2 k_{CL} C_H C_{CL}) M \\ + 2 g_O C_{CO} C_O + 2 r_O + C_{NO} C_O \quad (2.7)$$

This  $R_e$  term represents the rate at which dissociated species can be removed kinetically by the chemical equations:



where the  $k$ 's and  $P_O$ ,  $q_O$ , and  $r_O$  are the specific rate constants in moles/cc sec if two-body and moles  $2/\text{cc}^2\text{sec}$  if three body. In a B-containing system reactions such as  $\text{H} + \text{BF}_2 = \text{HF} + \text{BF}$  and  $\text{BO} + \text{BO} = (\text{BO})_2$  should also be included but are omitted in the present treatment because of the lack of kinetic data. The present analysis therefore serves as a lower limit for recombination rates in the  $\text{OF}_2/\text{B}_2\text{H}_6$  cases.

Numerical values of rate constants are somewhat uncertain. Values were taken at  $2500^\circ\text{K}$  and were assumed independent of temperature and the nature of the third body M. Recombination rate constants decrease slightly with increasing temperature and the present temperatures usually ranged from 2500 to  $3500^\circ\text{K}$ . However, the present results were insensitive to the numerical values of the rate constants. The value of values of  $k_H$  and  $k_{OH}$  were arbitrarily taken as 90% of the values reported at  $1650^\circ\text{K}$  (Reference 9). The value of  $k_H$  is identical to the values used at  $2000^\circ\text{K}$  by Westenberg and Favin (Reference 2) and to the lower limit recommended at  $3500\text{--}4300^\circ\text{K}$  by Widowsky et al (10). The rate constants actually tend to vary somewhat with M although data are sparse. Sugden (Reference 9) concluded that  $\text{H}_2\text{O}$  was 10 times more effective than  $\text{H}_2$  or  $\text{N}_2$  in promoting  $\text{H} + \text{OH}$  recombination, but Zimman (11) considered that such a conclusion was premature. Patch (Reference 12) concluded that H was 7 times more effective than  $\text{H}_2$  in promoting  $\text{H} + \text{H}$  recombination but the H concentration in the present systems is only a few percent or less of the total concentration of species and the  $\text{H} + \text{H} + \text{H}$  reaction can be omitted with negligible error. The rate of the  $\text{NO} + \text{O} + \text{M}$  reaction also depends upon the nature of M (Reference 13).

Figure B-3 shows the results of a typical calculation of freezing coefficient for  $\text{OF}_2/\text{B}_2\text{H}_6$ . The freezing area ratio of a nozzle can next be determined

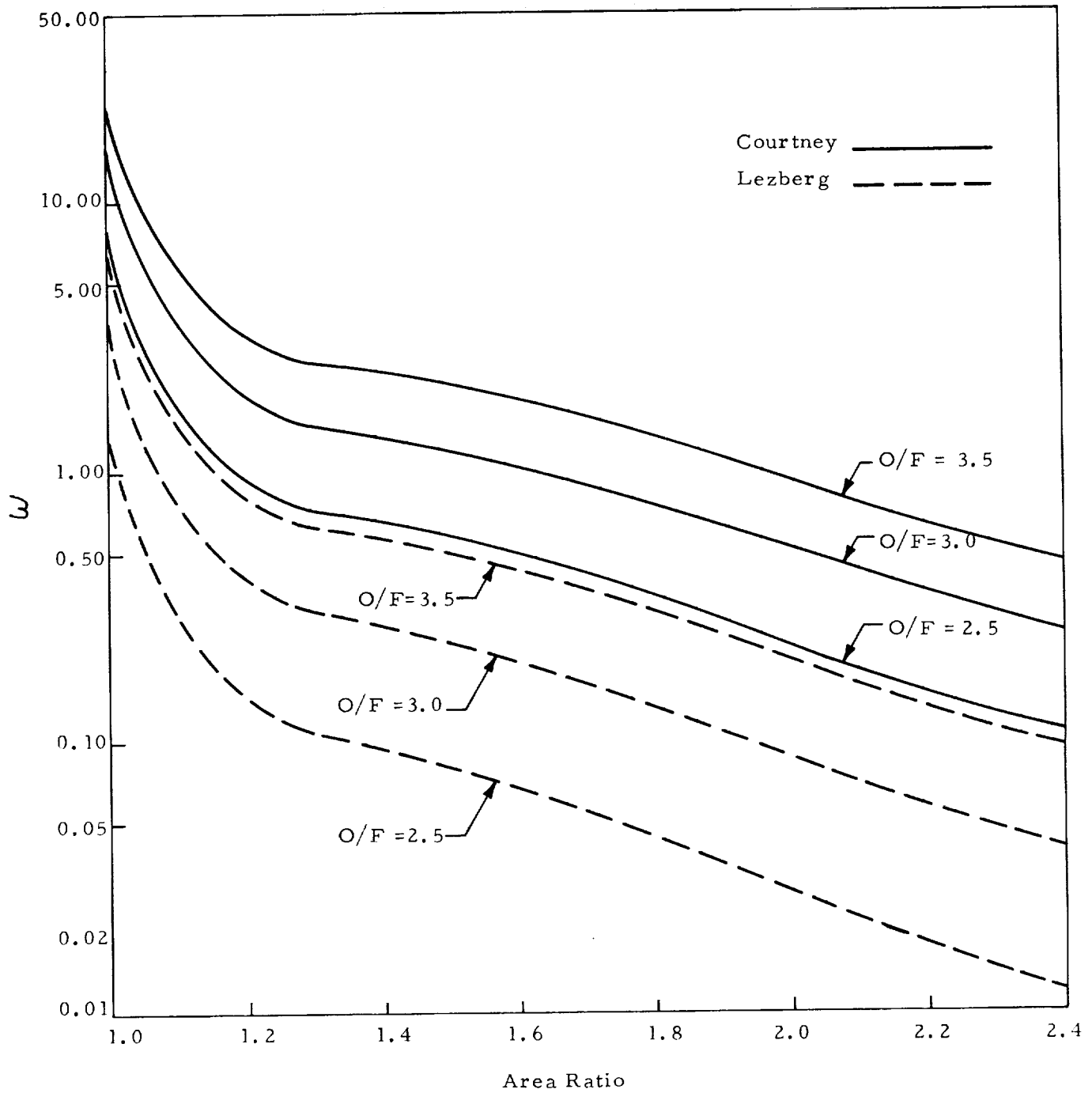


Figure B-3. Influence of Area Ratio on Propellant Freezing Coefficient  
( $w$ ) -  $\text{OF}_2/\text{B}_2\text{H}_6$

by superimposing on this plot the slope divided by the throat radius term of the nozzle. The intersection of these curves represents the freezing area ratio.

A second program was also available for the calculation of the kinetic performance of an engine as a function of freezing area ratio. This program combines the effects of shifting equilibrium up to the freezing area ratio and recognizes frozen flow from the freezing area ratio to the exit. Figure B-4 shows the results of such a calculation.

In summary, Figures B-5 and B-6 show the theoretical shifting, kinetic and frozen impulse values for chamber pressures of 120 and 150 and the AEDC altitude nozzle.

### 3.0 PERFORMANCE ANALYSIS OF $\text{OF}_2/\text{B}_2\text{H}_6$

#### 3.1 Performance Comparisons

In order to compare measured rocket performance with theory, two primary losses must be considered. These losses are combustion losses and expansion nozzle losses. For this analysis, the predicted losses described in the following sections were applied to the altitude performance test data in an attempt to obtain a better insight into the kinetic space performance potential of  $\text{OF}_2/\text{B}_2\text{H}_6$ .

Combustion losses normally considered are those associated with combustion upstream of the sonic point or throat and assume burning is completed prior to throat entry.

The expansion nozzle losses are comprised of geometrical losses (divergence,  $C_\lambda$ , and discharge,  $C_D$ ), drag losses (friction,  $C_f$ ), heat losses ( $C_q$ ), kinetic (dissociation,  $C_K$ ) and two phase flow losses ( $C_\phi$ ). These losses are described below.

(1) Divergence Loss ( $C_\lambda$ ) - The divergency loss was calculated by the following expression for a  $15^\circ$  half angle nozzle:

$$C_\lambda = - \frac{1 + \cos \alpha}{2} = 0.017 \quad (3.1)$$

(2) Discharge Coefficient Loss ( $C_D$ ) - The discharge coefficient loss, a transonic loss, represents a reduction in thrust coefficient attributed to non-uniform flow in the throat of a nozzle which in effect is manifested as a reduction of effective throat area. Figure B-7 shows the  $C_D$  loss as a function of the isentropic expansion coefficient,  $\gamma$ , and upstream radius ratio ( $R_c/r_{th}$ ) for the altitude nozzle was two (2) and therefore  $C_D$  from Figure B-7 gives a value of .0022.

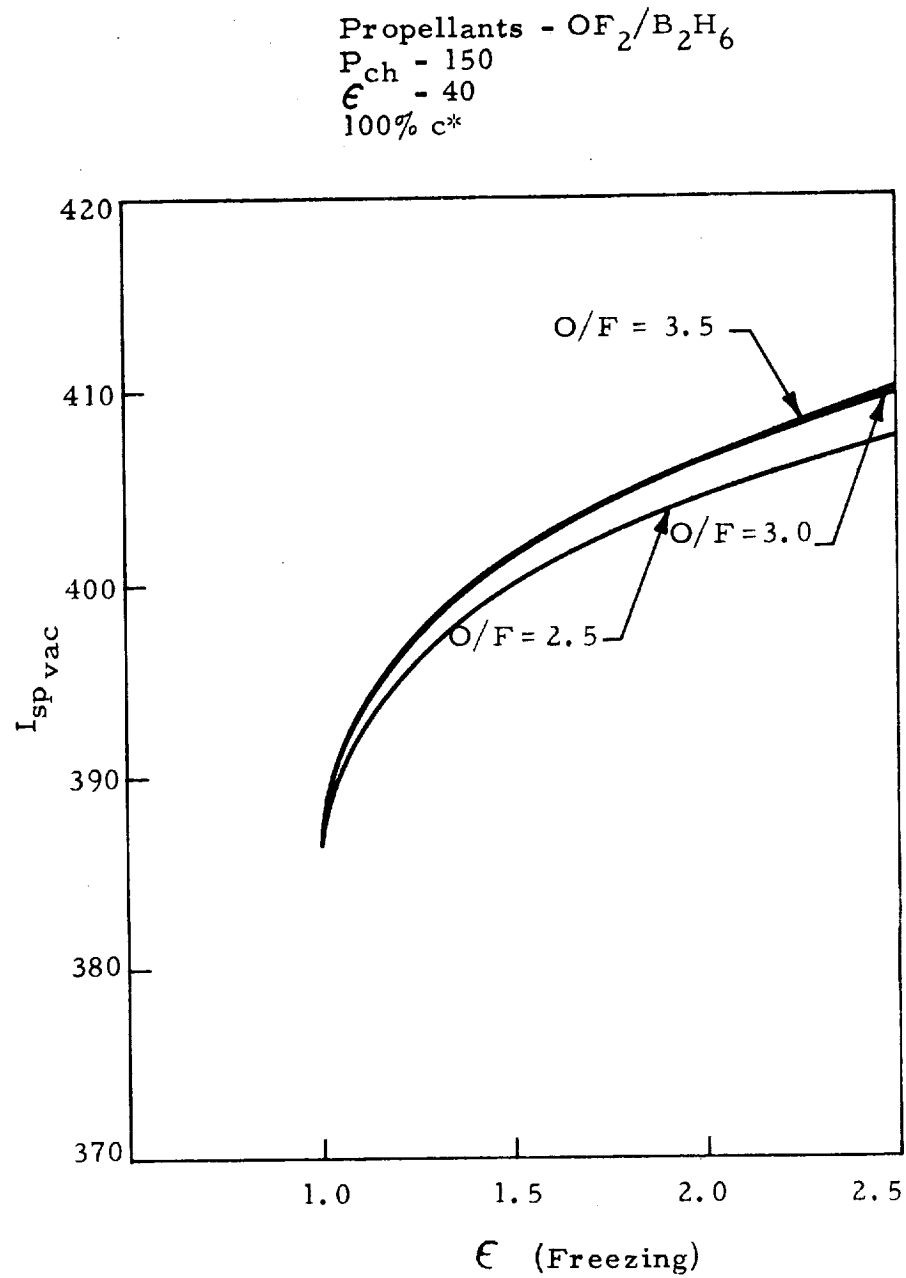


Figure B-4. Influence of Freezing Area Ratio of Kinetic Impulse -  $\text{OF}_2/\text{B}_2\text{H}_6$

$P_{ch} = 120$  psia  
 $\epsilon = 40$   
 Nozzle -  $15^\circ$  Conical  
 $D_t = 3.32$  in.

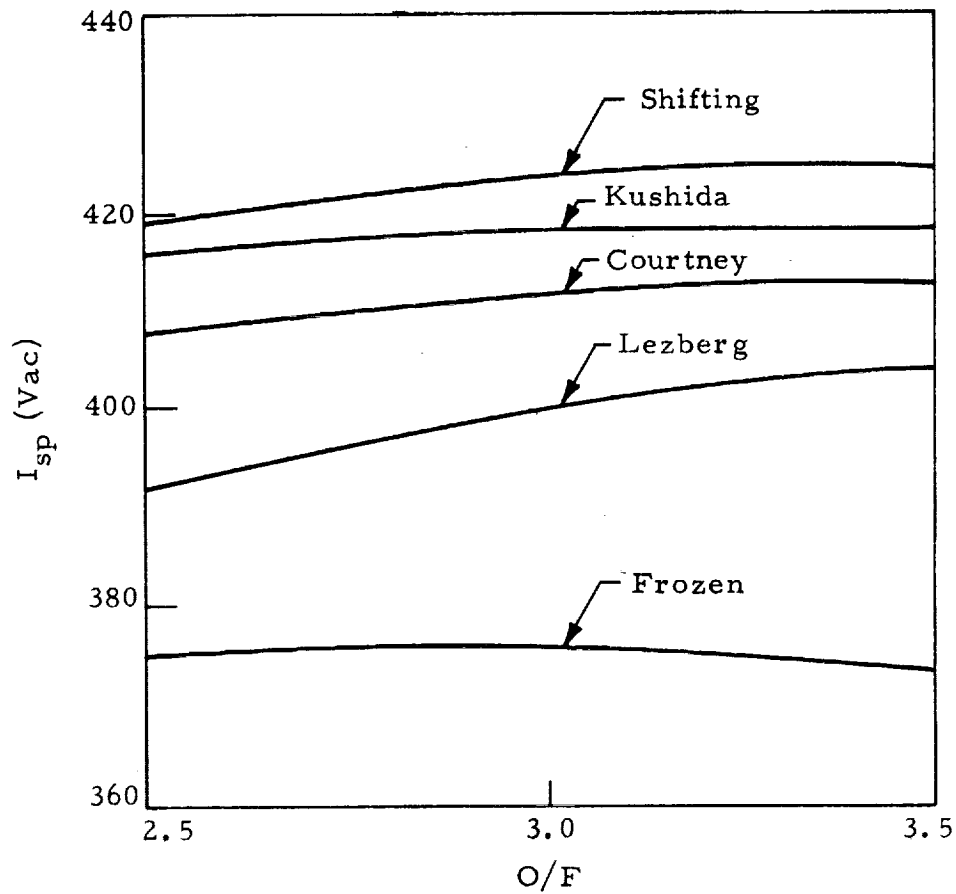


Figure B-5. Theoretical and Predicted Performance -  $OF_2/B_2H_6$



$P_{ch}$  - 150 psia  
 $\epsilon$  - 40  
Nozzle - 15° Conical  
 $D_r$  - 3.32 in.

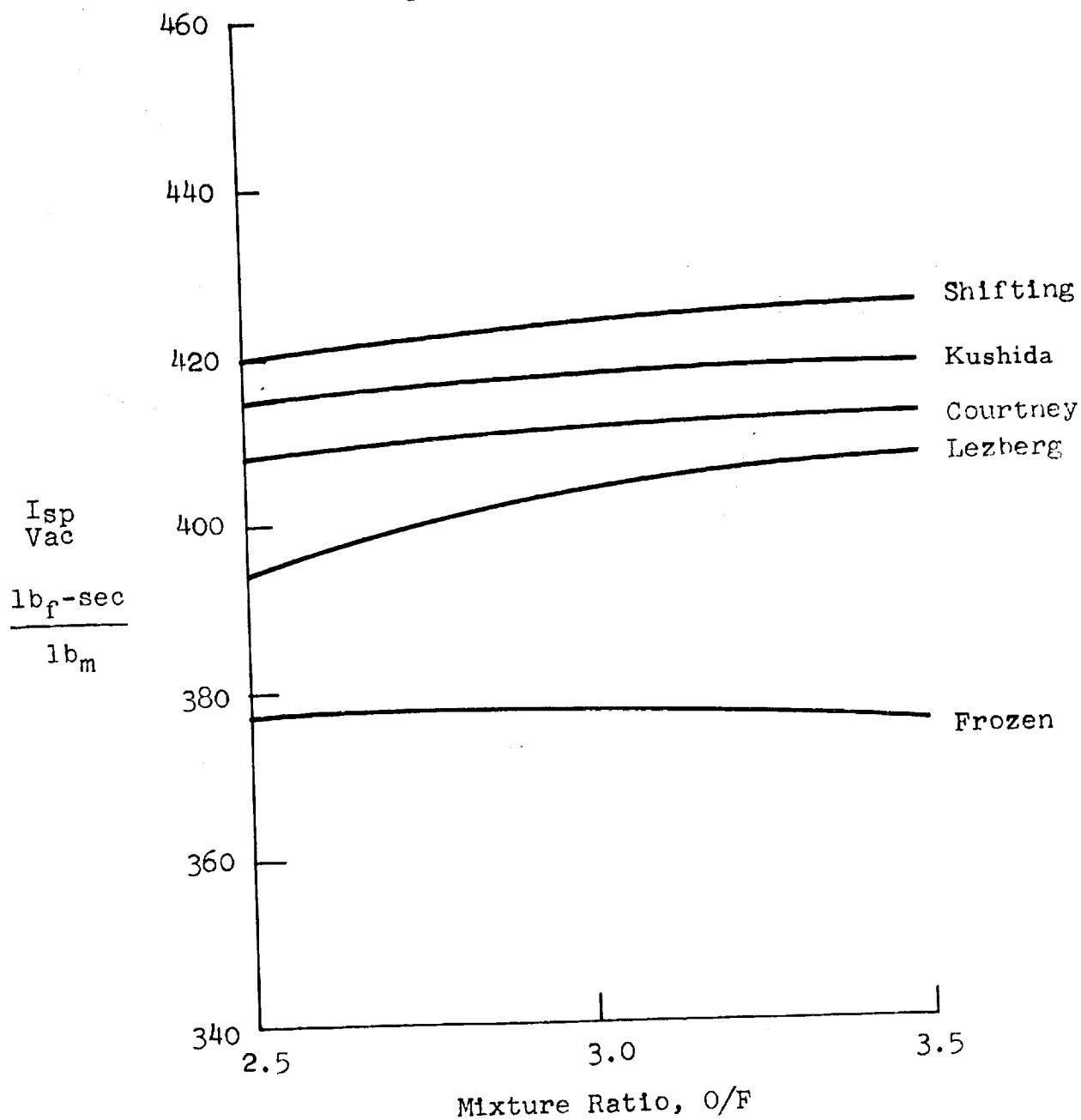


Figure B-6. Theoretical and Predicted Performance -  $OF_2/B_2H_6$

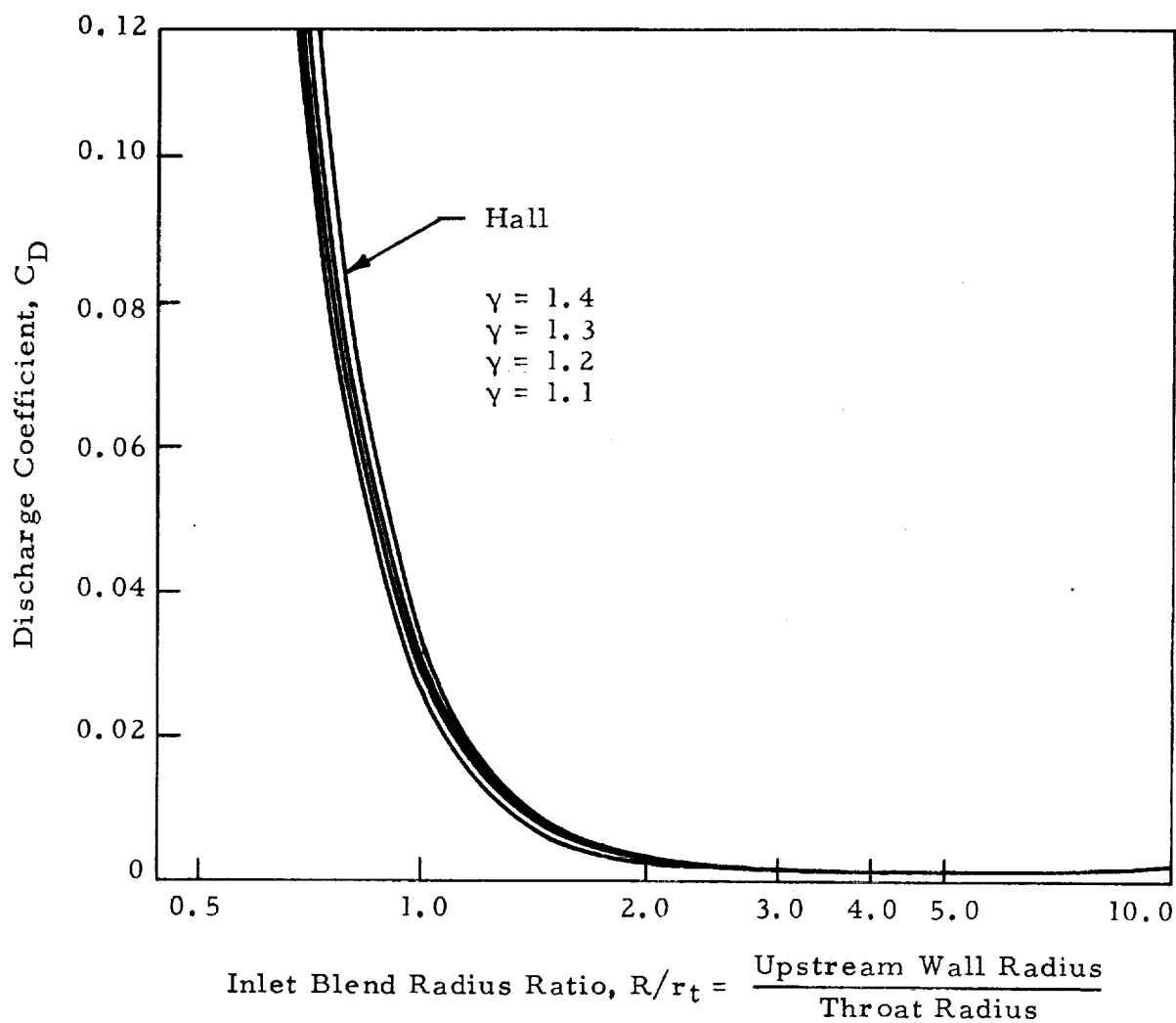


Figure B-7. Variation of Discharge Coefficient With Upstream Nozzle Wall Radius

(3) Drag Coefficient Loss ( $C_V$ ) - The drag loss ( $C_V$ ) of a nozzle is caused by frictional effects in a nozzle resulting in a reduction of thrust. Figure B-8 (Reference 15) shows the drag coefficient for a conical nozzle versus area ratio for various values of the product of thrust and chamber pressure. For a 2500 pound thrust engine operating at 150 psia, with  $OF_2/B_2H_6$  at an area ratio of 40:1, the drag coefficient is 0.0275.

(4) Heat Loss Coefficient - The heat loss coefficients were based on the actual heat transfer measurements obtained from the altitude tests. The heat loss was determined by a series, piece-wise integrations using the film coefficients obtained from high response, foil type thermocouples installed in the nozzle. The gas heat transfer coefficients were used to determine the heat transfer rate which was, in turn, integrated over the nozzle area to obtain the total heat rejection to the nozzle wall. The performance loss due to heat transfer can then be determined using the energy equation in the following form:

$$C_q = 1 - \sqrt{\frac{(I_{sp \text{ theo}})^2 - \frac{2QJ}{gw}}{I_{sp \text{ theo}}^2}} \quad (3.2)$$

The heat loss coefficient to the nozzle wall for the AEDC tests was 0.024.

(5) Two Phase Flow Loss - Two phase flow losses could not be evaluated since combustion specie data were not acquired.

(6) Kinetic Flow Loss - The kinetic flow losses are difficult to determine because of a lack of basic reaction rate data for the  $OF_2/B_2H_6$  combustion species. In an attempt to determine the kinetic loss, the test data was first corrected for the losses described in the preceding paragraphs. This corrected data was then compared with shifting and frozen impulse values to determine the kinetic losses. The theoretical shifting and frozen equilibrium performance and predicted kinetic performance based on three methods; Lezberg and Franciscus, Courtney and Kushida were discussed previously (Section B.2, Ref. Figures B-5 and B-6).

Figure B-9 shows the theoretical shifting, kinetic (Lezberg method) and frozen specific impulse curves with superimposed test data, adjusted for  $c^*$  efficiency and divergent losses only. It is apparent from this figure that the corrected experimental impulse values fall about 2% below the theoretical shifting curve. In comparing this result with the ARS Journal report by Olsen (Reference 16), the same type of result is apparent.

Table II shows the corrections made for each experimental point for the remaining losses considered ( $C_D$ ,  $C_V$ ,  $C_q$ ). The final values of specific impulse are shown in the right hand column. Figure B-10 shows the comparison between theoretical and experimental  $I_{sp}$  lie appreciably (2.5%) above the theoretical values.

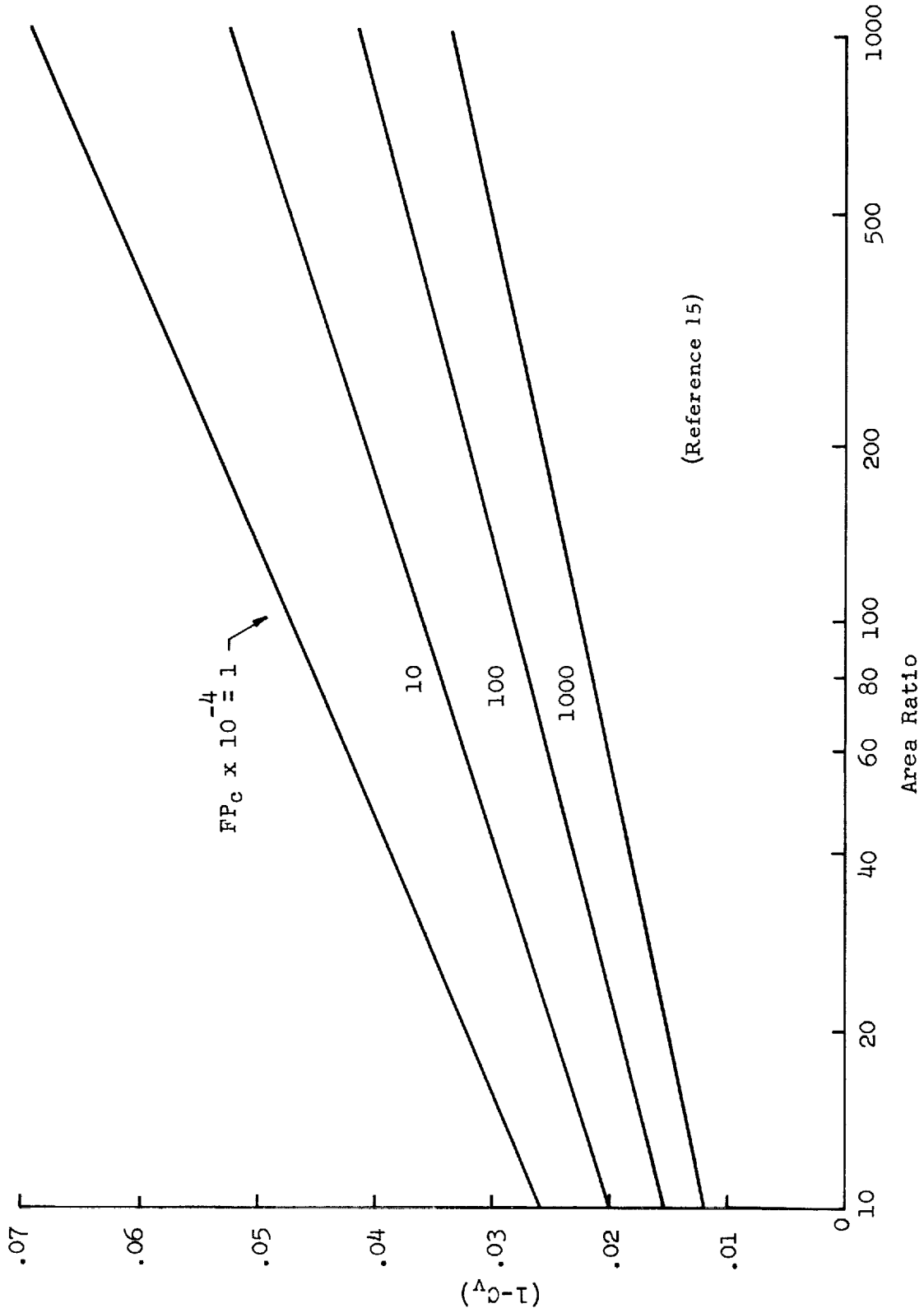


Figure B-8. Turbulent Flow Shear-Drag Loss For Conical Nozzles

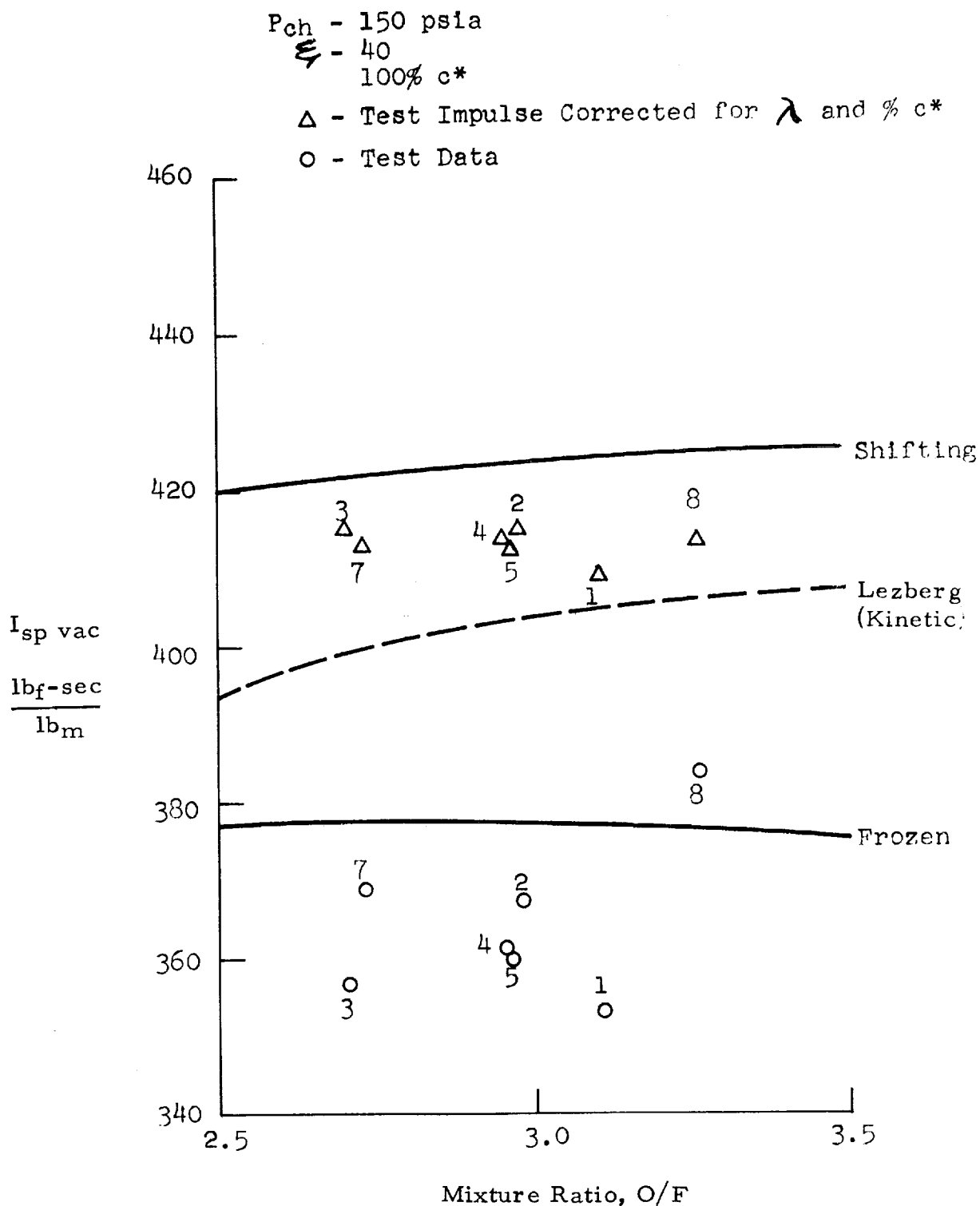


Figure B-9. Theoretical and Experimental Performance Comparison -  $OF_2/B_2H_6$

$P_{ch}$  - 150 psia  
 $\epsilon$  - 40  
 100%  $c^*$   
 $\Delta$  - Test Impulse Corrected for all Losses  
 $\circ$  - Test Data

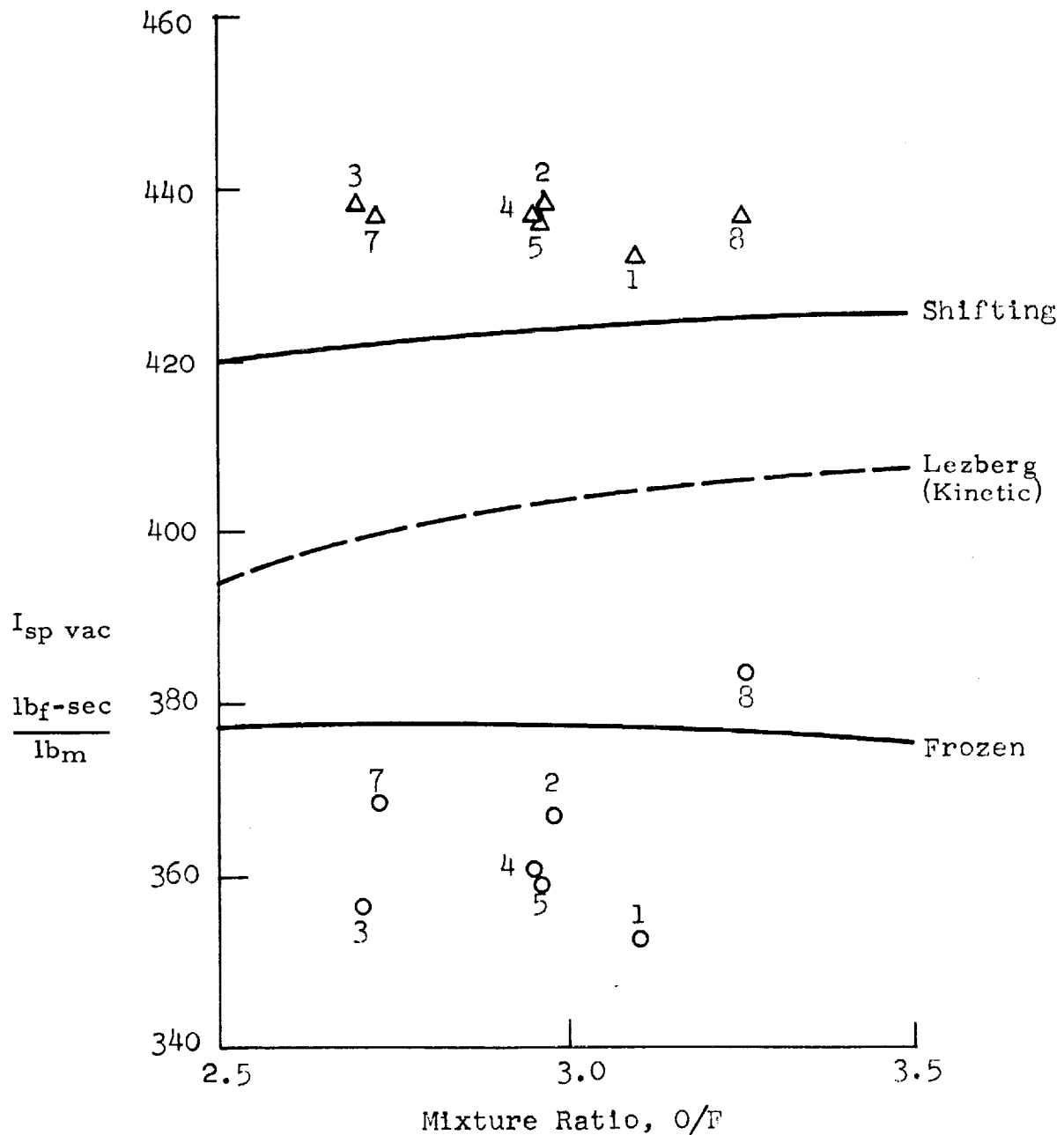


Figure B-10. Theoretical and Experimental Performance Comparison -  $OF_2/B_2H_6$  — B-20 —

TABLE II  
Corrected Vacuum Specific Impulse

Run	$I_{sp}$ Test	% $c^*$	$I_{sp}$ (1)	$I_{sp}$ (2)	$I_{sp}$ Theo Shifting
1	353.7	87.9	409.3	432.4	425
2	367.6	90.1	415.0	438.5	424
3	356.4	87.3	415.3	438.8	422
4	361.2	88.8	413.8	437.0	424
5	359.9	88.7	412.8	436.0	424
7	368.8	90.7	413.6	436.9	422
8	384.3	94.5	413.7	437.1	425

(1) Test Impulse corrected for  $(C_\lambda)$ ,  $(\%c^*)$

(2) Test Impulse corrected for all losses.  $(C_\lambda, \%c^*, C_D, C_V, C_q)$

The result indicates that there must be an inconsistency involved in the path toward the corrected experimental specific impulse since the theoretical shifting curves represent the maximum achievable performances. This effect is also noted in the data reported by Olsen when corrections for all losses except kinetic gave experimental impulses above theoretical shifting equilibrium.

In order to explain this inconsistency, it was decided to investigate (analytically) combustion in the nozzle itself. It is believed that with the combustion efficiencies obtained during test, there would be enough fuel-oxidizer constituents to support supersonic combustion, similar to experiments made passing air-hydrogen mixtures through a shock wave (Reference 17). This hypothesis is partially confirmed in Reference 18 where concentration samples were taken along various portions of the nozzle, indicated that oxidation reaction had indeed taken place in the nozzle. Under these conditions, assuming supersonic combustion in the nozzle, the measured characteristic exhaust velocity would not reflect the true or actual combustion efficiency across the total engine envelope. Thus, a conventional data adjustment based upon a measured characteristic exhaust velocity discounts this "after burning" and in effect applies a portion of the combustion correction redundantly. The supersonic combustion calculations were made using two methods, (1) constant pressure compressible flow relations and (2) the specific impulse program. The specific impulse data corrected for all conventional losses (i. e.,  $C_\lambda, C_D, C_V, C_q$ ) and a  $c^*$  correction based on supersonic combustion agree within 1% of the theoretical shifting equilibrium values.

## REFERENCES

1. K. N. C. Bray, "Simplified Sudden-Freezing Analysis for Non-Equilibrium Nozzle Flows", Journal of the ARS, June 1961.
2. Westenberg, A. A. and Favin, S., "Complex Chemical Kinetics in Supersonic Nozzle Flow", Ninth Symposium (International) on Combustion (Academic Press Inc., New York, 1963), pp. 785-798.
3. Zupnik, T. F., et al., "Application of the Method of Characteristics Including Reaction Kinetics to Nozzle Flow" AIAA Preprint No. 64-97, presented at Aerospace Sciences Meeting, New York, N. Y., Jan. 20-22, 1964.
4. P. P. Wegnener, "Experiments on the Departure from Chemical Equilibrium in a Supersonic Flow", Journal of the ARS, April 1960.
5. Lezberg, E. A., Franciscus, L. C., "Effects of Exhaust Nozzle Recombinations of Hypersonic Ramjet Performance", I. Experimental Measurements AIAA J. 1, 2071-2076, (Sept. 1963).
6. Courtney, W. B., "Recombination in Nozzles", RMD Report DS 230-05-179, November 11, 1964.
7. Kushida, R., "An Approximate Method of Analyzing Non-Equilibrium Recombination Effects in Exhaust Nozzle", Marquardt Corporation Report 20091, March 3, 1960.
8. Koppang, R. R., Bahn, E. J. and Giffoni, S., "Jet Propulsion Exhaust Nozzle Research Program", Marquardt Corporation, Report 25027 on BuWeps Contract AS59-614S-C (February 24, 1961).
9. Bluowicz, E. M. and Sugden, T. M., "The Recombination of Hydrogen Atoms and Hydroxyl Radicals in Hydrogen Flame Gases", Trans. Faraday Soc. 54, 1855-1860 (1958).
10. Widowsky, A., Oswalt, L. R., and Harp, J. L., "Experimental Determination of the Hydrogen Recombination Constant", ARSJ., 32, 1927-1929 (1962).
11. Zinman, W. G., "Recent Advances in Chemical Kinetics of Homogeneous Reactions in Dissociated Air", ARSJ., 30, 233-238 (1960).



REFERENCES (cont)

12. Patch, R. W., "Shock-tube Measurements of Dissociation Rates of Hydrogen", J. Chem. Phys., 36, 1919-1924 (1962).
13. Ogryzlo, E. A., and Schiff, H. I., "The Reaction of Oxygen Atoms with NO" , Can. J. Chem., 37, 1690-1695 (1959).
14. Hull, I. M., "Trasonic Flow in Two-Dimensional and Axially Symmetric Nozzles", Aeronautical Research Council (Britain), ARC 23, 347, December 18, 1961.
15. "Study of High Effective Area Ratio Nozzles for Spacecraft Engines", Aerojet NAS 7-136-F, June 1964.
16. Olsen, W. T., "Recombination and Condensation Process in High Area Ratio Nozzles", ARS Journal, 672-680, May 1962.
17. Rhodes, R. P. Rubins, P. M. and Chriss, D. E., "The Effect of Heat Release on the Flow Parameters in Shock-Induced Combustion", AEDC-TDR-62-78 (AD 275366), May 1962.
18. Lewis, J. D., "A Study of Combustion and Recombination Reactions During Expansion Process of a Liquid Propellant Rocket Engine", Ninth Symposium (International) on Combustion (Academic Press, Inc., N. Y., 1963) , pp. 366-374.



APPENDIX C  
TEST PROCEDURE FOR THE DETERMINATION  
OF THE SPECIFIC HEAT OF LIQUID OF<sub>2</sub>

APPENDIX C

TEST PROCEDURES FOR THE DETERMINATION  
OF THE SPECIFIC HEAT OF LIQUID  $\text{OF}_2$

1.0 INTRODUCTION

The following sections describe the apparatus, calibrations and test procedures employed to determine the specific heat of liquid  $\text{OF}_2$ .

2.0 APPARATUS DESIGN

A brief description of the apparatus is presented in Section C-3. The apparatus design was based on designs successfully employed to measure the heat capacity of liquid fluorine. Since  $\text{OF}_2$  and fluorine behave similarly, the materials of construction of the calorimeter were the same as that used for the liquid fluorine design. The design concept was discussed and reviewed with National Bureau of Standards personnel who concurred with the design approach. The following paragraphs describe the apparatus in more detail.

A schematic diagram of the calorimeter used is shown in Figure C1. The sample container (1) is an internally finned copper cylinder having a volume of approximately 120 cc to which is wound 40 gauge platinum wire (1a). This coil performs a dual function. It serves as a source of energy and secondly it is utilized as a temperature sensing element. The sample is introduced into the sample container via a 1/8 in. copper tube (2) brazed to the top of the sample container. Mounted above the sample container are two heat shields (3 and 4) constructed of copper. These units are employed to decrease heat losses due to conduction via the electrical wires and the sample filling tube. Since the mass of these shields are relatively large, energy is dissipated with only a slight temperature change. This, therefore, greatly diminishes the losses into the calorimeter. The shields are also wrapped with manganin wire so that its temperature can be controlled.

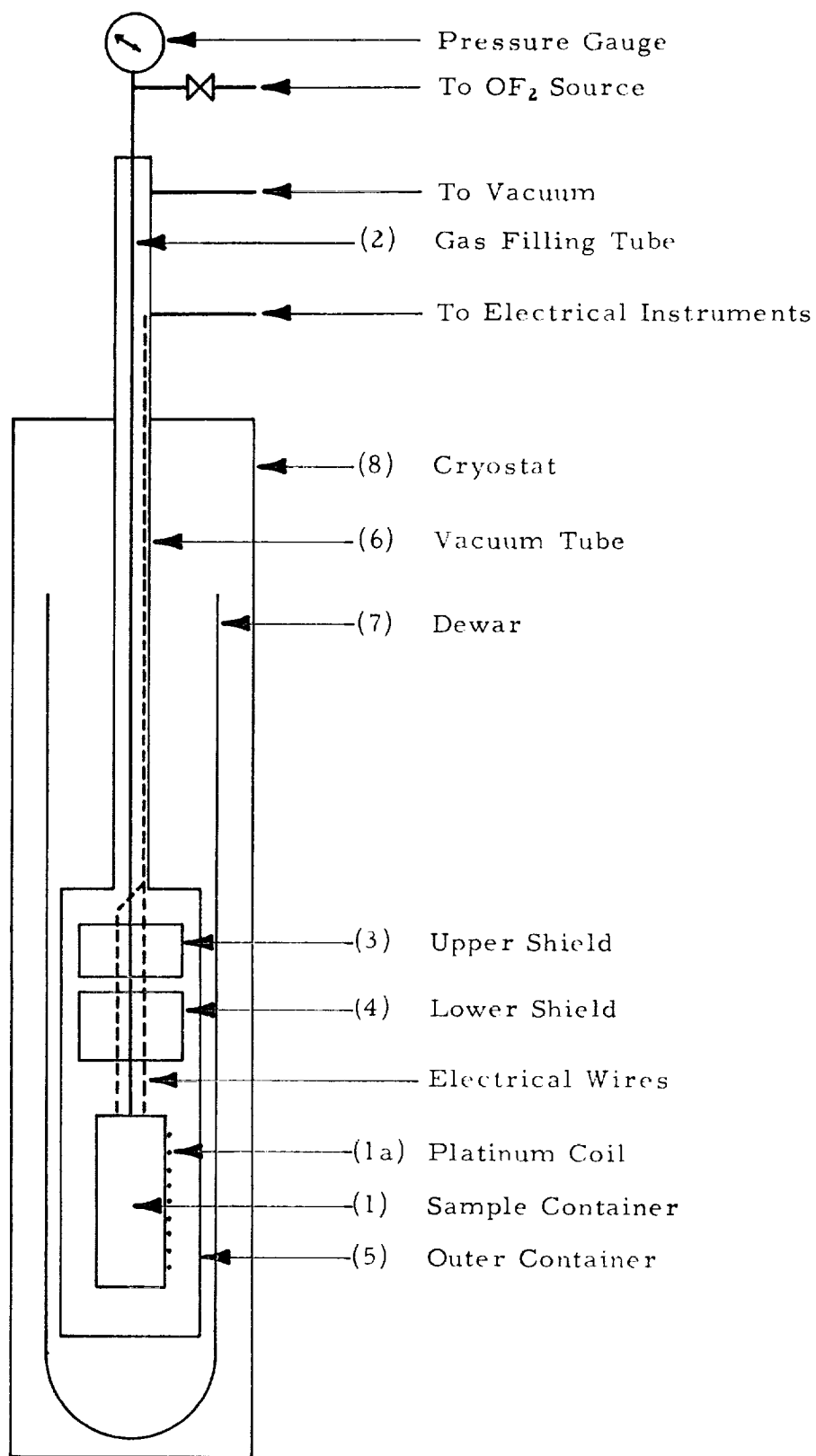


Figure C-1.  $\text{OF}_2$  Specific Heat Apparatus Schematic

The sample container and shields are sealed in an outer container (5) which is constructed of copper. This container serves as a vacuum jacket during a measurement and is evacuated through a 3/4 in. copper tube (6). This unit is suspended within a glass De war (7) which is set in a glass cryostat (8). The cryostat is vacuum tight and connected to a source of vacuum.

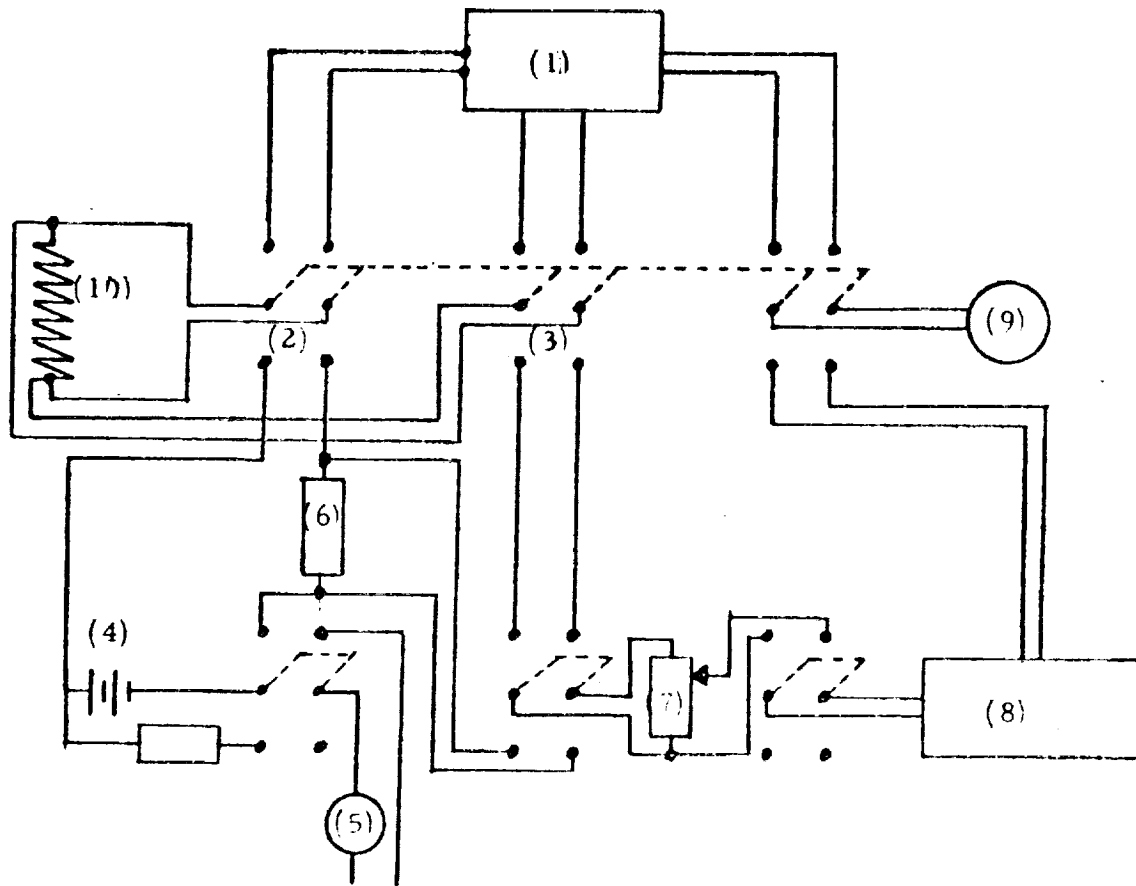
The electrical circuit for the  $\text{OF}_2$  calorimeter is shown in Figure 2. As mentioned, the platinum coil wrapped around the sample container is employed both as a heating source and also a temperature sensing element, therefore two separate electrical measuring circuits must be employed. In determining temperature, the platinum coil performs as a resistance thermometer; that is, its resistance will change as a function of temperature. Accurate resistance measurements will be obtained utilizing a Leeds and Northrup G-2 Mueller bridge (1) and can detect changes of better than  $\pm 1 \times 10^{-4}$  ohms. This, when converted to temperature is equivalent to  $\pm 0.001^\circ\text{C}$ ,

Temperature and energy input measurements cannot be obtained simultaneously, therefore, a series of knife switches (2 and 3) are connected across the potential and current leads of the platinum coil which serve to isolate the two systems.

Current to the heating coil is supplied by either a 12 or 24 volt lead acid battery (4). Since total energy input must be measured, a precision clock (5) accurate to  $\pm 0.1$  sec is activated at the same instant that current is applied to the heating coil. As current is flowing through the coil, its resistance changes due to the rise in temperature and as a result the current will also change. In addition, as current is being drained from the battery, there will be a slight variation in its output voltage. To ascertain these variations and to locate where these changes are occurring, a standard resistor (6) of a known value and with a negligible temperature coefficient, is placed in series with the platinum coil. By monitoring of the voltage drop across this resistor, the output voltage from the battery can be obtained.

The voltage measurements are obtained by utilization of a precision ratio bridge (7) in conjunction with a Leeds and Northrup K-3 potentiometer (8). With this instrumentation accuracies in the voltage measurement will be better than  $\pm 0.001$  volts.

With the above mentioned measurements accurate temperature and heat input data can be realized. It is expected that the heat capacity data generated from this study will be accurate to better than  $\pm 0.5\%$ .



1. Mueller Bridge
2. Knife Switch
3. Knife Switch
4. Lead Acid Battery
5. Precision Timer

6. Standard Resistor
7. Ratio Bridge
8. K-3 Potentiometer
9. Galvanometer
10. Platinum Coil

Figure C-2. Electrical Circuit for Heat Capacity Apparatus

### 3.0 APPARATUS CALIBRATION

#### 3.1 Temperature Sensing Element Calibration

The platinum resistance wire was calibrated in terms of resistance change as a function of temperature. This was accomplished by obtaining resistance measurements at various vapor pressure points of liquid oxygen. Since the vapor pressure-temperature relationship is well known for liquid oxygen it was an ideal temperature calibrating media for the temperature range of interest. Table I presents the vapor pressure, temperature and resistance relationships obtained.

Analysis of the resistance versus temperature relationship yield the following relationship for the temperature sensing element of the calorimeter:

$$t = \frac{R - 109.868}{0.4455}$$

where:     R     =     resistance (ohms)  
          t     =     temperature (°C)

#### 3.2 Calorimeter Constant Determination

Liquid oxygen and liquid propane were used to obtain the calorimeter constant for the apparatus. This was obtained by actual measurements of the temperature rise in the calorimeter for a given quantity of heat injected into the calorimeter. The calorimeter constant was obtained by substitution into the following equation:

$$K = \frac{E - C_p (\Delta T) g}{\Delta T}$$

where:     E         =     total energy input (cal)  
          C<sub>p</sub>       =     heat capacity of calibrating medium (Cal/g°C)  
          ΔT       =     change in temperature (°C)  
          g         =     mass of the calibrating fluid (grams)

A plot of the calorimeter constant as a function of temperature is given in Figure 3. As can be seen, the plot is not linear. This is due to the fact that heat losses vary as a function of the differential between the calorimeter



TABLE I  
CALIBRATION OF PT RESISTANCE THERMOMETER USING VAPOR  
PRESSURE-TEMPERATURE RELATIONSHIP FOR LIQUID O<sub>2</sub>

P (mm)	R (ohm)	t (°C)	P (mm)	R (ohm)	t (°C)	P (mm)	R (ohm)	t (°C)
147	21.980	-196.1	234	23.400	-193.0	608	26.850	-185.2
149	22.020	-196.0	237.5	23.450	-192.9	615	26.900	-185.1
156.5	22.170	-195.7	241.5	23.500	-192.8	623	26.950	-185.0
159	22.200	-195.6	245	23.550	-192.7	630	27.000	-184.9
161.5	22.250	-195.5	249	23.600	-192.6	637.5	27.050	-184.8
164	22.300	-195.4				645	27.100	-184.7
167	22.350	-195.2	402	25.320	-188.8			
169.5	22.400	-195.1	408.8	25.350	-188.6	2766	34.326	-169.0
172.5	22.450	-195.0	416	25.400	-188.5	4651	37.580	-161.4
175	22.500	-194.9	422.5	25.450	-188.3	8117	41.880	-152.0
			429	25.500	-188.2	10549	44.000	-147.3
201	23.000	-194.0	435	25.550	-188.0	12852	45.700	-143.55
208	23.050	-193.8	441	25.600	-187.9			
216	23.150	-193.5	446.5	25.650	-187.8			
219.5	23.200	-193.4						
223.5	23.260	-193.3	582	26.670	-185.6			
226.5	23.300	-193.2	587.5	26.700	-185.5			
230	23.350	-193.1	601	26.800	-185.3			

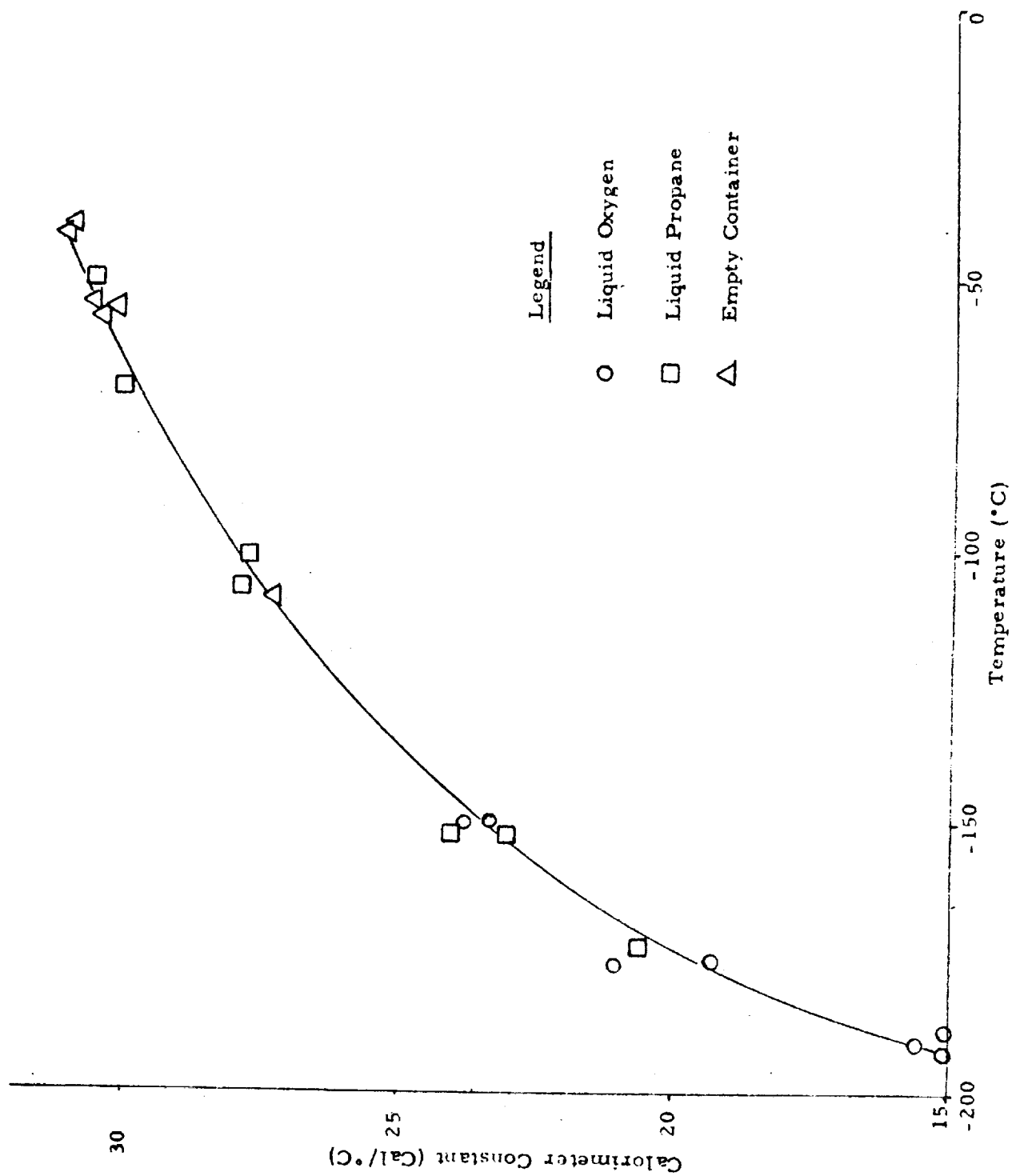


Figure C-3. Calorimeter Constant as a Function of Temperature

and its external environment. Examination of Figure C3 shows that the temperature range of the measurements with oxygen and propane overlap thus establishing excellent correlation.

#### 4.0 TEST PROCEDURE

Prior to the  $\text{OF}_2$  measurements, the sample container was subjected to cold cycling ( $\pm 320^\circ\text{F}$  to ambient) and pressure checked to 500 psig. The sample container and inlet system was passivated with gaseous fluorine at 200 psig for a period of 24 hours.

The outer container was evacuated to better than  $10^{-4}$  mm Hg and the heat leak to the calorimeter through the lead wires, etc., was allowed to become constant before an experiment was initiated. Upon maintaining a constant heat leak, the resistance of the platinum thermometer was recorded every half minute for a period of 4.5 minutes --- defined as the before period (Figure C4). During this time the 12 volt batteries were being discharged through a dummy resistance of approximately the same value as the calorimeter heater in order to minimize the voltage surge and voltage drop when the heater was switched on.

At time equal to 5 minutes, the heater was turned on and the heating maintained for approximately 6.5 minutes. The voltages across the calorimeter heater and the standard cell were measured at 21% of the heating time and again at 79%. This enabled the calculation of an "E" value. The time of heating was measured using a clock accurate to 0.01 sec. Voltages were measured to within  $\pm 0.00005$  volts.

At time equal to 12 minutes, the resistance of the platinum thermometer was again recorded every half minute for 15 minutes --- defined as the after period (Figure C4). To account for heat losses, the before period was extrapolated forward to 63% of the heating period and the after period extrapolated backward to the 63% point. The  $\Delta t$  was then taken as the difference in temperature at this 63% point between the before and after periods. Heat capacities are then computed from the following equation:

$$C_p = \frac{E - K (\Delta T)}{g(\Delta T)}$$

where:

$C_p$	=	heat capacity (cal/g $^\circ\text{C}$ )
$E$	=	total energy input (cal)
$K$	=	calorimeter constant (cal/ $^\circ\text{C}$ )
$\Delta T$	=	temperature rise due to heating
$g$	=	mass of sample (grams)

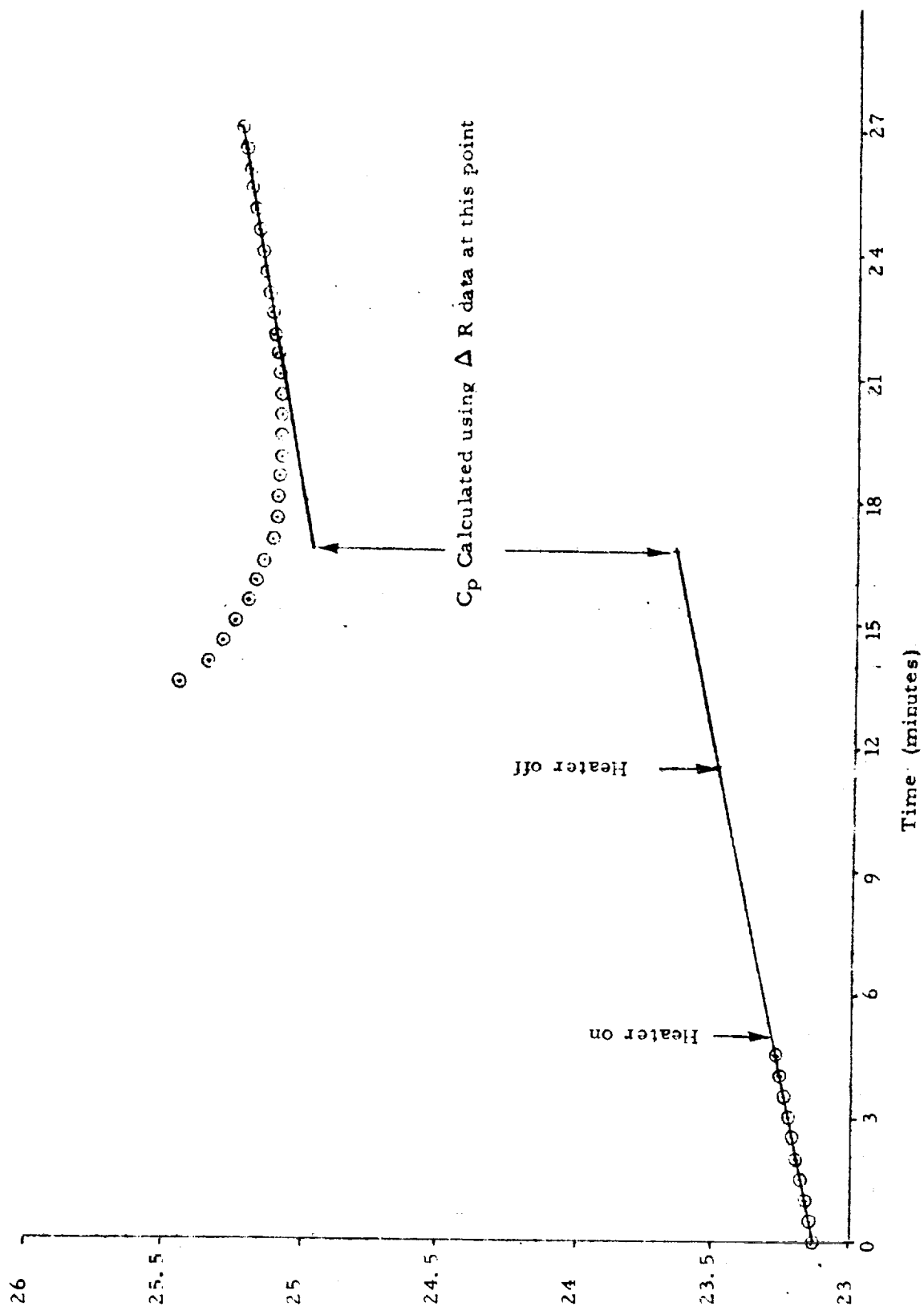


Figure C-4. Calorimeter Experimental Data

## 5.0 TEST RESULTS

Heat capacity measurements on  $\text{OF}_2$  were carried out over a temperature range of  $-196^\circ\text{C}$  to  $-75^\circ\text{C}$  employing the procedure as described. These data are presented in Section D. Data for a typical experiment are given in Table II.

TABLE II  
CALORIMETER EXPERIMENT  $\text{OF}_2$

Run #1 (4/14/65)

Before Period		After Period			
Time (min)	R (ohm)	Time (min)	R (ohm)	Time (min)	R (ohm)
0	23.142	12	---	18	25.101
	23.157		---		25.093
1	23.172	13	---	19	25.089
	23.187		25.420		25.088
2	23.202	14	25.350	20	25.089
	23.217		25.300		25.094
3	23.232	15	25.250	21	25.099
	23.247		25.210		25.105
4	23.262	16	25.175	22	25.114
	23.278		25.150		25.123
5	heater on	17	25.118	23	25.133
			25.113		25.144
				24	25.156

Heating period --- 6 min, 30.050 sec (390.050 sec)  
g --- 83.5.5 gm  $\text{OF}_2$

	$V_s$	$V_r$
21% time	.13760	.97573
79% time	.13715	.97488
ave.	.13738	.97531

